Copyright Warning & Restrictions

The copyright law of the United States (Title 17, United States Code) governs the making of photocopies or other reproductions of copyrighted material.

Under certain conditions specified in the law, libraries and archives are authorized to furnish a photocopy or other reproduction. One of these specified conditions is that the photocopy or reproduction is not to be "used for any purpose other than private study, scholarship, or research." If a, user makes a request for, or later uses, a photocopy or reproduction for purposes in excess of "fair use" that user may be liable for copyright infringement,

This institution reserves the right to refuse to accept a copying order if, in its judgment, fulfillment of the order would involve violation of copyright law.

Please Note: The author retains the copyright while the New Jersey Institute of Technology reserves the right to distribute this thesis or dissertation

Printing note: If you do not wish to print this page, then select "Pages from: first page # to: last page #" on the print dialog screen

ABSTRACT

NON-LINREAR EVALUATION OF CONCRETE-FILLED STEEL TUBULAR COLUMNS

by
Mohammad H. Shams

Concrete-filled steel tubular (CFT) columns have become increasingly popular in structural applications due to their high strength, high ductility, and large energy absorption capacity. These structural properties are the result of integral behavior of the concrete core and the steel tube. This research provides an analysis of the interaction of the concrete core and the steel tube in CFT columns.

While there have been many experimental studies of CFT columns, there has been no analytical work modeling the confining effect of the steel tube on the concrete core. Furthermore, current design procedures tend to underestimate the ultimate strengths of CFTs since they neglect the confining effect of the steel tube on the concrete core. Since experimental programs are expensive, time consuming and limited to small ranges of parameters, it is important to develop an analytical model for CFT members.

In this study emphasis is placed on the non-linear response of CFT columns subjected to axial and combined loadings. A three-dimensional finite element model is developed for CFT columns. The concrete core is modeled with 3-D solid elements which use the Pramono-William concrete model and the steel tube is modeled using shell elements which allow large deformation and contain a von Mises plasticity model with kinematic hardening. Gap elements are used to model concrete and steel interface. The finite element model is calibrated against existing experimental results.

Analyses of columns under axial loading indicate that the stress-strain properties of the concrete core are highly affected by the geometrical configuration of the columns as well as material properties of concrete core. CFT columns exhibit high flexural capacity with a hardening type of behavior due to higher ductility and larger compressive capacity of concrete core which is provided by confining effect of steel tube. The circular CFTs show a hardening type of response under axial loading while, a degrading type of behavior is observed in square columns.

Simple models are developed in order to define the axial and flexural capacity of CFT columns. The proposed methodology is calibrated against experimental data.

NON-LINEAR EVALUATION OF CONCRETE-FILLED STEEL TUBULAR COLUMNS

by
Mohammad Shams

A Dissertation
Submitted to the Faculty of
New Jersey Institute of Technology
in Partial Fulfillment of the Requirements for the Degree of
Doctor of Philosophy

Department of Civil and Environmental Engineering

January 1997

APPROVAL PAGE

NON-LINEAR EVALUATION OF CONCRETE-FILLED STEEL TUBULAR COLUMNS

Mohammad H. Shams

Dr. M. Ala Saadeghvaziri, Thesis Advisor — Date
Associate Professor of Civil and Environmental Engineering, NJIT

Professor Edward Dauenheimer, Committee Member — Date
Professor and Associate Chairman of Civil and Environmental Engineering, NJIT

Dr. C. T. Thomas Hsu, Committee Member — Date
Professor of Civil and Environmental Engineering, NJIT

Dr. Ahmad Rahimian, Committee Member — Date
Vice President, The Cantor Seinuk Group P.C., New York, N.Y.

Dr. William Spillers, Committee Member — Date
Distinguished Professor and Chairman of Civil and Environmental Engineering, NJIT

BIOGRAPHICAL SKETCH

Author: Mohammad H. Shams

Degree: Doctor of Philosophy

Date: January 1997

Undergraduate and Graduate Education:

- Doctor of Philosophy in Civil Engineering,
  New Jersey Institute of Technology, Newark, NJ, 1997
- Master of Science in Civil Engineering,
  New Jersey Institute of Technology, Newark, NJ, 1992
- Bachelor of Science in Civil Engineering,
  Shiraz University, Shiraz, Iran, 1985

Major: Civil Engineering

Presentations and Publications:

Spillers, W. R. and M. Shams
"Three-Dimensional Beam-Columns," Computers and Structures, Vol. 52, No. 3, 1994, pp. 449-460.

Saadeghvaziri, M. Ala and M. Shams
"Effect of Vertical Motion on the Response of Highway Bridges: A case Study from the Northridge Earthquake," Proceedings, 2nd International Conference on Seismology and Earthquake Engineering, May 15-17, 1995, Tehran, Iran, pp. 579-586.

Shams, M. and M. A. Saadeghvaziri
"The State-of-Art of Concrete-Filled Steel Tubular Columns," ACI Structural Journal, Accepted for publication, 1996.

Shams, M. and M. A. Saadeghvaziri

"Steel Jacketing of Substandard RC Columns, A Retrofitting Scheme," Poster Presentation, ASCE, Structural Seminar on Seismic Assessment of Regional Lifelines, March 1996, New Jersey Institute of Technology, Newark, NJ.

This thesis is dedicated to

my dear mother and beloved late father.

ACKNOWLEDGMENT

At the very outset, I would like to acknowledge my most sincere gratitude and appreciation to Dr. Ala Saadeghvazeri for his support and guidance all through this research study. His expertise in finite element analysis went a long way in helping me through some very difficult problems at critical times in my research study. Of special mention is the support extended to me by Dr. William R. Spillers from the very beginning of my graduate studies at NJIT. It would not have been possible to bring this research study to fruition without his valuable inputs and inspiration. I would also like to express sincere appreciation for the support extended to me by Professor Edward Daunheimer. I would like to thank Dr. Thmos Hsu for his guidance and moral support. I would like to acknowledge the help I received from Dr. Rahimian who provided me with many of the resources that I needed for this research study. Special thanks to Dr. Larisa Krishtopa for her support and inspiration. I would like to take this opportunity to thank Mr. Allyn Luke, Dr. Raj Navlurkar, Mr. Saied Rashidi and Dr. Sudhi Mukherjee for their help during the conduct of this research study. Financial support from NJIT and the Department of Civil and Environmental Engineering is gratefully acknowledged. I would like to mention that the emotional and moral support extended to me by my family and friends served as a source of inspiration all through this research study.

TABALE OF CONTENTS

Chapter **Page**

TABALE OF CONTENTS
(Continued)

Chapter **Page**

TABALE OF CONTENTS
(Continued)

Chapter **Page**

TABALE OF CONTENTS
(Continued)

Chapter **Page**

TABALE OF CONTENTS
(Continued)

Chapter **Page**

LIST OF TABLES

LIST OF FIGURES

Figure **Page**

LIST OF FIGURES
(Continued)

Figure **Page**

LIST OF FIGURES
(Continued)

Figure **Page**

LIST OF FIGURES
(Continued)

Figure **Page**

LIST OF FIGURES
(Continued)

Figure **Page**

LIST OF FIGURES
(Continued)

Figure **Page**

CHAPTER 1

INTRODUCTION

1.1 General

It is widely recognized that the innovative use of two or more materials in structures generally leads to more efficient systems for resisting seismic forces. Therefore, the structural application of hybrid systems and composite elements are becoming popular. Composite members are structural members, components or connections in which there is a high degree of interaction between structural steel and concrete. Hybrid systems refer to structural systems consisting of combination of steel, reinforced concrete and composite elements. Among the composite structural members, concrete-filled steel tubular (CFT) columns have attracted special attention. This is partly due to their excellent earthquake resistant properties such as high strength, high ductility and large energy absorption capacity. A CFT column is a structural member that uses a combination of steel tubes and concrete to provide adequate load carrying capacity to sustain either axial or combined loadings. A CFT column is simply constructed by filling a hollow rectangular or circular structural steel tube with concrete. Figure 1.1 shows a schematic cross-sectional view of CFT columns. The interactive and integral behavior of the concrete and the steel tube makes the CFT column a very cost effective and efficient member in structural applications.

The enhanced structural properties come from the composite action of constituent elements. The confinement effect created by steel casing enhances the material properties of concrete by putting the concrete under a triaxial state of stresses thereby increasing the

strength and ductility of concrete. Additionally, the inward buckling of the steel tube is prevented by the concrete, thus increasing the stability and strength of the column as a system. Among other advantages of CFT columns are the speed of construction, saving on formwork for the concrete core and possible use of simple standardized connections.

The use of CFT columns in structural frames has increased in the United States, Japan and China during the past ten years. The composite frames consisting of CFT columns have been used in the construction of a number of unique high rise buildings (Giffis, 1992). Among them, the Bank of China Building in Hong Kong is the tallest one. The 1209 foot tall Bank of China Building is the fifth tallest building and, the tallest composite frame structure in the world. It is supported on only five mega composite columns which are connected together by giant CFT diagonals. These diagonals are steel box members filled with concrete. In the construction of the composite frame only 23 psf of structural steel were used which is a dramatic reduction compared to an all-steel frame. This is particularly significant considering that Hong Kong is one of the windiest cities in the world.

1.2 Research Work on Overall Response of CFT Columns

Since the beginning of the twentieth century many researchers have attempted to understand the behavior of CFT columns. In 1915, Swain and Holmes studied the elastic behavior and strength of concrete-pipe columns. Kloppel and Goder (1957) carried out tests on the collapse load of CFT columns with different slenderness ratios. The elasto-plastic behavior of CFT columns was investigated and the test results compared with the predicted loads obtained from a proposed numerical method (Neogi and San, 1969). In

the proposed method, a uniaxial stress-strain relationship was used for the concrete core and the increase in the compressive strength of concrete due to confinement was ignored. To determine the ultimate axial capacity of CFT columns, several design equations have been developed (Gardner and Jacobson, 1967; Furlong, 1976; Knowles and Park, 1976; Rangan and Joyce 1992). In the proposed procedures the confinement effect of the steel tube on the concrete core and the composite action between them were ignored. As a result, a close agreement between test results and the predicted ultimate capacities was not achieved. Test results have shown that the increase in strength of CFTs due to confinement are in the range of 1.2 to 3.5 for square columns and 1.2 to 4.5 for circular columns (Sugano and Nagashima, 1992).

In 1977, an extensive experimental program was performed on CFT columns (Tomii et al., 1977). The objective of this study was to investigate the effect of size, cross-sectional shape and mechanical properties of concrete on the behavior of axially loaded columns. It was found that the ultimate capacity of CFT columns were considerably affected by the diameter to wall thickness ratio, cross-sectional shape and slenderness ratio. The effect of bond strength between the steel tube and the concrete core on the behavior of CFT columns was studied by a number of researches (Okamoto and Maeno, 1988; Matumura et al., 1990; Matui et al., 1991). Okamoto suggested that the bond strength does not influence the flexural capacity of CFT columns. Conversely, the experimental studies by Matumura and Matui indicated that bending moment capacity will increase by improving the bond between the steel tube and the concrete core. The effect of bond strength on the behavior of CFT columns is not completely understood.

Few experimental studies on the thin-walled CFT columns are available (Ge and Usami, 1992; Bridge and Webb, 1992). Local buckling of steel tube was observed in thin-walled columns. The mechanism of local buckling of steel tube is not entirely clear.

During last two decades, a number of experimental studies have been performed on the seismic response of CFT columns (Nagashima et al., 1989; Sugano and Nagashima, 1992; Chai, 1992; Boyd et al., 1995). Due to complexity of the problem and lack of information, no realistic hysteresis model has been proposed yet. The current state of knowledge is not sufficient to model every aspect of hysteresis response. Research (Sugano and Nagashima, 1992) has shown that important parameters such as cross-sectional shape, level of axial force and wall thickness have significant effect on the primary curves (e.g. load-deflection and moment-curvature curves). However, the level of sensitivity of primary curves to each parameter is not well defined.

Even though, experimental and analytical studies have been performed on CFT columns, there still exists problems concerning the response of CFTs under static and dynamic loadings. These problems are summarized in the following section

1.3 Research Needs

A large number of issues can be mentioned which reflect on the problems associated with understanding the behavior of CFT columns. To predict the behavior of CFTs, the response in pre-peak as well as in post-peak regime needs to be clearly understood. The main problem has to do with the fact that the state of stresses that exist in the CFT columns are rather complex. The concrete core is under a triaxial state of stress and the

steel tube is under a biaxial state of stress. The confining pressure which is developed between the concrete core and the steel tube interface varies at different stages of loading. The changes in the confining pressure is not well predicted. As a result, the overall response of CFTs under static and dynamic loadings is not well understood due to lack of knowledge on the behavior of its constituent components and the interaction between them. Hence, a number of potential research needs can be noted as:

1. Ultimate strength of CFT columns is not well predicted and the effect of important parameters such as cross-sectional shape, width-wall thickness ratio (aspect ratio), confined compressive strength of the concrete core and the bond strength on the load carrying capacity are not well understood.
2. Stiffness, ductility and strength of CFTs are highly affected by the aspect ratio, cross-sectional shape and slenderness ratio. However, the level of sensitivity of response to each parameter is not well defined (e.g. maximum aspect ratio).
3. High strength concrete has drawn attention in structural applications. The use of high strength concrete to construct the columns in high rise buildings is extremely advantageous as substantial savings in material quantities can be achieved. However, the application of high strength concrete to structures, especially in seismic zones is questioned since the material has poor ductility when unconfined. The ductility can be increased by confining the high strength concrete with structural steel tubes. However, the superior properties of high strength concrete may not be fully utilized if the steel tube is not thick enough to eliminate the possibility of local buckling. The optimum use of high strength concrete needs to be investigated in more details (thin-walled columns vs. high strength concrete) since there is uncertainty about whether

local buckling of the steel tube or crushing of the concrete core occurs first. Therefore, the mechanism of local buckling needs to be studied in detail.

4. Over the course of last three decades different design codes such as the American Concrete Institute; Building Code Requirements for Reinforced Concrete (ACI 318-95), the American Institute of Steel Constructions; Structural Specification Liaison Committee (AISC-SSLC), Manual of Steel Construction; Load Resistance Factor Design (LRFD), and Architectural Institute of Japan (AIJ-1987) have been used to design the CFT columns. The discrepancies among them and also the large difference between design codes and experimental results (Sugano and Nagashima, 1992) is shown in Figure 1.2. As can be seen, the current design codes can not accurately predict the capacity of CFT columns. In most cases, the load carrying capacity of CFTs is underestimated, up to 50% of the actual capacity. These discrepancies and differences indicate that there is a need for a more accurate, yet practical, design method. Such methodology must consider the important aspects of response such as confinement of concrete core and should be developed in conjunction with a detailed analytical study.
5. Parameters such as the level of axial force, cross-sectional shape, and bond strength have significant effect on primary curves (e.g. axial load-deflection and bending moment-curvature curves), but the level of sensitive of primary curves to each parameter is not well known.
6. Degree of strength decay depends on many parameters including confinement of concrete and shear strength, but there is not sufficient experimental information in

order to investigate the sensitivity of strength decay to each parameter. Moreover, it is not clear how strength decay can be delayed and its effects reduced.

7. Few experimental data is available on seismic performance of thin-walled columns. However, it is believed that the aspect ratio has significant effects on important features of the response such as pinching and stiffness degradation. Experimental and analytical studies including a wide range of aspect ratios are required to study the impact of aspect ratio on the hysteresis response of CFTs.
8. It is important to evaluate the seismic performance of full scale moment resistance frames, using CFT columns. To achieve this purpose, efficient and accurate global models should be developed. Therefore, it is essential to establish a realistic hysteresis model for CFT columns and important features of hysteresis response such as primary curve (i.e., stiffness, strength, toughness/ductility and hardening), stiffness degradation and strength decay needs to be evaluated.
9. Experimental and analytical work on the seismic performance of structural systems with CFT columns are practically nonexistent. Since experimental study is costly and practically impossible, analytical studies can be used for analysis of these systems.

The intent of the present study on non-linear response of CFT columns is to shed more light on some of these problems.

1.4 Objectives and Methodology of the Present Study

Even though extensive experimental work has been carried out on the CFT columns, no analytical work considering the triaxial effect of concrete and the behavior of steel under

biaxial state of stresses has been undertaken to date. Experimental studies have provided sufficient information to develop analytical models. Such models can be very useful tools for detailed analysis and parametric studies to aid engineers in more efficient design of CFT columns.

The main objective of this study is to develop a reliable finite element model in order to study the non-linear response of CFT columns under static axial and lateral loadings. A comprehensive parametric study will be performed using non-linear three-dimensional finite element analysis which includes a wide range of aspect ratios, concrete with different compressive strengths, various cross-sectional shapes and slenderness ratios. The results of this parametric study will be used to predict the ultimate strength, stiffness and ductility of CFT columns.

In order to study the non-linear response of CFT columns a three-dimensional finite element model, using the general purpose software "ABAQUS", is developed. Three-dimensional quadratic solid elements are used to model the concrete core. The steel tube is modeled by isoparametric shell elements. The interaction between the steel tube and the concrete core interface is modeled by gap elements. The von Mises elasto-plastic material model with kinematic hardening is used for the steel tube. The Pramano-William's concrete material model, implemented in ABAQUS (Xie et al., 1994) as a user subroutine, is used for the concrete core.

The characteristics and behavior of CFT columns is entirely understood through the detailed finite element analysis. Moreover, the stress-strain relationship of concrete core at every stage of loading is studied in detail. As a result, the behavior of concrete core is accurately predicted. In addition, the possibility and mechanism of local buckling

is completely investigated. A practical design method is established that accounts for important parameters effecting the response of CFT columns.

Hence, the main objectives of this study can be summarized as follows:

1. To develop a three-dimensional finite element model for CFT columns to handle the most common loading patterns and to verify its effectiveness by comparing its analytical results with previous experimental tests. The finite element model should be able to simulate the important features of response such as confinement of concrete core, local buckling of steel tube and interaction between concrete core and steel tube interface.
2. To obtain much needed "basic" information of practical importance, e.g., load transfer mechanism, stress-strain properties of the concrete core and confining effect of steel tube in increasing strength and ductility.
3. To investigate the effect of important parameters such as aspect ratio, cross-sectional shape and bond strength on the structural properties of CFTs e.g., ultimate strength, stiffness and ductility columns through a detailed parametric study.
4. To develop simplified analytical models to predict the load carrying capacity and to define the stress-strain relationship for the concrete core.
5. To propose new practical design guidelines for CFT columns.

1.5 Impact

As recommended by US-Japan Cooperative Earthquake Research Program (US-Japan Planning Groups, 1992), an extensive analytical study, including modeling of behavior

and parametric study is required to understand the response of CFT columns to static and dynamic loadings. The present study is meant to provide tools to predict the structural characteristics of CFTs such as strength, stiffness and ductility, which will lead to efficient use of CFT columns in structural systems. In view of the advantages and opportunities for innovation that CFT columns provide for earthquake resistance systems, design procedures are developed during this study that certainly advances the state-of-the-art in design.

CHAPTER 2

BACKGROUND AND MOTIVATION

2.1 Introduction

Major part of this chapter deals with an objective review of the previous research works on CFT columns. In the following sections the previous research works on CFT columns, including experimental and analytical studies are discussed. In the next section, experimental work including the discussion of behavior and response of the CFT columns under various loading conditions is presented. This includes the effects of bond improvement, hysteresis response of CFTs and performance of thin-walled columns. An overview of the analytical studies on CFT columns then follows. Finally, comparison of different design codes and their shortcomings are presented.

2.2 Experimental work

2.2.1 Characteristics and Behavior of CFT Columns

Use of CFT columns dates back to the early nineteen hundreds when a number of bridges and buildings were built using CFT columns. To name a few, Almondsbury Motorway Interchange (England), Charleroi Railways (Belgium), International Labor Organization at Geneva, and a gymnasium at Martigny-Boury in Switzerland (Bode, 1976). The hollow steel sections in these structures were filled with concrete to achieve higher stability (Kloppel and Goder, 1957; Russell, 1953). In addition, CFT columns can be credited with more advantages such as:

1. Excellent axial and flexural load carrying capacity,
2. High shear resistance,
3. Large ductility and energy absorption capacity,
4. Greater critical load in buckling (i.e., higher stiffness),
5. Possible use of standard and simple connections,
6. Saving of formwork for the concrete core.

The enhanced properties of CFTs can be explained in terms of composite action between the steel tube and the concrete core. In the early stages of loading the Poisson's ratio for concrete is lower than that for steel. Thus, the steel tube has no confining effect on the concrete core. As the longitudinal strain increases, the lateral expansion of the unconfined concrete gradually becomes greater than that of the steel. A radial pressure subsequently develops at the steel-concrete interface. At this stage, the concrete core is stressed triaxially and the steel tube biaxially. Because of the presence of hoop tension (i.e., biaxial state of stress), the steel tube can not sustain the normal yield stress, therefore there is a transfer of load from the tube to the core (Neogi and San, 1969). The load corresponding to this mode of failure can be considerably greater than the sum of the uncoupled steel and concrete failure loads. The level of increase in the failure load caused by the confining effect of the steel tube on the concrete core depends on several factors, namely the thickness of steel tube, slenderness ratio, eccentricity and cross-sectional shape. In the case of circular CFT columns, the steel tube has more confining effect than in the square columns. The center and the corners of square sections go under a higher confining pressure than the sides, but a uniform distribution of lateral pressure is expected in the circular columns.

An extensive study has been done to investigate the effects of the cross sectional shape, aspect ratio and column length on the behavior of CFT columns (Tomii and Yoshimaro, 1977). Tests were conducted on 286 columns under concentric axial loads. Six sizes of circular, square and octagonal steel tubing with different wall thicknesses were used during the test. It was found that CFT columns can fail in two modes. In the case of longer columns, general buckling and in shorter columns, crushing of concrete was observed. The ultimate strength of CFT columns was considerably affected by the slenderness ratio, the thickness of steel tubing as well as the cross-sectional shape. A confining effect can be expected for circular columns, while for square columns, there was no increase in axial strength due to triaxial effects, despite small slenderness ratios and large wall thickness. The load-deformation behavior of the columns (Figures 2.1a and 2.1b) was also remarkably affected by the cross-sectional shape, aspect ratio (diameter to wall thickness ratio) and concrete strength (Tomii and Yoshimaro, 1977). The load-deformation relation for circular and octagonal columns showed strain hardening or an elastic-perfectly plastic behavior, while for all square columns, the load-deformation curve was of a degrading type (Figures 2.1a and 2.1b).

The performance of CFTs under sustained loads is different from ordinary reinforced concrete columns. In RC columns, concrete experiences contraction as it sets during its early age. This is followed by a lengthy period of shrinkage and creep under load. In the case of CFT columns, because of the humid environment inside the steel tube, the coefficient of contraction is low and shrinkage proceeds very slowly. However, inside corrosion of the steel tube can be expected. Concrete expands more than its steel

jacket under large longitudinal strain. Thus, contraction of the concrete hardly affects the load carrying capacity of CFTs (Bode, 1976).

The only observation of creep in CFT columns was reported by Furlong (Furlong, 1967). He carried out tests on 22 circular and 17 square columns. These columns were subjected to various levels of constant axial force as moments were increased. In addition eight circular and five square columns were loaded only axially. The interaction of the steel tube and the concrete core was studied by measuring the longitudinal and transverse strain at four faces of the specimens. Figure 2.2 shows a typical longitudinal load-strain relationship.

A sudden increase in the ratio of transverse and longitudinal strain showed that the steel tube had provided confining pressure for the concrete core (Furlong, 1967). It was observed that after the steel tube began to yield, the creep of concrete caused a load reduction as high as 15%. The lack of information on behavior of CFTs under sustained loads indicates a need for further research in this area.

2.2.2 Composite Action

A higher buckling capacity is expected in CFT columns due to the composite action and increased stiffness. It has been suggested that composite action is only achieved with relatively stocky columns (i.e., slenderness ratio less than 50) (Roeder, 1992). Test results have shown that the composite action can also be expected in longer columns (Ghosh, 1977; Kenny and Broce, 1994). The test was conducted on two columns, a concrete-filled steel tube and a hollow steel tube, each 14.32 m (47 ft) in height, 32 cm

(12.75 inches) in diameter and with the wall thickness of 6 mm (0.25 in.) (Ghosh, 1977). Each column was subjected to axial and lateral loadings. The Canadian Standard (S16-1969) was used to analyze the columns. Comparison of the behavior of the two columns showed that concrete contributed significantly toward resisting the axial load and bending moment. Although the standard (S16-196) ignored the stiffening effect of concrete for columns where the slenderness ratio is greater than 85, while the slenderness ratio of tested columns was 129. The failure mode of the two columns was reported as an Euler-type of buckling. In general, the buckling mode of hollow cylindrical tubes can be categorized based on their slenderness ratios (Farshad, 1994).

(1) The buckling mode of short cylinders is predominately a so-called ring-buckling. Ring-buckling consists of an axisymmetric deformation with longitudinal waves along the length of cylinder.

(2) The chess-board buckling mode is the result of linear buckling analysis for cylinders with intermediate length. This mode of buckling is a regular pattern of inward and outward deformations in both longitudinal and circumferential directions. However, in experiments (Farshad, 1994) , diamond-shape buckling has been observed; a pattern of similar nature but not quite the same. The so-called diamond-shape buckling occurs in the postbuckling stage of loading. At this stage, the loaded cylinder snaps from one equilibrium shape to another which requires less energy to be maintained. The second deformed shape has a pattern of diamond type with inward and outward deformations.

(3) In long cylindrical tubes an Euler-type of buckling can occur. Since, long cylinders behave as columns, the critical buckling load can be obtained by using the classical

column theory. However, this mode of failure can be combined by the ovalization of cross section, so-called Brazier effect (Brazier, 1927), which tends to decrease the critical buckling load.

Both hollow and concrete-filled tubes were categorized as long columns. The concrete-filled column was considered as a composite member and theoretical analysis was carried out using the classical column theory. The test results showed good agreement with theoretical analysis (Ghosh, 1977). In addition, the observed flexural stiffness was greater than the sum of the uncoupled concrete and steel stiffnesses, indicating that the composite action was achieved between the concrete and the steel tube The enhanced structural behavior of the concrete-filled column can be explained in terms of composite action between the steel tube and the concrete core. Moreover, the circumferential deformation and ovalization of cross section were prevented, which results in higher stiffness and larger critical buckling load.

2.2.3 Bond Effects

It is accepted that CFT columns as composite members allow stress transfer (bond stress) between the steel tube and concrete core. It is believed that the bond strength has a significant effect on the behavior of composite members. However, careful examination of numerous test results indicates that there is still uncertainty about the effect of bond strength on the overall response of CFTs.

Okamoto investigated the effect of bond strength between the steel tube and concrete core on the behavior of CFT columns filled with high-strength concrete

(Okamoto and Maeno, 1988). The objective of this study was to investigate the effects of the aspect ratio, level of axial force and bond strength on the bending capacity of the columns. Tests were conducted on nine square columns filled with high strength concrete (f_c' = 98.1 MPa). In order to control the bond strength, a mortar layer with a thickness of 10 mm was placed between the steel tube and the concrete core. Table 2.1 shows the list of tested specimens.

According to the test results (Figures 2.3a and 2.3b), it was concluded that; (1) the bond strength does not significantly affect the flexural capacity of CFT columns, (2) the flexural capacity considerably increases by increasing axial load, (3) steel tube has a significant effect on improving the compressive strength of concrete and preventing the brittle failure that is normally associated with unconfined high strength concrete.

The range of variables used in Okamoto's study was limited (Table 2.1). Moreover, for each test the two main variables (level of axial force and mortar strength) were changed at the same time. In this situation, a solid conclusion is difficult to be made.

More recently, the experimental studies carried out by Matumara and Matai. indicated that the bending moment capacity will increase by improving the bond between steel tube and concrete core (Yoshioka, 1992). To improve bond strength, steel tubes with inner ribs were used. The tests were carried out on eight cantilever square columns. In this research the effects of inner ribs and level of axial force were investigated. Voids were provided at the top of columns to clarify the effect of the inner ribs. A typical test setup and the test program are shown in Figures 2.4 and 2.5. Each column was subjected

to constant axial load and cyclic lateral load. Columns with inner ribs showed larger energy dissipation and higher ductility (Figure 2.6).

It seems that when the slippage of the concrete core in the steel tube is prevented the bond strength does not have significant effect on the flexural capacity of CFTs. In columns where the slippage is permitted (i.e., Columns with voids at the top), the effect of bond strength is significant on the overall response of CFT columns. The comparison between the response of R3C (with ribs, no voids) and F3C (without ribs, no voids) shows that the performance of the column did not significantly improved by using steel tube with ribs. This indicates that the stiffness of the column did not considerably increased by employing steel tube with ribs.

2.2.4 Behavior of CFT Columns with Large Aspect Ratio

Very few experimental studies on concrete-filled thin-walled steel tubes with large aspect ratio (i.e., width-thickness ratio) are available. In 1992 Usami and Ge studied the behavior and performance of thin-walled square columns under axial loading (Ge and Usami, 1992). Six concrete-filled columns and four hollow steel tube columns were tested. In order to investigate the effect of stiffening of steel tube, two columns were equipped with stiffeners. Figure 2.7 shows the details of the specimens. For the columns with stiffeners, γ_t is the flexural rigidity of stiffeners and γ_{req} is the optimal value of the rigidity obtained from linear buckling theory. The width-thickness ratio parameter R was defined as $R = (b/t)\sqrt{12(1-\nu^2/(\pi^2 k)}\sqrt{\sigma_y / E}$, where b = flange or web width; t = plate thickness; σ_y = nominal yield stress of the plate; E = Young's modulus; and ν =

Poisson's ratio. k is the buckling coefficient with the value of $k = 4n^2$ and n is the number of subpanels in each plate panel (e.g. $n=1$ for unstiffened plate and $n=2$ for stiffened plate). Tables 2.2 and 2.3 shows the dimensions of specimens.

Typical failure and longitudinal load-strain relationships of stiffened and unstiffened columns are shown in the Figures 2.8 and 2.9, respectively.

In the hollow steel tubes local buckling occurred at the central part before the maximum load was reached. At the two opposite sides, buckling took place inward, and at the other two sides outward. While, in the concrete-filled columns it was observed that; (1) the local buckling occurred in one of the sides just before the peak load, and the other sides buckled after that, and (2) the outward buckling took place at all faces. After removing the steel tube, it was found that the concrete at the buckled portion was completely crushed, while no damage was observed in the other parts. Thus, it was concluded that local buckling of steel tubes was induced after crushing of the concrete core. It is also possible that these two phenomena occurred in reverse order. As it is identified later under research needs, a detailed analytical evaluation could shed more light on the mechanism of local buckling.

Bridge and Webb tested two thin-walled circular CFT columns, each with 2.021 mm thickness, 250.02 mm diameter and a height of 750.0 mm (Bridge and Webb, 1992). Each column was subjected to axial loading. Concrete with compressive strength of 59.5 (MPa) was used to fill the tubes. In addition, two hollow steel tubes were tested to determine the axial capacity and the influence of local buckling on the strength. In the case of hollow steel tube columns, local buckling occurred near the mid-height just prior to the maximum load although the magnitude of the buckling deformation was small.

Local buckling was observed to form well prior of the maximum load for both concrete-filled columns. It is not mentioned at which level of axial force local buckling occurred in the concrete-filled columns. It is possible that local buckling occurred almost at the same level of axial load in both the hollow and the filled columns. If so, then the use of high strength concrete in thin-walled columns is questionable.

2.2.5 Hysteresis Response of CFT Columns

Sugano and Nagashima investigated the effect of level of axial force, aspect ratio and the strength of the constituent materials on the overall response of CFT columns. Tests were carried out on thirty-eight circular and square columns (Sugano and Nagashima, 1992). Each column was subjected to constant axial load and cyclic lateral load. Figure 2.10 shows a typical test setup.

Circular columns demonstrated rich hysteresis curves (i.e., large ductility with stable loops). In the case of thin-walled circular columns, where the aspect ratio (D/t) was larger than 39, the maximum load was determined by the local buckling of the steel tube. Local buckling was formed in the square columns with the aspect ratio greater than 33. Square columns with a smaller aspect ratio indicated richer hysteresis curves. It was observed that the circular columns behaved in a ductile manner despite the level of axial force and aspect ratio. Ductile behavior can be expected only from those square columns where the aspect ratio is small and when the level of axial force is low (Sugano and Nagashima, 1992; Morino, et al., 1992; Nagashima et al., 1989). A typical shear force-drift angle relationship is shown in the Figure 2.11 for both types of cross-section.

Seismic performance of circular CFT columns was studied by F. Boyd et al. Tests were carried out on five circular columns (Boyd et al., 1995). Table 2.4 shows the details of tested columns and the test setup is shown in Figure 2.12. One of the circular columns was equipped with shear studs to improve the bond between the concrete core and steel tube.

Each column was subjected to a constant axial force of 178 kN (40 kips). A lateral cyclic load was applied near the top of the columns. All columns demonstrated higher flexural stiffness and load capacity than the ACI predicted stiffnesses and capacities. Figure 2.13 shows the hysteresis response of the columns. Pinching and strength decay was observed in hysteresis loops after a ductility factor of 2. The column with shear studs showed a monotonic load capacity (i.e., no strength decay was observed). It was concluded that the irregularities in the hysteresis response of the columns (i.e., pinching and humps) were caused by local buckling of steel tubes. The hysteresis response of the columns was similar to the response of ordinary RC columns with poor confinement. However, RC columns with proper confinement exhibit stable hysteresis loops with no strength decay (Saatcioglu, 1991). Thus, the use of CFT columns with a large aspect ratio is questionable. Moreover, the discrepancies between tests results (Sugano vs. Boyd) indicates a need for further research in this area.

2.2.6 Steel Jacket Retrofitting

Ductility and strength of existing substandard reinforced concrete columns can be enhanced by steel jacketing. In this technique the existing column is encased in a steel

tube and the gap is filled with a cement-based grout, resulting in a system that more or less is similar to CFT columns (Figure 2.14). Research results have shown that the confining effect of a steel jacket increases the compressive strength, flexural capacity and ductility of the columns (Chai, 1992; Priestly et al., 1994). To investigate the effectiveness of steel jacketing, tests were carried out on two RC-columns, each 61 cm (24 inches) in diameter and 381 cm (150 inches) in length. One column was retrofitted with a steel jacket. The steel jacket was fabricated from 4.8 mm (3/16 inch) thick hot rolled steel with the length of 120 cm (48 inches). A 6.3 mm (1/4 inch) gap was provided between the steel jacket and the column, which was filled with a cement-based grout. Each column was subjected to a constant axial load of 1780 kN (400 kips) and cyclic lateral load. The hysteresis response of both columns are shown in the Figure 2.15.

In the case of the unretrofitted column, bond failure was indicated at the lap-splice during the early stages of loading. The column sustained up to 97% of the theoretical flexural capacity followed by a rapid degradation of strength and stiffness. The strength envelope was observed to degrade after a ductility factor of 1.5. The response of the retrofitted column under cyclic loading demonstrated stable hysteresis loops up to a ductility factor of seven, which corresponds to a drift ratio of 5.3% (Chai, 1992).

2.3. Analytical Studies

Over the course of the last five decades different theories and design procedures have been suggested by many research groups. In 1957 Kloppel and Goder established lower and upper limits to predict the strength of concentrically loaded CFT columns (Kloppel

and Goder, 1957). The lower limit was expressed as the buckling load of the transformed area of the composite section. The upper limit was determined by calculating the buckling load considering an equivalent stiffness as the sum of steel and concrete stiffnesses. The proposed upper limit was found to be conservative for short columns.

In 1968 Furlong proposed that the lower limit of the axial capacity of CFT columns could be established as the force necessary to cause the steel to yield plus the force which is required to develop the same strain in the concrete (Furlong, 1968). The plastic moment of steel alone is the lower limit to the pure bending capacity. These values can be expressed as follow:

$$P_0 = A_s F_y + A_c f_c' \sqrt{F_y / 0.018 E_s} \qquad \text{with} \qquad F_y/.0018E_s \le 1 \tag{2.1}$$

$$M_0 = (F_y / 6)(D_0^3 - D_i^3) \qquad \text{circular columns} \tag{2.2a}$$

$$M_0 = (F_y / 4)(D_0^3 - D_i^3) \qquad \text{square columns} \tag{2.2b}$$

where D_0 and D_i are the external and internal dimensions of steel tube, respectively. To establish the interaction behavior of CFT columns an elliptical equation was suggested (Furlong, 1968). It can be written as:

$$(M_u / M_0)^2 + (P_u / P_0)^2 \le 1 \tag{2.3}$$

where $\boldsymbol{P_0}$ and $\boldsymbol{M_0}$ are the minimum axial and flexural capacity of the column respectively. It was found that Eq. (2.3) is conservative and usually underestimates the

strength of CFT columns. In the case of long columns, an equivalent stiffness was used to obtain the critical load. This equivalent stiffness was considered to be the algebraic sum of stiffness for each component as if each material acted separately. Thus:

$$(AE)_{eq} = A_c E_c + A_s E_s \tag{2.4a}$$

$$(IE)_{eq} = I_c E_c + I_s E_s \tag{2.4b}$$

where $(AE)_{eq}$ and $(IE)_{eq}$ are the equivalent stiffness under axial and flexural load, respectively. It was assumed that the flexural stiffness is constant. In fact, similar to RC columns an increase in the axial load increases the flexural stiffness of CFT columns. However, when the axial load is higher than 50% of the axial capacity ($\boldsymbol{P_0}$), the flexural stiffness tends to decrease. Thus, to account for this Eq. (2.4b) is modified as follow:

$$(IE)_{eq} = (4P / P_0)(1 - P / P_0)[I_c E_c + I_s E_s] \qquad 0.5P_0 \le P \le P_0 \tag{2.4c}$$

thereby, the effective radius of gyration and critical load can be obtained:

$$r_{eff} = \sqrt{(IE)_{eq} / (AE)_{eq}} \tag{2.5}$$

$$P_{cr} = (\pi / h)^2 (EI)_{eq} \tag{2.6}$$

where $\boldsymbol{h}$ is the effective length of the column. Equation (2.6) showed close agreement with test results.

A simple straight line interaction formula was used by Knowles and Park to estimate the moment-axial load relationship for concrete-filled steel tubular columns (Knowels and Park, 1969).

$$M_u / M_0 + P_u / P_0 = 1 \tag{2.7}$$

in which P_u and M_u are the ultimate axial load and bending moment capacity, P_0 is the ultimate axial load when there is no bending moment and M_0 is the ultimate bending moment when the axial load is zero. Experimental results showed that using Eq. (2.7) is unsafe for slender columns and conservative for short columns (Knowels and Park, 1969). Later, Park and Knowles developed a design equation to determine the ultimate axial load of long CFT columns (Knowels and Park, 1970). In the suggested procedure, the buckling load of a column could be predicted by summing the tangent modulus loads for the steel tube and concrete core acting as independent columns. There was a close agreement between the calculated loads and the test results for columns with a slenderness ratio greater than 44.3. But the ultimate loads for shorter columns were 12% to 42% greater than predicted loads, indicating that an increase in concrete strength due to the confinement by the steel tube did occur. In this procedure the composite action between steel and concrete which increases the flexural stiffness was ignored.

In 1969 a numerical procedure was developed by Neogi and San to study the load-deformation behavior of concrete filled tubes over the elasto-plastic range (Neogi and San, 1969). The following assumptions were made; (1) uniaxial stress-strain curves for

steel and concrete are used with no tensile strength for concrete, (2) stress-strain curves with unloading and reloading characteristics are used, (3) complete interaction takes place between steel and concrete, (4) failure due to local buckling or shear does not occur. Tangent modulus load of composite section had been considered as the critical load for concentrically loaded columns, and can be determined from the following equations:

$$P_{\tan} = \pi^2 / l^2 (E_{Ts} I_s + E_{Tc} I_c) \tag{2.8}$$

$$P_{\tan} = A_s \sigma_s + A_c \sigma_c \tag{2.9}$$

where A_s and A_c are the areas, σ_s and σ_c, are the longitudinal stresses, I_s and I_c moment of inertia and E_{Ts} and E_{Tc} are tangent modules of steel tube and concrete core, respectively. The above equations can be written as:

$$\pi^2 / l^2 (E_{Ts} I_s + E_{Tc} I_c) - (A_s \sigma_s + A_c \sigma_c) = 0 \tag{2.10}$$

and

$$\sigma_s = f(\varepsilon) \tag{2.11}$$

$$\sigma_c = g(\varepsilon) \tag{2.12}$$

where $\boldsymbol{\varepsilon}$ is the longitudinal strain, thus Equation (2.10) can be expressed as:

$$\pi^2 / l^2 (f'(\varepsilon) I_s + g'(\varepsilon) I_c) - (A_s f(\varepsilon) + A_c g(\varepsilon)) = 0 \tag{2.13}$$

An iterative method was used to solve Eq. (2.13). In the case of eccentrically loaded columns the governing equation has the form of:

$$S_x(d^2y/dx^2) + PY = 0 \tag{2.14}$$

since the flexural stiffness S_x is a complicated function of the axial force P and the deformed shape Y, analytical integration of Eq. (2.14) is practically not possible and numerical integration is required. To simplify the numerical procedure, the deflected shape of the column was assumed to be in the form of a trigonometric function, and the cross section was divided into a finite number of fibers. Thus the internal axial force (P_i) and moment (M_i) can be expressed by the equations:

$$P_i = \sum \sigma_{si} A_{si} + \sum \sigma_{ci} A_{ci} \tag{2.15}$$

$$M_i = \sum \sigma_{si} d_i A_{si} + \sum \sigma_{ci} d_i A_{ci} \tag{2.16}$$

where d_i is the distance of fiber i from the neutral axis of the cross section. An iterative method was used to solve the set of equations (2.14 to 2.16). The suggested procedure showed close agreement with the test results for long columns, where no confining effect of steel is expected (Figure 2.16). In the case of short columns the difference between the results was significant. The main deficiency is that a uniaxial stress-strain relation was

used for the concrete and the increase in the ultimate strength of concrete due to confinement was ignored.

San proposed that in circular CFT columns with length-diameter ratio less than five, the axial strength reaches 1.6 times the sum of axial strength of steel tube and concrete core (i.e., $A_s F_y + A_c f_c^{'}$) (Bode, 1976). This increased axial capacity can be expressed by the following equation:

$$P_{inc} = .75 F_y A_s + A_c [f_c^{'} + 3.8 t F_y / (d - t)] \tag{2.17}$$

where d and t are diameter and thickness of steel tube, respectively.

In 1967, Gardner and Jacobson proposed that as the steel tube restrains the concrete core at failure (Gardner and Jacobson, 1967), an internal pressure (σ_r) develops between the steel tube and concrete, creating a tensile hoop stress (σ_t) in the steel tube. Due to this confining effect, the compressive strength of the concrete will be augmented and was found to be:

$$\sigma_c = f_c^{'} + k\sigma_r \quad \text{and} \tag{2.18a}$$

$$\sigma_t = r\sigma_r / t \tag{2.18b}$$

where k is an empirical factor and is determined to be approximately 4 (Gardner and Jacobson, 1967). The axial capacity can be determined using the following equation:

$$P_u = A_c f_c^{'} + A_c k\sigma_t (t/r) + A_s \sigma_{sl} \tag{2.19}$$

To calculate the ultimate load, the magnitude of k, σ_t and σ_{sl} must be determined. However, due to the complex behavior of concrete under triaxial state of stresses, it is difficult to determine σ_t, even by experiment. But if the longitudinal strain of concrete at crushing is determined, the axial compressive stress in the steel tube can also be determined, and a reasonable estimate of the hoop stress can be made using the maximum shear theory:

$$\sigma_t + \sigma_{sl} = \sigma_y \tag{2.20}$$

Test results have shown that Eq. (2.19) underestimates the strength of CFT columns, but the maximum difference between the theoretical and experimental results is less than 20%.

An iterative technique was used by Rangan and Joyce to design slender columns (Rangan, 1991; Rangan and Joyce, 1992). In this procedure it is assumed that the axial capacity (P_u) of a slender eccentrically loaded steel tubular column filled with concrete is reached when the maximum moment M_n is equal to the ultimate bending moment M_u at the mid-height of the column, and failure occurs when the extreme compressive fiber in concrete reaches a limiting value of 0.003. The following formulas can be obtained considering equilibrium at cross sectional level:

$$P_n = C_s + C_c - T \tag{2.21}$$

$$M_n = C_s Z_{sc} + C_c Z_c + T Z_{st} \tag{2.22}$$

where Z_s and Z_c are the moment arms of forces measured from the plastic centered. C_s and C_c are the compressive forces in steel and concrete, respectively. T is the tensile force in the steel tube. The value of $\boldsymbol{P_u}$ is related to $\boldsymbol{M_u}$ by:

$$M_u = P_u(e + \Delta_{cp} + \Delta_u) \tag{2.23}$$

where $\boldsymbol{e}$ is the eccentricity of the axial load, Δ_{cp} and Δ_u are the creep and mid-height deflections of the column, respectively. A uniaxial stress-strain relation (i.e., Hognastad's parabola) for concrete was assumed and the capacity of the columns were obtained by solving Equations 2.21 to 2.23 using an iterative method. The calculated $\boldsymbol{P_u}$ was found to underestimate the experimental results with the maximum difference of 68%.

2.4 Design Codes

Over the course of the last two decades, three different specific codes for the design of concrete filled steel tubular columns have been used in the U. S. Even though some of the design codes have used the same design philosophy and experimental data as their foundations, large discrepancies exist among them.

The Building Code Requirements of Reinforced Concrete (ACI 318-95) traditionally had been the only source for composite column design. According to the ACI 318-89, a composite column is a concrete column reinforced with a structural steel shape or tubing in addition to reinforcing bars. In the absence of reinforcing bars the maximum nominal axial strength can be expressed as:

$$P_0 = 0.85(A_s F_y + 0.85 A_c f_c^{'}) \tag{2.24}$$

It is assumed that all fibers are subjected to 0.3% strain. The load-moment interaction relation can be established using the same rules as ordinary reinforced concrete columns. In order to consider the slenderness effects, an equivalent radius of gyration and flexural stiffness are used:

$$r = \sqrt{((E_c I_g / 5) + E_s I_s) / ((E_c A_g / 5) + E_s A_s)} \tag{2.25}$$

$$EI = (E_c I_g / 5) / (1 + \beta_d) + E_s I_s \tag{2.26}$$

where β_d is the sustained load ratio, and without any sustained load, it should be taken as zero. To prevent local buckling, thickness of the steel tube should be greater than:

$$t \geq b\sqrt{f_y / 3E_s} \qquad \text{for square sections of width } b \tag{2.27}$$

$$t \geq h\sqrt{f_y / 8E_s} \qquad \text{for circular sections of diameter } h \tag{2.28}$$

These limiting values are based on achieving yield stress in a hollow steel tube under monotonic axial loading (Park et al., 1983). Previous research has shown that this requirement is unnecessarily restrictive for CFT columns (Boyd et al., 1995).

The Structural Specification Liaison Committee (SSLC) procedures are based on the allowable stress limit under service load conditions using stress allowances equal to those of the American Institute of Steel Constructions (AISC) specification for steel alone (Furlong, 1983). A pseudo yield stress and stiffness (F_{my} and E_m) are defined to accommodate the composite action and steel tube. The equations for pseudo yield strength and stiffness are derived from superposition of the constituent material strengths and stiffnesses. For concrete filled tubes they can be expressed as:

$$F_{my} = F_y + 0.85(A_c / A_s) f_c^{'} \tag{2.29}$$

$$E_m = E_s + 0.4(A_c / A_s) E_c \tag{2.30}$$

where A_c and A_s are the areas of concrete core and the steel tube, respectively. The radius of gyration is taken as the radius of gyration for steel alone or for concrete alone, whichever is larger. The section modulus is equal to elastic modulus of the steel tube in the absence of any reinforcing bars. Since no iterative calculation are necessary, analysis of strength by the SSLC procedure is considerably easier than ACI procedure. A parabolic beam column relationship is employed instead of the linear relationship of the AISC specifications:

$$(f_a / 0.6F_{my})^2 + f_b / F_b = 1 \qquad \text{strength alone} \qquad (2.31)$$

$$(f_a / 0.6F_{my})^2 + (f_b / F_b)(C_m / (1 - f_a / F_e')) = 1 \qquad \text{including stability} \qquad (2.32)$$

where the C_m, F_a, F_b, f_a and f_b are the end moment coefficients, allowable axial stress, allowable bending stress, computed axial stress and computed bending stress, respectively. The reduced Euler buckling stress (F_e') is equal to $(12/23)(\pi^2 E_m / (kl/r_m)^2)$.

In Manual of Steel Construction, Load and Resistance Factor Design (LRFD-AISC, 1994) the nominal strength is estimated on the basis of ultimate resistance to the load, and reduction factors are then applied. Expressions for nominal cross section strength are very similar to those recommended by the SSLC report and are as follows:

$$P_0 = A_s F_{my} \qquad (\text{thrust capacity}) \qquad (2.33)$$

$$M_n = S_m F_y \qquad (\text{nominal flexural strength}) \qquad (2.34)$$

The nominal axial load capacity is reduced according to the slenderness ratio λ_c. The nominal buckling stress is defined as:

$$\lambda_c = (kl / r_m) / (\pi^2 E_m / F_{my})^{1/2} \qquad (2.35)$$

$$F_{cr} = (1.3 - 0.57\lambda_c) F_{my} \qquad \text{when} \quad \lambda_c \le 1.53 \qquad (2.36)$$

$$F_{cr} = F_{my} / \lambda_c^2 \qquad \text{when} \qquad \lambda_c > 1.53 \tag{2.37}$$

and the nominal axial strength is expressed as:

$$P_n = A_c F_{cr} \tag{2.38}$$

The resistance factor ϕ_c must be applied to the nominal axial strength and a value of 0.75 should be used for filled tubes. A linear function describes the limiting values for P and M for $(0.3 < P_n / P_0 < 1.15)$ and it can be expressed as:

$$P / (1.3P_0) + M / (S_m F_y) = 1 \tag{2.39}$$

When $P_n = 0.3P_0$ a linear interaction function applies such that when $P_n = 0$, the resistance factor for flexural, $\phi_b = 0.9$ applies. The magnitude of the allowable service load can be determined by dividing values of ϕP_n and ϕM_n by the appropriate load factors. Load factors for LRFD are to be taken as 1.2 for dead load and 1.6 for live load, but total strength can not be taken as less than 1.4 of dead load (Furlong, 1968).

In all three design procedures the flexural stiffness is underestimated and the confining effect of the steel tube on the concrete core is ignored. Table (2.5) shows the differences between the results obtained using the three different design procedures (as discussed) to analyze a square CFT column. It must be emphasized that these capacities are nominal capacities (i.e., reduction factors are not applied). The column has a cross

section of 250x250 mm and it is 173 cm long with a wall thickness of 8 mm. The steel tube had a yield strength of 373 MPa and the ultimate strength of the concrete was 38 MPa (Sugano and Nagashima, 1992). The disagreement between the results shown in Table (2.5) indicates that research is needed to provide more accurate design guidelines. It should be noted that only this single case is compared because the intention is to highlight the inaccuracy of current design codes not comparison over a wide range of loadings. This example was chosen because experimental results (Sugano and Nagashima, 1992) were available.

2.5 Summary

The earlier analytical works generally have focused on applying the classical theory of mechanics with employing the uniaxial concrete stress-strain relationship to CFT columns. However, due to the complex stress-strain properties of the concrete core and puzzling interaction between the concrete core and the steel tube interface, these approaches have not been successful. Although, the different design guide lines have been developed based on the experimental date, the CFT columns have been treated as ordinary RC or steel columns. Hence, the load carrying capacity of CFTs is underestimated. Moreover, the large discrepancies among the design specifications indicates a need for accurate design guide lines. The experimental works have provided significant information which can be used to develop accurate analytical models. Through a detailed study using the developed analytical model, the response of CFTs to

axial and combined loadings can be entirely understood. As a result, a new design method can be developed which will accurately predict the capacity of CFT columns.

CHAPTER 3

FINITE ELEMENT MODELING

3.1 General

In recent years the finite element technique has become a powerful tool for analyzing structures. There are two major reasons for application of finite element models to concrete structures specially CFT columns. First, although experiments have played significant role in research on CFT columns, they are expensive and time consuming. Extensive data are needed to understand the behavior of CFT columns. Tests covering various aspect ratios, different type of loadings and various cross-sectional shapes are needed for a detailed study on CFT columns. A parametric study using finite element models is affordable and allows the study of virtually limitless combinations of the parameters of interest. In addition, tests can not provide as much insight into the complicated pattern of stress distribution revealed by numerical simulations. Finite element analysis provides supplementary information to the experiments. Therefore, a detail analysis of CFTs using finite element analysis is a useful approach as long as the analytical model is calibrated with experimental results.

In order to analyze the nonlinear response of CFT columns a practical and reliable finite element model needs to be developed. The use of appropriate finite element software has significant role in performance of the analytical model. Such a model should be able to simulate important characteristics of CFTs such as confinement of concrete core and local buckling of steel tube. General purpose finite element program "ABAQUS" is used in the present study. This program is capable of modeling non-linear

material behavior, large deformation and contact analysis which are required in finite element simulation of CFT columns.

3.2 Finite Element Modeling

The concrete core is modeled with twenty-node, three-dimensional reduced integration quadratic solid elements with hourglass control. The advantages of reduced integration elements are that the strains and stresses are calculated at the locations that provide optimal accuracy, the so-called Barlow points (Barlow, 1976). Even though in materially nonlinear analysis high order integration analysis is more effective at capturing more accurate behavior of the material (Saadeghvaziri, 1988), the reduced number of integration points decreases CPU time and storage requirements. The reduced integration scheme is based on the uniform strain distribution. In this procedure, the number of integration points is sufficient to exactly integrate the contributions of the strain field that are one order less than the order of interpolation. This method first publish by Flanegan and Belytschko (1981), ensures that the reduced integration elements passes the patch test. The uniform strain method yields the exact average strain over the element volume. Using an average strain is significant when the constitutive model is non-linear, since the strains passed into the constitutive routines are a better representation of the actual strain.

Steel tube is modeled with isoparametric shell elements. The formulation of shell elements allows large displacement analysis, which is used to investigate the possibility of local buckling. Gap element is used to model the interaction between concrete core and steel tube interface. Gap contact elements are special purpose contact elements

which allow for contact between two nodes. Gap contact elements placed between nodes allow for the nodes to be in contact or separated with respect to particular directions and separation conditions. For this particular problem gap elements are placed between adjacent nodes of steel tube and concrete core with a fixed contact direction perpendicular to surface of the steel tube. In the case of circular columns, the contact direction is in the radial direction. The initial separation distance is specified as zero, in which case the gap is initially closed (i.e. the concrete and steel tube are initially in contact with each other). The opening of the gap element is determined by comparing the relative displacements of the nodes in the contact direction, **n**. Thus, the gap opening, h, can be expressed as;

$$h = \mathbf{n} \cdot (\mathbf{u}^2 - \mathbf{u}^1) \tag{3.1}$$

where $\mathbf{u}^1$ and $\mathbf{u}^2$ are the total displacements at the first and the second node of the gap element.

Due to symmetry of geometry and loading conditions, only one half of the square columns and one quarter of the circular columns were modeled. In Figures 3.1 and 3.2, the finite element meshes are shown for circular and square columns.

3.3 Material Models

3.3.1 Steel Plasticity Model

The classical plasticity model for steel is standard von Mises model failure surface with associated plastic rule. The yield surface assumes that the yield of metal is independent

of the equivalent pressure stress. This assumption is experimentally confirmed for metals under compressive stress. Associated plastic flow means that, as the material is yielding, the inelastic deformation rate is in the direction of the normal to the yield surface. The von Mises yield surface is used for initially isotropic metals. It is defined by giving the value of uniaxial yield stress as function of uniaxial equivalent plastic strain and temperature. The work hardening defines the way the yield surface changes with plastic straining. Three assumptions can be used in order to model the hardening of metals: perfect plasticity, isotropic hardening, and kinematic hardening. Perfect plasticity means that the yield surface does not change with plastic strain. In isotropic hardening the yield surface changes size uniformly in all directions, so the yield stress increases or decreases in all stress directions as plastic straining occurs. This hardening model is useful for cases involving gross plastic straining, or in which the straining at each point is essentially in the same direction in strain space throughout the analysis. In kinematic hardening the yield surface stays the same size in the stress space. The von Mises elastic-plastic model with kinematic hardening is used for the steel tube. Figure 3.3 shows a typical input for steel in ABAQUS and Figure 3.4 represent the von Mises yield surface in principal stress space

3.3.2 Concrete Material Model

The concrete core in CFT columns has a very complex material behavior: non-linear stress-strain behavior in a triaxial state of stress with confining pressure changes. Due to this complexity, selection of a proper constitutive model describing the concrete behavior

under confining condition is a challenging task for developing an accurate finite element model. In this section a comparison between different concrete material models is made. The outlines of fracture energy-based plasticity model (Pramono and William, 1989) are introduced and the extension of the model to three dimensional state of stress is discussed. This model is calibrated for concrete with different compressive strength using experimental data.

Material models developed for finite element analysis of concrete structures can be categorized in three groups: (1) elasticity-based, (2) plasticity-based , and (3) fracture energy-based plasticity models. In the following sections, a brief review of these three groups is presented.

3.3.3 Elasticity-Based Models

Isotropic Linear Elastic Model: Isotropic linear elasticity approximates the behavior of concrete under tensile-type loading well. Before the peak stress the stress-strain relation is almost linear in such a loading environment. This model can also represent the behavior of concrete under small compressive loading, but the model is unacceptable as the applied compressive loads increases. Non-linear elastic model improves this drawback significantly.

Cauchy Elastic Model: The simplest way of introducing nonlinearity is to employ a non-linear function to define the stress-strain relationship of concrete. For unconfined compressive behavior of concrete many models in the form of Eq. (3.2) have been proposed (Saenz, 1964; Popovics 1973; Carrenia and Chu 1985; Tasi 1988 among

others). When extended to multiaxial state of stress, Cauchy model can be expressed as Eq. (3.3). This equation often takes the form of representing secant stiffnesses (D^{δ}_{ijkl}), which are functions of stress state (Eq. 3.4).

$$\sigma = f(\varepsilon) \tag{3.2}$$

$$\sigma = F_{ij}(\varepsilon_{ij}) \tag{3.3}$$

$$\sigma = D^{\delta}_{ijkl}\,(\sigma_{pq})\,\varepsilon_{kl} \tag{3.4}$$

This type of model with arbitrarily introduced nonlinear functions may generate energy under a certain loading-unloading cycle (Chen, 1982). Such behavior is physically inadmissible since it violates the laws of thermodynamics.

Hyperelastic (Green Elastic) Model: This model is based on the postulate of the existence of a strain energy function Φ or a complementary energy density function Ω. The stress-strain relationship is defined by:

$$\sigma_{ij} = \frac{\partial \Phi}{\partial \varepsilon_{ij}} \quad \text{or} \quad \varepsilon_{ij} = \frac{\partial \Omega}{\partial \sigma_{ij}} \tag{3.5}$$

This ensures no energy can be generated through any load cycle, and thermodynamic laws are always satisfied. Based on assumed polynomial expansions of the function Ω in terms of the three stress invariants, a third order stress-strain relationship has been developed (Evans and Pister; 1966). The material constants of this class of model do not

have physical interpretation in general, so that it is not easy to quantify the values of those constants experimentally. Although it can model many characteristics of concrete such as nonlinearity, dilatation, and stress-induced anisotropy, this class of formulation is not popular for modeling the behavior of concrete.

Hyperelastic models provide a one-to-one relationship between the current state of total stress and that of total strain. Thus, these material models are independent of deformation path in the sense the stresses are uniquely determined from the current state of stress or vice versa. Therefore, these models have an inherent limitation in applications, since loading-path dependence of deformation state of concrete is well recognized. Hypoelastic models over come this drawback of hyperelastic models.

Hypoelastic Model: in hypoelastic model the material behavior is described in terms of the increments of stress and strain. Thus, the stress-strain relationship can be expressed using tangent stiffness which varies with current stress state. Therefore, this class of model is dependent on deformation history. The general form of a hypoelastic material can be expressed as follows:

$$d\sigma_{ij} = D^{t}_{ijkl}(\sigma_{pq}, \varepsilon_{rs})\, d\varepsilon_{kl} \tag{3.6}$$

where D^{t}_{ijlk} is the tangent stiffness. The hypoelastic type of formulation encounters an inherent difficulty in the construction of the constitutive relationships. In the highly non-linear range near peak stress, concrete becomes anisotropic, even if the initial behavior is isotropic. This anisotropy implies that the behavior in the principal direction is different from each other and the principal axes of stress and strain are not coincident, introducing

coupling between normal and shear quantities. This phenomenon is the so-called dilatancy behavior, i.e. volumetric expansion under shear load. This indicates that twenty one material moduli need to be defined, but it is not a practical approach since formulation becomes too complicated. Hence, hypoelastic models are appropriate for moderate nonlinear problems.

To summarize, elasticity-based models are rather simple and reasonably good for moderate non-linear problems. However, these models are not suitable when the general behavior of concrete needs to be modeled. In this case, plasticity-based models appear to be more effective and attractive.

3.3.4 Plasticity-Based Models

There are three basic assumptions used in the development of classical theory of plasticity: an initial yield surface, a hardening rule, and a flow rule. An initial yield surface in stress space defines a stress level at which plastic deformation begins. A hardening rule regulates the evolution of subsequent loading surfaces during the course of plastic flow. A flow rule defines an incremental plastic stress-strain relationship using a plastic potential function. The formulation of plasticity theory can be expressed by the following incremental stress-strain relationship (Chen and Han, 1988).

$$d\sigma_{ij} = D^{ep}_{ijkl}\, d\varepsilon_{kl} \tag{3.7}$$

where

$$D^{ep}_{ijkl} = D^{e}_{ijlk} - \frac{\dfrac{\partial f}{\partial \sigma_{mn}} D^{e}_{mnkl} D^{e}_{ijst} \dfrac{\partial g}{\partial \sigma_{st}}}{h + \dfrac{\partial f}{\partial \sigma_{pq}} D^{e}_{pquv} \dfrac{\partial g}{\partial \sigma_{uv}}} \tag{3.8}$$

in which D^{e}_{ijkl} and D^{ep}_{ijkl} are elastic and elastic-plastic material tensors, f is a loading function (surface), g is a potential function and h is a scalar function related to the hardening rule associated with a particular material. For an associate flow rule, f is equal to g while f≠g is assumed for a non-associated flow rule. This implies that symmetry of D^{ep}_{ijkl} is violated in the case of non-associated flow rule.

It is well known that plasticity theory was originally developed for metals. Consequently, its application for concrete requires considerable modification on the shape of yield surface, hardening rule, and flow rule. Isotropic hardening plasticity model is the best-known earliest plasticity-based model (Chen and Chen, 1975). In this model two similar functions are utilized to define the yield surface in tension and tension-compression region. Due to this similarity, the initial yield surface is open toward the hydrostatically compressive direction. It is experimentally observed that pure hydrostatic loading can not cause failure (Chinn and Zimmerman, 1965), which justifies an open-end failure surface. In this model a linear elastic is employed to define the stress path in pre-peak region. However, it is unrealistic for material like concrete to exhibit a linear elastic response along the stress path even under large magnitude of loads. In fact, experimental results indicate a closed elastic limit (Launay and Gachon, 1971). This observation is one of the drawbacks of Chen-Chen model.

In nonuniform hardening plasticity modeling a closed initial yield surface is employed (Han and Chen, 1985) which encloses all the loading surfaces. During hardening , the loading surface expands and changes its shape from the initial yield surface to the final shape that matches with the failure surface. The associated flow rule is used in the development of the model which overestimates the volumetric strain. In order to overcome this shortcoming, the non-associated flow rule is utilized to control the volumetric strain. However, the model does not include strain-softening which is an important feature of concrete stress-strain relationship. It appears that the plasticity concept by itself is insufficient for describing the concrete behavior.

3.3.5 Fracture Energy-Based Plasticity Model

Unlike metal, fracture occurs at early stage of deformation in concrete. In order to capture all aspects of concrete behavior, the concept of fracture mechanics is implemented into the constitutive models (Maekawa and Okamura, 1983). The Maekawa-Okamura model assumes that concrete is composed of constituent elements located in parallel surfaces and the overall response of concrete is the sum of these elements' stresses. Each element behaves as a strain-hardening material and it does not sustain stress as it reaches its fracture strength. The model describes the concrete behavior under two-dimensional loading condition and it has the following features: (1) in low deformation range the level of element stress is low and stress-strain relationship is linear; (2) the stress-strain relationship in hardening regime is described as:

$$\sigma_e = E_0 \varepsilon_e \tag{3.9}$$

$$\sigma = K E_0 \varepsilon_e \tag{3.10}$$

$$\varepsilon_e = \varepsilon - \varepsilon_p \tag{3.11}$$

where σ and σ_e are microscopic stress and element stress, ε, ε_e, and ε_p are total, elastic and plastic strain, respectively. E_0 is elastic stiffness and K is a fracture parameter. KE_0 represents the unloading stiffness so the degradation of unloading stiffness is modeled systematically; (3) at certain stage of loading (i.e. peak load) the increase in the element stress is canceled out by the reduction of stress due to fracture of elements. The application of the model is limited since the model is based on two-dimensional loading conditions.

Bazant and Kim (1979) combined the incremental plasticity and linear fracture theory to obtain a nonlinear triaxial constitutive relation for concrete. In this model, plastic deformation is defined by the flow theory of plasticity and the stiffness degradation is modeled by the fracture theory of Dougill. In this approach, there are some difficulties in the definition of loading criterion, since it involves two loading surfaces: one is the yield surface specified in stress space and the other is the fracturing surface specified in strain space.

Among the proposed fracture-based plasticity models, Pramano-William's model has the ability to fit the triaxial compression tests more accurately. This feature of the model is a very important aspect in analysis of CFT columns where confinement plays a significant role. The model is developed to capture the triaxial behavior of plain

concrete. The formulation covers the full load-response spectrum in tension as well as in compression. The constitutive model is based on the non-associated flow theory with hardening in prepeak regime and fracture energy based softening in the post-peak regime. The Pramano-William's model forms the basis of model used in this study and is discussed in the next section.

3.4 Pramono-William's Fracture-Energy Based Plasticity Model

The model assumes that the concrete behaves elastically as long as the stress state lies within an initial yield surface. When loading progresses beyond the initial yield surface, plastic flow occurs and the yield surface hardens isotropically up to a failure surface. In this range the plastic strain rate is governed by a plastic potential different from the yield surface, thus the hardening rule is non-associated. This gives the model an added flexibility and allows a better fit of concrete behavior.

As the plastic flow continues beyond the limit necessary to reach the failure surface, the material behavior becomes isotropic softening. At this stage, the failure surface degrades to a residual surface, and the flow is now refined to satisfy the energy of fracture. In the following sections the various concepts describes above are presented. This presentation is largely based on the work done by Pramono and William (1989), and Xie et al. (1994).

3.4.1 Leon's Triaxial Strength Failure Criterion

This strength formulation combines the two-parameter Mohr-Coulomb friction law and the one-parameter tension cut-off condition of Rankine. The isotropic failure criterion is expressed in terms of the major and minor principal stresses:

$$F(\bar{\sigma}^*) = f(\sigma_1, \sigma_3) = (\frac{\sigma_1 - \sigma_3}{f_c'})^2 + m_0 \frac{\sigma_1}{f_c'} - c_0 = 0 \qquad (3.12)$$

where $\bar{\sigma}^*$ is the principal stress vector, σ_1 and σ_3 are principal stresses with tension being positive. The effect of intermediate principal stress is omitted similar to Tresca and Coulomb conditions of maximum shear. The triaxial failure condition is characterized by the uniaxial compressive strength f_c', the frictional parameter m_0 and the cohesion c_0 which has the value of 1.0 at failure. The frictional parameter m_0 is determined by substituting a uniaxial tension state in Eq. 3.12 (i.e. $\sigma_1 = f_t'$, $\sigma_3 = 0$).

$$m_0 = \frac{f_c'^2 - f_t'^2}{f_c' f_t'} \qquad (3.13)$$

in which f_t' is the tensile strength. The triaxial failure of Leon is presented in Figure 3.5 in a principal stress sectional view.

The performance of the Leon criterion is illustrated in Figures 3.6, in which $R_d = \sqrt{2J_2}$ is the deviatoric length and $R_h = I_1 / \sqrt{3}$ is the hydrostatic length. I_1 and J_2 are the first and the second stress variants, respectively. The Leons' compressive and

tensile meridians show good agreement with experimental data (Richart, 1928; Mills; 1970, Launay, 1970; and Xie, 1994).

3.4.2 Isotropic Hardening for Pre-Peak Behavior

The Pramono-William model uses the Leon triaxial concrete strength criterion. The main reason for adopting the Leon model is its simplicity. It combines the basic features of the Mohr-Coulomb criterion with those of tension cut-off condition within a single mathematical description.

In order to account for cap action near the hydrostat the Leon model is extended in such a way that the elastic limit is bounded by a closed surface in the compression that expands isotropically with increasing plastic deformations until the failure surface is reached. The position of loading surface is expressed in terms of hardening parameter $0 \le k \le 1$ as:

$$F(\sigma_1,\sigma_3,k) = \left[(1-k)\frac{\sigma_1^2}{f_c'^2} + \frac{\sigma_1 - \sigma_3}{f_c'} \right]^2 + k^2 m_0 \frac{\sigma_1}{f_c'} - k^2 c_0 = 0 \qquad (3.14)$$

In this case the initial loading surface grows in a self-similar fashion when the hardening parameter increases monotonically from its initial value $k = k_0 > 0$ to the final value at peak $k = k_p = 1$. Different loading stages in a meridian plane are shown in Figure 3.7 for concrete with compressive strength of 9.0 Ksi.

The constitutive model assumes that the material is initially isotropic and remains isotropic during the entire deformation history irrespective of the orientation and magnitude of principal stresses. Therefore, the inherent anisotropy as well as induced anisotropy are neglected. The strain rate is decomposed into independent elastic and plastic components (Eq. 3.15) and the elastic response is governed by the linear operator $\boldsymbol{E}$ (Eq. 3.16).

$$\Delta\bar{\varepsilon} = \Delta\bar{\varepsilon}_e + \Delta\bar{\varepsilon}_p \tag{3.15}$$

$$\bar{\sigma} = \boldsymbol{E}\Delta\bar{\varepsilon}_e \tag{3.16}$$

3.4.3 Non-Linear Hardening Response

The strain hardening theory describes the current state of inelastic deformation process in terms of a scalar-valued kinematic variable ε_p defining the length of plastic strain trajectory. The effect of confinement on the rate of hardening is introduced in terms of the ductility measure x_p, which defines the accumulated plastic strain at peak. Thus, the hardening parameter is expressed as a monotonically increasing elliptic function of plastic strain:

$$\boldsymbol{k} = \boldsymbol{k}_0 + \frac{1-\boldsymbol{k}_0}{\varepsilon_p}\sqrt{2\varepsilon_p x_p - \varepsilon_p^2} \tag{3.17a}$$

The equivalent plastic strain increment is defined as a Euclidean norm of the plastic strain increment:

$$\Delta\varepsilon_p = \sqrt{\Delta\bar{\varepsilon}_p^T \cdot \Delta\bar{\varepsilon}_p} \tag{317b}$$

in which $\Delta\bar{\varepsilon}_p$ is the vector of principal plastic strain increments. The ductility measure x_p introduces the effect of confining pressure on the rate of hardening and it is expressed as a quadratic polynomial:

$$x_p = A_h\left(\frac{\sigma_1}{f_c'}\right)^2 + \frac{B_h\sigma_1}{f_c' + C_h} \tag{3.18}$$

where σ_1 is the major principal stress. Ductility parameters A_h, B_h, and C_h are dimensionless parameters which are determined from experimental results at three different confinement levels such as the direct tension test (i.e. no confining pressure), and a low as well as a high confined compression test.

3.4.4 Non-Associated Flow Rule

The inelastic dilatancy is controlled by the hydrostatic component of the plastic strain increments. In the case of pressure-sensitive flow the volumetric plastic stress is not coaxial with plastic strain increment because of the Poisson effect. This phenomenon of pressure- sensitive loading surface is illustrated in Figure 3.8.

The flow rule has significant effect on the performance of constitutive model and its triaxial response. In the case of associated flow rule, it assumes that the loading surface and the potential function are equal. Therefore, the plastic stress and strain increments are coaxial, which yields to an over estimation of volumetric changes. In the Pramono-William model a non-associated flow rule is adopted which defines the plastic strain rate as:

$$\Delta\bar{\varepsilon}_p = (\Delta\lambda)\,\bar{m} \quad \text{where} \quad \bar{m} = \frac{\partial Q}{\partial \bar{\sigma}^*} \tag{3.19}$$

The plastic multiplier $\Delta\lambda$ controls the magnitude while the gradient $\bar{m}$ controls the direction of the plastic strain increments. The plastic potential function Q for non-associated flow is based on a modification of the loading surface:

$$Q(\sigma_1,\sigma_3,k,m_Q) = \left[(1-k)\frac{\sigma_1^2}{f_c'^2} + \frac{\sigma_1-\sigma_3}{f_c'}\right]^2 + k^2 m_Q \frac{1}{f_c'} - k^2 c_0 = 0 \tag{3.20}$$

with the friction parameter $m \rightarrow m_Q$ being redefine in terms of the major principal stress as:

$$\frac{\partial m_Q}{\partial \sigma_1} = D\exp E\left(\frac{f_t' - \sigma_1}{f_c'}\right) + F \tag{3.21}$$

The material parameters D, E and F are determined from three sets of experiments at different confining levels. The gradient of the plastic potential in Eq. 3.20 is evaluated as:

$$\bar{\boldsymbol{m}} = \frac{\partial \boldsymbol{Q}}{\partial \bar{\sigma}^*} = \frac{\partial \boldsymbol{Q}}{\partial \sigma_1}\frac{\partial \sigma_1}{\partial \bar{\sigma}^*} + \frac{\partial \boldsymbol{Q}}{\partial \sigma_2}\frac{\partial \sigma_2}{\partial \bar{\sigma}^*} + \frac{\partial \boldsymbol{Q}}{\partial \sigma_3}\frac{\partial \sigma_3}{\partial \bar{\sigma}^*} \tag{3.22}$$

where

$$\begin{Bmatrix} \dfrac{\partial \boldsymbol{Q}}{\partial \sigma_1} \\ \dfrac{\partial \boldsymbol{Q}}{\partial \sigma_2} \\ \dfrac{\partial \boldsymbol{Q}}{\partial \sigma_3} \end{Bmatrix} = \frac{1}{\boldsymbol{f}_c'} \begin{Bmatrix} \boldsymbol{s}_h\{2(1-\boldsymbol{k})\sigma_1 + 1\} + \boldsymbol{k}^2 \dfrac{\partial \boldsymbol{m}_Q}{\partial \sigma_1} \\ 0 \\ -\boldsymbol{s}_h \end{Bmatrix} \quad \text{where} \tag{3.23}$$

$$\boldsymbol{s}_h = 2\left[(1-\boldsymbol{k})\frac{\sigma_1^2}{\boldsymbol{f}_c'^2} + \frac{\sigma_1 - \sigma_3}{\boldsymbol{f}_c'}\right] \tag{3.24}$$

Similar to Coulomb condition, there is no inelastic component in the direction of the intermediate principal stress. Moreover, only the major principal stress component is needed in Eq. (3.21) because of the gradient operation for $\bar{\boldsymbol{m}}$. The explicit form of the plastic multiplier in Eq. (3.19) is determined by the differential consistency condition $\Delta \boldsymbol{F}_n = 0$:

$$\Delta\lambda = \frac{\Delta \boldsymbol{L}_p}{\boldsymbol{E}_p + \boldsymbol{E}_n} \qquad \text{where} \tag{3.25}$$

$$E_n = \bar{n}\bar{E}\bar{m} \tag{3.26}$$

$$E_p = \frac{\partial F}{\partial k}\Delta k \tag{3.27}$$

In sum, the differential flow rule in Eq. (3.19) defines the evolution of plastic deformations in terms of the prescribed strain rate as:

$$\bar{\varepsilon}_p = \frac{\bar{m}\bar{n}^T}{E_p + E_n}\bar{E}\bar{\varepsilon} \tag{3.28}$$

3.4.5 Isotropic Softening for Post-Peak Behavior

There exists a critical difference between concrete behaviors before and after peak stress. Under the tensile type of loading , this fact has been well recognized. For instance, the experimental results (Gopalaratnam and Shah, 1985) have clearly revealed the localized deformation after peak stress, presenting a striking contrast to homogenous deformation before peak stress. Namely, in the post peak regime most deformation is found to be related to the expansion of the crack while it is unloading. On the other hand, the softening response in compressive loading is not well understood. The localized deformation under compression has been recognized and accepted recently (Read and Hegemier, 1984; Chen, 1985).

The pre-peak behavior of concrete is associated with the extension of bond cracks (cracks around aggregates) while the extensive development of mortar cracks is observed in post-peak regime. With the advancement of non-linear fracture mechanics concepts,

concrete behavior under tensile loading has been studied extensively. The field of fracture mechanics has been focusing on crack processes for years. However, these concepts have not been widely accepted because of questions related to diffuse fracture in matrix-aggregate composite. Moreover, the smeared analysis tools is more reliable, in which microscopic as well as macroscopic discontinuities in the form of discrete cracks are distributed and represented by equivalent continuum concepts. In view of need for models which account for strength degradation in a rational manner, Pramono-William model uses a smeared description. In this model the fracture energy-based strain softening flow is formulated in terms of fracture mode and is extended to compressive splitting and shear faulting. The description of the strength degradation is presented in the following section.

3.4.6 Degradation of Triaxial Strength

The principal issue of the fracture energy-based strain-softening formulation revolves around the definition of strain-softening modulus E_f. The differential consistency condition $\Delta F = 0$ yields an explicit form of the tangential modulus. Therefore, the selection of a rational expression for residual strength envelop *(F)* in post-peak regime is essential. In the case of softening behavior in tension and shear, the uniaxial tensile and compressive strength is reduced to zero at residual level and only frictional resistance can be mobilized due to granular action. Thus, the Eq. 3.12 degenerates to:

$$F_r(\sigma_1, \sigma_3) = \left(\frac{\sigma_1 - \sigma_3}{f_c'}\right) + m_r \frac{\sigma_1}{f_c'} = 0 \tag{3.29}$$

in which the cohesion factor is zero and m_r is the residual friction factor. The overall softening mechanism is described by degradation of tensile strength σ_t as:

$$c_s = \frac{\sigma_t}{f_t'} \quad \text{and} \quad m_s = m_r - (m_r - m_0)c_0 \tag{3.30}$$

such that $c_0 = 1$ when $m = m_0$ and $c_r = 0$ when $m = m_r$. Thus, the intermediate softening stage is defined by the modification of Eq. 3.12 as follows:

$$F_s(\sigma_1, \sigma_3) = \left(\frac{\sigma_1 - \sigma_3}{f_c'}\right) + m_s \frac{\sigma_1}{f_c'} - c_s = 0 \tag{3.31}$$

In fracture mechanics the degradation of tensile strength is related to the crack-mouth opening u_f rather than the tensile strain. In Pramono-William model an exponential expression based on experimental results (Hurlbut, 1985) is used to described the degradation of tensile strength as:

$$\sigma_t = f_t' \exp\left(-5\frac{u_f}{u_r}\right) \tag{3.32}$$

in which u_r is the rapture displacement. Consequently, the fracture energy released rate is expressed as:

$$G_f = \int_0^{u_f} \sigma_t du_f \tag{3.33}$$

Beyond peak, the fracture rule defines direction and magnitude of the inelastic fracture strain in the equivalent elastic-plastic continuum as:

$$\Delta\bar{\varepsilon}_f = \Delta\lambda\,\bar{m} \quad \text{where} \tag{3.34}$$

$$\bar{m} = \frac{\partial Q}{\partial \bar{\sigma}} = \begin{Bmatrix} \frac{\partial Q}{\partial \sigma_1} \\ \frac{\partial Q}{\partial \sigma_2} \\ \frac{\partial Q}{\partial \sigma_3} \end{Bmatrix} = \begin{Bmatrix} \frac{m_q}{f_c'} + 2(\sigma_1 - \sigma_3)_q \\ 0 \\ 2(\sigma_1 - \sigma_3) \end{Bmatrix} \tag{3.35}$$

In the case of direct tension, since only the strain increment in major stress direction is used, the incremental crack-mouth opening is expressed in terms of tensile crack spacing h_t (Eq. 3.36). For the cases other than direct tension, an equivalent crack-mouth opening in terms of equivalent crack spacing h_c is introduced (Eq. 3.37).

$$\Delta u_f = h_t \Delta\varepsilon_f \tag{3.36}$$

$$\Delta u_f = h_c \Delta \varepsilon_f \tag{3.37}$$

The crack spacing is an important concept in the stain softening analysis of concrete. In Pramono-William model, the equivalent crack spacing is expressed as a function of the major principal stress:

$$\frac{h_t}{h_c} = A_s\left(\frac{\sigma_1 - f_t'}{f_c'}\right)^4 + B_s\left(\frac{\sigma_1 - f_t'}{f_c'}\right)^2 + 1 \tag{3.38}$$

where the softening parameters A_s and B_s are determined from low and high confined compression test. However, the proposed expression is not successful in modeling unconfined concrete and concrete with low confining pressure. The fracture energy of concrete in compression is overestimated and the model is unrealistically stiff. In order to overcome this problem, a new expression for h_c was suggested (Xie et al., 1994). In this expression, the definition of h_c is different depending on whether the major principal stress is compressive or tensile:

$$\frac{h_t}{h_c} = A_s\sqrt{\left(1 + B_s\frac{\sigma_1}{f_c'}\right)} \qquad \text{when} \qquad \sigma_1 < 0 \tag{3.39}$$

$$\frac{h_t}{h_c} = 1 - \left(1 - A_s\right)\left(1 - \frac{\sigma_1}{f_t'}\right)^2 \qquad \text{when} \qquad \sigma_1 \geq 0 \tag{3.40}$$

3.4.7 Extension of the Model to Three Dimensional Loading Case

As shown in the previous sections, the loading surface and the potential function are both expressed in terms of principal stress components σ_1 and σ_3. In both expressions, the effect of intermediate principal stress is ignored. In order to extend a two-dimensional plasticity model to a three-dimensional one, a transformation matrix is required for mapping the stress tensor into principal stress vector. The differentiation of loading and potential surfaces against principal stress vector can be multiply by the transformation matrix in order to obtain the differentiation against the general stress tensor. This transformation can be expressed as follows:

$$\frac{\partial F}{\partial \{\bar{\sigma}\}} = \frac{\partial F}{\partial \bar{\sigma}^*} \frac{\partial \bar{\sigma}^*}{\partial \{\bar{\sigma}\}} \tag{3.41}$$

in which $\bar{\sigma}$ and $\bar{\sigma}^*$ are general stress tensor and principal stress vector, respectively. Here $\frac{\partial \bar{\sigma}^*}{\partial \{\bar{\sigma}\}}$ is transformation matrix which was introduced by Xie et al. 1994. The principal stress vector and the general stress array $\{\bar{\sigma}\}$ are defined as:

$$\{\bar{\sigma}\} = \left\langle \sigma_x, \sigma_y, \sigma_z, \tau_{xy}, \tau_{yz}, \tau_{zx} \right\rangle^T \tag{3.42}$$

$$\bar{\sigma}^* = \begin{Bmatrix} \sigma_1 \\ \sigma_2 \\ \sigma_3 \end{Bmatrix} = \frac{2\sqrt{J_2}}{\sqrt{3}} \begin{Bmatrix} \sin(\theta + 2\pi/3) \\ \sin\theta \\ \sin(\theta - 2\pi/3) \end{Bmatrix} + \frac{I_1}{3} \begin{Bmatrix} 1 \\ 1 \\ 1 \end{Bmatrix} \tag{3.43}$$

in which θ is called the angel of similarity and defined as:

$$\theta = \frac{1}{3}\sin^{-1}\left[-\frac{3\sqrt{3}J_3}{2\,(J_2)^{3/2}}\right] \quad \text{with} \quad (-\pi/6 < \theta < \pi/6) \tag{3.44}$$

where I_1, J_2, and J_3 are the three stress invariants and expressed as:

$$I_1 = \sigma_x + \sigma_y + \sigma_Z \tag{3.45a}$$

$$J_2 = \frac{1}{2}\left[\sigma_x^{'2} + \sigma_y^{'2} + \sigma_z^{'3}\right] + \tau_{xy}^2 + \tau_{yz}^2 + \tau_{zx}^2 \tag{3.45b}$$

$$J_3 = \sigma_x^{'}\sigma_y^{'}\sigma_z^{'} - \sigma_x^{'}\tau_{yz}^2 - \sigma_y^{'}\tau_{zx}^2 - \sigma_z^{'}\tau_{xy}^2 + 2\tau_{xy}\tau_{yz}\tau_{zx} \tag{3.45c}$$

where $\sigma_x^{'}$, $\sigma_y^{'}$, and $\sigma_z^{'}$ are stress deviators and defined as:

$$\sigma_n^{'} = \sigma_n - \frac{I_1}{3} \quad \text{where} \quad n = x,\ y,\ \text{and}\ z \tag{3.46}$$

A stress invariant vector $\bar{J} = < I_1, \sqrt{J_2}, J_3 >$ is defined for simplicity. Since $\bar{\sigma}^*$ and $\bar{J}$ are uniquely invariable, it can be shown that:

$$\frac{\partial \bar{\sigma}^*}{\partial\{\sigma\}} = \frac{\partial \bar{\sigma}^*}{\partial I_1}\frac{\partial I_1}{\partial\{\sigma\}} + \frac{\partial \bar{\sigma}^*}{\partial \sqrt{J_2}}\frac{\partial \sqrt{J_2}}{\partial\{\sigma\}} + \frac{\partial \bar{\sigma}^*}{\partial J_3}\frac{\partial J_3}{\partial\{\sigma\}} \tag{3.47}$$

in which

$$\frac{\partial \bar{\sigma}^*}{\partial I_1} = \left\langle \frac{1}{3}, \frac{1}{3}, \frac{1}{3} \right\rangle^T \tag{3.48a}$$

$$\frac{\partial \bar{\sigma}^*}{\partial \sqrt{J_2}} = \left\langle -\frac{2\sin(2\theta - 2\pi/3)}{\sqrt{3}\cos(3\theta)}, -\frac{2\sin(2\theta)}{\sqrt{3}\cos(3\theta)}, -\frac{2\sin(2\theta + 2\pi/3)}{\sqrt{3}\cos(3\theta)} \right\rangle^T \tag{3.48b}$$

$$\frac{\partial \bar{\sigma}^*}{\partial J_3} = \left\langle -\frac{\cos(\theta + 2\pi/3)}{J_2\cos(3\theta)}, -\frac{\cos(\theta)}{J_2\cos(3\theta)}, -\frac{\cos(2\theta - 2\pi/3)}{J_2\cos(3\theta)} \right\rangle^T \tag{3.48c}$$

$$\frac{\partial I_1}{\partial\{\sigma\}} = \langle 1,\ 1\ ,1,\ 0,\ 0,\ 0 \rangle \tag{3.49a}$$

$$\frac{\partial \sqrt{J_2}}{\partial\{\sigma\}} = \frac{1}{2\sqrt{J_2}} \left\langle \sigma_x^{'},\ \sigma_y^{'},\ \sigma_z^{'},\ 2\tau_{xy},\ 2\tau_{xz},\ 2\tau_{yz} \right\rangle \tag{3.49b}$$

$$\begin{aligned} \frac{\partial J_3}{\partial\{\sigma\}} = \Big\langle\ & (\sigma_y^{'}\sigma_z^{'} - \tau_{yz}^2 + \frac{J_2}{3}),\ (\sigma_x^{'}\sigma_z^{'} - \tau_{xz}^2 + \frac{J_2}{3}),\ (\sigma_x^{'}\sigma_y^{'} - \tau_{xy}^2 + \frac{J_2}{3}) \\ & 2\left(\tau_{yz}\tau_{xz} - \sigma_z^{'}\tau_{xy}\right),\ 2\left(\tau_{xz}\tau_{xy} - \sigma_x^{'}\tau_{yz}\right),\ 2\left(\tau_{xy}\tau_{yz} - \sigma_y^{'}\tau_{xz}\right)\ \Big\rangle \end{aligned} \tag{3.49c}$$

Pramono-William model was coded in FORTRAN 77 by Xie et al. The model is implemented as a user subroutine "UMAT" into ABAQUS.

3.5 Calibration and Performance of the Material Model

The Calibration was performed using substantial data from experiments conducted at the University of Colorado on concrete with different compressive strengths (i.e., 3.0 to 5.5 ksi) (Hurlbut, 1985 and Smith, 1987). Each experiment was performed in a modified

Hoek cell which accepts a NX-core size specimen of dimension 4.25 in. height by 2.125 in. diameter. Stiff steel platens were used and no friction reducing material was used between the steel-concrete interface. Thus, the boundary conditions were rigid. A finite element model is developed in order to simulate the triaxial compression tests which is described in the following section.

Due to the geometric and loading symmetry, axisymmetric elements are used to model the concrete specimen as shown in Figure 3.9. In order to simulate the effect of the rigid loading platen, the deformation along the top of concrete cylinder is suppressed. The analysis is performed using displacement control.

The calibration of the model is carried out for concrete with different compressive strengths. A comparison between analytical and experimental results is shown in Figures 3.10a-3.10b. Material parameters, including ductility and strain softening parameters are presented in Table 3.1. As demonstrated in Figs 3.10a-3.10d, the Pramono-William's model can accurately predict the triaxial behavior of concrete especially when the confining pressure is higher than 10% of uniaxial compressive stress. Since the confining pressure in CFT columns increases rapidly as will be discussed in the next chapter, this deficiency of the material model can not have significant effect on the accuracy of the finite element model.

3.6 Large Deformation Analysis

The possibility of local buckling of steel tube is investigated by employing large deformation analysis. This section illustrates the technique which was used in finite

element analysis to predict the buckling of steel tube. As mentioned earlier, the shell element is used to model the steel tube. Since the shell carries the loading primarily as membrane, its initial response is stiff (i.e. it exhibits only small elastic deformations prior to buckling). If the membrane state created by the external loading is compressive, there is a possibility that the membrane equilibrium state will become unstable and the structure will buckle.

In general, shell buckling stability studies require a two-step analysis. First, eigenvalue analysis is used to obtain estimates of buckling loads and modes. The second step is to perform load-displacement analysis, using imperfections suggested by the eigenvalue analysis. The imperfections are applied in the locations which can provide the most important buckling modes. This type of analysis can not be used for the investigation of the local buckling of composite systems such as composite shells and steel tube in CFT columns in which the component elements are initially in contact with each other. Therefore, a one-step analysis approach is introduced in the present study. In this approach, the main assumption is that the expansion of concrete core provides the necessary imperfections for the buckling of steel tube. This technique is verified by examination of the buckling of a simply supported thin plate. The analytical solution for the buckling load for this case as given by Timoshenko and Gere (1961) is:

$$N_{cr} = \frac{4\pi^2 D}{b^2} \tag{3.50}$$

where N_{cr} is the critical value of the edge load per unit length of the edge, b is the length of each edge and $D = Et^3 / 12(1-\nu^2)$ is the elastic bending stiffness of the plate, with Young modulus E, Poisson's ratio ν, and plate thickness t.

For this particular example, a 2x2 inch plate with thickness of 0.01 inches was analyzed, so that the plate is rather thin (b/t=200). Since the solution is known to be symmetric, only one quarter of the plate was modeled. A mesh of 2x2 was used. Four eight-node shell elements were used to model the plate and the concrete block was modeled with 20-node solid elements.

Two versions of the problem were solved and both results were compared with exact solution. In the first case, the eigenvalue analysis was performed on the simply supported plate which was followed by load-displacement analysis with geometric imperfection. In the second case, the plate is attached to a confined concrete block. The interaction between the plate and the concrete was modeled with gap elements. The plate and the concrete block were compressed in one direction. Load-displacement analysis was performed with no geometric imperfection. Figure 3.11 shows the deformed shape of the plate for the latter case. In Table 3.2 the critical buckling loads are compared with exact solution. As can be seen, the one-step buckling analysis can provide accurate results. However, it should be noted that in two-step analysis the solution is strongly imperfection sensitive (Figure 3.12). This means that as the initial imperfection increases, a lower buckling load when compared to exact solution will be obtained. As can be seen in Figure 3.12, this shortcoming of geometric imperfection analysis has been overcome in a one-step analysis method which is used in the present study.

3.7 Verification of Present F.E. Models

Developing a reliable finite element model is essential for accurate and practical analytical work. Therefore, verification of the developed model is a critical step in any analytical study. To verify the developed model a number of tests on CFT columns are simulated and checked against actual experiments.

The present F.E. model is verified by simulating a number of experimental works performed by different researchers (Tomii et. al., 1977; Okamoto et al, 1988 and Sugano et al, 1992). These experimental tests were conducted on circular and square CFT columns under axial and combined loadings. The test program performed by Tomii examined columns using concrete with a range of uniaxial compressive strengths and various aspect ratios. For each series of compressive strength and aspect ratio a total of three test results were reported. The properties of the columns are summarized in Table 3.3. In Figures 3.13-3.22 the comparison of axial load-strain response between the test and analytical results is presented. The results of finite element analysis and experimental data are in good agreement.

Okamoto investigated the flexural behavior of square CFT columns and Sugano tested circular and square columns. In both experimental work, each column was subjected to axial and lateral loadings. First, a constant axial load was applied and then the lateral load was increased gradually. The details of the tested columns are summarized in the Table 3.4. The comparison between the test results and finite element

results is shown in the Figures 3.23, 3.24 and 3.25. As can be seen, experimental data verifies the finite element model.

As demonstrated, the present F.E. model can accurately predict the response of CFTs under axial and combined loadings. After verification of the present finite element model, a comprehensive detailed analysis is performed on CFT columns. The next two chapters present the discussion of the results for this study.

3.8 Summary

A three-dimensional finite element model is developed using the general purpose software "ABAQUS". The concrete core is modeled with 3-D quadratic solid elements and isoparametric shell elements are used to model the steel tube. The interface between the steel tube and the concrete core is modeled using gap elements. The von Mises elasto-plastic material model with kinematic hardening is used for the steel tube. The finite element model takes advantage of Pramono-William concrete material constitutive relationship. The Pramono-William model is implemented in ABAQUS as a user subroutine. The calibration and verification of the concrete material model is performed using available test data. The method which is used to investigate the possibility of local buckling of steel tube is introduced and verified. The capability of the developed finite element model to correctly predict the response of CFT is also discussed.

CHAPTER 4

4.1 General

In this chapter, the results of analytical studies on CFT columns under axial loading is discussed and important aspects such as load carrying capacity, load transfer mechanism, confinement of concrete core and local buckling of steel tube are explained. In the next section a comparison between the test results and analytical work is made. This will be followed by a discussion of the characteristics and behavior of CFTs under axial loading. Finally, in the last section, the conclusion and summary will be presented.

4.2 Characteristics and Behavior

As demonstrated in the previous chapter, the finite element model developed in this study can accurately predict the response of CFTs. In this section the analytical work is extended in order to study the mechanics of the behavior of CFTs in more detail. The following characteristics of CFTs are discussed in the proceeding sections.

- Load transfer mechanism
- Confinement of concrete core
- Stress-strain relationship for concrete core and steel tube
- Ultimate concrete core compression strain
- Stress distributions
- Local buckling of steel tube

A total of 63 square and 63 circular columns are analyzed. The above characteristics are discussed for only one square and one circular columns in order to make understanding the results easier. Parametric study using various cross-sectional shapes, different aspect ratios and different material properties is presented in Chapter Six. In the following sections the detailed F.E. analysis of a 6x6x24 inches square and a 6x24 inches circular CFT column with wall thickness of 0.17 inches are discussed. The steel tubes have a yield strength of 43.0 (ksi) and the concrete cores have a uniaxial compressive strength of 2.0 (ksi).

4.2.1 Load Transfer Mechanism

It has been observed (Furlong, 1967) that the ultimate axial capacity of CFT columns is larger than the sum of uncoupled steel and concrete failure loads. The increase in the failure load is caused by the confining effect of steel tube on the concrete core. The structural behavior of CFTs are considerably affected by the difference between the Poisson's ratios of the steel tube and concrete core. In the initial stage of loading, the Poisson's ratio for the concrete is lower than that of the steel. Thus, the steel tube has no confining effect on the concrete core. As longitudinal strain increases, the lateral expansion of concrete core gradually becomes greater than expansion of steel tube. At this stage, the concrete core becomes triaxially stressed and steel tube biaxially stressed. The steel tube under a biaxial state of stress can not sustain the normal yield stress, causing a transfer of load from tube to the core. The load transfer mechanism at each

columns, respectively. The load transfer mechanism is similar in square and circular CFT columns. In the first stage of loading the steel tube sustains most of the load until it yields (point A). At this point (A) there is a load transfer from the steel tube to the concrete core. The steel tube exhibits a gradual decrease in load sharing until the concrete reaches its maximum compressive strength (A to B). After this stage of loading (point B), there is a redistribution of load from concrete core to the steel tube. At this point (B) the steel exhibits a hardening behavior with almost the same slope as in the uniaxial stress-strain hardening relationship (E_t).

Even though the load transfer mechanism in circular and square CFTs is similar, the maximum confined compressive stress of concrete core in circular columns is higher than square columns. This can be explained in terms of a larger confining effect of circular steel tubes, which is described in the following sections.

4.2.2 Stress-Strain Relationship for Concrete Core and Steel Tube

Circular and square CFT columns exhibit different pattern of cross-sectional stress distribution in concrete core. In the case of square columns, the cross-sectional stress distribution is not uniform. The center and the corners of square sections go under a higher confining pressure than the sides. Figure 4.2 shows cross-sectional lateral pressure for square columns. The lateral stresses at the sides and corners are about 35% and 50% of maximum stress at the center, respectively. The axial stress distribution is presented in Figure 4.3. As can be seen, the compressive axial stress in the central zone is about 30% and 40% higher than the stresses at corners and sides, respectively. In the case of circular

and 40% higher than the stresses at corners and sides, respectively. In the case of circular columns, the axial and lateral stress distribution at the cross section are radially uniform (Figure 4.4)

Since the axial stress distribution at the cross section is not uniform due to the nonuniform distribution of lateral stresses (i.e., the corners go under a higher confining pressure than the sides), an equivalent axial stress is defined which is obtained by dividing the total concrete core axial load by the cross-sectional area of concrete core. The stress-strain relationship of the concrete core and steel tube are presented in Figures 4.5a and 4.5b, respectively. It is well known that confined concrete exhibits higher compressive strength and larger ductility than unconfined concrete. In Figure 4.5a a comparison between the uniaxial and confined stress-strain relationship is made for circular and square CFT columns. In the case of square column, the compressive strength of concrete core is almost twice the uniaxial compressive strength ($f_{cc}^{'} / f_{c}^{'} = 1.91$). In the circular column the concrete core reaches a compressive capacity of 4.8 (ksi) which is 2.4 times of uniaxial compressive strength. The confined strain at maximum stress in both cases is about four times larger than the unconfined strain at maximum stress in uniaxial compression test ($\varepsilon_{c0} / \varepsilon_{0} = 3.89$ in the square column and $\varepsilon_{c0} / \varepsilon_{0} = 4.20$ in the circular column). The level of increase in the compressive strength depends on the aspect ratio of the column and uniaxial compressive strength of the concrete core. However, the degree of increase in ductility depends only on the aspect ratio. These two phenomena are discussed in chapter six under results of parametric study.

In the prepeak portion of stress-strain curve for the concrete core two parts are distinguished (*OA* and *AB* in Figure 4.5a). A decrease in the stiffness of concrete core is observed at point A in Figure 4.5a which corresponds to point A' of Figure 4.5b when the steel tube yields. The yield stress of steel tube is lower than the normal yield stress due to the presence of hoop stresses (i.e., biaxial effect). Beyond this point (A', Figure 4.5b), steel exhibits a strain softening behavior until it reaches point B', which corresponds to point B of Figure 4.5a, when the concrete reaches its maximum compressive capacity. The softening behavior of steel tube is due to the fact that when decrease in the stiffness of concrete core starts (point A), the lateral expansion of concrete core increases rapidly resulting in a higher internal pressure between concrete and steel tube interface. Higher internal pressure causes larger hoop stress which results a reduction in compressive stress in steel tube. It should be noted that the steel tube has already yielded. At this point (B') the compressive stress in the steel tube is in the range of 85% to 95% of normal yield stress. The degree of reduction in the stress depends mainly on the thickness of the steel tube. In thinner tubes more reduction of stress is expected. For these particular columns (t=0.17 in.), the stress of steel tube at this stage of loading is about 93% of F_y. It has been observed that the value of F_y has no effect on the level of reduction in compressive stress in steel tube. After this point (B') the steel tube exhibits a hardening behavior with the same slope as in uniaxial stress-strain hardening relationship. The axial stress contours for the concrete core and the steel tube are presented in the Figure 4.6. As expected, the axial state of stress remains constant along

the height of the columns. The axial stress at the top is about 2% higher than the axial stress at mid-height of the column.

4.2.3 Ultimate Concrete Core Compression Strain

So far no expression for the ultimate strain of concrete core in CFTs is available. A number of investigators (Baker and Amarakone, 1964; Corley, 1966; Mattock, 1967) have proposed several empirical equations for the ultimate strain in RC columns, as follows:

$$\varepsilon_{cu} = 0.0015[1 + 150\rho_s + (0.7 - 10\rho_s)\frac{d}{c}] \leq 0.01 \quad \text{(Baker and Amarakone, 1964)} \qquad (4.1)$$

$$\varepsilon_{cu} = 0.003 + 0.02\frac{b}{Z} + \left(\frac{\rho_s F_y}{20}\right)^2 \quad \text{(Corley, 1966)} \qquad (4.2)$$

$$\varepsilon_{cu} = 0.003 + 0.02\frac{b}{Z} + 0.2\rho_s \quad \text{(Mattock, 1967)} \qquad (4.3)$$

where ρ_s is the ratio of the volume of transverse steel to the volume of the concrete core, d is the effective depth, b is the width of the cross section, c is the distance of neutral axis from the exterior compression fiber, Z is the distance from the critical section to the point of contraflexure and F_y is the yield strength of the transverse steel.

These equations were developed based on the experimental studies on confined RC columns. In addition, the upper limit for Eq. (4.1) is $\varepsilon_{cu} = 0.01$ which is conservative for concrete core in CFT columns where the confinement is entirely provided by the steel

tube which results in a ductile behavior. Eqs. (4.2 and 4.3) are applicable for low values of ρ_s (less than 0.02). Hence, these expressions are not applicable for the concrete core in CFT columns where ρ_s is relatively large.

More recent work reported by Mander et al. (1984) proposes a rational method for the prediction of ultimate strain in confined RC columns based on an energy balance approach. In this method, the additional ductility of confined concrete members is considered to be due to the energy stored in the transverse reinforcement. The energy balance method is used in the present study in order to determine the ultimate strain of concrete core in CFT columns.

Consider the stress-strain relationships for unconfined and confined concrete shown in Figure 4.7. The area under each curve presents the total strain energy per unit volume required to cause failure in the concrete. The increase in the strain energy of the concrete core can only be balanced by the strain energy capacity of the steel tube as it yields in tension. By equating the ultimate strain energy capacity of the steel tube per unit volume of the concrete core (U_{sh}), to the difference in area between the confined (U_{cc}) and the confined (U_{co}) concrete stress-strain curves, plus additional energy required to maintain yield in the steel tube in compression in the longitudinal direction (U_{sc}), the ultimate strain of the concrete core can be calculated. Thus,

$$U_{sh} = U_{cc} + U_{sc} - U_{co} \qquad \text{where} \tag{4.4}$$

$$U_{sh} = \rho_s A_{cc} \int_0^{\varepsilon_{sf}} f_s d\varepsilon_s \tag{4.5}$$

$$U_{cc} = A_{cc} \int_0^{\varepsilon_{cu}} f_{cc} d\varepsilon_{cc} \tag{4.6}$$

$$U_{sc} = \rho_{sl} A_{cc} \int_0^{\varepsilon_{cu}} f_{sl} d\varepsilon_{cc} \tag{4.7}$$

$$U_{co} = A_{cc} \int_0^{\varepsilon_{sp}} f_c d\varepsilon_c \tag{4.8}$$

where ρ_s is the ratio of the area of steel tube in the transverse direction to the area of the concrete core along one unit length, A_{cc} is the area of the concrete core, f_s and ε_s are hoop stress and strain in the steel tube, ε_{sf} is the fracture strain of the steel tube, ρ_{sl} is the ratio of the cross-sectional area of steel tube to the concrete core, f_{cc} and ε_{cc} are the longitudinal stress and strain in the concrete core, f_c and ε_c are the stress and strain for unconfined concrete, f_{sl} is longitudinal stress in the steel tube and ε_{sp} is the spalling strain of unconfined concrete. Substituting Eqs 4.5 to 4.8 in Eq. 4.4 gives:

$$\rho_s A_{cc} \int_0^{\varepsilon_{sf}} f_s d\varepsilon_s = A_{cc} \int_0^{\varepsilon_{cu}} f_{cc} d\varepsilon_{cc} + \rho_{sl} A_{cc} \int_0^{\varepsilon_{cu}} f_{sl} d\varepsilon_{sl} - A_{cc} \int_0^{\varepsilon_{sp}} f_c d\varepsilon_c \tag{4.9}$$

The left hand term of Eq. (4.9) contains the total area under the stress-strain curve (U_{sf}) for the steel tube up to the fracture strain ε_{sf}.

$$U_{sf} = \int_0^{\varepsilon_{sf}} f_s d\varepsilon_s \tag{4.10}$$

Results from tests carried out by Mander et al. (1984) indicate that U_{sf} is independent of size or yield strength, and can be taken as 15.94 (kips-in./in.^{3}) within $\pm$ 10%, and the fracture strain is in the range of 0.24 to 0.29. Hence, with the knowledge of stress-strain relationships for the concrete core and the steel tube, Eq. (4.9) can be solved numerically and the ultimate strain of the concrete core obtained.

Eq. (4.9) is solved numerically using the stress-strain curves (Figures 4.5 a and 4.5b) for concrete core and steel tube obtained during finite element analysis. The areas under the stress-strain curves are calculated numerically using Quattro Pro software and trial and error method is used to determine ultimate confined strain (ε_{cu}) for concrete core. Same analysis is performed for CFT columns with different aspect ratios, unconfined concrete compressive strengths and cross-sectional shapes. The results of this analysis is presented in Table 4.1. Even though there is no experimental data that can be compared with analytical results, the obtained confined ultimate strains seem reasonable for CFT columns. Therefore, energy balance approach gives a good definition for ultimate strain in concrete core.

As expected in circular CFT columns, the ultimate strain of the concrete core is higher than in square CFTs. The level of increase in the ultimate strain of the confined concrete in CFT columns is in the range of 6 to 12 times of the ultimate strain for unconfined concrete. The degree of increase in the ultimate strain is mainly affected by

the aspect ratio. As expected, the ultimate strain of concrete core is higher in thick wall CFT columns with compare to thin wall columns. This is due to the fact that in CFT columns with small aspect ratios (i.e., thick wall columns) higher amount of energy is stored in the steel tube. Therefore, a higher strain energy in concrete core is required to balance the stored energy in steel tube A relationship between aspect ratio and ultimate strain is determined based on the parametric study which will be discussed in chapter six.

4.2.4 Confinement Pressure

The confinement pressure on the concrete core varies at each stage of loading. Figure 4.8 shows the details of this variation for circular and square CFTs. In the first stage of loading, the steel tube expands more than the concrete core so no confining pressure is developed at this stage (OA portion of Figure 4.8). At point A, the lateral expansion of concrete core reaches the steel tube. Subsequently, the concrete core expands more than the steel jacket, as a result, confining pressure develops and increases rapidly until the steel yields. As the steel tube yields, there is a drop in the confining pressure (point B of Figure 4.8) in the square column. Thereafter, it increases at a slower rate. In the case of circular column, the confining pressure increases at a slower rate with no drop as steel yields. The increase in the confining pressure continues until the concrete reaches its maximum compressive capacity, (point C of Figure 4.8 which corresponds to point B of Figure 4.5a). The confining stress is almost linear and constant in the post peak. A higher confining pressure develops in circular columns. The confining pressure in circular columns is almost 35% higher than square columns.

4.2.5 Poisson's Ratio-Axial Strain Relationship for Concrete Core

The structural behavior of CFT columns is highly affected by the changes in the Poisson's ratio of the concrete core. The Poisson's ratio of the concrete core increases rapidly from 0.2 to 0.55. At this point the concrete core reaches it maximum compressive strength. Thereafter, the Poisson's ratio remains constant. The changes in the Poisson's ratio of concrete core is demonstrated in the Figure 4.9. For low strains the value of Poisson's ratio for concrete is about 0.2 and for the strains larger than the peak-strain the value can raise to 0.55. The concrete core is not a linear material, therefore its Poisson's ratio can be more than 0.5. As the peak-strain reaches and the Poisson's ratio approaches a constant value of 0.55, the confining pressure remains constant.

4.2.6 Load-Deflection Relationship

The load-deflection relationship for CFT columns can be categorized in two groups; strain hardening type and degrading type. The circular columns show strain hardening type of behavior. The degrading type of response is observed in square CFTs in which there is a rapid deterioration of axial capacity after the peak load (point A, Figure 4.10). The decrease in the axial load continues until the defection reaches two to four times of peak deflection in thick to thin wall square columns (point B). In circular columns (Figure 4.1b), after the peak load the load-deflection relationship is linear (i.e., load increases with a constant rate). The rate of increase depends on the aspect ratio. In the thick wall columns, the axial load increases with a higher rate.

The axial stiffness of CFT columns is defined as the slope of axial load-deflection curve, and is equal to the sum of axial stiffnesses of the concrete core and steel tube. Figure 4.11 shows that the axial stiffness of the column can be obtained by adding the stiffness of its constituent elements. As expected, the stiffness of steel tube stays constant until it yields (point A', Figure 4.11). Up to this point (A), the stiffness of the CFT column has a similar shape to the stiffness of concrete core, but with a higher values (i.e., stiffness of concrete core plus stiffness of steel tube which is constant). Thereafter, there is a sudden drop in the stiffness of CFT column (i.e., from point A to B) since the steel tube yields (point A') and its stiffness becomes negative due to biaxial effect. After this point (B), the stiffness of CFT column is almost equal to the stiffness of its concrete core until the concrete core reaches its maximum axial capacity. In the post-peak regime, hardening and degrading type of behavior are observed in circular and square columns, respectively.

The axial stiffness of concrete core is higher than the axial stiffness of a plane concrete column with the same geometry and material properties. The ratio between the axial stiffnesses of concrete core and plain concrete column is defined as Stiffness Index (S_I). The variation in stiffness index is presented in the Figure 4.12. It can be observed that at the initial stage of loading, the stiffness index is equal to one. Thereafter, it increases linearly up to a value of two until the concrete reaches its uniaxial peak strain, after which the stiffness index increases rapidly.

4.2.7 Local Buckling of Steel Tube

The initiation of local buckling can be determined by examination of the contact force between the steel tube and concrete core. Figure 4.13 shows history of this force as the system is deflected. The variation of internal force is similar to the changes in confining pressure (Figures 4.8 and 4.13). The only difference is in the area where local buckling of the steel tube occurs. At this point the confining pressure at the location of local buckling is linearly released to zero, but the confining pressure still increases in other regions. The initiation of the local buckling of the steel tube can be observed at the mid-height of the column at a deflection of 0.2 inch for the particular square column considered (point D on Figure 4.13). Figure 4.14 shows the deformed shape and stress distributions of steel tube at the initiation of local buckling, respectively. The aspect ratio has a significant effect on the local buckling of steel tube. Based on the results obtained from detailed F.E. analyses, it is found that for square CFT columns with aspect ratio of more than 78, the local buckling of steel tube forms at the peak load. While, in thicker columns (i.e., lower aspect ratio) the steel tube buckles after the peak load is reached. In the case of circular columns, the local buckling of the steel tube occurs at the peak load in columns with aspect ratio more than 95. In both cases ductile behavior is observed even after local buckling has occurred, however, the circular columns show a more ductile behavior.

Based on the results obtained from F.E. analysis, at the first stage of loading, local buckling of steel tube occurs at the top and bottom of the column. The large amount of shear stress at the steel and concrete interface near the supports causes the separation of

the steel tube from the concrete core which results in the local buckling of the steel tube. At this point the axial stress in the concrete core is much less than its maximum compressive capacity. In practice the separation of steel tube and concrete core at supports is prevented by employing internal diaphragms. In most experimental work, rigid steel plates were used at supports which restrained the separation of steel from concrete. In short CFT columns with diaphragms, the separation of the steel tube from the concrete core forms at mid-length of the column. In the case of longer columns, the separation of steel and concrete first occurs below the location of diaphragms and then the separation of concrete and steel forms at different locations.

The response of thin steel tubes in CFTs to the applied loading (e.g. compressive force and internal pressure) is very different from the behavior of hollow tubes under compressive forces. In general, the prebuckling deformation of shells is not a rotation free procedure. This means that hollow shells under compressive forces may experience bending as well as membrane deformation. However, the rotation of the steel tube in CFTs is prevented due to the bond between the steel and concrete interface and when the bond is broken, only an outward rotation can occur. In addition, the internal pressure between the steel and concrete interface eases the outward rotation of steel tube. If the steel tube is thick enough, the separation of the steel tube from the concrete core may happen after the peak load. In the thin-walled CFT columns, local buckling of the steel tube can occur at peak load. The local buckling of steel tube is due to the separation of steel and concrete. At such a stage, the concrete core maintains its compressive capacity until the separation completed. Thereafter, cracking and spalling of concrete at the separated area can occur. Even though, the CFT column can not sustain a higher load

after local buckling occurs, it still maintains its load carrying capacity. This behavior is similar to post-buckling of plates.

4.3 Summary

The characteristics and behavior of CFT columns under axial loading are discussed. The load transfer mechanism between steel tube and concrete core is explained. At the first stage of loading, the steel tube sustains most of the load until it yields. Thereafter, the load transfers to the concrete core. As the concrete core reaches its maximum compressive capacity, the load is redistributed from the concrete core to the steel tube. The axial and lateral stress distributions in square and circular columns are identified. In the case of square columns, corners and center exhibit higher compressive stress than the sides due to nonuniform lateral stress distributions. The cross-sectional stress distribution is more uniform in circular columns. The stress-strain properties of concrete core is discussed. The increase in compressive capacity of concrete core due to confining effect of steel tube is identified. The ultimate strain in the concrete core is defined based on energy balance approach. The mechanism of local buckling of steel tube is studied. In CFT columns with thin wall steel tubes, the separation of steel tube and concrete core results in local buckling of steel tube. It is found that in square and circular columns with aspect ratio larger than 78 and 95, respectively, the local buckling of steel tube occurs before the concrete core reaches its maximum compressive capacity.

CHAPTER 5

CHARACTERISTICS AND BEHAVIOR OF CFT COLUMNS UNDER COMBINED LOADING

5.1 Introduction

In practice, most of CFT columns are subjected to moments as well as axial forces. Even though a number of experimental studies (Boyd et al., 1995; Sugano et al, 1992; among others) have been carried out, limited information is available on the behavior of CFTs when subjected to both axial and lateral loadings. The experimental investigations were mainly concerned with the study of circular columns under combined loading. Some experimental work on the square CFT columns has been reported (Sugano et al, 1992; Okamoto et al, 1988). When the design is concerned, the CFT columns have been treated as regular RC columns due to lack of information. However, in CFTs the overall response and the behavior of each component element are much different from the RC or steel columns. The results of the finite element analysis on the non-linear response of CFTs under axial and lateral loadings is presented in this chapter. In the next section, flexural response of square and circular CFT columns is presented. This is followed by the discussion of characteristics and behavior of CFTs under combined loading.

5.2 Flexural Behavior of CFT Columns

To better understand the flexural response of CFT columns, detailed finite element analysis is performed on a number of square and circular columns (i.e., 14 circular and 14 square columns). The results of F.E. analysis of only one square (i.e., a 10x10 inches)

and one circular (i.e., 10 inch diameter) columns with a height of 70 inches and wall-thickness of 0.16 inches are discussed in order to make understanding the results easier. The steel tube has a yield strength of 54.0 ksi and the concrete has an unconfined compressive strength of 2.0 ksi. The important features of flexural response such as moment-deflection relationship, ultimate flexural capacity, stress distribution and stress-strain relationship of concrete core and steel tube are discussed.

5.2.1 Moment -Deflection Relationship

The flexural response can be expressed in the form of moment-curvature or moment-deflection relationship. Figures 5.1 and 5.2 show typical moment-deflection relationships for the square and circular CFT columns, respectively. As demonstrated in Figures 5.1 and 5.2, ductile behavior can be expected from CFT columns with a strain hardening type of behavior. In the ordinary RC columns, the flexural behavior in the post-peak regime depends mainly on the steel content. Lightly reinforced sections result in a practically linear moment-curvature relationship up to the point of steel yielding. When the steel yields, a large increase in the curvature occurs at nearly constant bending moment. In heavily reinforced sections, the moment-curvature relationship becomes nonlinear when the concrete enters the inelastic part of its stress-strain relationship, and failure can be quite brittle unless the concrete is confined by closed stirrups.

To investigate the benefits of confinement on the flexural response, a combined section is introduced. The so called combined section, is a plane concrete section surrounded by a steel tube in which the confining effect of steel tube is ignored. The

combined section is analyzed as an ordinary RC column using an unconfined stress-strain relationship for concrete. The moment-curvature of the combined section shows a degrading type of behavior with no brittle failure due to the stirrup action of the steel tube. A comparison between the moment-curvature relationships of a combined section and a CFT column is presented in the Figure 5.3. The flexural rigidity of is defined by,

$$EI = \frac{dM}{d\varphi} \tag{5.1}$$

where EI is the flexural rigidity, M is the moment and φ is the curvature.

In the cases of combined sections, the flexural rigidity decreases significantly after the steel yields in compression (point A' in the Figure 5.3). The crushing of concrete commences before the steel tube yields in tension. As the crushing of concrete starts, the flexural rigidity becomes negative (point B' in Figure 5.3). However, in the case of CFT columns, the flexural rigidity is nearly constant before the steel tube yields in compression (point A). At this point a decrease in the flexural rigidity is observed until the steel tube yields in tension (point B). Thereafter, the flexural rigidity decreases significantly until the concrete core reaches its maximum compressive capacity (point C). Then, the moment increases linearly and the flexural rigidity remains constant. Since the steel tube yields before the concrete core reaches its maximum compressive capacity, ductile behavior is ensured.

5.2.2 Ultimate Flexural Capacity

As discussed earlier in chapter three, compressive strength and ductility of the concrete core in CFTs is higher than the unconfined concrete. The amount of increase in strength and ductility mainly depends on the aspect ratio and the unconfined compressive strength of concrete core. The flexural capacity of unconfined RC columns is reached when the exterior fiber of concrete in compression reaches a strain of 0.003 (ultimate strain), which is approximately 1.5 times unconfined strain at maximum stress (i.e., 0.002). However, as mentioned earlier, the ultimate strain of the concrete core can be up to 12 times larger than the ultimate strain in an unconfined uniaxial test which results in a higher flexural capacity as well as higher ductility.

The flexural capacity of CFT columns and combined sections are compared with each other. The flexural capacity of the combined sections are calculated using the fiber method considering the unconfined stress-strain relationship for concrete. In this method, the section is divided into a finite number of strips parallel to the neutral axis. The area and centroid of each fiber can easily be calculated. In the first step of analysis, a neutral axis is assumed at any arbitrary location. The location of neutral axis then can be modified by comparing the axial compressive and tensile forces. The trial and error continues until equilibrium is satisfied.

The results are compared with the flexural capacity of CFT columns obtained from finite element analysis. Figure 5.4 presents a comparison between the results obtained from finite element analysis and fiber method. As demonstrated in the Figure 5.4, the increase of CFTs' flexural capacity due to confinement can be in the range of 1.7

to 2.2 for square columns and 1.8 to 2.6 for circular columns. The circular columns exhibit more increase in the flexural capacity than square columns since confinement effect in circular columns is higher than in square CFTs. Moreover, the cross-sectional stress distribution in the steel is not uniform. Due to the complex pattern of stress distribution (i.e., biaxial effect), the corners sustain a lower stress than the sides. The detailed discussion of stress distribution of CFT columns under combined loading is presented in the next section.

5.2.3 Stress Distribution

The flexural strength of reinforced concrete sections can be determined if the stress distribution of the cross section is available. In the case of ordinary RC sections (i.e., sections with poor confinement), the compressive stress distribution in concrete has the same general shape as for an unconfined uniaxial compression test. However, the maximum stress is less than the maximum uniaxial compressive stress (Wang and Salmon, 1985). Experimental results (Hognestad et al, 1955; Granholm, 1965) have established the relationship between the uniaxial compression test and the concrete compressive stress distribution along the section (i.e., the maximum stress is found to be 85% of the maximum uniaxial compressive stress). The stress-strain properties of steel are well defined. Normally, a bilinear stress-strain curve is assumed and the strain hardening is neglected. The nominal strength of the section is assumed to be reached when the strain in the extreme compression fiber is equal to the ultimate strain of concrete. At this point, the strain in the tension steel could be either larger or smaller

than the yield strain, depending on the relative proportion of steel to concrete. If the amount of steel were low enough, the steel would yield prior to crushing of concrete, resulting in a ductile failure mode. A large quantity of steel would allow the steel to remain elastic at the time of crushing of the concrete causing a brittle mode of failure.

In the case of CFT columns, the stress distribution on the cross section is not defined due to lack of information on the flexural behavior of CFTs. Moreover, no experimental results exist that relate the compressive stress distribution of concrete at the cross section with the stress-strain properties of the concrete core under pure compression. Hence, the finite element analysis of CFTs under combined loading is extended to study the stress distribution of the steel tube and the concrete core to reach some understanding of the distribution of stresses. Figures 5.5-5.9 show the longitudinal and cross-sectional stress contours for the square and circular CFT columns. As can be seen, the longitudinal and cross-sectional stress distributions are not uniform. In the longitudinal direction, on the extreme compressive side, the rate of decrease in compressive stress of concrete core is significant in the central area (i.e., mid-height of the column toward the supports). The steel tube exhibits a more gradual change in the longitudinal stress distribution. However, the cross-sectional stress distribution has rather complex pattern.

Figure 5.10 shows the stress distribution for the concrete core and the steel tube for the square CFT column. It can be seen from Figure 5.10 that the stress distribution in the concrete core and the steel tube are much different from the stress distributions in an ordinary reinforced section. The concrete core stress distribution has the same general

shape as the confined stress-strain relationship of concrete core under compression (Figure 5.11).

As demonstrated in Figures 5.10 and 5.12, the compressive and tensile stress distribution in steel tube along the cross section is not uniform. The complex state of stress at the corners of the steel tube causes the corners to sustain less stress than the mid-sections. Table 5.1 presents the values of stresses at corners in the extreme compression and tension fibers of steel tube. As can be seen, the maximum compressive stress and tensile stress at the corners are about 70% and 80% of the normal yield stress, respectively. Then, it increases linearly up to yield stress. The maximum average compressive stress and tensile stress along the cross-sectional width are 92% and 95% of yield stress. It should be noted that the steel tube has already yielded. Due to biaxial effect the corners yield at a lower stress than the normal yield stress.

Figure 5.13 shows the variation of the steel tube's stress distribution along the depth of the cross section. The non-linear stress-depth relationship of steel tube makes the determination of the flexural capacity of CFT columns even more difficult. The location of neutral axis mainly depends on the level of axial force, aspect ratio and uniaxial compressive strength of concrete core. Hence, it is rather difficult to estimate a linear relationship instead of the non-linear variation to ease the calculation. However, a an approximate stress block could be defined. The development of such an approximate method is discussed in the next chapter.

In the case of circular CFT columns, the stress distribution in the steel tube on the cross section is more uniform than the square columns. Figure 5.14 shows the stress distribution under combined loading. As shown in the Figures 5.14 and 5.15, the

concrete core, in circular CFT sections exhibit almost the same pattern of behavior as square sections but with a higher compressive stress and more ductility. The stress distribution in steel tube is much more uniform than the square columns. The steel tube experiences a maximum stress at the exterior compression fiber which on the average is 10% more than the normal yield stress (point A in Figure 5.16) due to the strain hardening. The stress in the steel tube remains constant up to point B. Then, it decreases linearly to zero at the neutral axis. In the tension zone, the stress increases linearly from zero to the maximum stress and remains constant up to exterior tension fiber. It can be seen from Figure 5.17 that employing an accurate stress block for the steel tube in the circular columns is more practical than in the square column.

5.3 Summary

The flexural behavior of CFT columns is studied. It is found that, the CFT columns exhibit higher flexural capacity than the combined sections due to higher ductility and larger compressive capacity of concrete core which is provided by confining effect of steel tube. The moment-curvature relationship for CFT columns shows a hardening type of behavior. The axial and lateral stress distributions in square and circular columns are studied. The cross-sectional stress distribution in concrete core and steel tube is not uniform. In the case of square columns, the corners of steel tube sustain a lower stress than the sides and the maximum stress at corners is in the range of 70% to 80% of the normal yield stress. The axial stress distribution in the concrete core at the cross section has the same general shape as the confined stress-strain relationship under compression.

However, the central part of concrete core normal to neutral axes exhibits higher capacity than the areas next to the steel tube.

CHAPTER 6

PARAMETRIC STUDY AND ANALYTICAL MODELS

6.1 Introduction

As discussed in the earlier chapters, the basic parameters such as aspect ratio, uniaxial compressive strength of concrete, slenderness ratio and cross-sectional shape have significant impact on the behavior of CFT columns. Experimental investigation on the effects of all these parameters is practically impossible, since it is expensive and time consuming. The present finite element model allows a comprehensive parametric study considering a wide range and combination of the parameters of interest to be investigated. The parametric study includes a wide range of aspect ratios ($10 \leq D/t \leq 100$), concrete uniaxial compressive strengths (2000 to 9000 psi), length-width ratios (3 to 25) and steel normal yield stresses (40 to 60 ksi). The effect of each parameter on the overall response as well as the behavior of individual component element is presented in this chapter. The results of this study is used to develop a practical design methodology for CFT columns under both axial and combined loading. The results of proposed model is compared with previous experimental data.

6.2 Parameters and Combinations

A wide range and combination of parameters of interest is used in this study. To investigate the effect of aspect ratio and uniaxial compressive strength of concrete tube on the stress-strain properties of concrete core, a combination of these two parameters is

used. Assuming a length-width ratio of 4, six different values of unconfined concrete compressive strengths (i.e., 2, 3, 4, 5, 6 and 9 ksi) are used. For each uniaxial compressive strength of concrete a total of nine different aspect ratios (i.e., 10, 20, 25, 35, 50, 60, 75, 85 and 100) with two different steel yield strengths are considered. To study the impact of slenderness ratio on the overall response, twenty four CFT columns with six different length-width ratios (i.e., 3, 5, 8, 12, 15 and 25) are analyzed. The results of this study is presented in the following sections.

6.3 Non-Linear Curve Fitting Algorithm

The results of parametric study are used to develop analytical models which can express the different aspects of response with considering effect of different parameters. To determine the constant parameters in each analytical model non-linear curve fitting algorithm is employed. For this purpose, "TableCurve 2D" software is used. The non-linear curve fitting algorithm is the Levenburg-Marquardt method (Bevington, 1969; Press, 1992) that uses the Gauss-Jordan procedure for the matrix inverse required in each iteration. In non-linear curve fitting, the parameters are iteratively adjusted to minimize a goodness of fit merit function. The analysis is successful when the coefficient of determination (r^2) remains constant for five consecutive iterations.

6.4 Stress-Strain Properties of Concrete Core

The mechanical properties of concrete core such as maximum compressive strength (f'_{cc}), strain at maximum stress (ε_{co}), ultimate compressive stress (f'_{cu}) and ultimate strain (ε_{cu})

are highly affected by aspect ratio (*D/t*), cross-sectional shape and uniaxial compressive strength of concrete (f_c'). In the following sections, the effect of these parameters on each mechanical property is discussed in details. It should be noted that an average stress-strain relationship under the pure axial load is considered since the cross-sectional stress distribution is not uniform (as discussed in chapter 4).

6.4.1 Maximum Compressive Strength of Concrete Core

The superior property of concrete core in CFTs (i.e., high compressive strength) has been ignored in the current design specifications due to lack of knowledge on determination of maximum compressive strength. This section presents the result of parametric study and introduces a practical and accurate method for determination of the maximum compressive strength of confined concrete core. Figure 6.1 presents the relationship between confinement ratio (f_{cc}' / f_c') and aspect ratio (*D/t*) for a square and a circular CFT column with concrete uniaxial compressive strength of 2000 psi and length-width ratio of 4. In both cases, the concrete core exhibits larger confined compressive strength (f_{cc}') with smaller aspect ratios (i.e., thicker tubes). The confined compressive strength is seen to vary between 1.77 and 1.11 times the uniaxial compressive strength for aspect ratios between 10 and 100 for the square column. The rate of increase in confined compressive strength is significant when the aspect ratio decreases from 100 to 25. Afterwards, the confined compressive strength increases with a lower rate and it almost remains constant for aspect ratios of less than 20. The low rate of increase in confinement ratio in thick wall columns is due to the fact that the stress distribution at the

cross section is not uniform (i.e., the corners and center go under more confining pressure than the sides). This means that the concrete core exhibits a higher compressive strength at so called effective area, corners and center of the cross section. When the wall thickness increases (i.e., smaller aspect ratio), there is a reduction in the effective area and therefore the average of stress at the cross section decreases.

Circular columns exhibit small changes in the rate of increase in confinement ratio as the aspect ratio decreases. In this case, the confinement ratio is in the range of 1.7 and 2.3. As the wall thickness increases in circular columns, the increase in the confinement is more significant than the square columns.

To investigate the influence of higher strength concrete on confinement ratio, similar analysis is performed on circular and square columns using concrete with different $f_c^{'}$ (i.e., 3, 4, 5, 6 and 9 ksi). Figures 6.2 and 6.3 show the effect of different unconfined concrete compressive strengths on the confinement ratio for square and circular columns. Interestingly, it is observed that for the same aspect ratio the confinement ratio for higher strength concrete is less than lower strength concrete. This is due to the fact that as the compressive strength increases, the stiffness of concrete also increases resulting in less lateral expansion. Thus, the concrete core experiences less confining pressure.

Based on the results obtained relating confinement ratio and aspect ratio, and between confinement ratio and uniaxial compressive strength (Figures 6.2 and 6.3), empirical equations are developed to determine the maximum confined compressive strength of concrete core. These equations are expressed as:

$$f_{cc}^{'} = f_c^{'}\left(1+\frac{A}{1+\left(\frac{D/t}{E}\right)^4}\right) \qquad \text{for square columns} \qquad (6.1)$$

$$f_{cc}^{'} = f_c^{'}\left(1+\frac{B}{1+\left(\frac{D/t}{F}\right)}\right) \qquad \text{for circular columns} \qquad (6.2)$$

where D is the diameter or width and t is the wall thickness of the column. A, B, E and F are empirical parameters. Table 6.1 shows values of A, B, E and F obtained based on the best fit for each group of aspect ratio and each concrete uniaxial compressive strength. A, B, E and F can be expressed in terms of $f_c^{'}$ as:

$$A = 1.335\, e^{-\left(\frac{f_c^{'}}{3.55}\right)} \qquad (6.3)$$

$$B = 1.831\, e^{-\left(\frac{f_c^{'}}{3.55}\right)} \qquad (6.4)$$

$$E = 47.492 + \frac{30}{f_c^{'}} \qquad (6.5)$$

$$F = -32.517 + \frac{510}{f_c^{'}} \qquad (6.6)$$

where ($f_c^{'}$) is in ksi. These relationships are obtained based on nonlinear regression analysis. As a result, with the knowledge of uniaxial compressive strength of concrete

core and thickness of the steel tube, the maximum confined compressive strength of concrete core can be accurately calculated, as shown in Figures 6.2 and 6.3. The maximum compressive stress in concrete core ($f_{cc}^{'}$) is determined using the proposed model (Eqs. 6.1 to 6.6). The strain at peak stress (ε_{co}) can also be determined which is discussed in the next section.

6.4.2 Confined Concrete Core Strain at Maximum Stress

The confined strain which corresponds to the confined peak stress, so called strain at maximum confined stress, mainly depends on the aspect ratio. The results obtained from finite element analysis (Figures 6.4 and 6.5) have shown that for CFT columns with the same aspect ratio and concrete core with various uniaxial compressive strengths, the strain at maximum stress is almost the same. This means that the unconfined compressive strength of concrete has no significant effect on the value of confined strain at peak stress if the same unconfined strain at maximum stress is assumed. Figures 6.4 and 6.5 present the relationships between the strain at maximum stress and aspect ratio for square and circular columns, respectively. These relationships can be expressed as:

$$\varepsilon_{co} = \varepsilon_{o}\left(1+\frac{3.51}{\left(\frac{D/t}{60}\right)^{4}}\right) \qquad \text{for square columns} \qquad (6.7)$$

$$\varepsilon_{co} = \varepsilon_o \left(1 + \frac{4.40}{\left(\frac{D/t}{100} \right)} \right) \qquad \text{for circular columns} \qquad (6.8)$$

where ε_{co} and ε_o are confined and unconfined strain at maximum stress, respectively. *(D/t)* is the aspect ratio.

The next step after determining the confined peak stress and peak strain of concrete core, is to define its stress-strain relationship.

6.4.3 Stress-Strain Relationship for Concrete Core

The most puzzling characteristics of CFT columns is the behavior of concrete core at every stage of loading. Based on the results obtained from finite element analysis and with the knowledge of confined peak stress and confined strain at peak stress, the stress-strain relationship of concrete core in CFTs can be expressed as follows:

$$\sigma_{cc} = f_{cc}' \left(\frac{a + bx + cx^2 + dx^3 + ex^4 + fx^5}{1 + gx + hx^2 + ix^3 + jx^4 + kx^5} \right) \qquad (6.9a)$$

where

$$x = \frac{e_{cc}}{\varepsilon_{co}} \qquad (6.9b)$$

in which, σ_{cc} and e_{cc} are the stress and strain ; f'_{cc} and ε_{co} are the peak stress and strain at maximum stress of concrete core, respectively. The empirical parameters *a, b, c, d, e, f, g, h, i, j* and *k* are determined based on a nonlinear regression analysis and have the values of:

a = 0.01810	b = 4.69430	c = -5.53100	d = 4.63689
e = -1.54584	f = 0.16773	g = 2.12912	i = 5.08680
j = -1.86773	k = 0.20046		(6.10)

The accuracy of the proposed model to predict the stress-strain relationship of concrete core in circular and square columns is remarkable. Figures 6.6-6.9 present a comparison between the proposed model and finite element results for square and circular CFT columns. As can be seen, the proposed model can predict the response of concrete core with high accuracy.

6.4.4 Maximum Compressive Stress in Steel Tube

As discussed in chapter four, the maximum stress that steel tube in CFT columns can sustain depends mainly on the wall thickness and length-width (*L/D*) ratio. The effect of aspect ratio and length-width ratio on the maximum load carrying capacity of steel tubes in CFTs is studied. This section presents the results of this investigation.

Steel tube under biaxial state of stress exhibits a lower yield stress. In the case of short columns, the level of decrease in the yield stress depends on the aspect ratio and

cross-sectional shape and it is independent of normal yield stress of steel tube. It is found that the maximum stress in circular columns is slightly higher than square columns (i.e., 2% to 4%). However, for simplicity in the derivation of formula, the results obtained for square columns are used. Table 6.2 shows the effect of aspect ratio on the yield stress of steel tube (F_{sy}) under biaxial state of stress. The decrease in the steel tube yield stress (F_{sy}) compared to its normal yield stress (F_y) is more significant in columns with higher aspect ratio and decreases to 85% of the normal yield stress. Based on the results obtained from finite element analysis, a reduction factor is proposed to consider the biaxial effect on the maximum stress in the steel tube. The reduction factor (R_1) of steel tube due to the effect of aspect ratio is defined as:

$$R_1 = \frac{F_{sy}}{F_y} \tag{6.11}$$

The relationship between the reduction factor and aspect ratio can be expressed as:

$$R_1 = 1.08 - 0.045 \ln\left(\frac{D}{t}\right) \tag{6.12}$$

in which (D/t) is the aspect ratio. Figure 6.10 presents a comparison between the proposed model and the finite element results.

The second parameter which has significant effect on the maximum load carrying capacity of CFT columns is length-width ratio (*L/D*) of the column. To investigate the

effect of (L/D) on the load carrying capacity, finite element analysis is performed on the thick-wall (i.e., D/t>20) square and circular CFT columns with length-width ratio of 3 to 25. Table 6.3 shows the details and the results obtained from the finite element analysis for square and circular columns. As can be seen, the level of decrease in the maximum stress is more significant in longer columns. However, the degree of reduction is constant for shorter columns up to a certain (L/D) ratio (i.e., $L/D<7$ for square columns and $L/D<10$ for circular columns). Therefore, the square columns with L/D less than or equal to 7 can be considered as short columns. In the case of circular columns, the limit length-width ratio is found to be 10. The reduction factor of steel tube due to the effect of length-width ratio (R_2) is defined as:

$$R_2 = \frac{F_{sy}}{F_y} \tag{6.13}$$

Interestingly, it is found that the maximum difference in R_2 for circular and square columns is less than 3% which is observed in shorter columns. To consider the effect of length-width ratio, the following expression for R_2 is proposed:

$$R_2 = 0.59 + \frac{0.38}{1+\left(\frac{L/D}{22.19}\right)^{3.93}} \tag{6.14}$$

in which (L/D) is the length-width ratio. As shown in Figure 6.11, the proposed model can accurately predict the effect of length-width ratio on the maximum stress of steel tube in CFT columns.

6.5 Ultimate Load Carrying Capacity of Axially Loaded CFT Columns

The determination of ultimate load of a column subjected to axial load is essentially a stability problem in which the effect of inelastic action must be considered. It is generally accepted that the tangent modulus theory is the best method for determining the ultimate load of a column fabricated from a single homogeneous material when it is loaded into the inelastic range. The tangent modulus formula for the ultimate buckling stress (f_u) of a column is given by:

$$f_u = \frac{\pi^2 E_t}{\left(\frac{KL}{r}\right)^2} \tag{6.15}$$

where E_t is the value of tangent modulus at this stress, KL is the effective length and r is the radius of gyration.

As discussed in Chapter Two, the tangent modulus method is not applicable to CFT columns in which two different materials have been used for their fabrication. In addition, as shown in Figure 4.12b in Chapter 4, E_t for steel tube has a negative value at the peak load. Moreover, the stress-strain properties of concrete core and steel tube vary with changes in the aspect ratio and cross-sectional shape. Therefore, for a CFT column

constructed from two different materials with different stress-strain relationships, the ultimate load carrying capacity can not be obtained using the tangent modulus method.

With the knowledge of maximum compressive stresses in the concrete core and steel tube, the ultimate load carrying capacity of CFT columns can be obtained easily by adding the maximum capacity of the concrete core and the steel tube. Hence, the maximum axial capacity of CFT columns (P_{CFT}) can be calculated as:

$$P_{CFT} = A_s F_{sy} + A_c f_{cc}^{'} \tag{6.16a}$$

where,

$$F_{sy} = R_1 R_2 F_y \tag{6.16b}$$

in which R_1 and R_2 are reduction factors indicating the effect of aspect ratio and length-width ratio, respectively. A_s and F_y are the cross sectional area and normal yield stress of steel tube, respectively. A_c and $f_{cc}^{'}$ are cross sectional area and maximum confined compressive stress of concrete core, respectively. F_{sy} is the maximum compressive stress that steel tube can sustain at the peak load. R_1 can be determined using Eq. (6.12) and R_2 is determined from Eq. (6.14). $f_{cc}^{'}$ is calculated using Eqs. (6.1 and 6.2). The proposed model (Eq. 6.15) is compared with numerous experimental data (Kloppel and Goder, 1957; Chapman and Neogi, 1964; Furlong, 1967; Gardner and Jacobson, 1967-1968; Knowles and Park, 1970). Tables 6.4 and 6.5 present the result of this comparison. As

demonstrated in Tables 6.4 and 6.5 the proposed procedure along with analytical model for $f_{cc}^{'}$ and F_{sy} can accurately predict the maximum axial capacity of CFT columns.

6.6 Ductility of CFT Columns under Axial Loading

One of the most significant characteristic of CFT columns, is the high ductility which makes CFTs good candidates for seismic resistance structural systems. So far, no information or formula is available which can be used to determine the ductility of CFT columns. Figure 6.12 presents a typical axial load-strain relationship for CFT columns. The ductility factor can be defined as:

$$\mu_e = \frac{\varepsilon_{cu}}{\varepsilon_{cy}} \tag{6.17}$$

where, μ_e is the ductility factor, ε_{cu} is the confined ultimate strain and ε_{cy} is the yield strain of CFT column. As described in Chapter 4, the ultimate strain can be determined using energy balance approach and the level of increase in the ultimate strain is mainly affected by the aspect ratio. The ultimate strain for circular and square CFT columns with different aspect ratios and various unconfined concrete compressive strength is determined. Table 6.6 presents the relationship between the aspect ratio, confined ultimate strain and confined strain at maximum stress. As discussed earlier, the confined ultimate strain depends on aspect ratio and cross-sectional shape. Interestingly, it can be seen that the ultimate strain is 3 to 4 times of strain at the maximum stress. Therefore,

the ultimate strain can be obtained using Eqs (6.7 and 6.8) by multiplying them by 3.0, which is conservative for columns with larger aspect ratio and has good accuracy for columns with smaller aspect ratio.

$$\varepsilon_{cu} = 3.0\varepsilon_o \left(1 + \frac{3.51}{\left(\frac{D/t}{60}\right)^4} \right) \qquad \text{for square columns} \qquad (6.18)$$

$$\varepsilon_{cu} = 3.0\varepsilon_o \left(1 + \frac{4.40}{\left(\frac{D/t}{100}\right)} \right) \qquad \text{for circular columns} \qquad (6.19)$$

Figures 6.13 and 6.14 present the axial load-strain relationship for square and circular columns with different aspect ratio. Interestingly, it is found that the yield strain for CFT columns with different aspect ratio is the same, and it can be seen from Figures 4.11a and 4.11b in Chapter 4 that the yield strain is equal to the yield strain of steel tube. Therefore,

$$\varepsilon_{cy} = \varepsilon_y = \frac{F_y}{E_s} \qquad (6.20)$$

where, ε_y and F_y are the yield strain and yield stress of steel tube, respectively. E_s is the elastic Young modulus of steel tube. Hence, the ductility factor of CFT columns can be calculated as follows:

$$\mu_e = 3.0\frac{E_s\varepsilon_0}{F_y}\left(1+\frac{3.51}{\left(\frac{D/t}{60}\right)^4}\right) \qquad \text{for square columns} \qquad (6.21)$$

$$\mu_e = 3.0\frac{E_s\varepsilon_0}{F_y}\left(1+\frac{4.40}{\left(\frac{D/t}{100}\right)}\right) \qquad \text{for circular columns} \qquad (6.22)$$

where ε_o is the unconfined strain at maximum stress of concrete core (e.g. 0.002) and *(D/t)* is the aspect ratio. As can be seen, the value of ductility factor depends on the material properties of steel tube and concrete core as well as geometry of the column. For example, the ductility factor is in the range of 10 to 25 for a square CFT column with F_y = 43.0 ksi, E_s = 30000 ksi and ε_0=0.002.

6.7 Flexural Capacity of CFT Columns

The nominal flexural strength is assumed to be reached when the strain in extreme compressive fiber is equal to confined ultimate strain (ε_{cu}). Based on the results obtained from extensive finite element analysis, a practical and rational method is developed to predict the flexural capacity of CFT columns. Similar to the method used for RC columns, equivalent stress blocks are defined for the concrete core and steel tube. The detailed discussion of the proposed method is presented in the following sections.

6.7.1 Equivalent Concrete Stress Block

With the knowledge of stress-strain properties of concrete core (Eqs. 6.9 and 6.19), the flexural capacity of concrete core can be obtained using fiber method. However, a simple and more practical method is more desirable for day to day use in design. Hence, equivalent stress blocks are defined for the compressive stress in concrete core and steel tube and also for tensile force provided by steel tube. Figure 6.15 presents a schematic view of stress distribution and equivalent stress block at the cross section. As can be seen, the width of the stress block is equal to maximum confined compressive stress ($f_{cc}^{'}$) and the depth (a_c) is a percentage of distance of neutral axis from the exterior compressive fiber:

$$a_c = \beta_{1c} X_n \tag{6.23}$$

where a_c is the depth of stress block and X_n is the distance of neutral axis from the compressive exterior fiber which will be obtained by equating the total compressive and tensile forces provided by the steel tube and the concrete core. β_{1c} is the concrete depth-neutral axis ratio, a positive number less than one. Table 6.7 gives the values of β_{1c} for concrete core with different unconfined concrete compressive strengths and various aspect ratios. As can be seen, β_{1c} has a value of 0.80 for all cases. In the case of reinforced concrete columns, the depth-neutral axis ratio has a value of 0.85 for concrete with $f_c^{'} \leq 4000$ psi, and is reduced continuously by 0.05 for each 1000 psi of strength in excess of 4000 psi. The reduction in depth-neutral axis ratio for high strength concrete is

mainly due to the less favorable shape of stress-strain curve of that concrete. However, in the case of CFT columns, the concrete core exhibits a ductile stress-strain relationship even for high strength concrete due to the confining effect of steel tube. Therefore, the value of β_{1c} can be fixed at 0.80 for all cases.

The resultant compressive forces of the actual and equivalent stress blocks have the same magnitude. The compressive force in concrete core (C_c) can be expressed as:

$$C_c = a_c b f_{cc}^{'} \qquad \text{for square columns} \qquad (6.24)$$

$$C_c = \left(\frac{D}{2}\right)^2 \left(\theta - \frac{1}{2} Sin(2\theta)\right) f_{cc}^{'} \qquad \text{for circular columns} \qquad (6.25)$$

where,

$$\theta = Cos^{-1}\left(1 - \frac{2a_c}{D}\right) \qquad (6.26)$$

in which, a_c is the depth of equivalent stress block. b and D are the cross-sectional width and diameter, respectively. $f_{cc}^{'}$ is the maximum confined compressive stress in concrete core.

6.7.2 Compressive and Tensile Stress in Steel Tube

The stress distribution at the compression and tensile fiber of steel tube is not uniform. Moreover, the pattern of stress distribution in circular and square columns are different In the case of square columns, the corners sustain a lower stress than the mid-sides (see

Figure 5.16, Chapter 5). Even though the cross-sectional stress distribution is not uniform, a practical method to calculate the compressive and tensile forces of steel tube is to define an equivalent stress block. Figure 6.16 presents a schematic view of stress distribution and equivalent stress block at the cross section for the steel tube. The steel equivalent stress block in compression has a width of $\alpha_c F_y$ and a depth of $a_s = \beta_{1s} X_n$. The depth of equivalent stress block in tension (h_s) is equal to $h_s = \beta_{1s}(D - X_n)$ and its width is equal to $\alpha_t F_y$.

It is found that α_c has a value of 0.92 and 1.0 and α_t is equal to 0.95 and 1.0 for square and circular columns, respectively. The value of β_{1s} (steel depth-neutral axis ratio) is found to be 0.85 for square columns and 0.80 for circular columns. X_n is the distance of neutral axis from the exterior compression fiber and it can be determined by equating the total compressive forces (C) to steel tensile force (T). In the following sections the determination of X_n and flexural capacity of square and circular columns are discussed.

6.7.3 Flexural Strength of Square Columns

The distance of neutral axis from the extreme compressive fiber can be obtained as follows:

$$C = T \tag{6.27}$$

The tensile force of steel tube at cross section in square sections is expressed as:

$$T = T_f + T_w \tag{6.28}$$

$$T_f = \alpha_t F_y b\ t \tag{6.29}$$

$$T_w = 2\alpha_t F_y t\ (h_s - t) \tag{6.30}$$

The total compressive force is provided by the concrete core (C_c) which is expressed by Eq. (6.24) and steel tube (C_s) which is expressed as:

$$C = C_c + C_s \tag{6.31}$$

$$C_s = C_f + C_w \tag{6.32}$$

$$C_f = \alpha_c F_y b\ t \tag{6.33}$$

$$C_w = 2\alpha_c F_y t\ (a_s - t) \tag{6.34}$$

where T_f and T_w are the tensile forces provided by flange and web of steel tube, respectively. C_f and C_w are the compressive forces provided by flange and web of steel tube, respectively. C_s is the compressive force in concrete core. If the expressions for a_c, a_s and h_s are substituted in Equations (6.24, 6.28-6.34), then:

$$T = \alpha_t F_y t\left(b + 2\beta_{1s}\left(D - X_n\right) - 2t\right) \tag{6.35}$$

$$C = \beta_{1c} b X_n f_{cc}^{'} + \alpha_c F_y t\left(b + 2\beta_{1s} X_n - 2t\right) \tag{6.36}$$

By equating Equations (6.35) and (6.36), the location of neutral axis can be found:

$$X_n = \frac{2\alpha\beta_{1s} F_y tD + (\alpha_t - \alpha_c) F_y tb - 2(\alpha_t - \alpha_c) F_y t^2}{\beta_{1c} b f_{cc}^{'} + 2(\alpha_t + \alpha_c)\beta_{1s} F_y t} \tag{6.37}$$

For simplicity and considering the fact that the difference between α_t and α_c is very small (i.e., 0.03), we can assume that $\alpha = \alpha_t = \alpha_c = 0.92$. It should be noted that b is equal to D for square sections. Therefore, Eq. (6.37) can be expressed as;

$$X_n = \frac{2\alpha\beta_{1s} F_y tD}{\beta_{1c} D f_{cc}^{'} + 4\alpha\beta_{1s} F_y t} \tag{6.38}$$

or,

$$X_n = \frac{1.564 F_y tD}{0.8 D f_{cc}^{'} + 3.128 F_y t} \tag{6.39}$$

Therefore, with the knowledge of location of neutral axis, the depth of steel and concrete stress blocks (a_s and a_c) is determined and the flexural capacity of the square section can be calculated as follows:

$$M = C_f(D-t) + C_w\left(D - \frac{a_s - t}{2}\right) + C_c\left(D - \frac{a_c - t}{2}\right) \tag{6.40}$$

Since no experimental data is available on pure bending of CFTs, the proposed model is compared with finite element results. Table 6.8 presents the result of this comparison. As can be seen, the proposed model shows good agreement with results obtained from finite element analysis.

6.7.4 Flexural Strength of Circular Columns

In the case of circular columns, the compressive force in the concrete core is determined using Eqs (6.25 and 6.26). Therefore, the tensile and compressive forces in the steel tube and concrete core can be expressed as:

$$T = DtF_y Cos^{-1}\left(1 - 2\beta_{1s}\left(1 - \frac{X_n}{D}\right)\right) \tag{6.41}$$

$$C_s = DtF_y Cos^{-1}\left(1 - \frac{2\beta_{1s}X_n}{D}\right) \tag{6.42}$$

$$C_c = \left(\frac{D}{2}\right)^2 f'_{cc}\left(Cos^{-1}\left(1 - \frac{2\beta_{1c}X_n}{D}\right) - \frac{1}{2}Sin\left(2Cos^{-1}\left(1 - \frac{2\beta_{1c}X_n}{D}\right)\right)\right) \tag{6.43}$$

and

$$T = C_c + C_s \tag{6.44}$$

By solving Eq. (6.44) X_n can be obtained. It is difficult to have a closed form solution to Eq. (6.44), therefore a simple computer program needs to be developed.

6.8 Concluding Remarks

A parametric study is performed using three-dimensional non-linear finite element analysis to identify the response of CFT columns under axial and combined loadings. Based on this study the following conclusion can be reached.

1. It is found that the aspect ratio, unconfined compressive strength of concrete core and cross-sectional shape have significant effect on the response of CFT columns. The confinement effect in circular columns is higher than in square columns due to a more uniform stress distribution. Concrete core with a lower unconfined compressive strength exhibits higher confinement ratio than higher strength concrete. The amount of increase in the maximum compressive strength of concrete core mainly depends on the aspect ratio, unconfined concrete compressive strength and cross-sectional shape. The strain at maximum stress depends on the aspect ratio and cross-sectional shape.
2. The important stress-strain properties of concrete core such as peak stress and peak strain is identified. Based on the results obtained relating confinement effect and aspect ratio, and between confinement ratio and unconfined compressive strength of concrete, analytical models are proposed to determine the maximum compressive stress and peak-strain in concrete core for circular and square CFTs.
3. In the experimental programs, the stress-strain relationship of concrete core can not be determined directly. Based on the proposed analytical model for confined stress-strain

curve of concrete core, the response of concrete core can entirely be determined. The accuracy of the proposed model is checked with finite element results. It should be noted that the finite element model has already been verified with experimental data.

4. The maximum compressive stress in the steel tube depends on the aspect ratio and length-width ratio. It is found that maximum compressive capacity of concrete core is independent of the normal yield stress of steel tube. The effect of these two parameters (i.e., D/t and $f_c^{'}$) on the maximum compressive capacity of the steel tube is identified.
5. The ultimate axial capacity of CFT columns is not well predicted. The current design specifications underestimate the load carrying capacity of CFTs. Therefore, developing an accurate and practical design procedure is essential. An analytical model is proposed to determined the ultimate axial capacity of CFT columns. It is shown that the proposed model can predict the load carrying capacity of CFTs with a high accuracy and it is easy to use.
6. One of the advantages of CFT columns is their high ductility. It is important that the ductility factor of CFTs can be determined analytically. The ductility factor for CFT columns subjected to axial loading is formulated as a function of material properties of steel tube and concrete core and geometry of the columns.
7. The ultimate flexural capacity of CFT columns is not well defined due to lack of knowledge on the cross-sectional stress distribution and overall behavior of CFTs under lateral loading. A difference up to 100% is observed between the experimental data and different design procedures (Sugano, et al., 1992). Current models are not

successful in predicting the flexural strength of CFTs, since the confinement effect and ductility are ignored (as discussed in chapter two). A practical method is developed to determined the maximum flexural capacity of CFT columns in which the confining effect of steel tube and large ductility of concrete core are considered. The proposed model is validated with results obtained from finite element analysis and it is easy to use.

CHAPTER 7

SUMMARY AND CONCLUSIONS

7.1 Summary

The overall objective of this study is to investigate the non-linear response of CFT columns subjected to axial and combined loadings. Experimental investigations have played significant role in research on CFT columns. However, experimental programs are expensive and time costuming. Moreover, they can not provide as much information about different aspects of response as revealed by numerical simulation. Therefore, there is an essential need to develop a reliable finite element model to evaluate the overall response of CFT columns. The finite element model allows the study of virtually limitless combinations of the parameters of interest.

A three-dimensional finite element model is developed for CFT columns. The concrete core is modeled with 3-D solid elements. The steel tube is modeled using shell elements which allow large deformation analysis. Gap elements are used to model the interaction between concrete and steel interface. The von Mises plasticity model with kinematic hardening is used for the steel tube. Concrete core has a complex behavior in CFT columns. To capture the actual response of concrete core under different loading conditions, a realistic material model needs to be employed. Among the different concrete material models, Pramono-William model has the ability to capture the response of concrete under triaxial state of stress with high accuracy. The material model is

implemented in the finite element software as a user subroutine and calibrated using substantial published test data.

Verification of the developed finite element model is made by analyzing sixteen CFT columns tested by different researches (Tomii et. al., 1977; Okamoto et al, 1988 and Sugano et al, 1992). The finite element analysis has successfully captured the axial load-deformation and bending moment-deflection response along with important features such as the development of triaxial state of stress in the concrete core, the decrease in the yield strength of steel tube due to biaxial effect and local buckling of steel tube.

A parametric study is performed on CFT columns subjected to axial and lateral loadings. The analysis includes a wide range of aspect ratios, concrete unconfined compressive strengths, steel normal yield stresses and slenderness ratios. Results of the parametric studied is used to develop practical design procedures to determine the axial and flexural capacity of CFT columns.

7.2 Conclusions

Based on the detailed finite element analysis the characteristics and behavior of CFT columns under axial and combined loading are explained and analytical models are developed to predict the different features of response. The results obtained can be summarized as follows:

1. The mechanism of load transfer from steel tube to the concrete core and redistribution of load from concrete core to steel tube is identified. There are three distinguished parts in the load transfer mechanism. The first part starts from the beginning of

applying load and ends when the steel tube yields. During this stage of loading, the steel tube sustains most of the load until it yields. In the second part, after the steel tube yields there is load transfer from steel tube to the concrete core. At this stage, the steel tube exhibits a softening type of behavior due to the effect of biaxial state of stress in steel tube until the concrete core reaches its maximum compressive capacity. Finally, there is a load redistribution from concrete core to the steel tube. In this stage of loading steel tube shows hardening behavior and concrete core exhibits softening behavior.

2. The cross-sectional stress distributions of square and circular CFTs under axial loading are described. It is found that the stress distribution in square sections is not uniform (i.e., center and corners exhibit a higher compressive capacity than the sides). Therefore, an equivalent axial stress-strain relationship for concrete core is introduced. The equivalent confined axial stress is defined as the concrete core axial force divided by its cross-sectional area. It is found that as the aspect ratio increases the confinement ratio decreases. The changes in the confinement ratio is different in circular and square columns. In the case of square columns, the rate of increase in confinement ratio changes significantly when the aspect ratio decreases from 100 to 25. In circular columns, the change in confinement ratio is more gradual for the same range of aspect ratio. Interestingly, it is observed that for higher strength concretes the confinement ratio is smaller if the same aspect ratio is considered (e.g. $f_c^{'} = 2.0$ ksi $\rightarrow (f_{cc}^{'} / f_c^{'}) = 1.91$; $f_c^{'} = 5.0$ ksi $\rightarrow (f_{cc}^{'} / f_c^{'}) = 1.32$) and it is independent of normal yield strength of steel tube. In the case of circular columns,

the confinement ratio is higher than the square columns. Based on the results obtained from parametric study, analytical models are proposed to predict the maximum confined compressive stress of concrete core in circular and square CFT columns.

3. The results obtained from finite element analysis have shown that for CFT columns with the same aspect ratio and concrete core with various uniaxial compressive strengths, the confined strain at maximum stress is almost the same. This means that the unconfined compressive strength of concrete has no significant effect on the value of confined strain at peak stress if the same unconfined strain at maximum stress is assumed. Based on the results obtained relating aspect ratio and unconfined strain at maximum stress with confined strain at maximum stress, analytical models are proposed.
4. The ultimate strain of concrete core is determined using energy balance method. It is found that only aspect ratio and unconfined strain at maximum stress have effect on the confined ultimate strain. As the aspect ratio decreases or by increasing the unconfined strain at the maximum stress the concrete core ultimate strain increases. Based on the results obtained relating confined ultimate strain and aspect ratio, and between confined ultimate strain and unconfined strain at the maximum stress, an analytical model is proposed to determine the confined ultimate strain in concrete core.
5. Based on the results obtained from finite element analysis and with the knowledge of confined peak stress and confined strain at peak stress, an analytical model is proposed to predict the stress-strain relationship of concrete core in CFTs. The

proposed model shows high accuracy for concrete core in circular and square columns.

6. The possibility of local buckling in steel tube is investigated. The initiation of local buckling can be identified by examination of the contact forces between steel tube and concrete core. In the area that local buckling occurs, the contact forces are released linearly to zero. However, the force increases in the other areas. Separation of steel tube from concrete core results in local buckling of steel tube. The concrete core maintains its capacity until the separation is completed. Local buckling of steel tube depends mainly on the wall thickness of steel tube. It is found that in square columns with aspect ratios larger than 78, local buckling of steel tube occurs before the concrete reaches its maximum compressive capacity. In the case of circular columns, the limiting value for aspect ratio is 95.
7. An analytical model is proposed to determined the ultimate axial capacity of CFT columns. The effect of important parameters such as confinement of concrete core, biaxial effect in steel tube and slenderness ratio are considered in the proposed model. The proposed model is easy to use. The results obtained from the present model are compared with experimental data. It is shown that the proposed model can predict the load carrying capacity of CFTs with high accuracy and it is easy to use.
8. The flexural response of CFT columns are different from RC columns since the concrete core exhibits larger compressive strength and higher ductility. The cross-sectional stress distribution is not uniform when the CFT columns are subjected to lateral loading. Development of the three-dimensional finite element model in this

study enables determination of the stresses which otherwise would have not been possible using a two-dimensional model or experimental investigations. The complex pattern of stress distribution at cross section is identified. Based on the cross-sectional stress distributions, equivalent stress blocks are defined for stresses in concrete core and steel tube. To characterize the concrete equivalent stress block, it is assumed that the CFT column reaches its maximum flexural capacity when the compressive strain in extreme fiber of concrete core is equal to confined ultimate strain. A practical method is developed to determined the flexural capacity of CFT columns. The proposed method considers the effect of confinement (i.e., higher concrete compressive stress and larger ductility) and it is easy to use.

7.3 Recommendations for Further Research

The following items could be considered for further research:

1. Strong consideration should be given to the investigation of seismic response of CFT columns. A realistic hysteresis model for CFTs could be developed using the present finite element model and with the help of experimental data. Effect of different parameters such as level of axial force, aspect ratio, cross-sectional and strength of concrete core on the seismic response of CFTs needs to be investigated.
2. Simple analytical model is needed to study the seismic performance of structural systems with CFT columns.

3. Load transfer mechanism between connections and columns could be studied using the present finite element model. Standardized and cost effective connections could be developed based on the obtained results.
4. The present finite element model can be used to investigate the flexural behavior of CFT columns under biaxial bending. Interaction diagrams (i.e., axial load-bending moment curves) can be developed using the results of the present study. The proposed stress-strain relationship for concrete core can be combined with fiber method through a simple computer program. A series of analysis is required to establish the interaction diagrams.

TABLES

Table 2.1 List of tested specimens.

Specimen	D (mm)	t (mm)	d/t	L (mm)	N_{axial} (MPa)	Mortar (MPa)
SPM-1	175	3.2	54.7	1700	0	19.62
SPM-2	175	3.2	54.7	1700	(1/3)Fc	9.81
SPM-3	175	3.2	54.7	1700	(1/6)Fc	No Mortar
SPM-4	175	4.5	38.9	1700	0	19.62
SPM-5	175	4.5	38.9	1700	(1/3)Fc	9.81
SPM-6	175	4.5	38.9	1700	(1/6)Fc	No Mortar
SPM-7	175	6.0	29.2	1700	0	19.62
SPM-8	175	6.0	29,.2	1700	(1/3)Fc	9.81
SPM-9	175	6.0	29.2	1700	(1/6)Fc	No mortar

*Fc = estimated strength of concrete, 98.1 MPa

Table 2.2 Measured dimension of specimens without stiffeners.

Specimen	b (mm)	B (mm)	A_S (mm^2)	A_c (mm^2)	L (mm)	r (mm)	b/t	R, with k=4
U9-S	197	213	3.654	-	592	81.0	43.7	0.844
U9-C	196	213	3.654	37.100	592	29.5	43.7	0.839
U12-S	263	279	4.842	-	789	108.0	58.3	1.126
U12-C	263	279	4.842	66.800	790	36.2	58.3	1.126
U12-HC	263	279	4.842	66.800	789	36.2	58.3	1.126
U15-S	329	345	6.030	-	988	118.0	73.0	1.409

Table 2.3 Measured dimension of specimens with stiffeners.

Specimen	b (mm)	B (mm)	b_S (mm)	t_S (mm)	A_s (mm^2)	A_c (mm^2)	r (mm)	γ_t/γ_{req}	R, with k=16
S75-S(1)	328	344	38.1	4.36	6.714	-	132.0	1.11	0.70
S75-C(1)	328	345	38.0	4.36	6.714	104.6	43.3	1.11	0.702
S75-C(0.35)	329	344	25.1	4.34	6.480	105.4	43.1	0.35	0.705
Note: L=1.36 mm									

*U refers to the column without stiffeners and, S refers to the columns with stiffeners.
**Numbers following U or S related to the aspect ratio.
***S or C represents hollow steel tube and concrete-filled columns respectively.

Table 2.4 Measured dimensions and details of tested columns.

Column No.	Diameter (in.)	Thickness (in.)	D/t	Shear studs	f_c' (ksi)	f_y (ksi)
1	8	.109	73	No	4.6	50
2	8	.109	73	No	4.6	50
3	8	.109	73	Yes	4.6	50
4	8	.075	107	No	4.6	41
5	8	.075	107	No	7.0	41

Table 2.5 Comparison between different design codes and experimental data for ultimate load carrying capacity of CFT columns

Axial Load (kN)	Moment (kNm)			
	LRFD	SSLC	ACI	Experiment*
1500	162.69	212.86	303.70	408.00
2500	113.89	172.19	241.33	423.00
3500	63.72	126.00	165.41	307.77
Average	71%	57%	42%	—

*Experimental data was adopted from Sugano and Nagashima, 1992.

Table 3.1 Material parameters for Pramano-William's concrete model

f_c' (ksi)	3.0	5.3	9.0	13.5
f_t' (ksi)	0.35	0.44	0.72	0.97
E (ksi)	2400	2800	3780	4630
A_h	-.0017	-.0017	0.02142	0.00745
B_h	-0.0140	-0.0140	-0.0320	-0.0360
C_h	0.0020	.0020	0.00250	0.0025
A_s	24.00	24.00	24.00	24.00
B_s	-2.00	-2.00	-4.00	-4.00
m_0	8.45	11.96	12.42	13.85

Table 3.2 Buckling load for the square thin plate.

Critical Edge Load (kips/in.)		
F.E Analysis (Geometric Imperfections)	F.E. Analysis (Plate & Concrete block)	Exact Solution (Timoshenko)
90.52	90.79	90.28

Table 3.3 Details of tested columns in pure axial compression tests.

Column	t (in.)	A_s (in.^{2})	A_c (in.^{2})	F_y (ksi)	f'_c (ksi)	E_c (ksi)	L (in.)
Square 6x6 in.	0.170	3.935	31.065	43.0	2.0	2470	24.0
	0.170	3.935	31.065	43.0	2.0	2470	30.0
	0.170	3.935	31.344	43.0	4.0	2860	18.0
	0.078	1.843	32.770	50.0	2.4	2700	24.0
	0.078	1.843	32.770	50.0	2.4	2700	30.0
Circular D=6.0 in.	0.170	3.082	24.662	40.0	4.0	3500	24.0
	0.078	1.471	25.964	49.0	3.5	3280	24.0
	0.170	3.082	24.662	40.0	4.2	3600	18.0
	0.118	2.285	25.220	42.0	4.2	3600	18.0
	0.170	3.082	24.662	40.0	3.2	3160	18.0

Table 3.4 Details of tested columns in combined loading tests.

Okamoto (1988)						
Column	D (in.)	t (in.)	L (in.)	f_c' (ksi)	F_y (ksi)	Axial Load (kips)
Square	6.89	0.039	67.0	14.0	43.0	110.0
	6.89	0.177	67.0	14.0	43.0	0
Sugano 1992						
Square	9.84	0.315	67.0	5.5	50.0	335.0
	9.84	0.315	67.0	5.5	50.0	558.0
	9.84	0.315	67.0	5.5	50.0	780.0
Circular	11.80	0.315	79.0	5.5	58.0	400.0
	11.80	0.315	79.0	5.5	58.0	600.0
	11.80	0.315	79.0	5.5	58.0	850.0

Table 4.1 Confined ultimate strain for concrete core in CFT columns.

Square Columns						
D/t	10	20	25	35	50	75
ε_{cu}	0.0320	0.0275	0.0249	0.0225	.0215	0.0204
Circular Columns						
ε_{cu}	0.0341	0.0306	0.0270	0.0245	0.0222	0.0211

Table 5.1 Stress at top and bottom corners of steel tube

Square Columns						
D/t	10	20	31.25	50	85	100
σ_{sc} *(ksi)*	44.6	41.11	37.94	37.23	35.78	35.97
σ_{st} *(ksi)*	45.78	43.50	43.39	44.11	44.52	42.69
σ_{sc} / F_y	0.83	0.76	0.70	0.69	0.65	0.67
σ_{st} / F_y	0.85	0.81	0.80	0.81	0.82	0.80

Table 6.1 Values for parameters effecting maximum confined compressive stress.

f_c' (psi)	2000	2600	4000	5300	6000	9000
A	0.738	0.647	0.508	0.274	0.201	0.115
B	1.342	1.229	1.032	0.814	0.734	0.459
E	62.80	58.97	51.10	52.82	52.64	51.06
F	221.23	163.75	107.45	63.76	52.67	24.20

Table 6.2 Effect of aspect ratio on maximum yield stress of steel tube.

D/t	10	20	25	35	75	100
$(F_{sy}/F_y)\%$	99.6	97.2	95.7	93.3	90.4	89.9

Table 6.3 Effect of length-width ratio on maximum yield stress of steel tube

Square Column 0.15x3x3 (in.)					
L (in.)	D (in.)	t (in.)	L/D	F_{sy} (ksi)	F_{sy}/F_y
10	3.0	0.15	3.34	45.31	0.96
20	3.0	0.15	6.67	45.31	0.96
30	3.0	0.15	10	45.12	0.95
45	3.0	0.15	15	43.85	0.93
55	3.0	0.15	18.34	42.34	0.90
70	3.0	0.15	23.34	40.00	0.86
Circular Columns 0.23x3.5 (in.)					
10	3.5	0.23	2.85	45.92	0.98
20	3.5	0.23	5.70	45.70	0.97
30	3.5	0.23	8.57	45.67	0.97
45	3.5	0.23	12.85	44.15	0.94
55	3.5	0.23	15.71	42.75	0.91
70	3.5	0.23	20	41.04	0.87

Table 6.4 Comparison between experimental and the proposed model.

Circular Columns										
Kloppel and Goder, 1957										
L (in.)	D (in.)	t (in.)	L/D	f_c' (ksi)	F_y (ksi)	F_{sy} (ksi)	f_{cc}' (ksi)	P_{cft} (kips)	P_t (kips)	P_t/P_{cft}
55.91	3.74	0.492	14.95	2.94	39.83	35.9	5.19	211.2	212.9	1.008
55.91	3.74	0.502	14.92	2.94	39.83	35.9	5.19	213.9	210.8	0.985
55.91	3.74	0.488	14.92	2.94	39.83	35.9	5.19	209.9	203.9	0.971
33.86	3.74	0.496	9.00	2.94	39.83	37.5	5.19	219.0	228.0	1.041
33.86	3.74	0.144	9.00	3.62	56.0	50.0	5.54	132.4	147.5	1.114
77.95	3.74	0.504	20.80	2.94	40.3	34.4	5.19	204.4	199.3	0.975
77.95	3.74	0.492	20.80	2.94	39.9	34.0	5.19	202.7	203.9	1.005
55.91	3.74	0.152	14.95	3.62	47.4	40.8	5.56	122.4	127.4	1.048
55.91	3.74	0.154	14.94	3.62	56.0	47.9	5.56	134.8	136.2	1.010
77.95	3.74	0.148	20.80	3.62	47.0	38.0	5.56	115.3	120.6	1.045
77.95	3.74	0.144	20.80	3.62	56.0	45.3	5.56	127.4	127.2	0.998
87.4	8.05	0.162	10.27	3.32	43.4	37.0	4.97	416.7	412.4	0.989
87.4	8.05	0.159	10.27	4.32	41.8	35.7	5.74	451.8	503.3	1.113
87.4	8.05	0.238	10.27	3.32	56.4	49.2	5.17	520.2	553.4	1.063
87.4	8.05	0.256	10.27	4.32	42.8	38	6.03	510.7	630.3	1.234
87.4	8.05	0.248	10.27	4.32	58.7	51.0	6.03	594.7	659.2	1.108

Table 6.4 Comparison between experimental and the proposed model (continued).

77.95	3.74	0.152	20.8	3.49	48.2	39.2	5.45	117.7	112.0	0.952
77.95	3.74	0.134	20.8	3.49	48.9	39.1	5.45	110.6	106.3	0.961
41.34	4.764	0.144	8.67	3.06	42.8	36.4	4.96	153.9	156.3	1.015
41.34	4.764	0.215	8.67	3.06	49.9	45	5.09	213.6	224.8	1.053
90.95	4.764	0.146	19.09	3.06	42.8	34.7	4.96	150.5	144.0	0.9956
Chapman and Neogi, 1964										
74.00	14.0	0.440	5.28	5.52	51.5	48.0	6.91	1835	2576	1.403
82.00	14.00	0.314	5.85	3.40	51.5	46.5	5.30	1372	1671	1.217
28.00	5.00	0.064	5.60	9.60	53.8	47.0	9.86	230.0	289.0	1.256
28.00	5.00	0.116	5.60	9.60	53.8	48.5	9.97	264.2	293.5	1.110
Furlong, 1967										
36.00	4.50	0.125	8.00	4.20	60.0	52.2	5.88	173.4	170.0	0.980
36.00	5.00	0.095	7.20	5.10	42.0	36.3	6.35	157.0	148.0	0.942
36.00	6.00	0.061	6.00	3.75	48.0	39.6	4.97	179.0	164.8	0.921
Gardener and Jacobson, 1967 and 1968										
60.00	4.00	0.121	15.00	4.52	87.76	72.8	6.16	176.1	180.0	1.022
60.00	4.00	0.121	15.00	4.95	87.76	72.8	6.54	180.2	184.0	1.021
41.34	4.75	0.161	8.70	4.29	65.5	57.9	6.04	228.0	245.0	1.074
41.34	4.75	0.161	8.70	4.99	65.5	57.9	6.56	235.2	260	1.105
24.00	3.00	0.068	8.00	5.93	58.69	51.8	7.04	77.4	92.0	1.188

Table 6.5 Comparison between experimental and the proposed model.

Square Columns										
Furlong, 1967										
L (in.)	D (in.)	t (in.)	L/D	f_c' (ksi)	F_y (ksi)	F_{sy} (ksi)	f_{cc}' (ksi)	P_{cft} (kips)	P_t (kips)	P_t/P_{cft}
36.00	4.00	0.084	9.00	3.40	48.0	41.7	4.55	121.4	117.8	0.970
36.00	4.00	0.125	9.00	4.18	48.0	42.5	5.72	162.4	152.0	0.935
36.00	5.00	0.189	7.20	6.50	70.0	62.0	7.80	391.0	360.0	0.921
Chapman and Neogi, 1964										
16.00	4.52	0.173	3.53	4.66	36.8	32.8	6.20	206.4	201.6	0.976
16.00	4.50	0.379	3.55	4.66	36.8	34.6	6.33	305.0	549*	1.80*
Knowles and Park, 1970										
10.00	3.00	0.133	3.34	5.92	47.0	41.9	7.36	119.1	115.0	0.965
20.00	3.00	0.133	6.64	5.92	47.0	41.0	7.36	117.6	113.7	0.966
32.00	3.00	0.133	10.67	6.53	47.0	39.0	7.80	117.8	104.0	0.882

* The tested column showed a very high compressive capacity. If it is assumed that the steel tube sustain the maximum possible load (i.e., $A_s F_y$), then the compressive stress in the concrete should be 23.0 ksi. This means that the increase in the compressive stress of concrete is almost five times of its uniaxial compressive stress which is practically impossible.

Table 6.6 Effect of aspect ratio on the confined ultimate strain.

Square Columns						
D/t	10	20	25	35	50	75
ε_{cu}	0.0320	0.0275	0.0249	0.0225	.0215	0.0204
$\varepsilon_{cu} / \varepsilon_{co}$	3.15	3.13	3.17	3.08	3.55	4.2
Circular Columns						
ε_{cu}	0.0341	0.0306	0.0270	0.0245	0.0222	0.0211
$\varepsilon_{cu} / \varepsilon_{co}$	3.28	3.25	3.14	2.95	3.46	3.58

Table 6.7 Values of depth-neutral axis ratio for concrete with different $f_c^{'}$.

β_{1c}						
$f_c^{'}$ (ksi)	D/t					
	75	50	35	25	20	10
2.0	0.787	0.815	0.803	0.817	0.827	0.808
4.0	0.824	0.828	0.821	0.801	0.801	0.794

Table 6.8 Flexural capacities obtained from F.E. results and the proposed model.

Square column 10x10 inches $F_y = 54$ ksi, $f_c^{'} = 2.0$ ksi								
D/t	$f_{cc}^{'}$ (ksi)	T (kips)	C_f (kips)	C_w (kips)	C_c (kips)	M_p (ft-k)	M_f (ft-k)	M_p/M_f
10.0	3.52	73.68	41.40	21.53	9.93	642.48	661.50	0.97
20	3.5	40.76	20.70	10.98	8.66	365.76	354.17	1.03
31.2	3.43	27.53	13.24	6.53	7.49	250.66	271.23	0.93
50.0	3.07	18.00	8.28	3.69	5.86	165.90	180.45	0.92
62.5	2.75	14.60	6.62	2.85	5.00	135.22	141.96	0.95
85.0	2.33	10.87	4.84	1.97	3.95	101.18	111.72	0.90
100.0	2.2	9.39	4.14	1.62	3.55	87.67	93.66	0.93

FIGURES

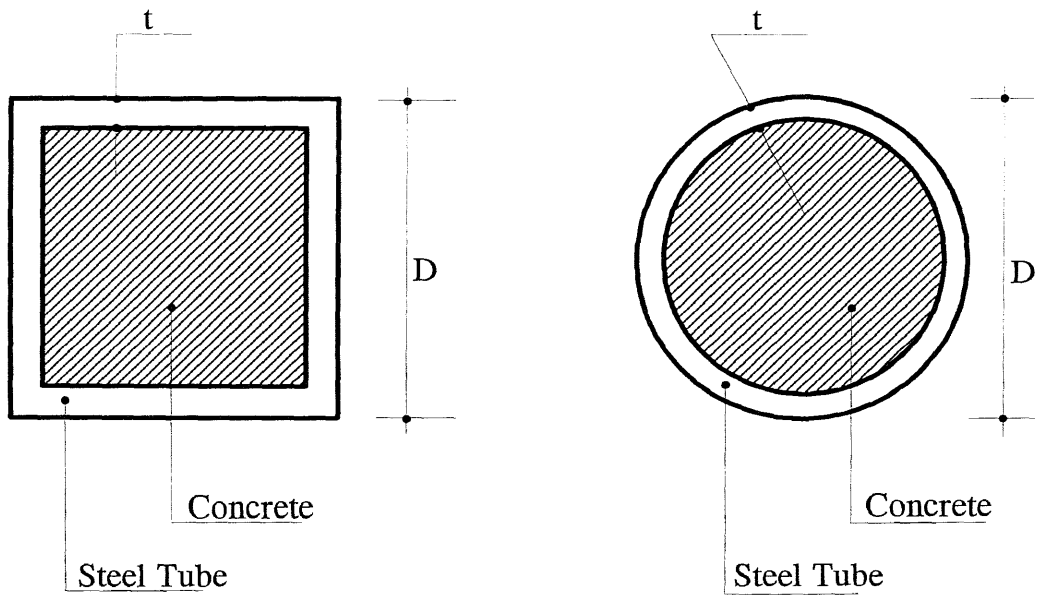

Figure 1.1 Schematic cross-sectional view of CFT, (a) square (b) circular columns.

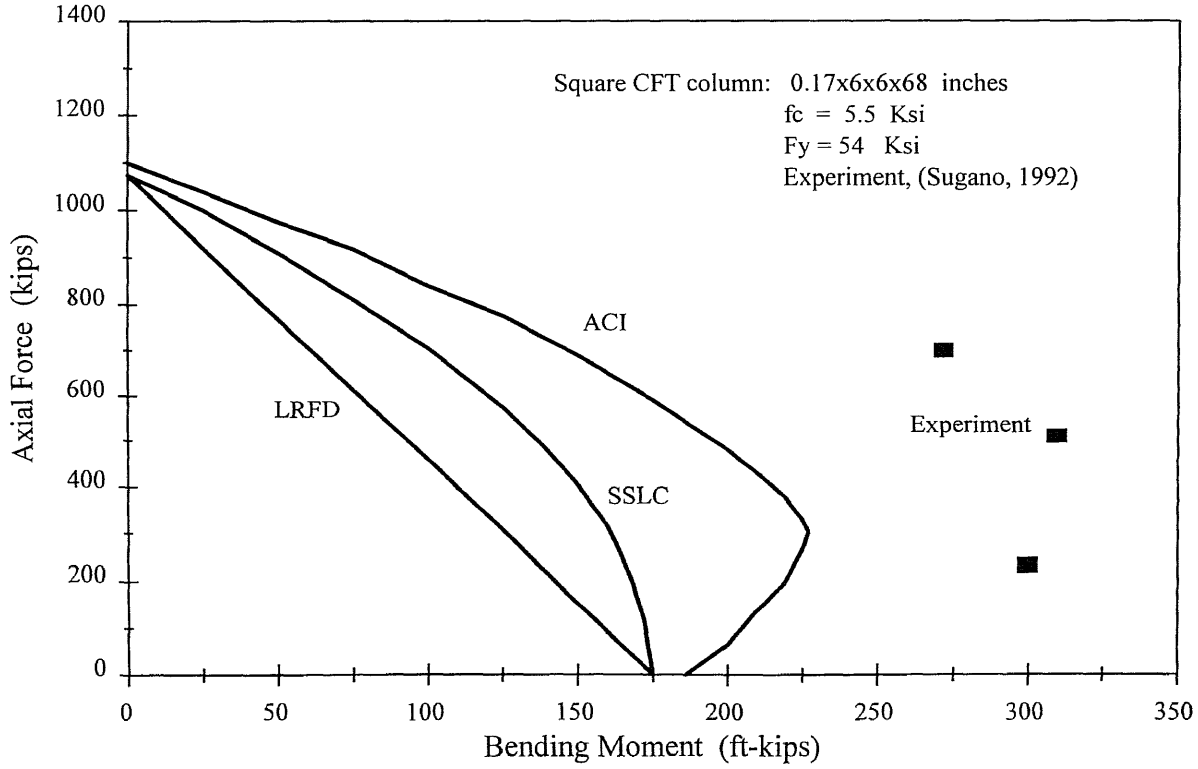

Figure 1.2 Ultimate capacity for a square CFT Column, comparison of different design codes and experiment.

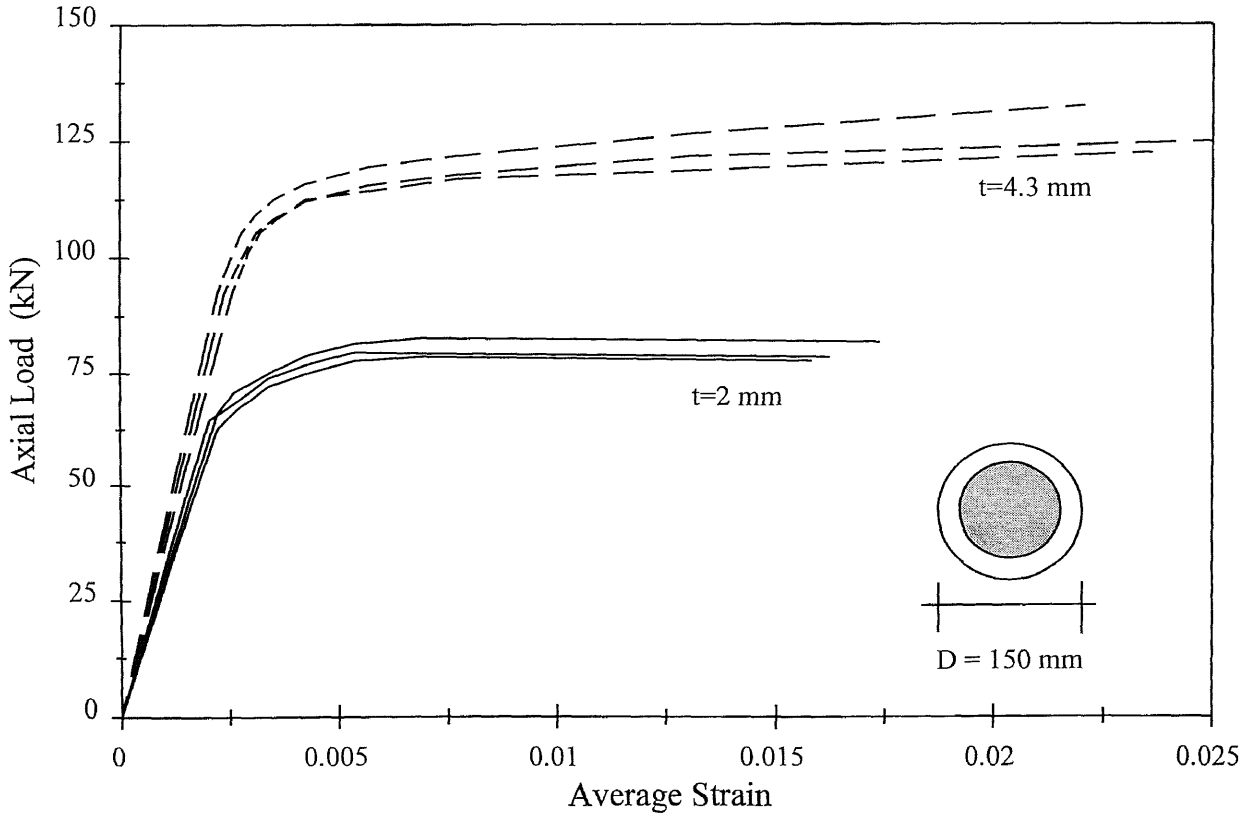

Figure 2.1a Load-strain relationships for axially loaded circular CFT columns (Tomii and Yoshimaro, 1977).

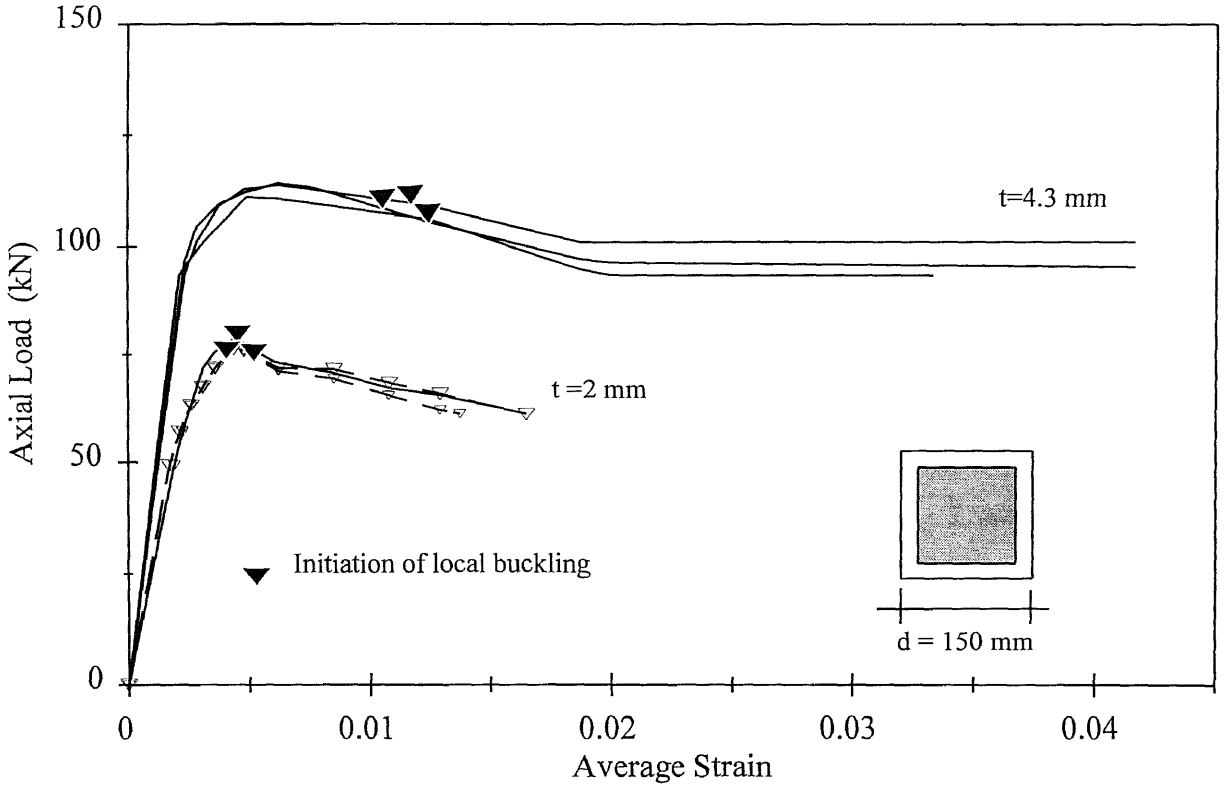

Figure 2.1b Load-strain relationships of axially loaded square CFT columns (Tomii and Yoshimaro, 1977).

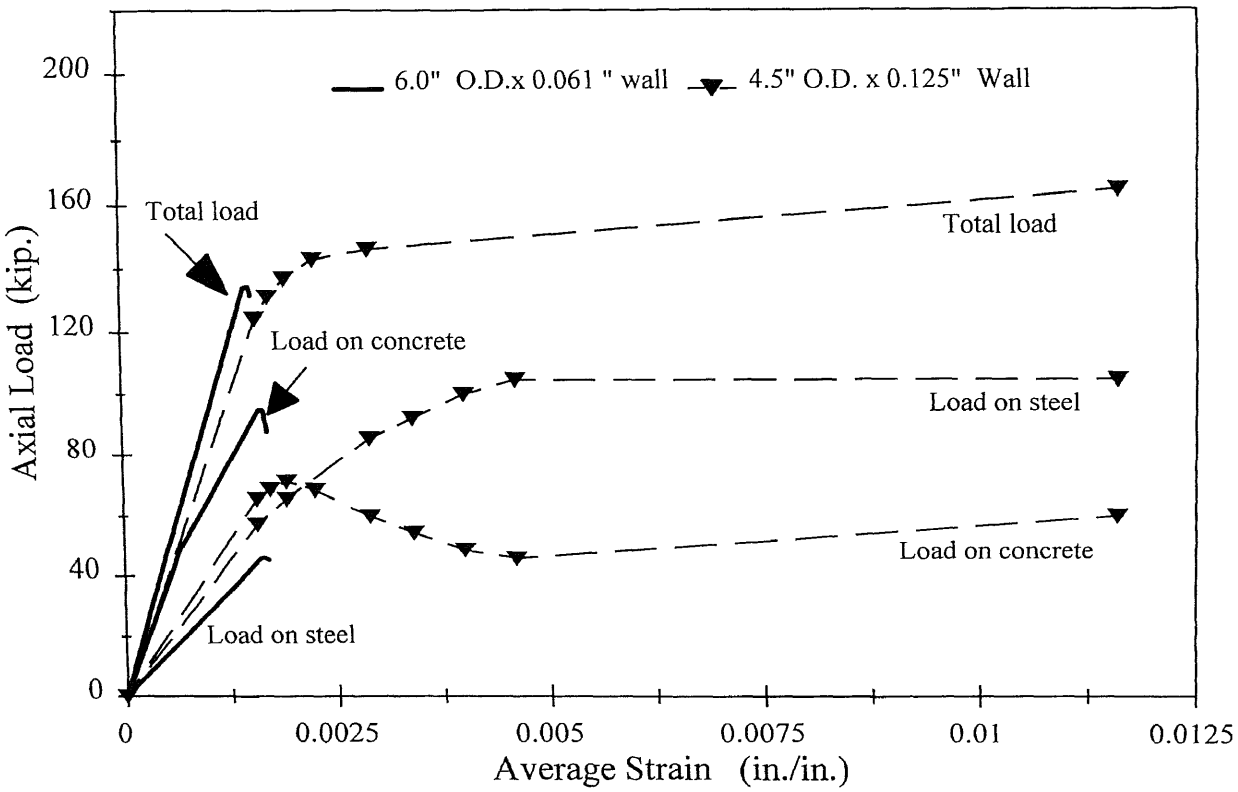

Figure 2.2 Load-strain behavior in typical axial load test (Furlong, 1967).

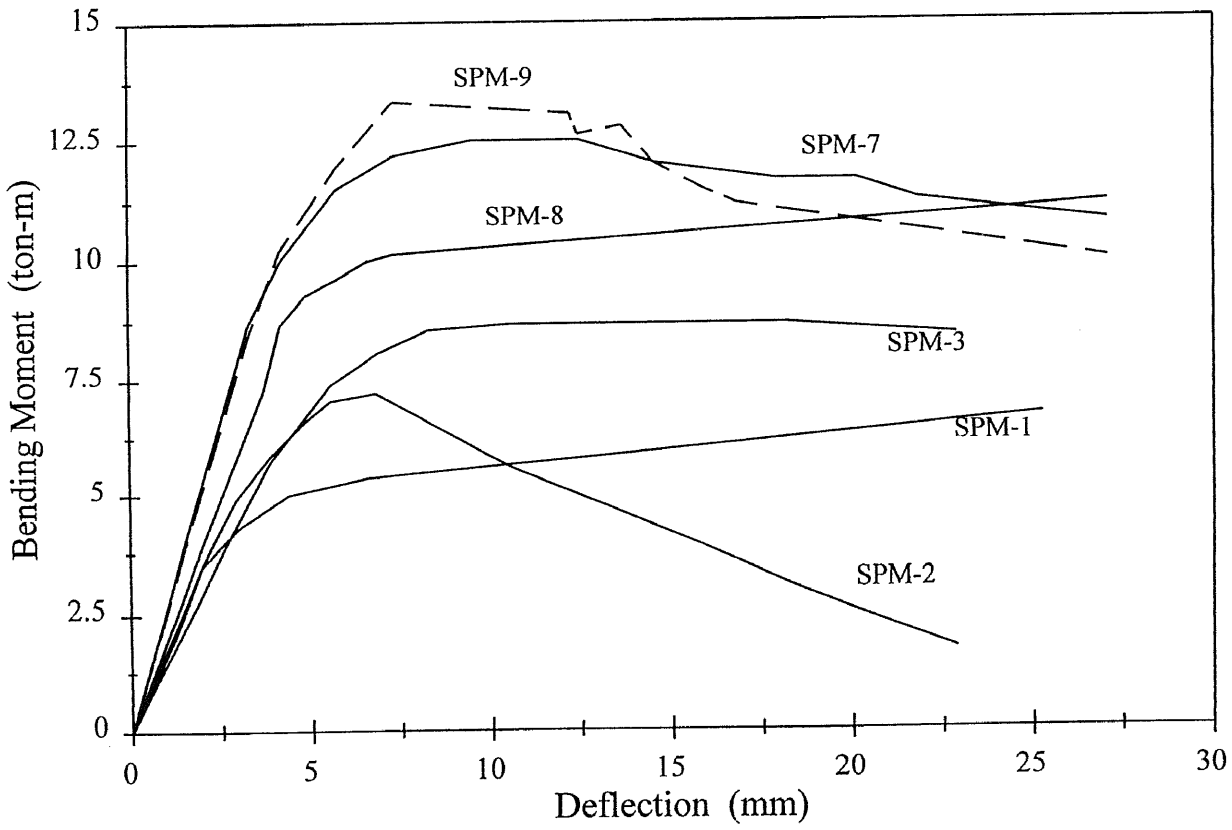

Figure 2.3a Bending moment-deflection curves; bond effect (Okamoto and Maeno, 1988).

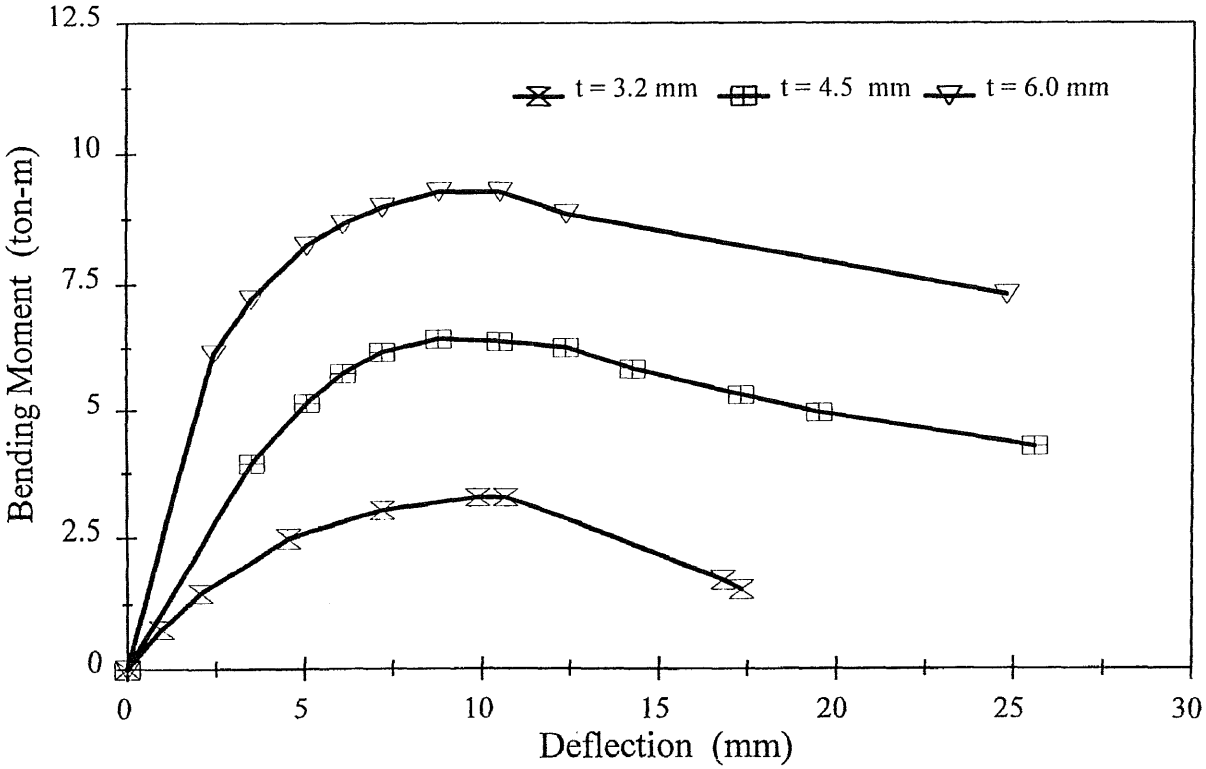

Figure2.3b Bending moment-deflection curves for CFT columns with different aspect ratios (Okamoto and Maeno, 1988).

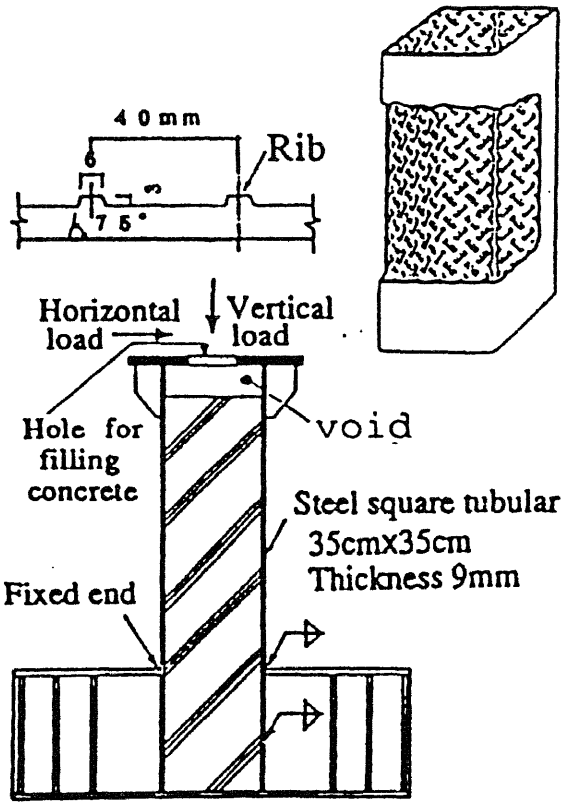

Figure 2.4 Typical test setup (Yoshioka, 1992).

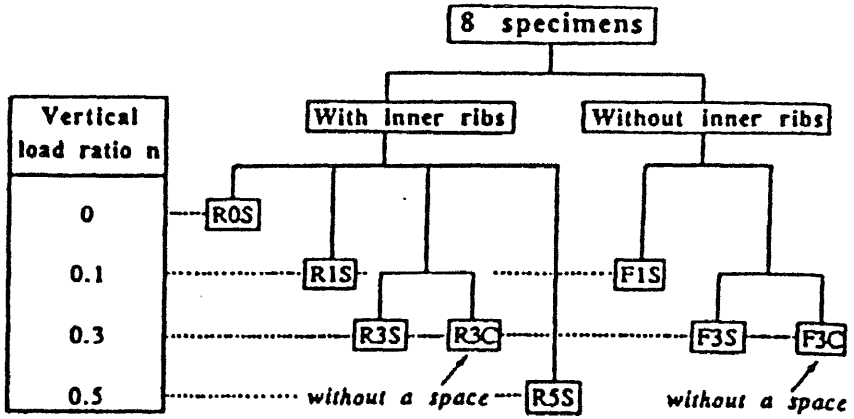

Figure 2.5 Test program (Yoshioka, 1992).

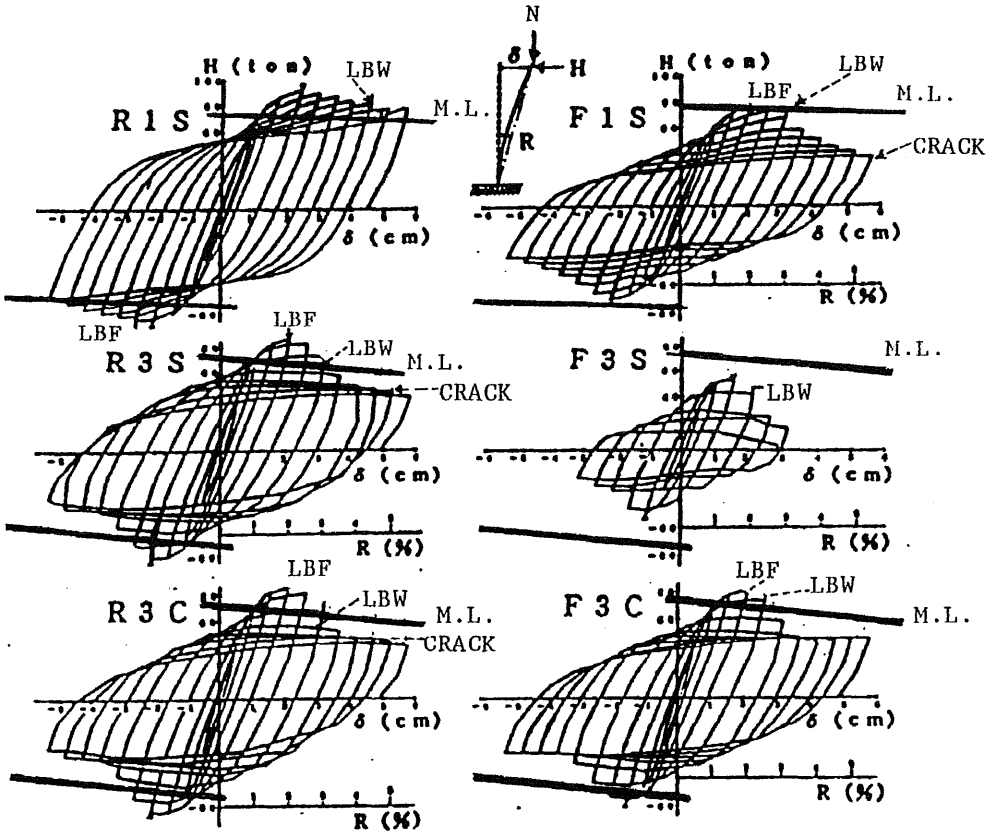

Figure 2.6 Load-deflection relationship (Yoshioka, 1992).

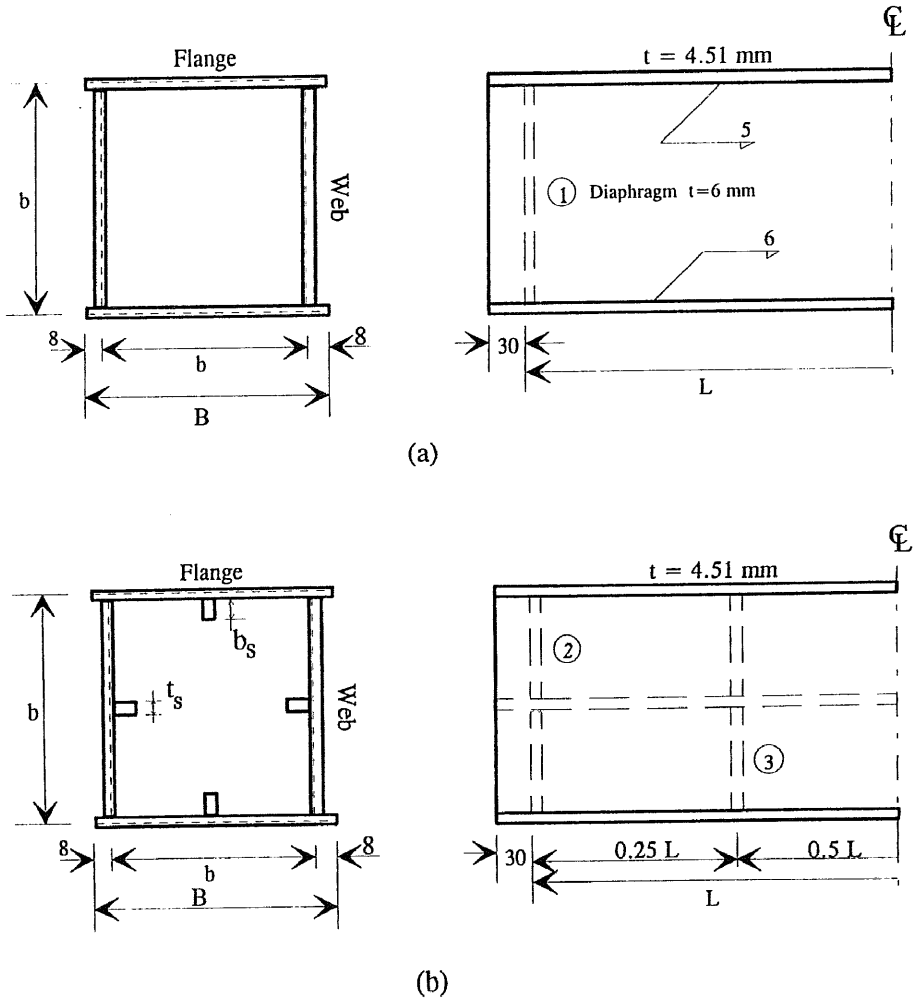

Figure 2.7 (a) Unstiffened section; (b) Stiffened section (Ge and Usami, 1992).

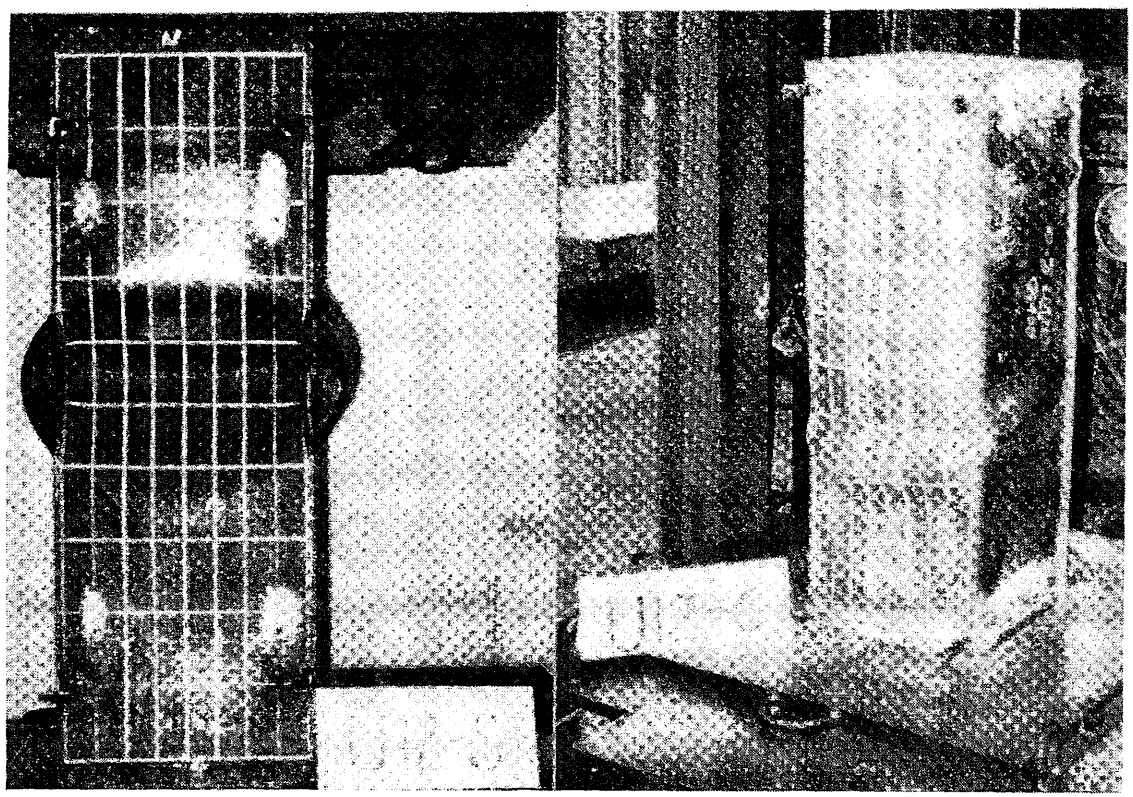

(a) (b)

Figure 2.8 Typical failure of (a) hollow steel tube, (b) concrete-filled column (Ge and Usami, 1992).

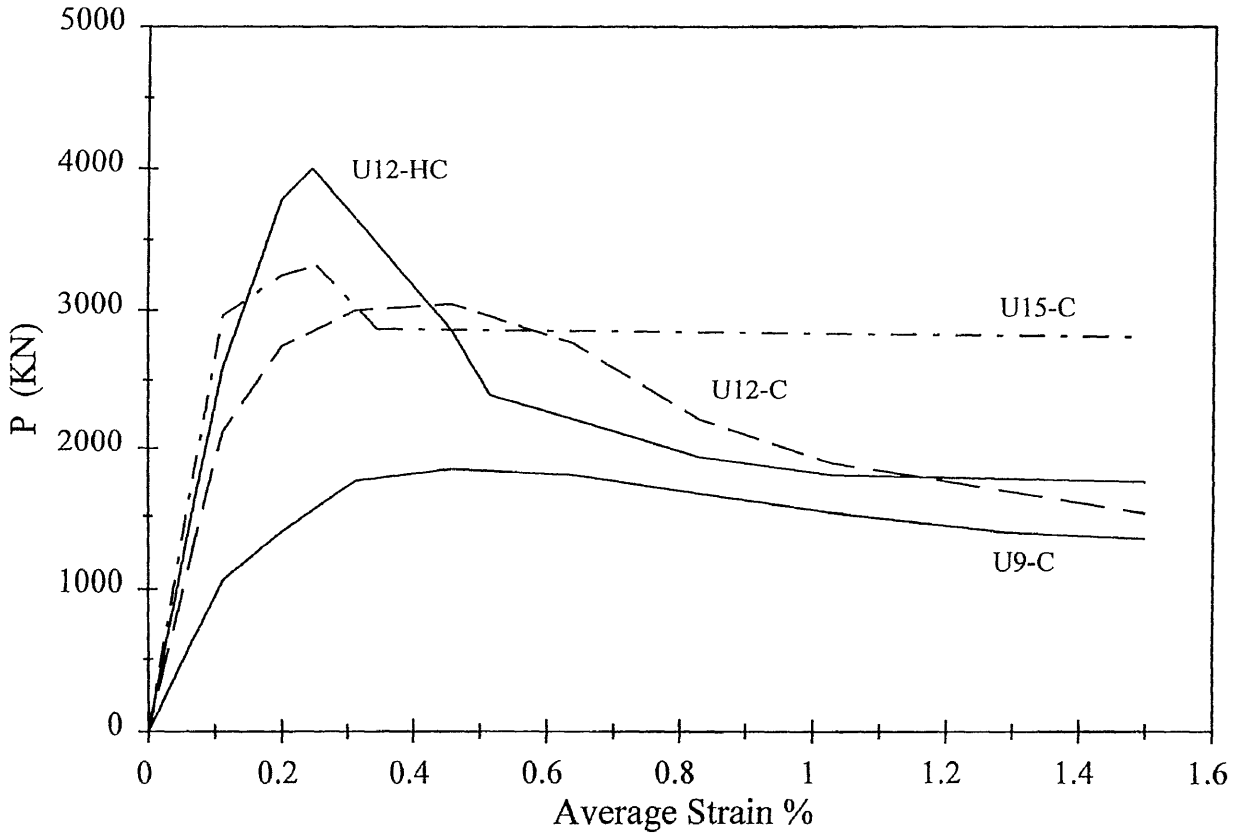

Figure 2.9a Load strain relationship for unstiffened CFT columns (Ge and Usami, 1992).

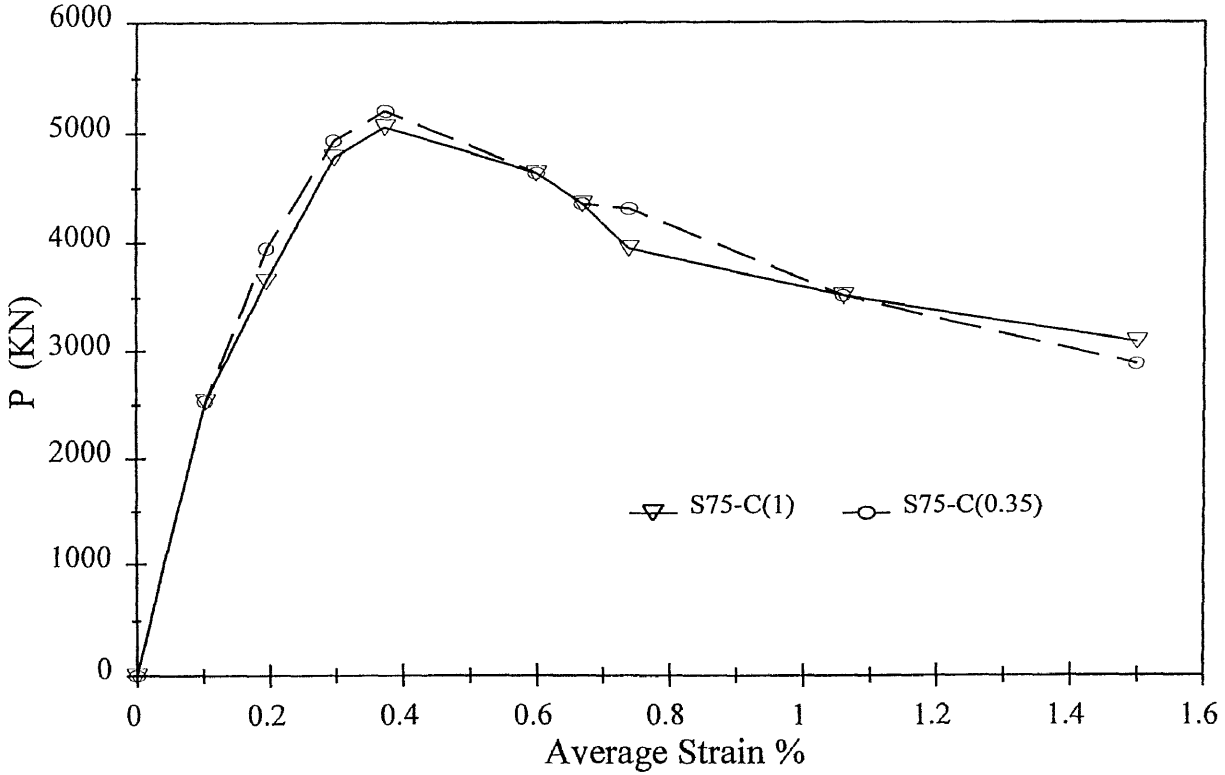

Figure 2.9b Load-strain relationship for stiffened CFT columns (Ge and Usami, 1992).

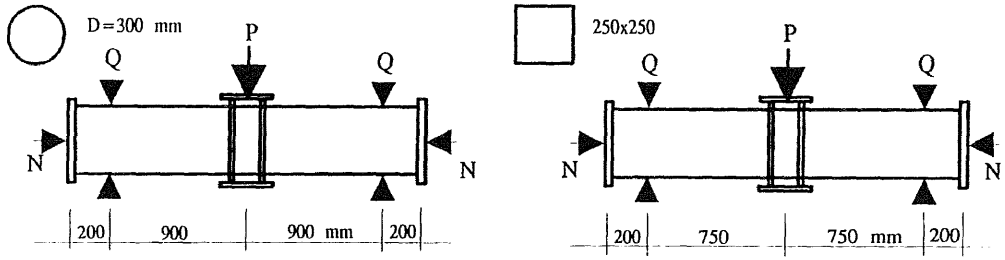

Figure 2.10 Typical test setup (Sugano and Nagashima, 1992).

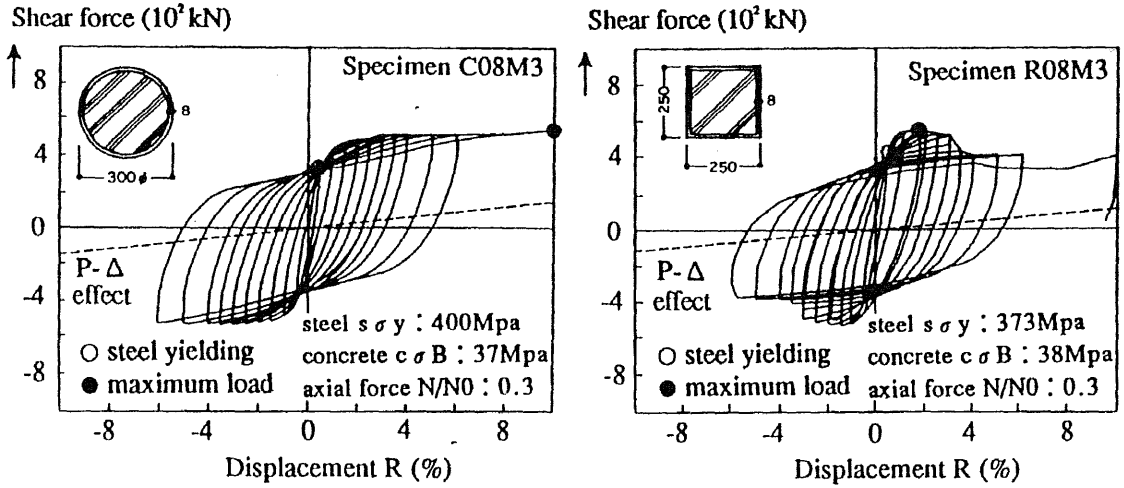

Figure 2.11 Typical hysteresis curves for circular and square columns (Sugano and Nagashima, 1992).

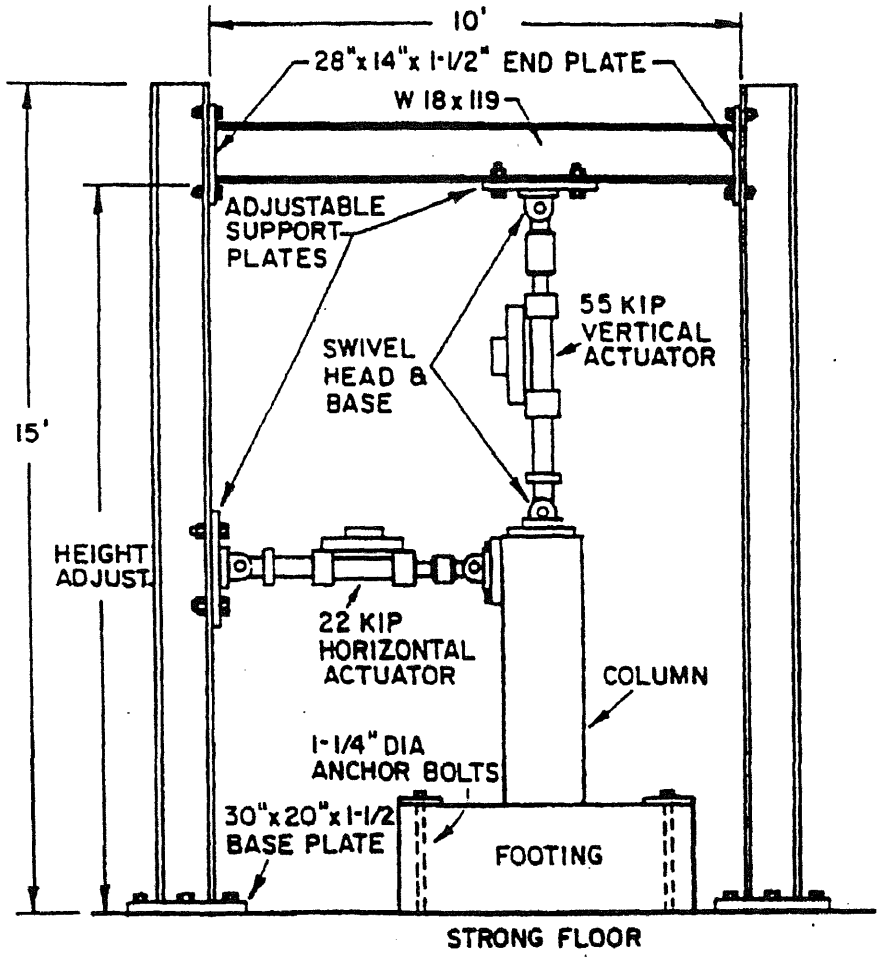

Figure 2.12 Test setup (Boyd et al., 1995).

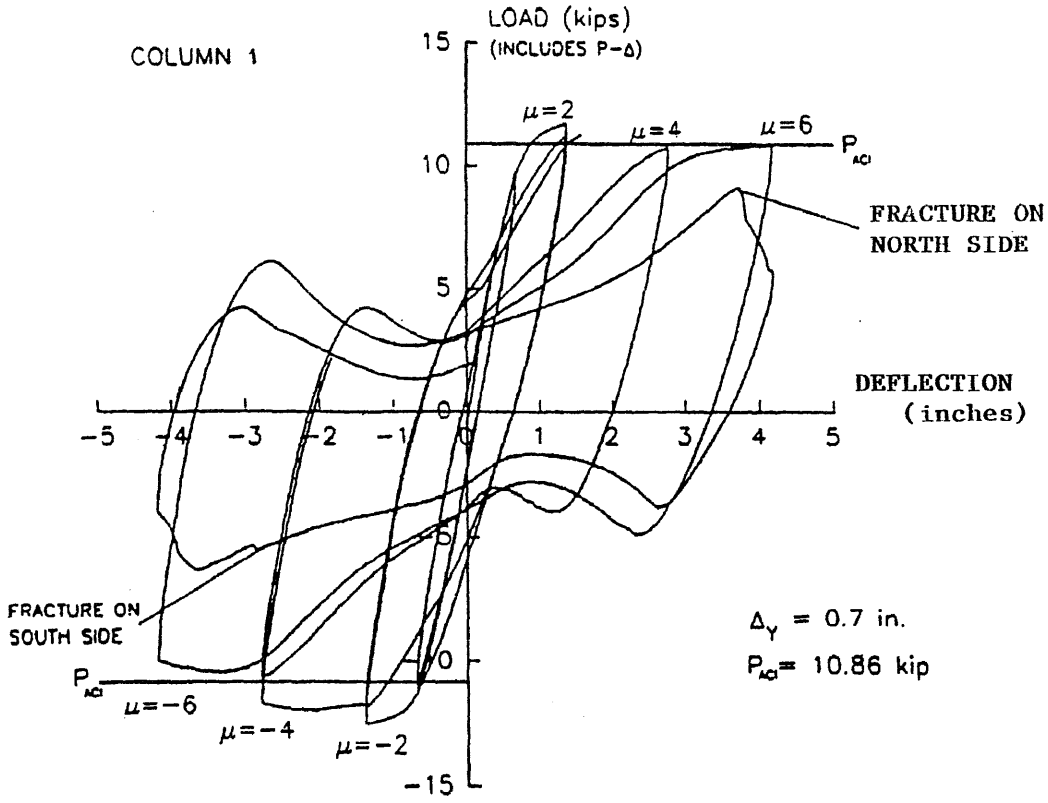

Figure 2.13 Hysteresis response (Boyd et al., 1995).

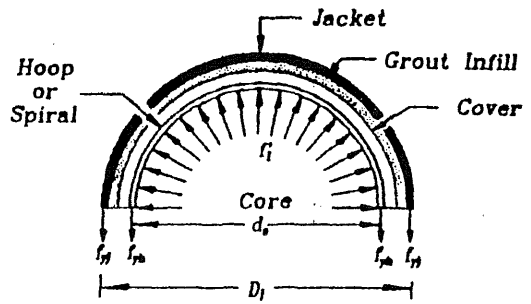

Figure 2.14 Confining action of steel jacket (Chai, 1992).

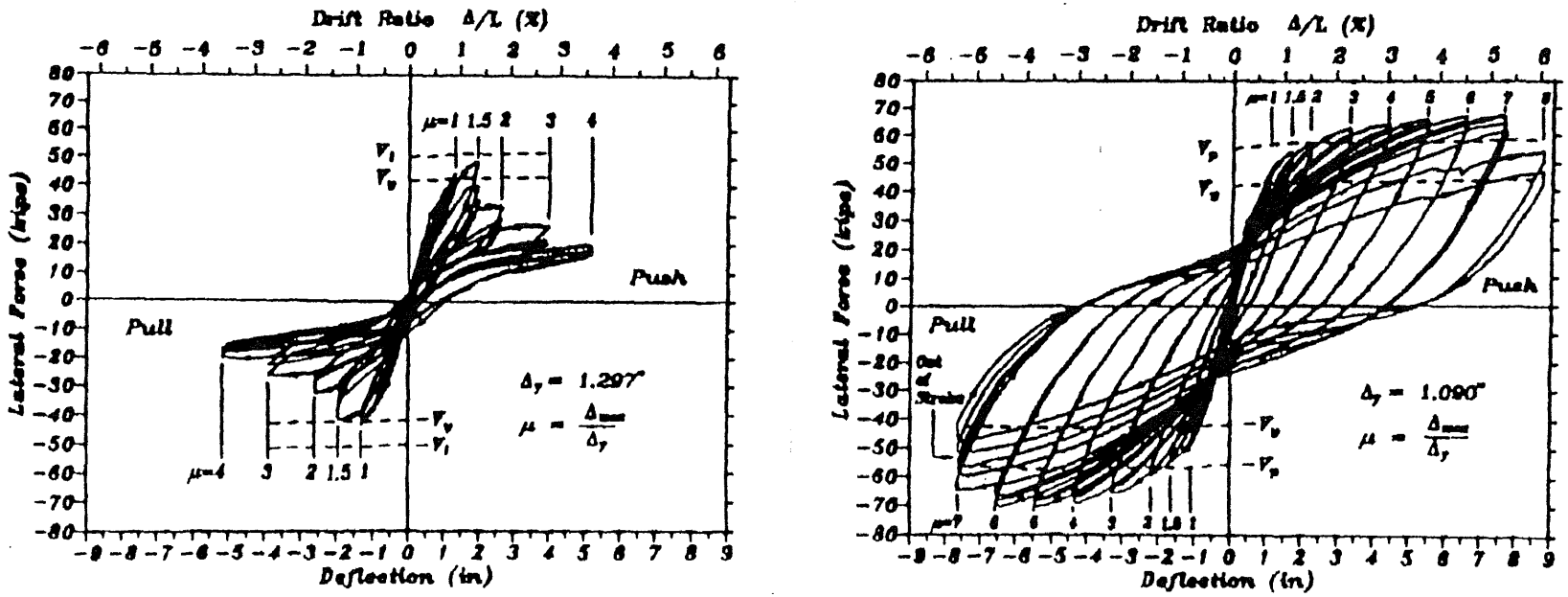

Figure 2.15 Hysteresis response of (a) RC column, (b) retrofitted column (Chai, 1992).

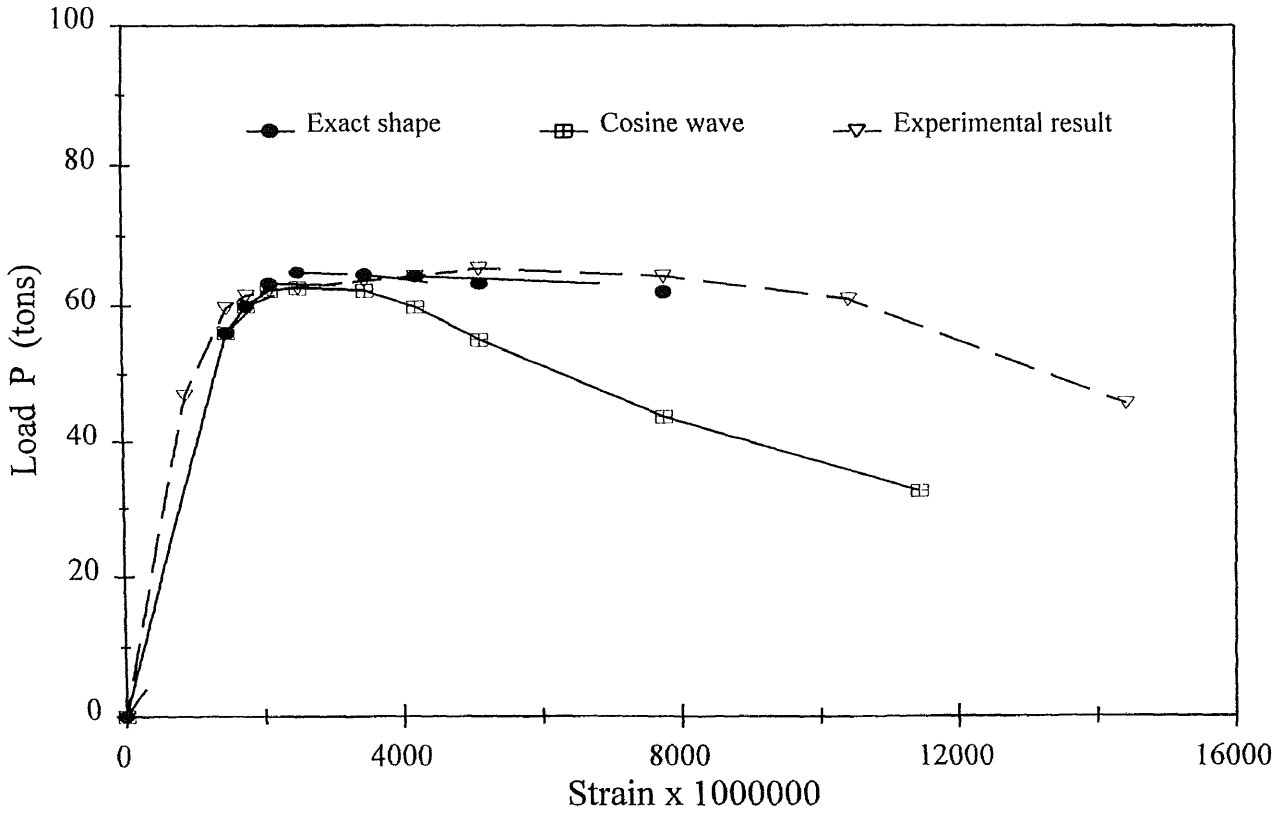

Figure 2.16 Comparison between theoretical and experimental results for long CFT columns (Neogi and San, 1969).

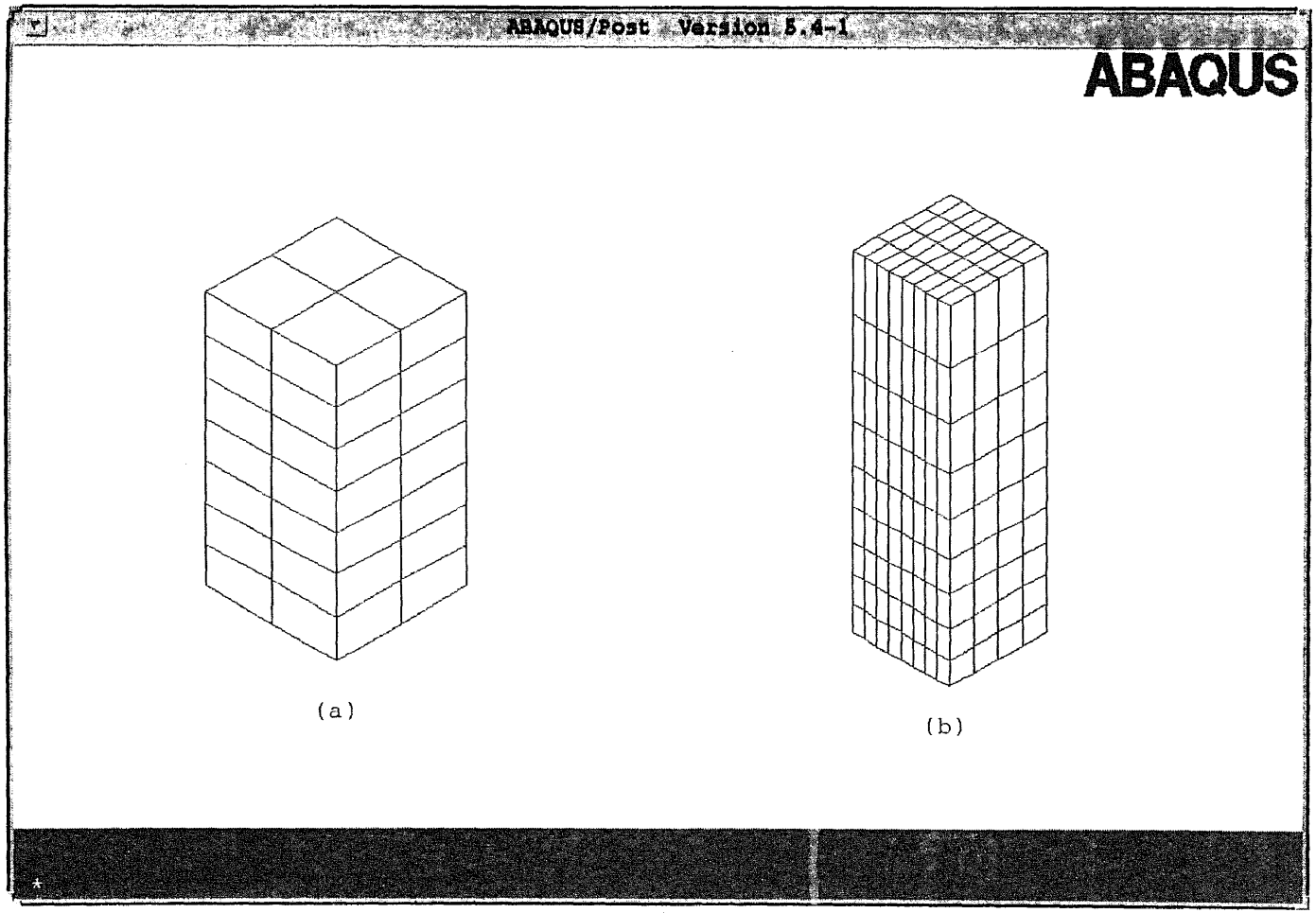

Figure 3.1 Three-dimensional finite element mesh for square CFT columns (a) used in axial loading (b) used in combined loading.

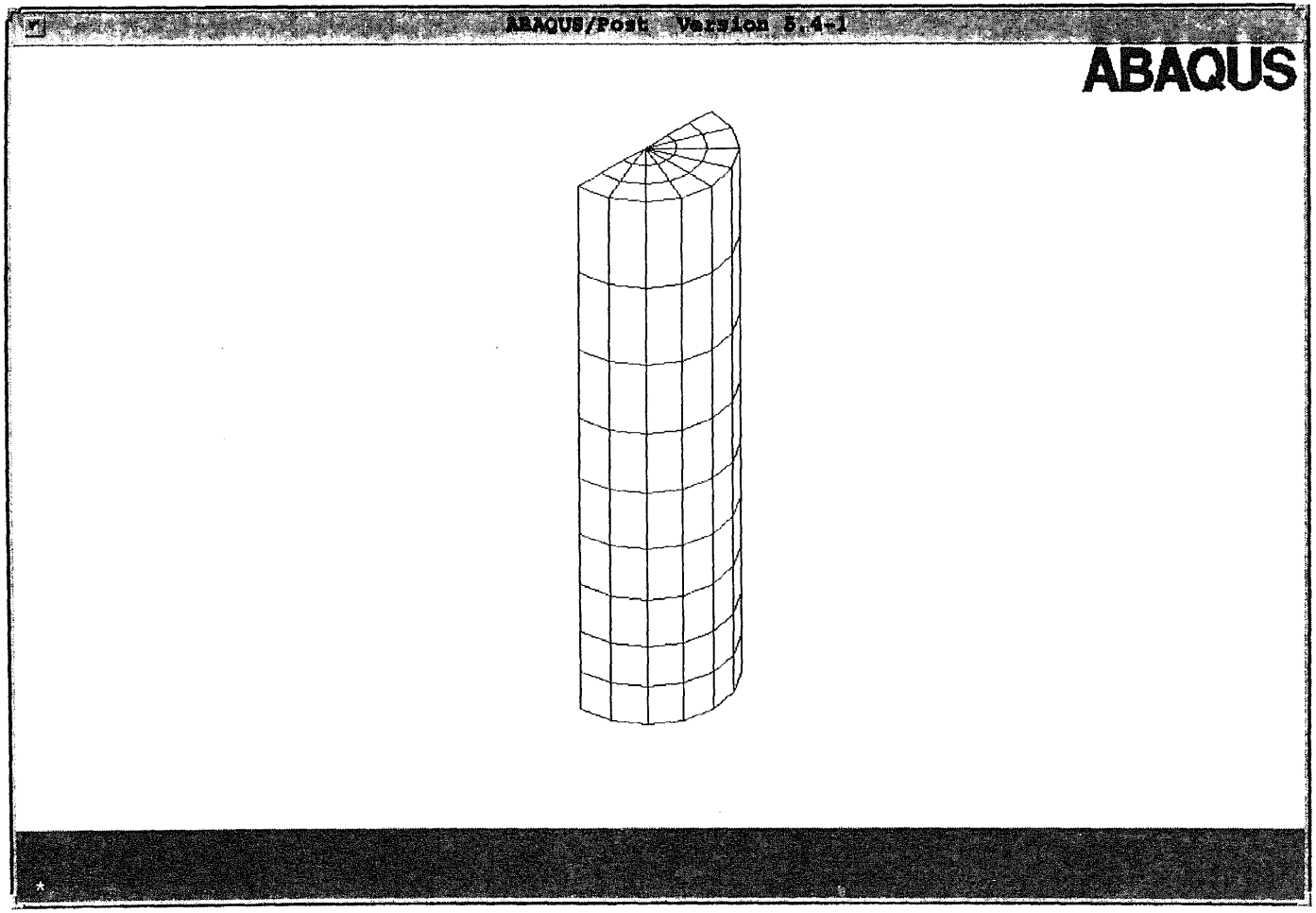

Figure 3.2 Three-dimensional finite element mesh for Circular CFT columns.

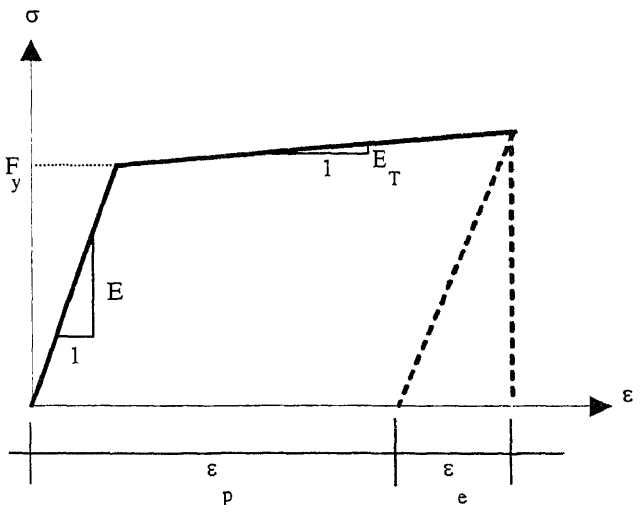

Figure 3.3 Typical steel stress-strain relationship.

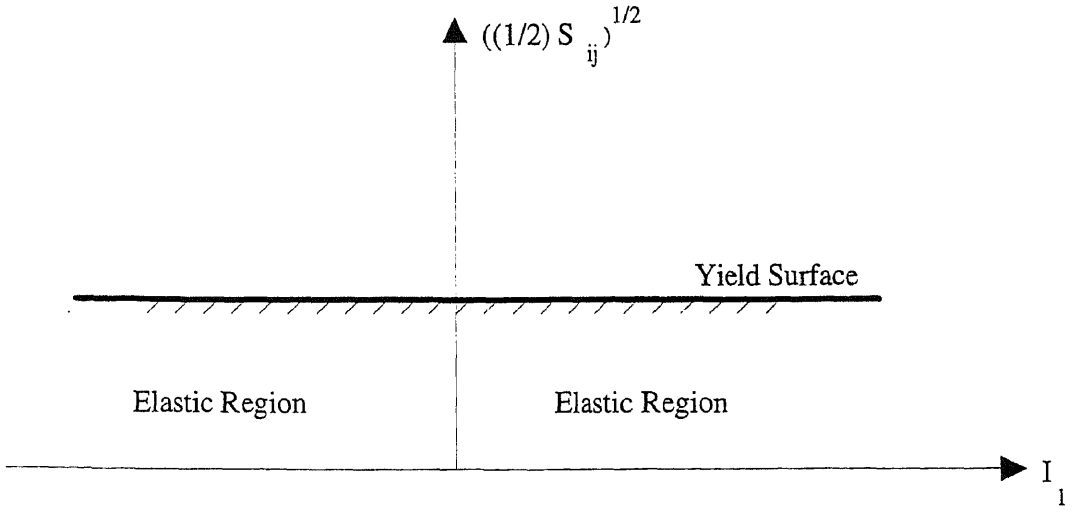

Figure 3.4 The von Mises yield surface.

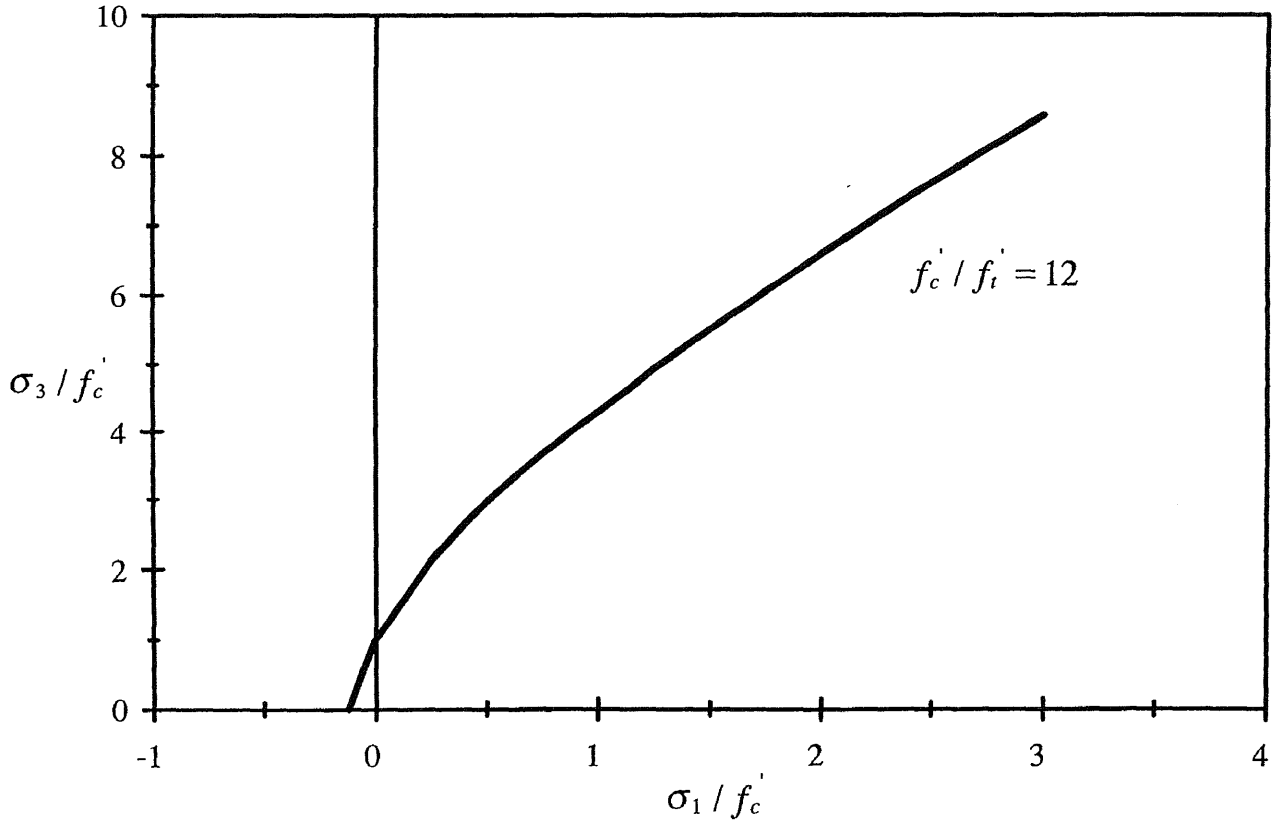

Figure 3.5 Triaxial failure envelope of Leon's model in principal stress section.

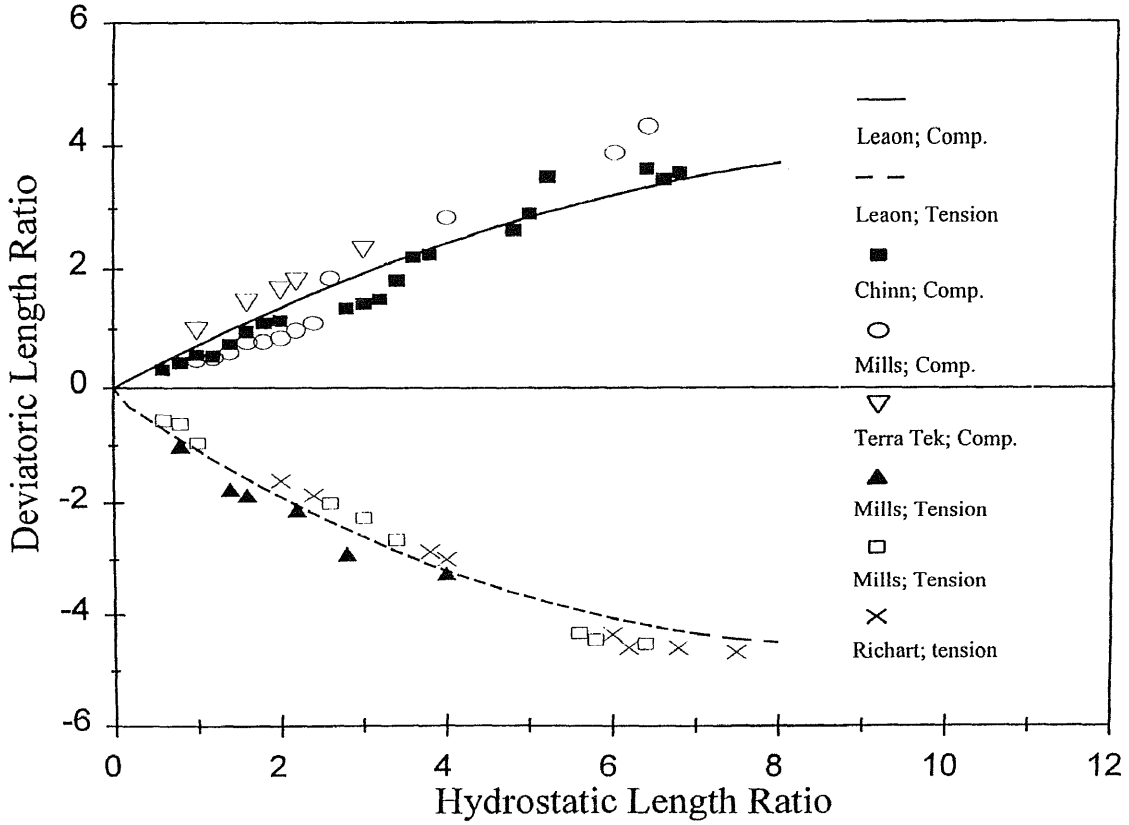

Figure 3.6 Leon's tensile and compressive meridians with test results.

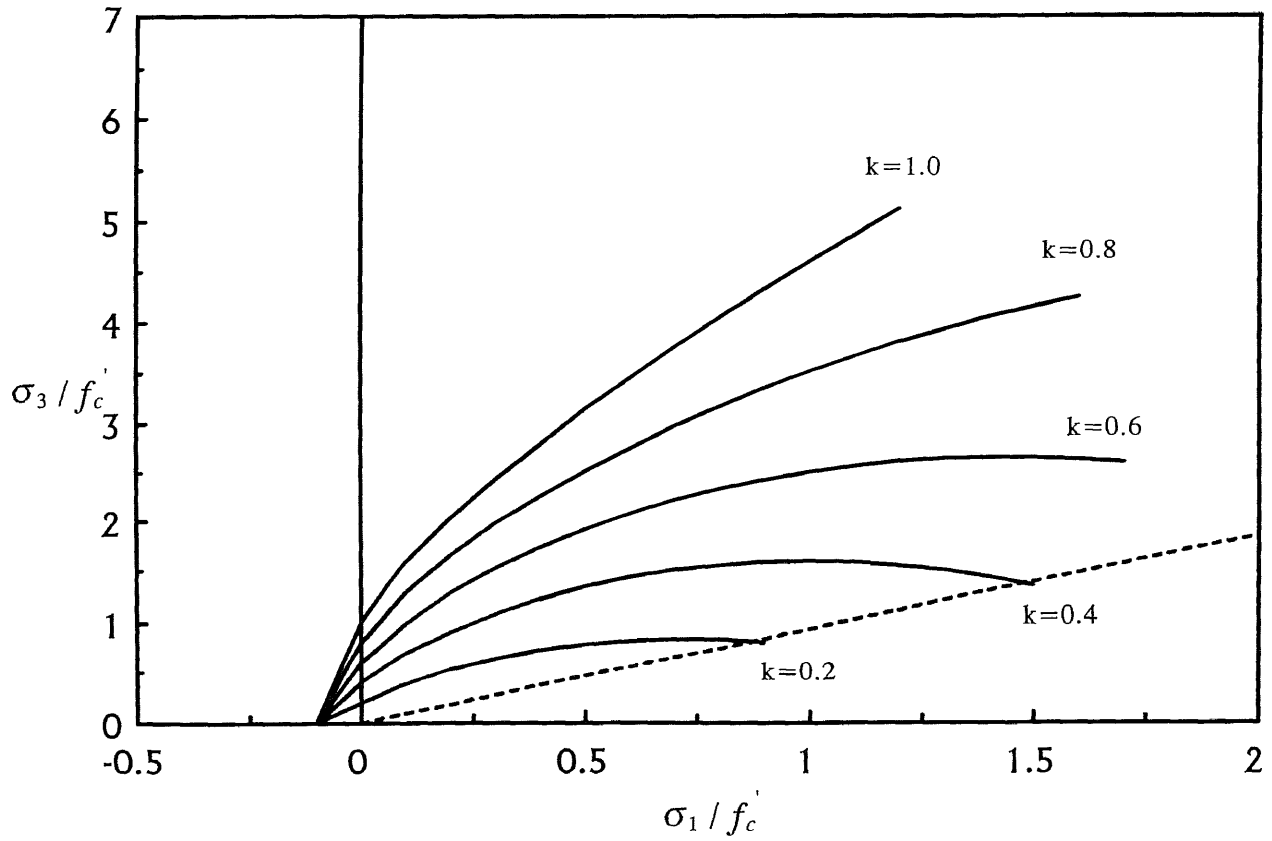

Figure 3.7 Loading surface of isotropic hardening model.

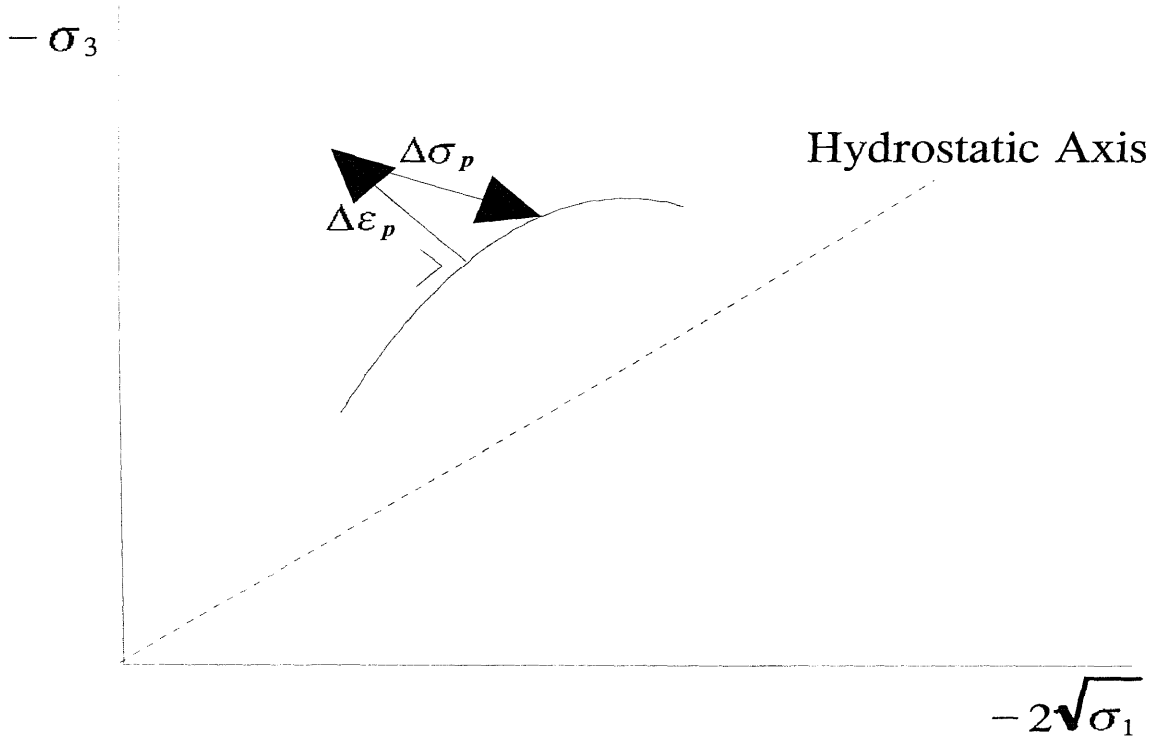

Figure 3.8 Inelastic volume change and plastic stress corrector.

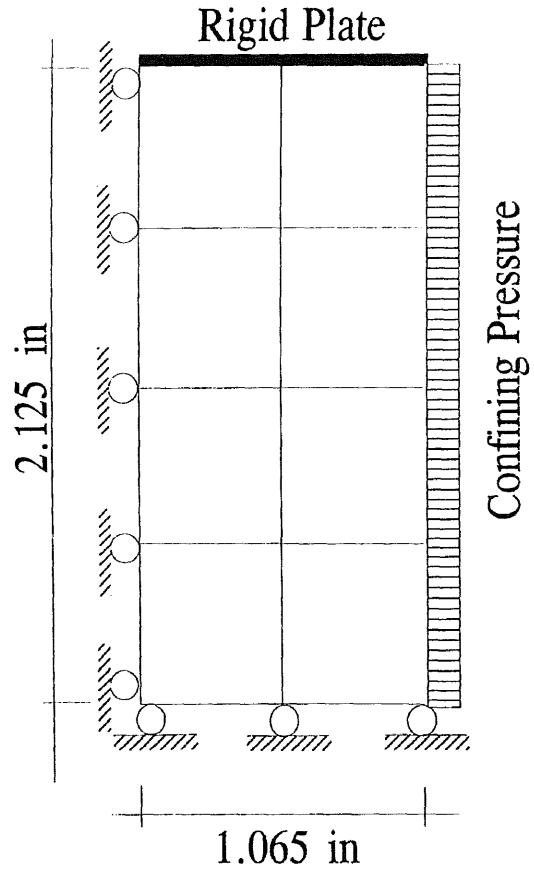

Figure 3.9 Finite element model for concrete triaxial compression test.

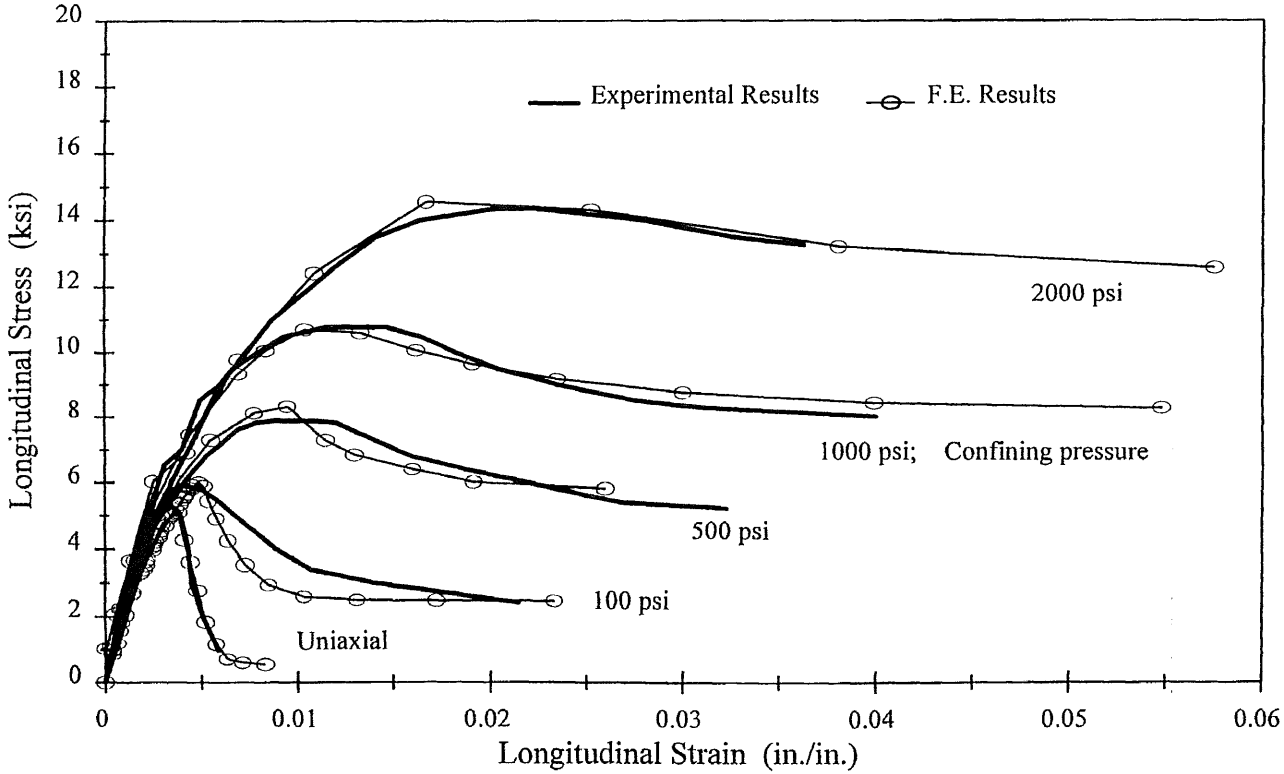

Figure 3.10a Stress-strain relationship for concrete with $f_c^{'}$ = 5.3 Ksi

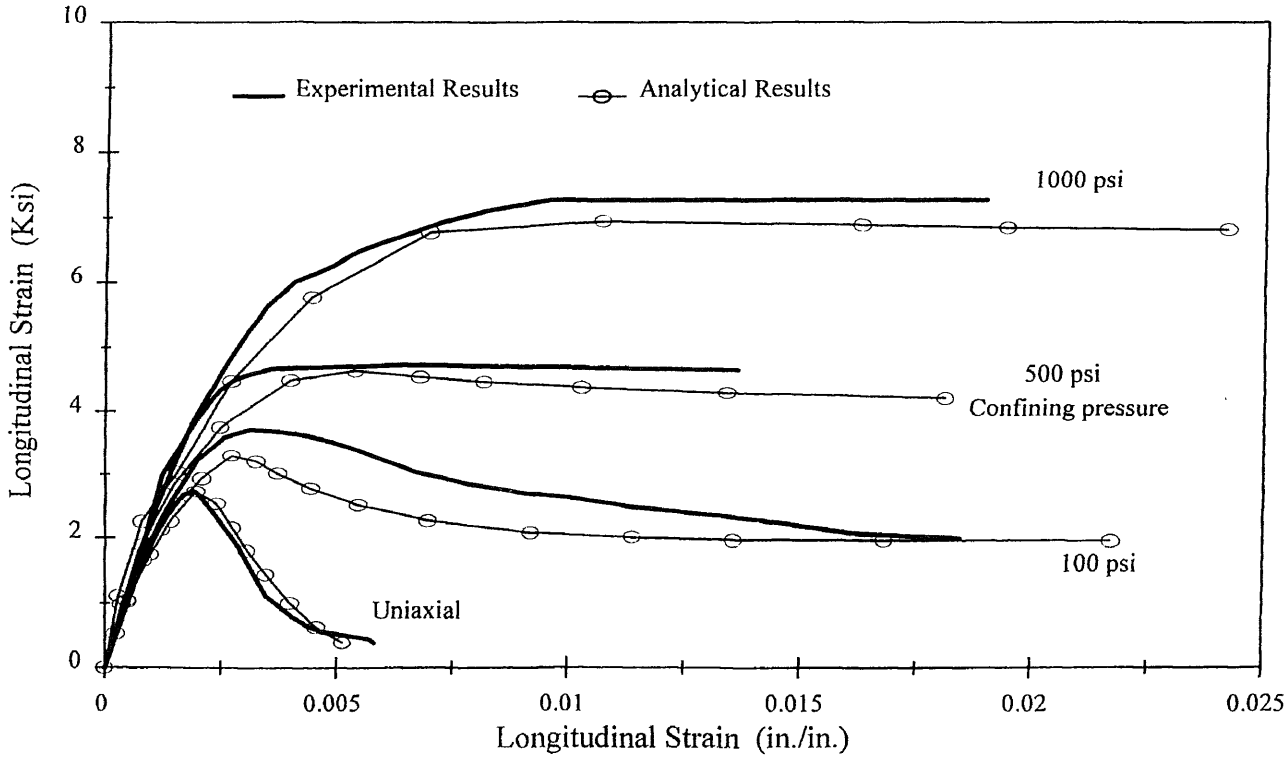

Figure 3.10a Stress-strain relationship for concrete with $f_c^{'}$ = 3.0 Ksi.

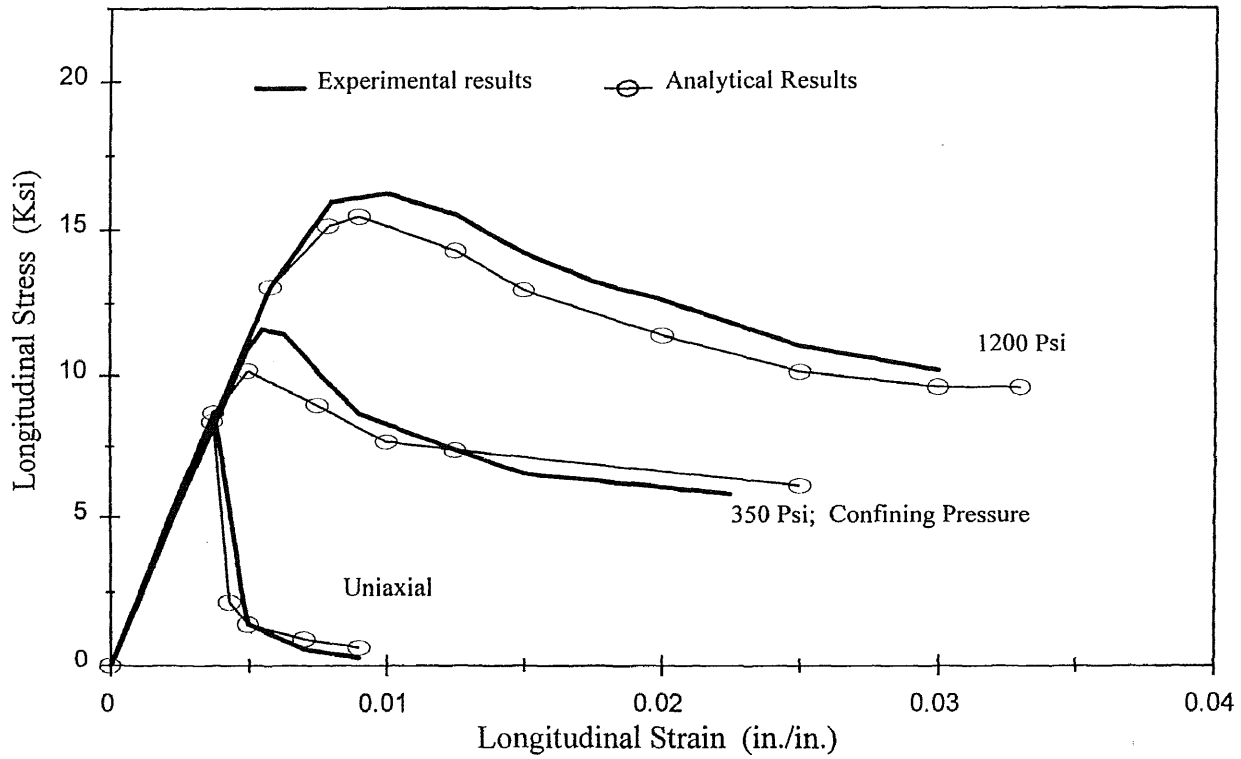

Figure 3.10c Stress-strain relationship for concrete with $f_c^{'}$ = 9.0 Ksi.

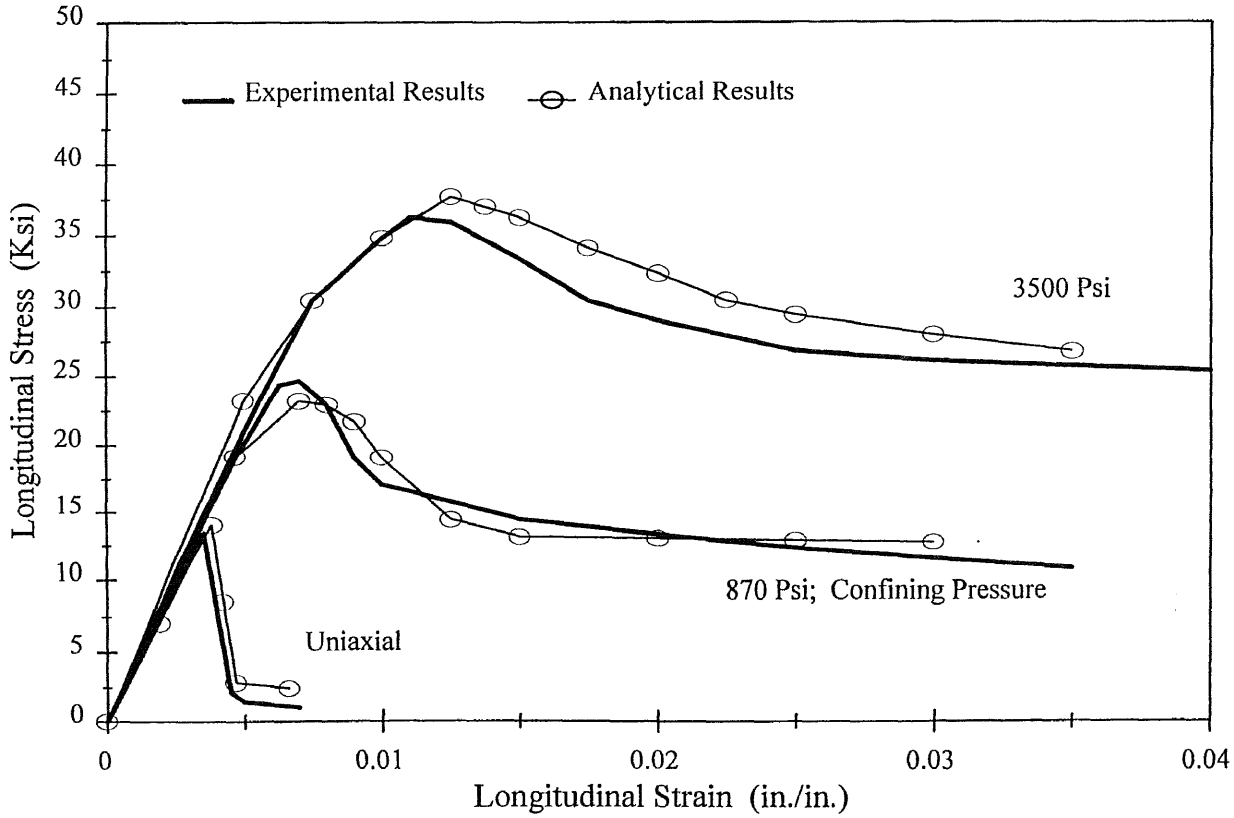

Figure 3.10d Stress-strain relationship for concrete with $f_c^{'} = 13.5$ Ksi

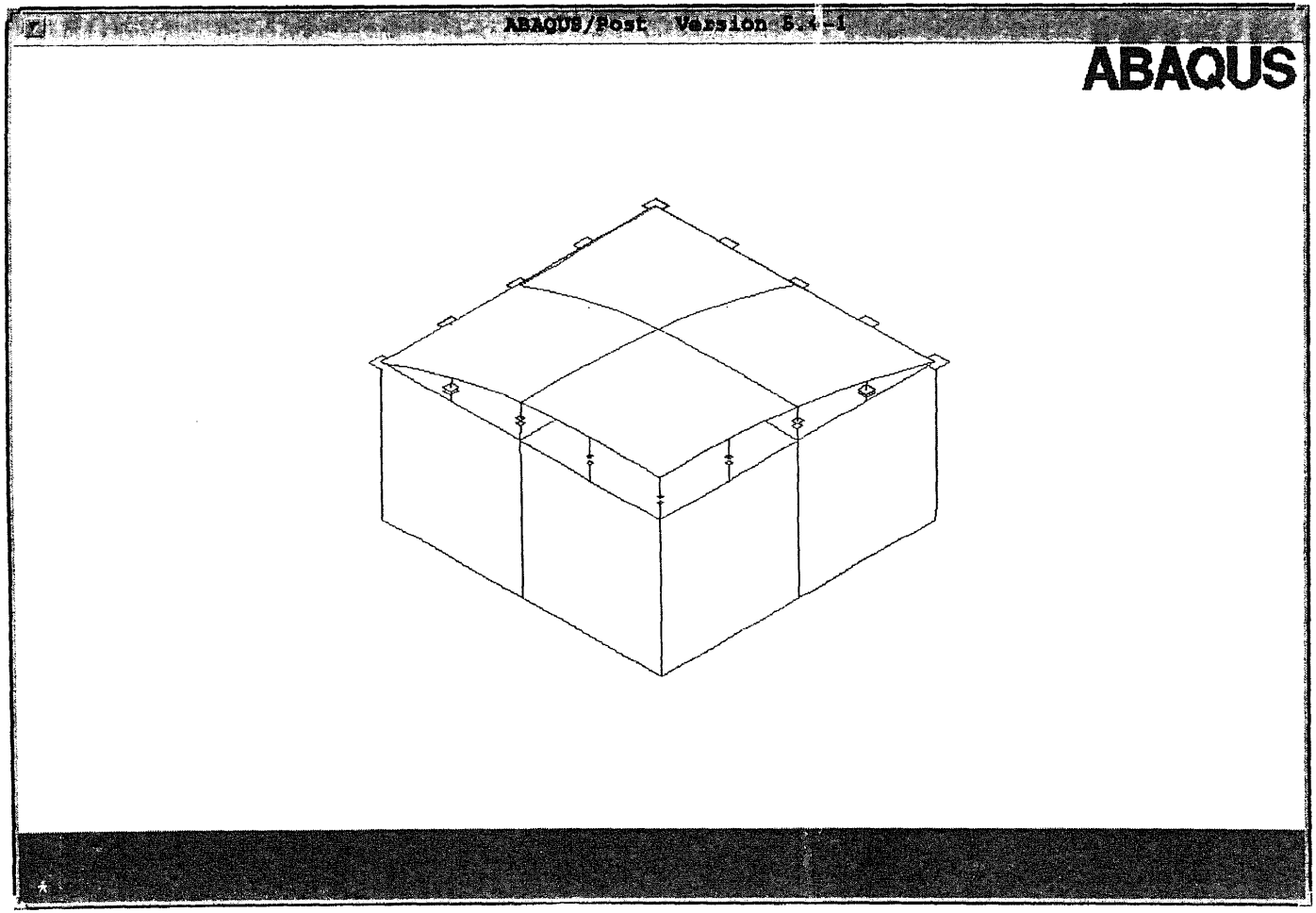

Figure 3.11 Buckling of a square thin plate which attached to a concrete block.

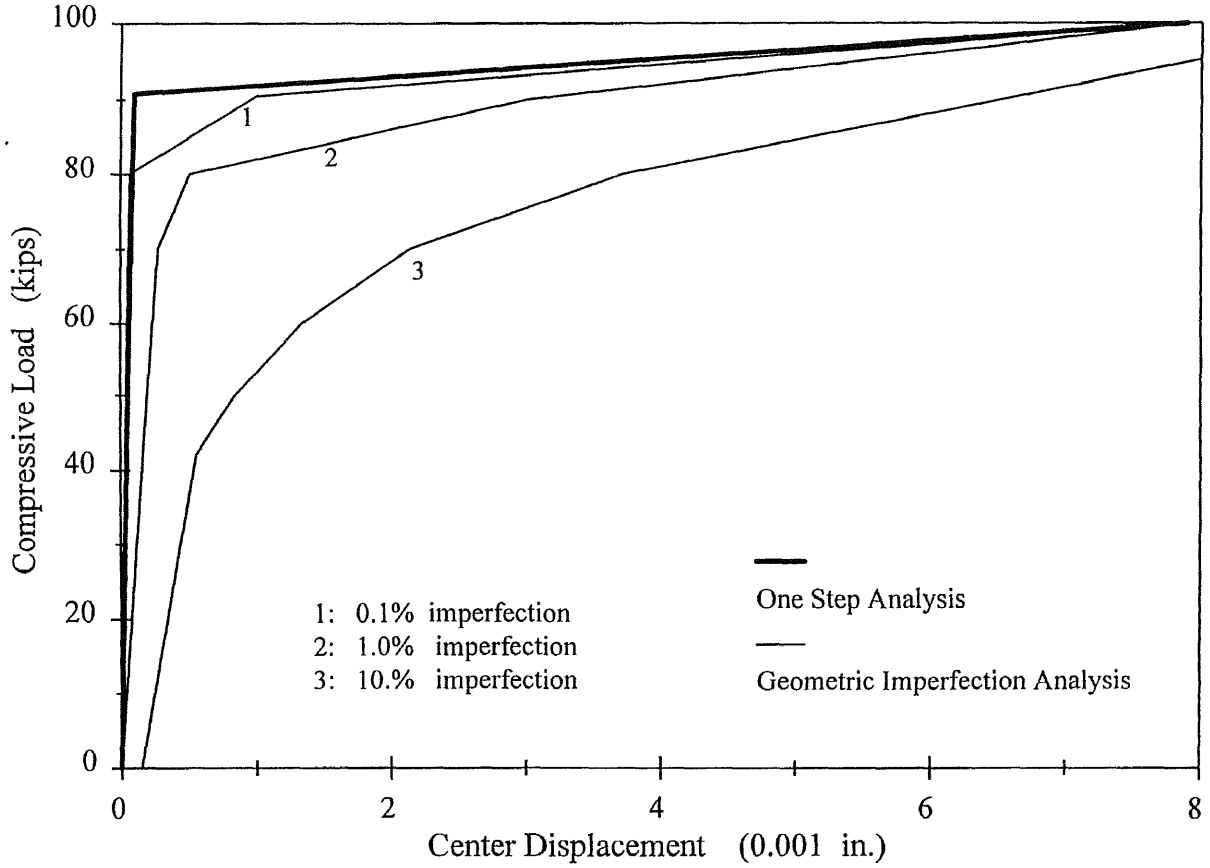

Figure 3.12 Load-displacement relationship for a simply supported square plate.

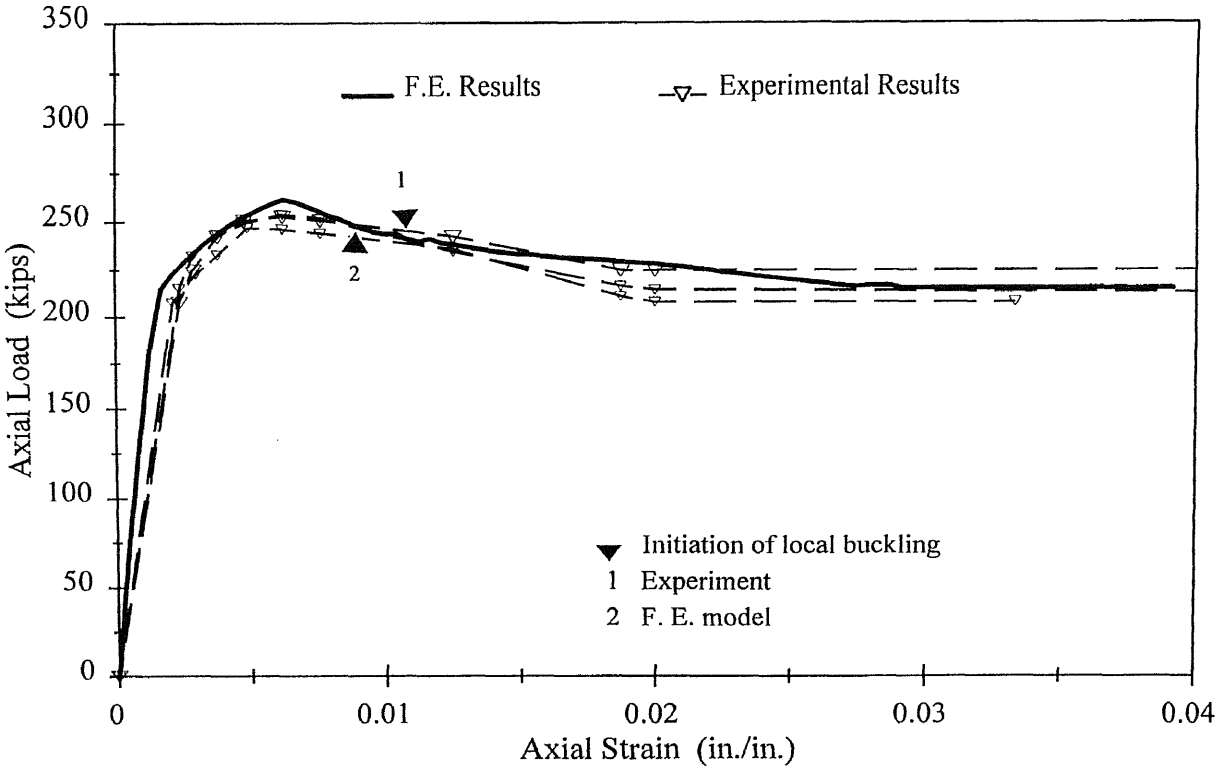

Figure 3.13 Axial load-strain relationship for Square CFT column .17x6x6x24 inches.

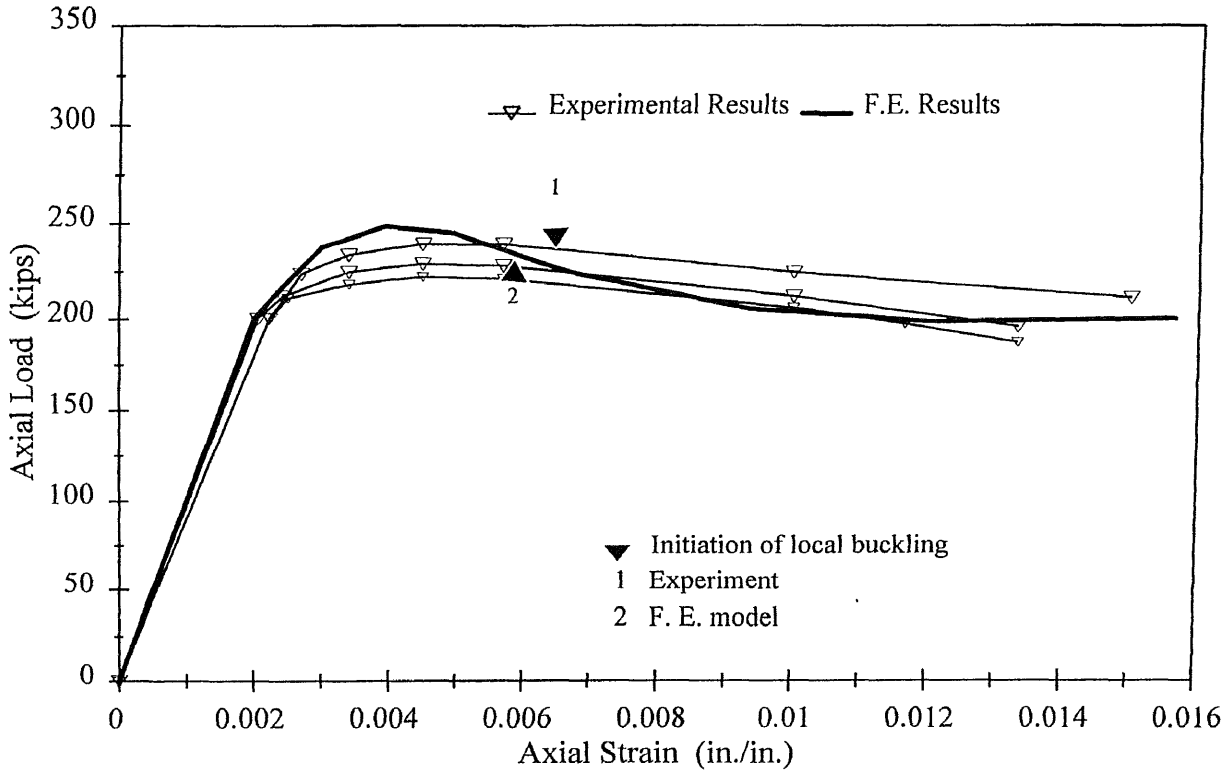

Figure 3.14 Axial load-strain relationship for Square CFT column .17x6x6x30 inches.

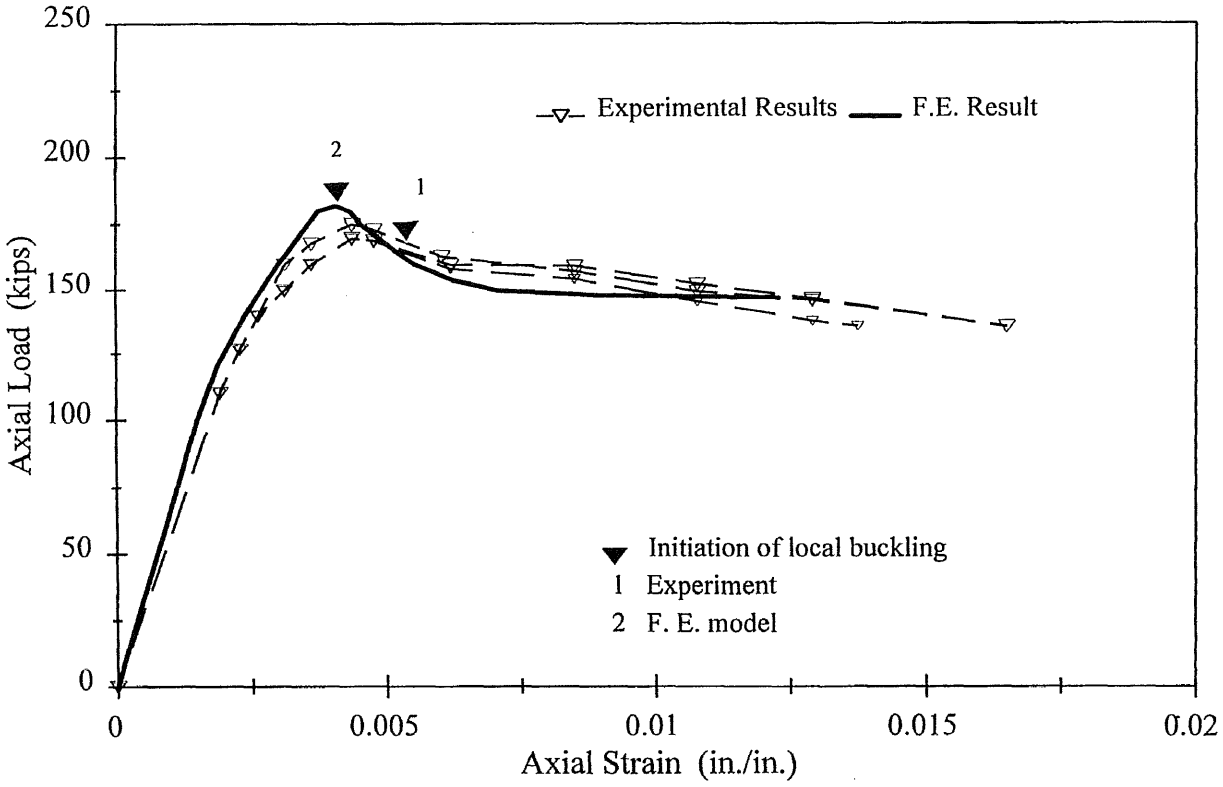

Figure 3.15 Axial load-strain relationship for Square CFT column .078x6x6x18 inches.

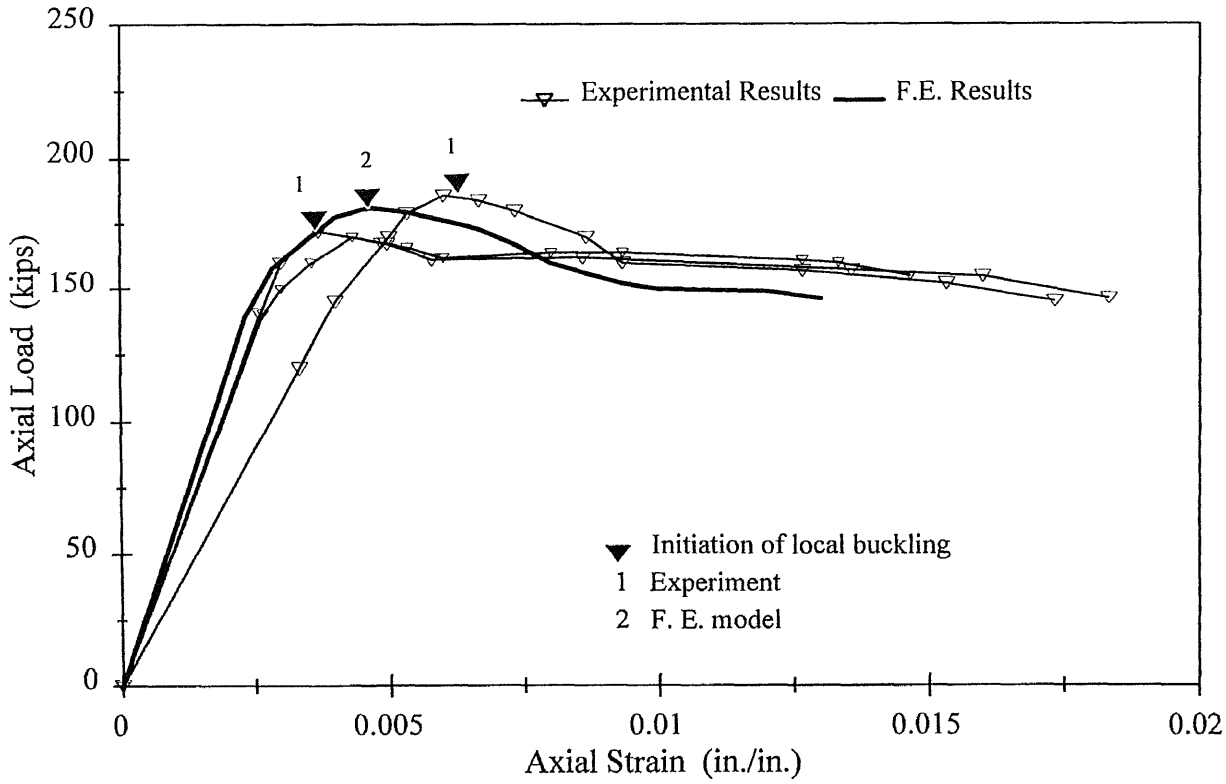

Figure 3.16 Axial load-strain relationship for Square CFT column .078x6x6x24 inches.

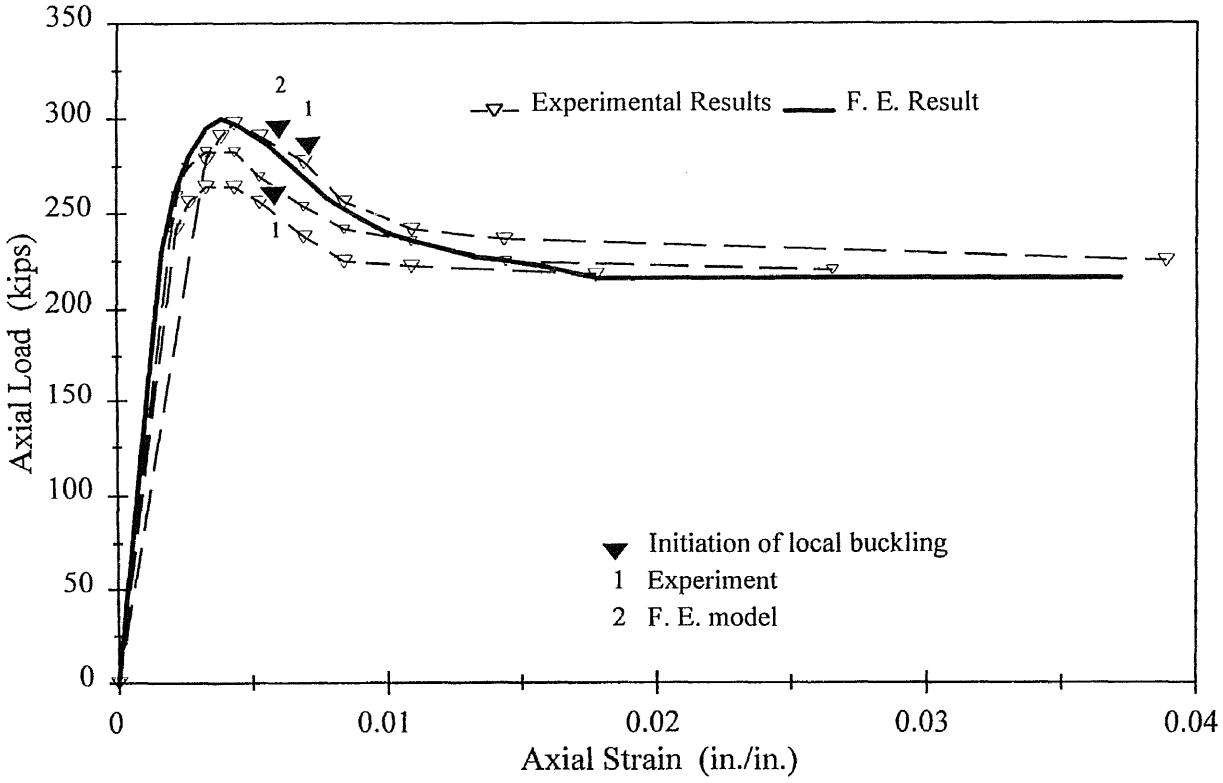

Figure 3.17 Axial load-strain relationship for Square CFT column .17x6x6x18 inches.

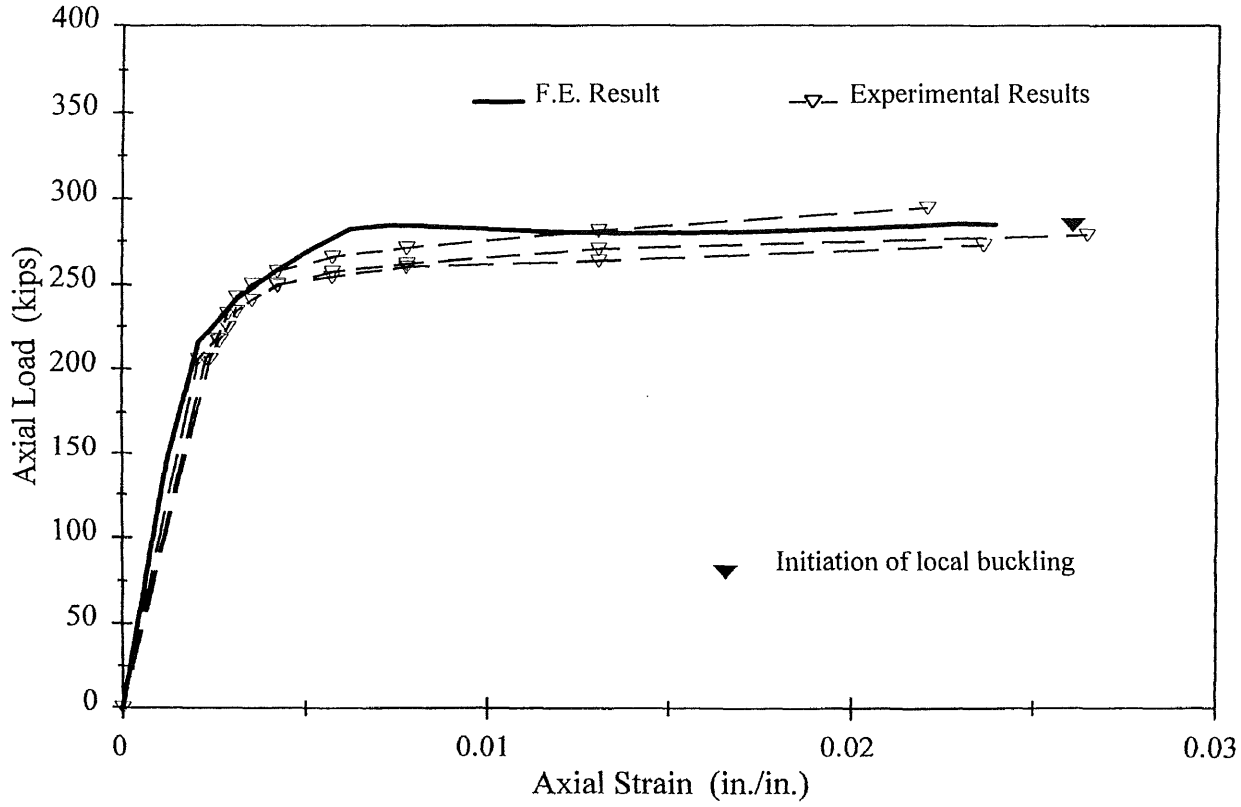

Figure 3.18 Axial load-strain relationship for circular CFT column .17x6x24 inches.

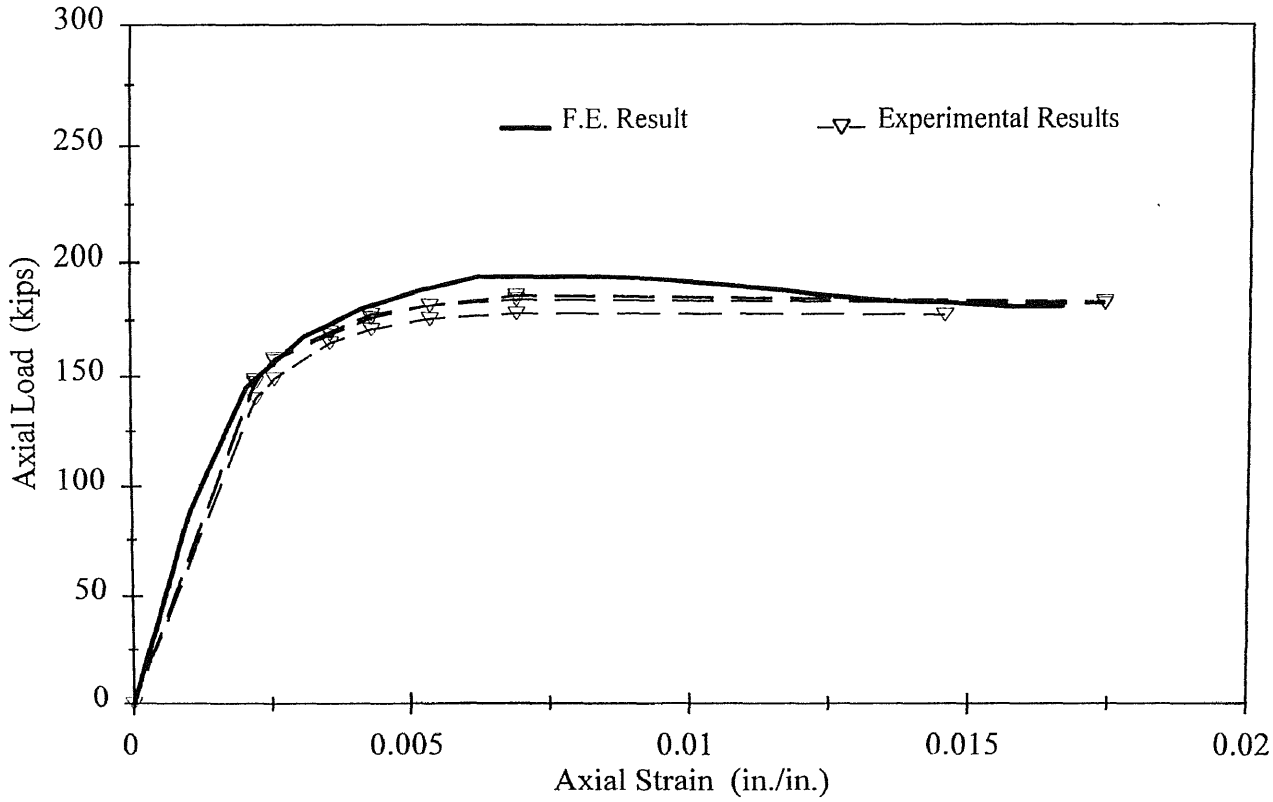

Figure 3.19 Axial load-strain relationship for circular CFT column .078x6x24 inches.

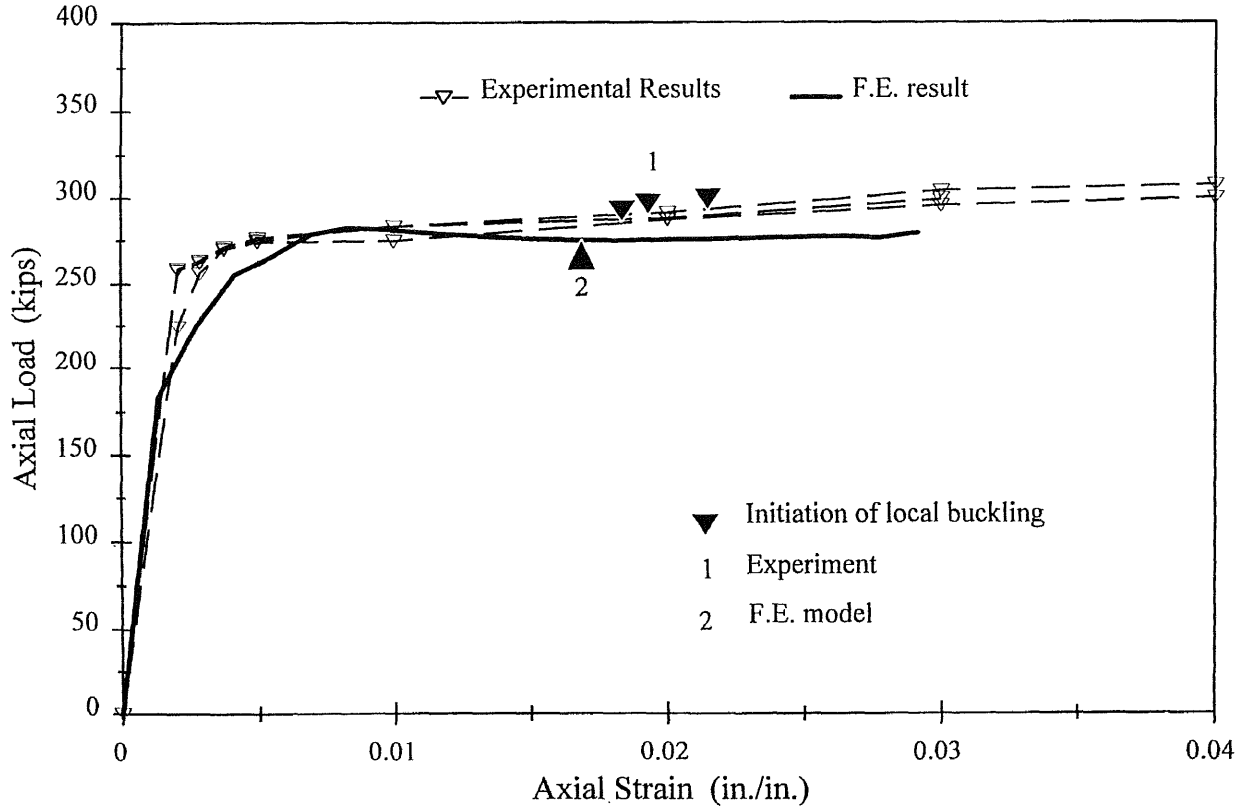

Figure 3.20 Axial load-strain relationship for circular CFT column .17x6x18 inches (f_c' .= 4.2 ksi).

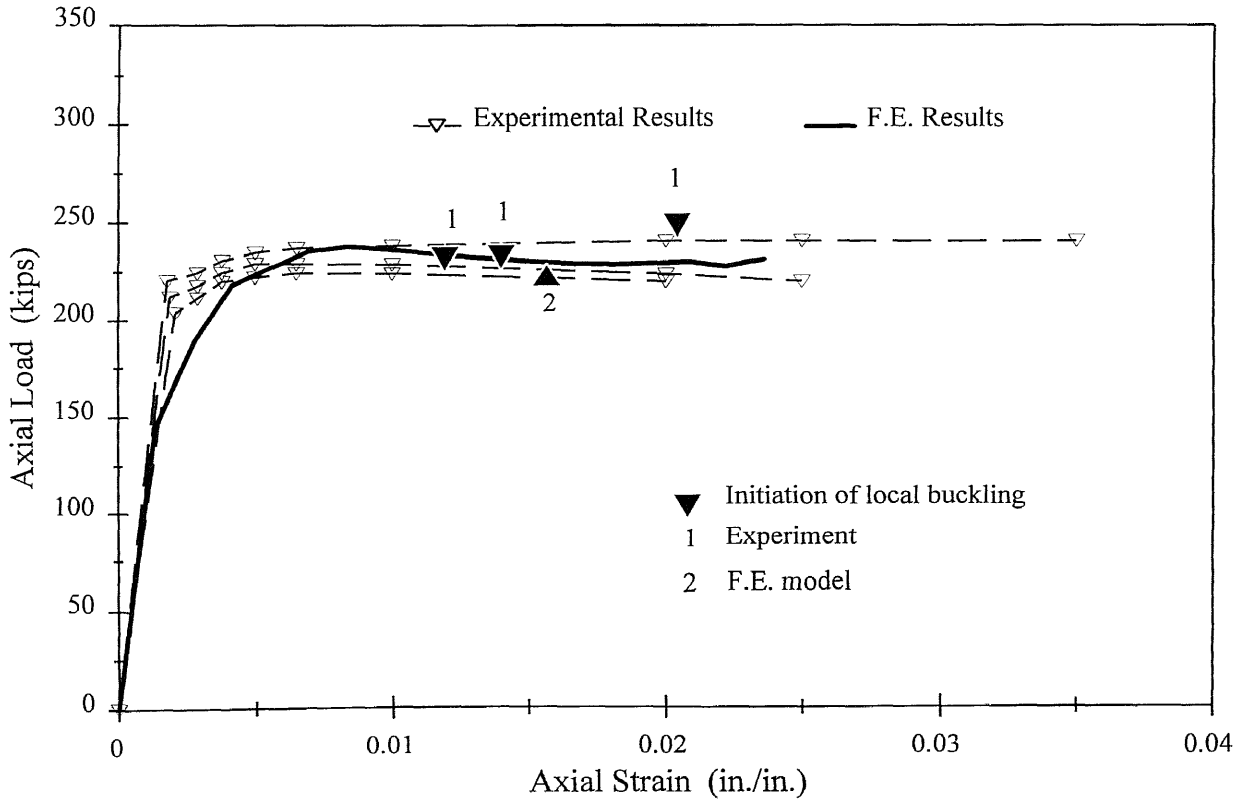

Figure 3.21 Axial load-strain relationship for circular CFT column .118x6x18 inches.

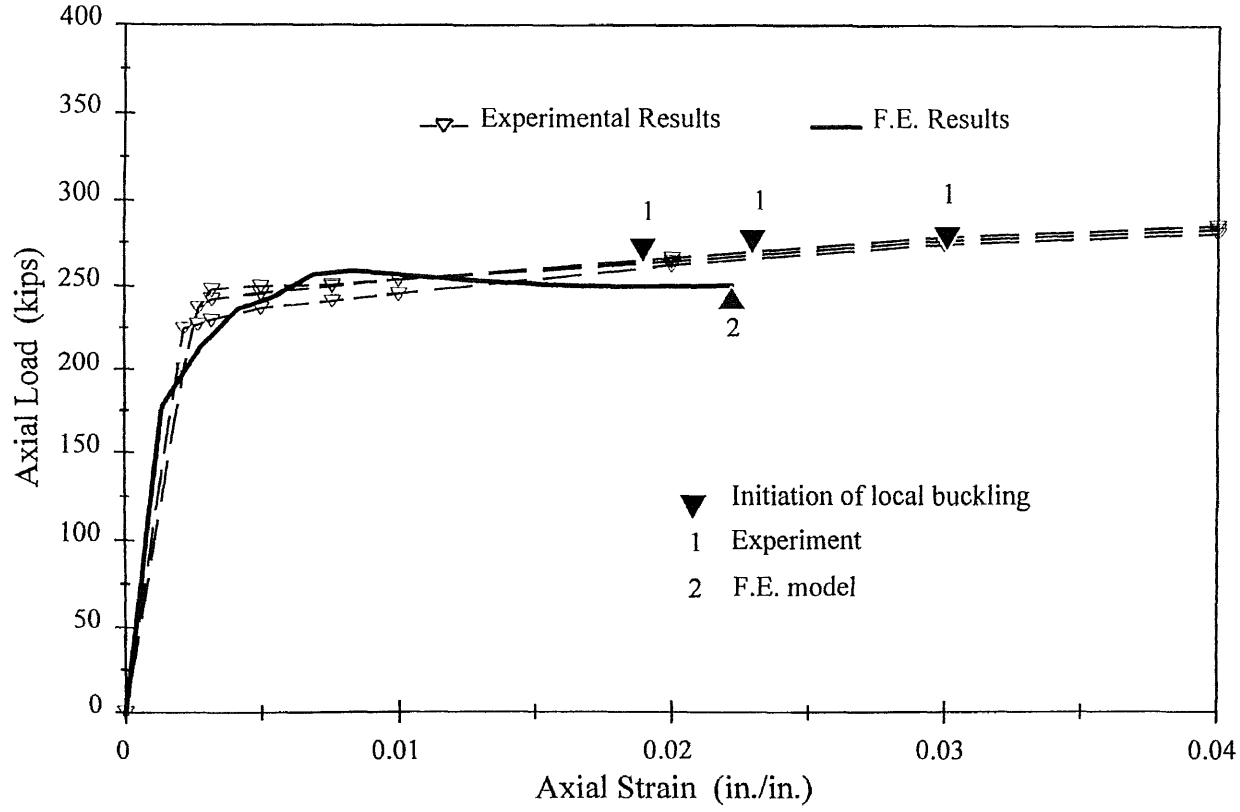

Figure 3.22 Axial load-strain relationship for circular CFT column .17x6x18 inches ($f_c^{'}$.= 3.2 ksi).

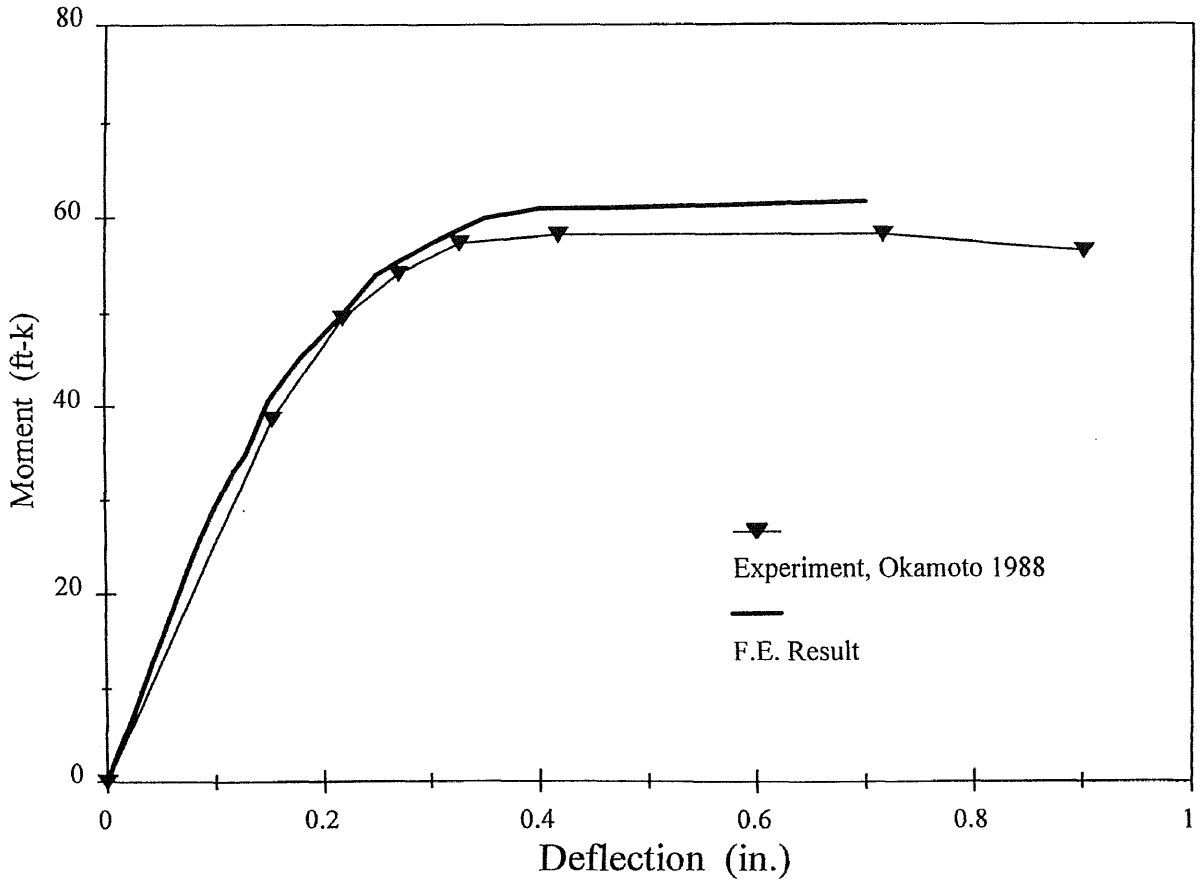

Figure 3.23 Moment-deflection relationship for square CFT column (0.039x6.89x6.89x67 inches).

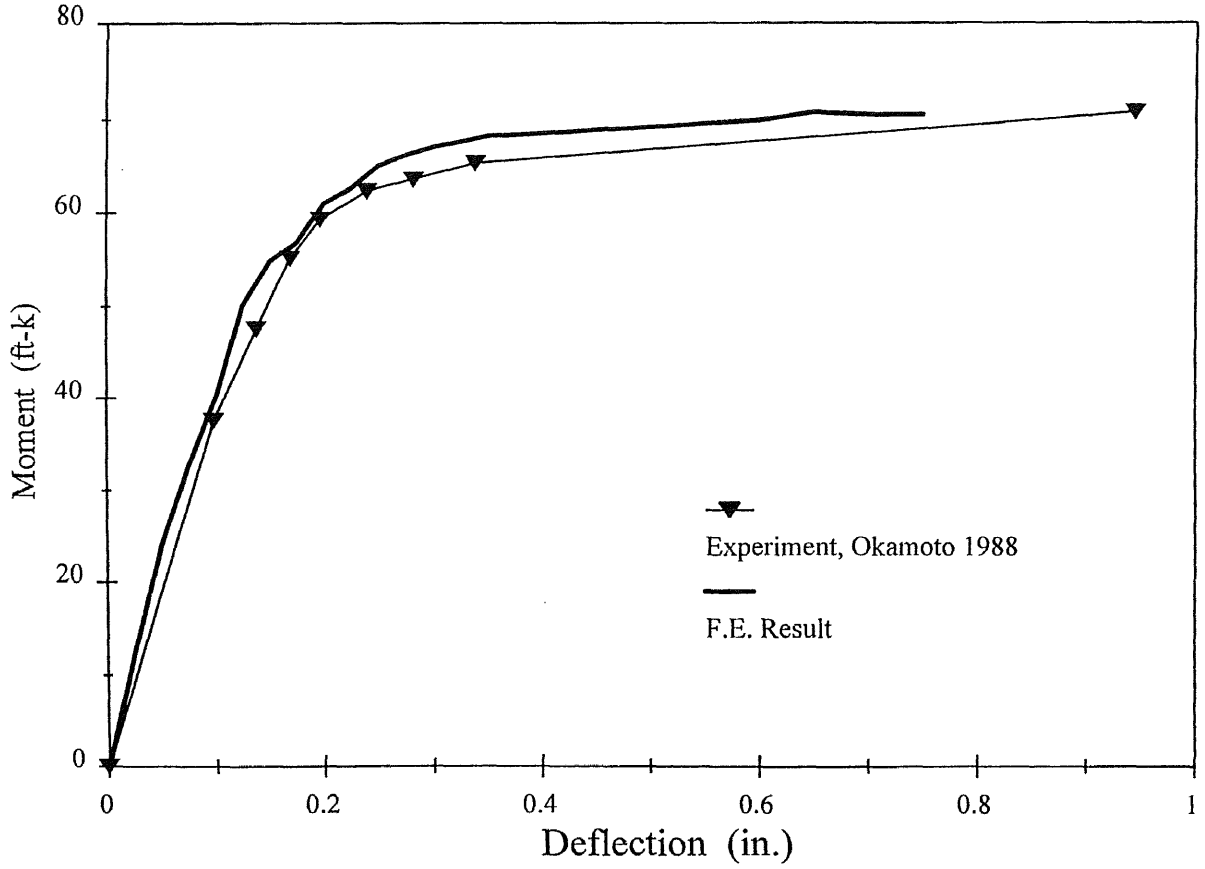

Figure 3.24 Moment-deflection relationship for square CFT column (0.117x6.89x6.89x67 inches).

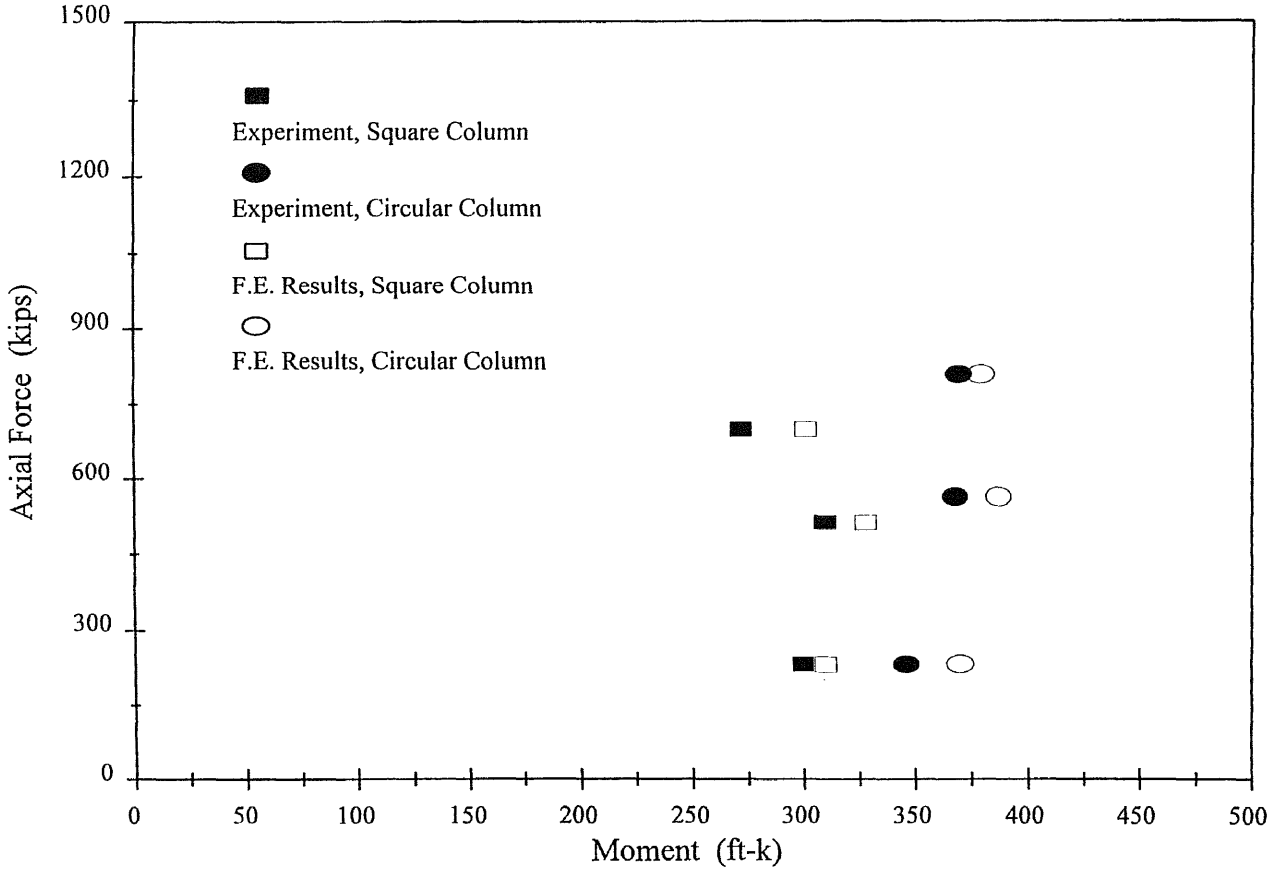

Figure 3.25 Flexural capacity of CFT columns under combined loading, a comparison between test and F.E. results.

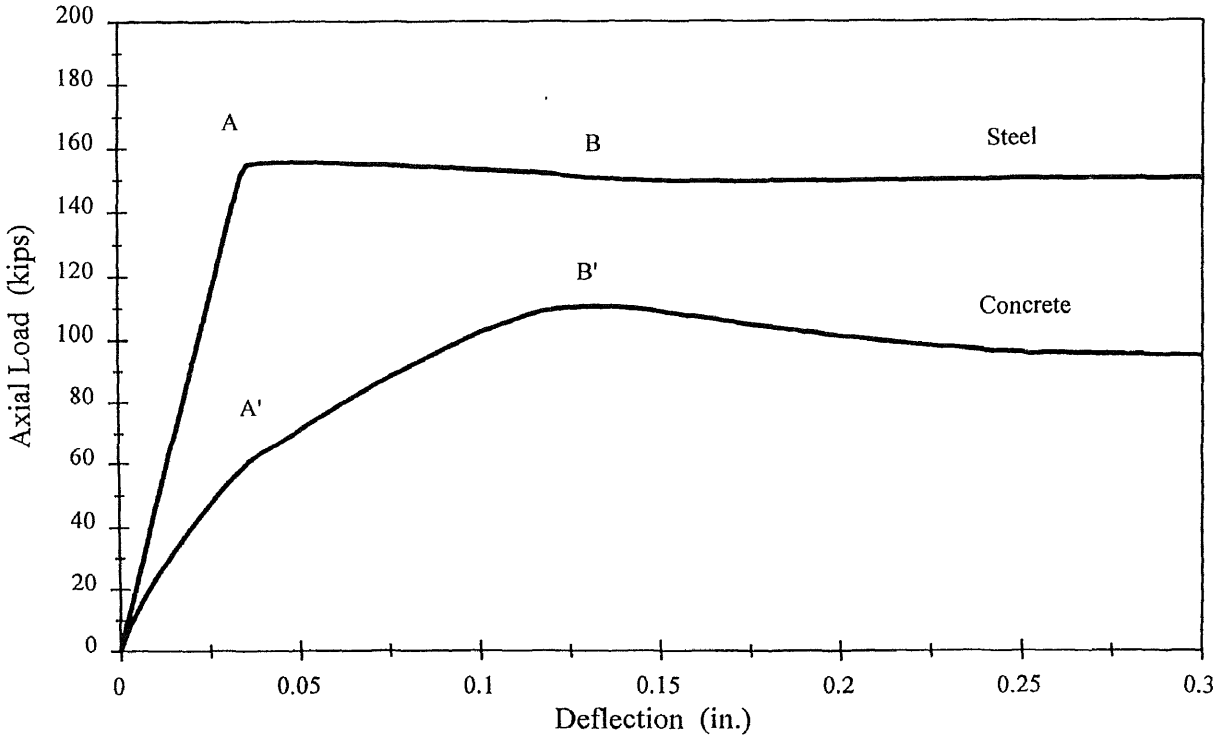

Figure 4.1a. Load-deflection relationship for concrete core and steel tube.
(Square CFT column B=6.0 in., L=24.0 in., $f_c^{'}$ = 2.0 ksi)

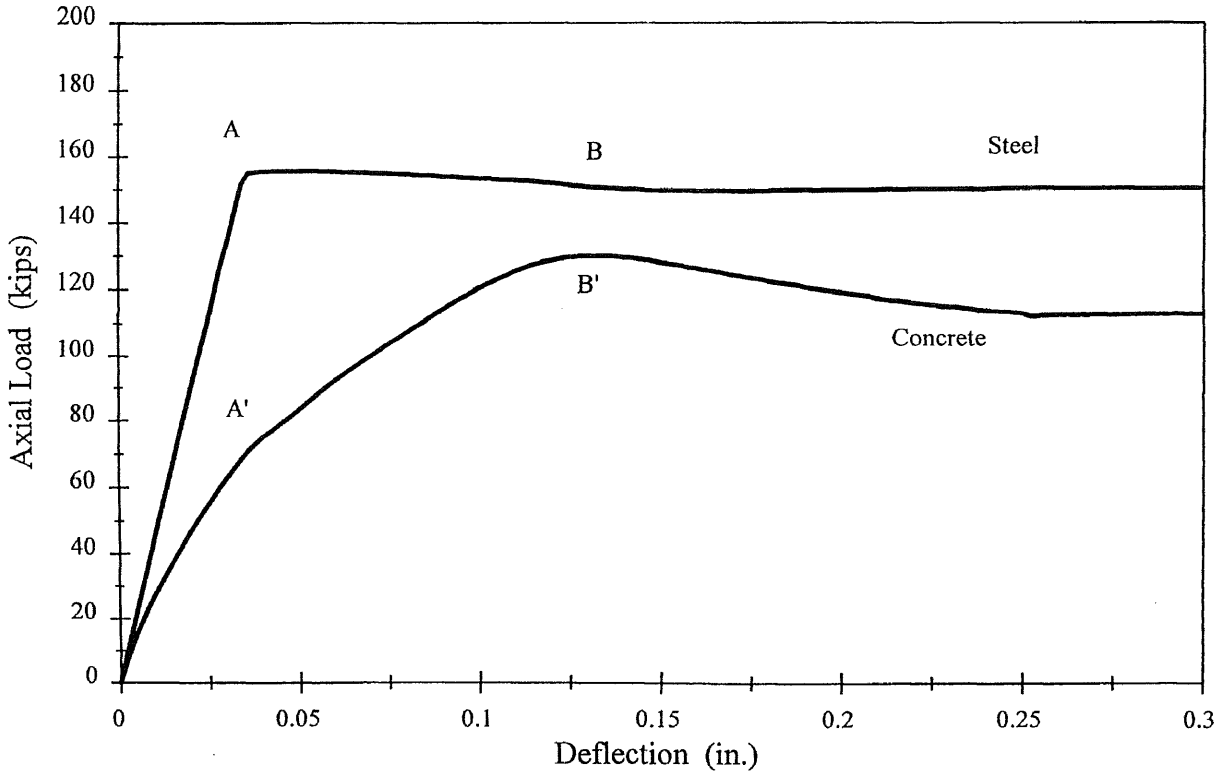

Figure 4.1b Load-deflection relationship for concrete core and steel tube.
(Circular CFT column D=6.0 in., L=24.0 in., $f_c^{'}$ = 2.0 ksi)

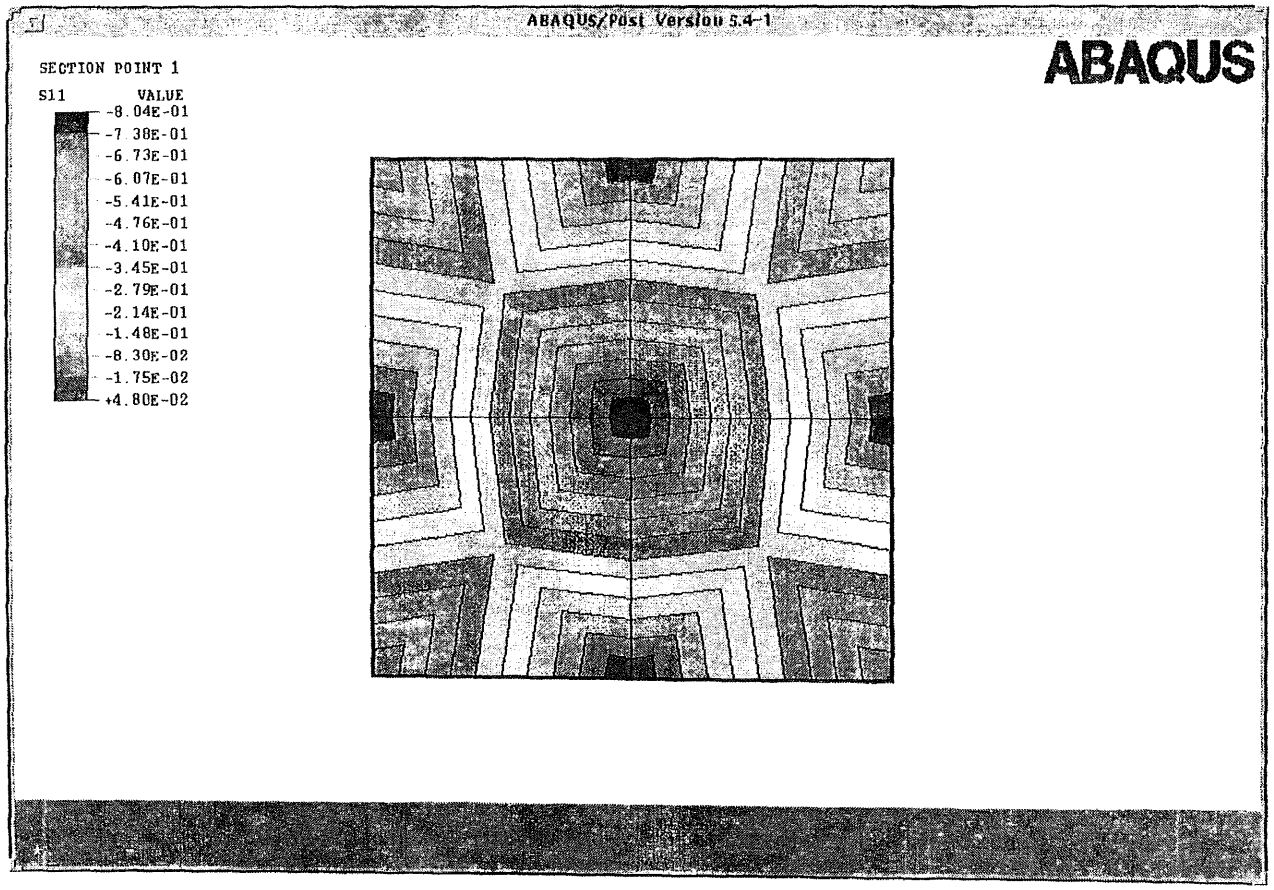

Figure 4.2 Lateral stress distribution at cross-section in square columns under axial loading.

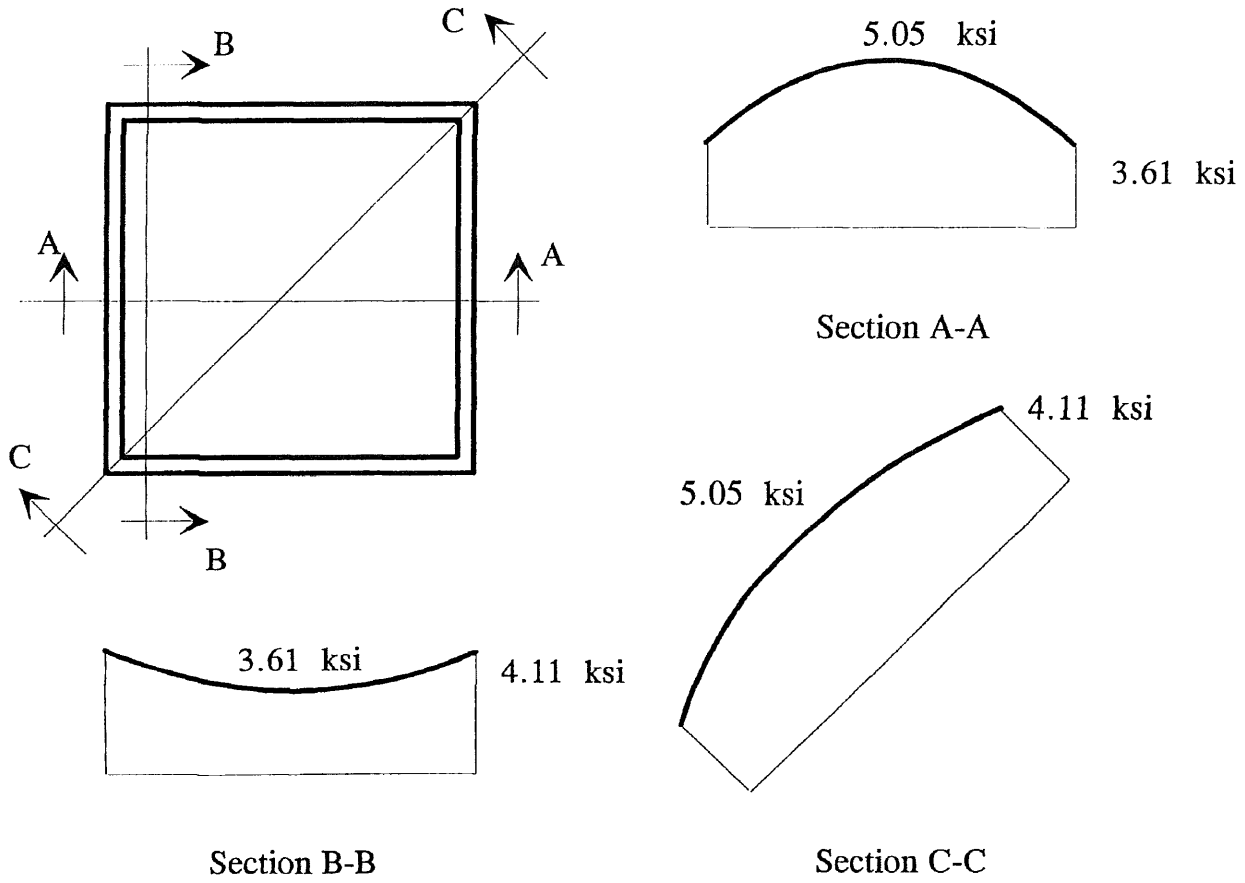

Figure 4.3 Axial stress distribution at the cross section.

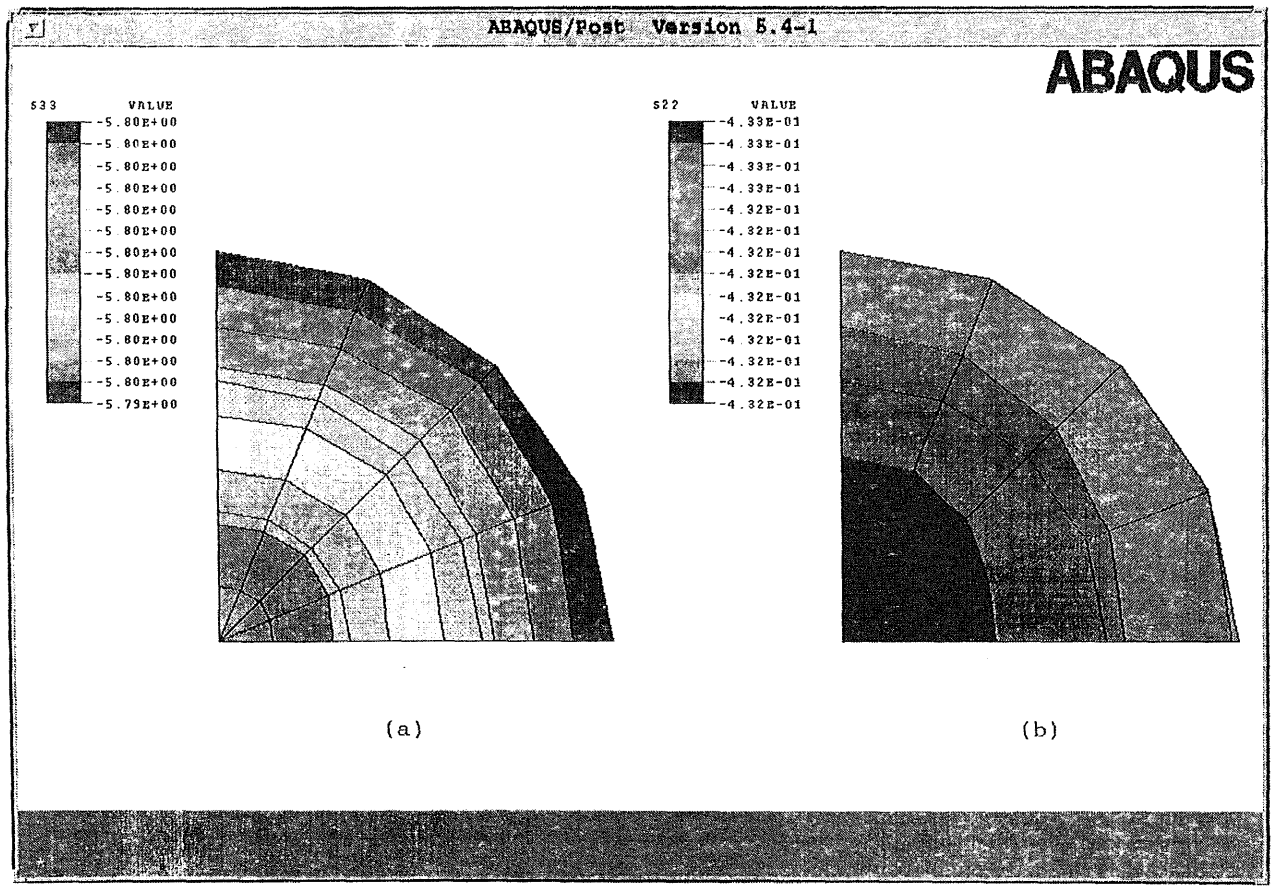

Figure 4.4 Lateral stress distribution at cross-section in circular columns under axial loading.

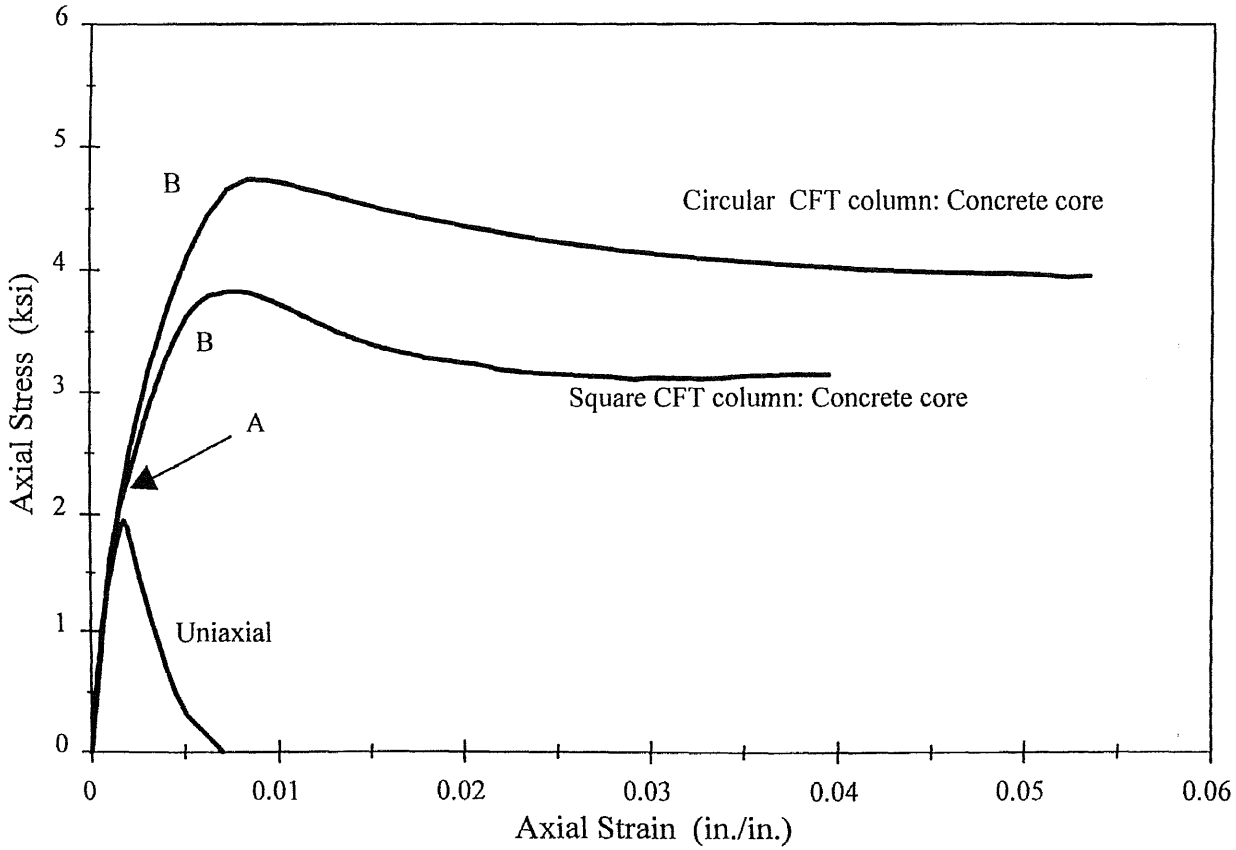

Figure 4.5a Concrete stress-strain relationship for concrete core.

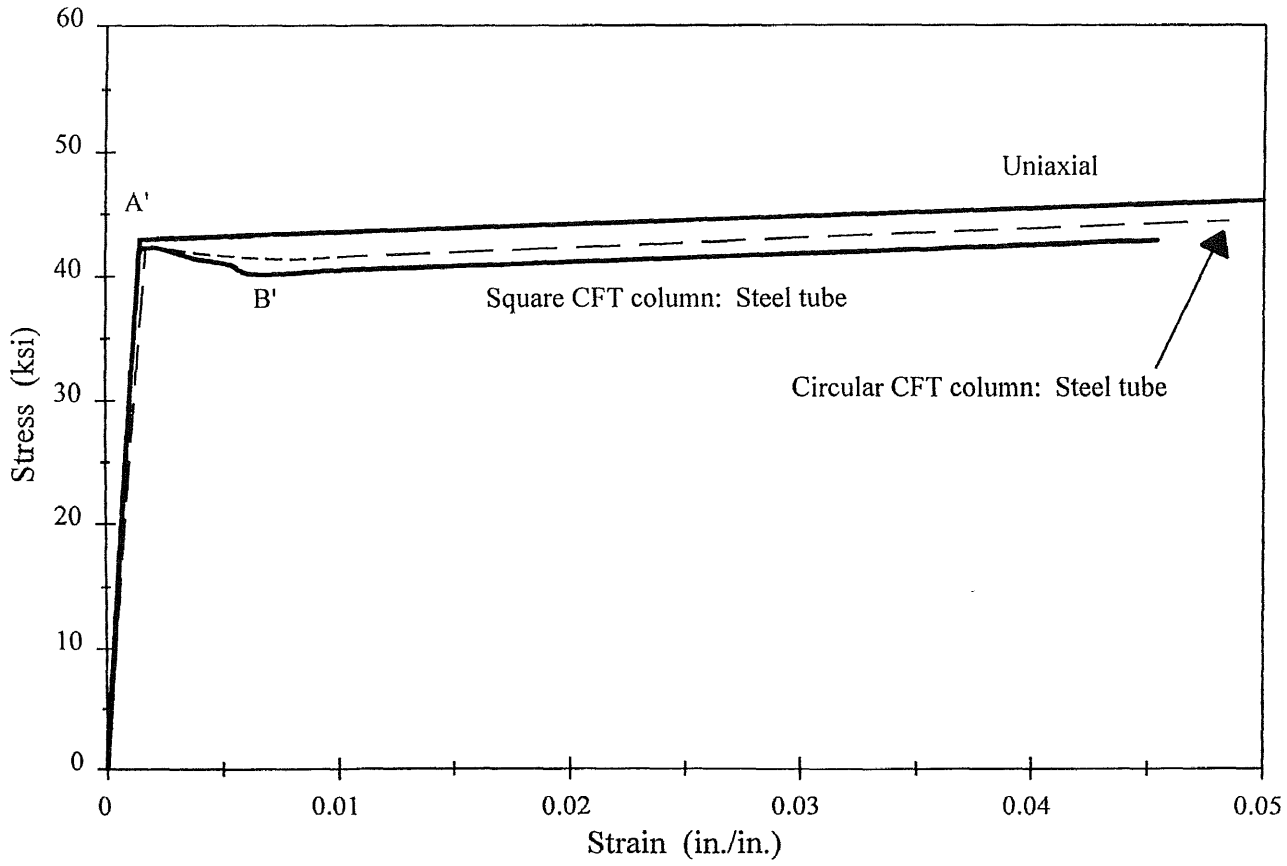

Figure 4.5b Steel stress-strain relationship.

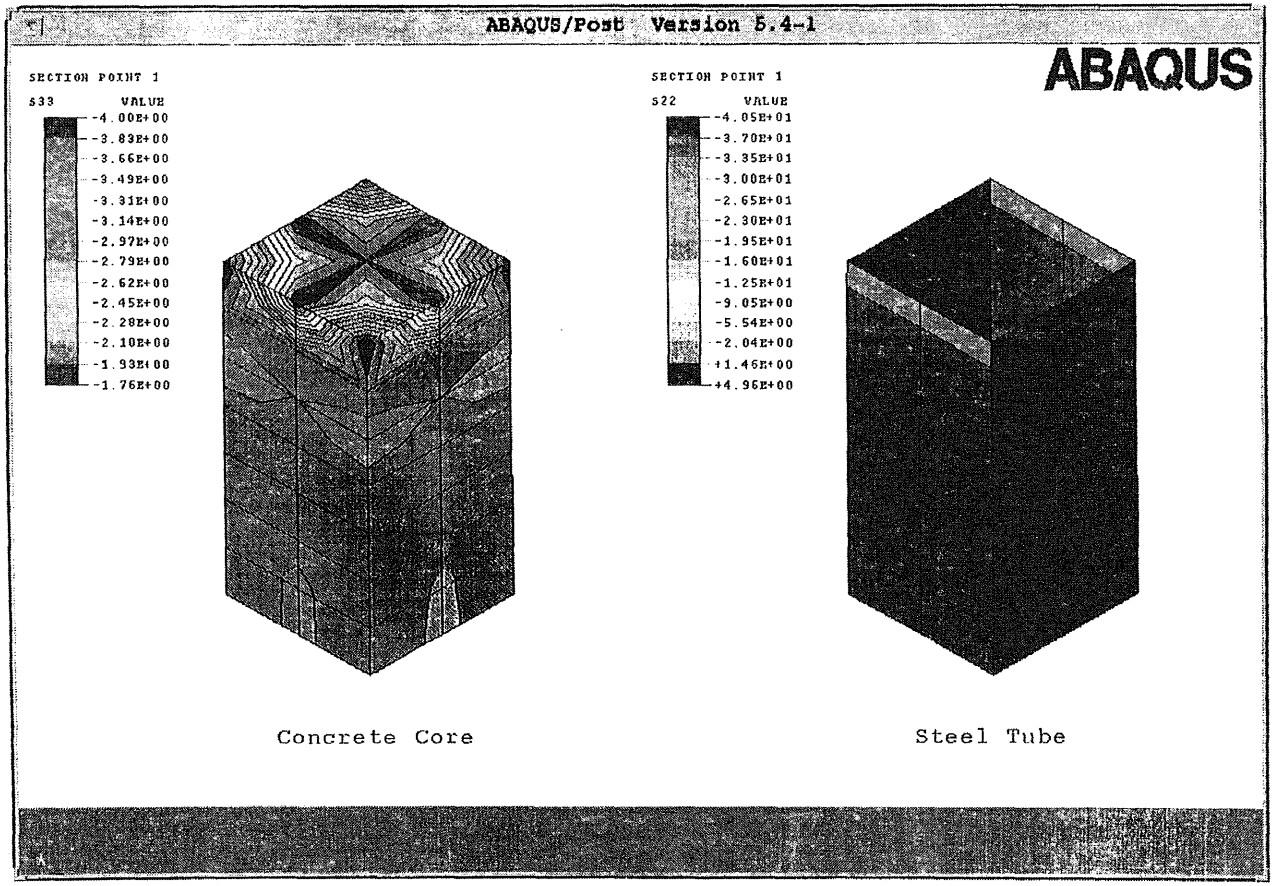

Figure 4.6a Axial stress contours for the steel tube and the concrete core in square CFT column.

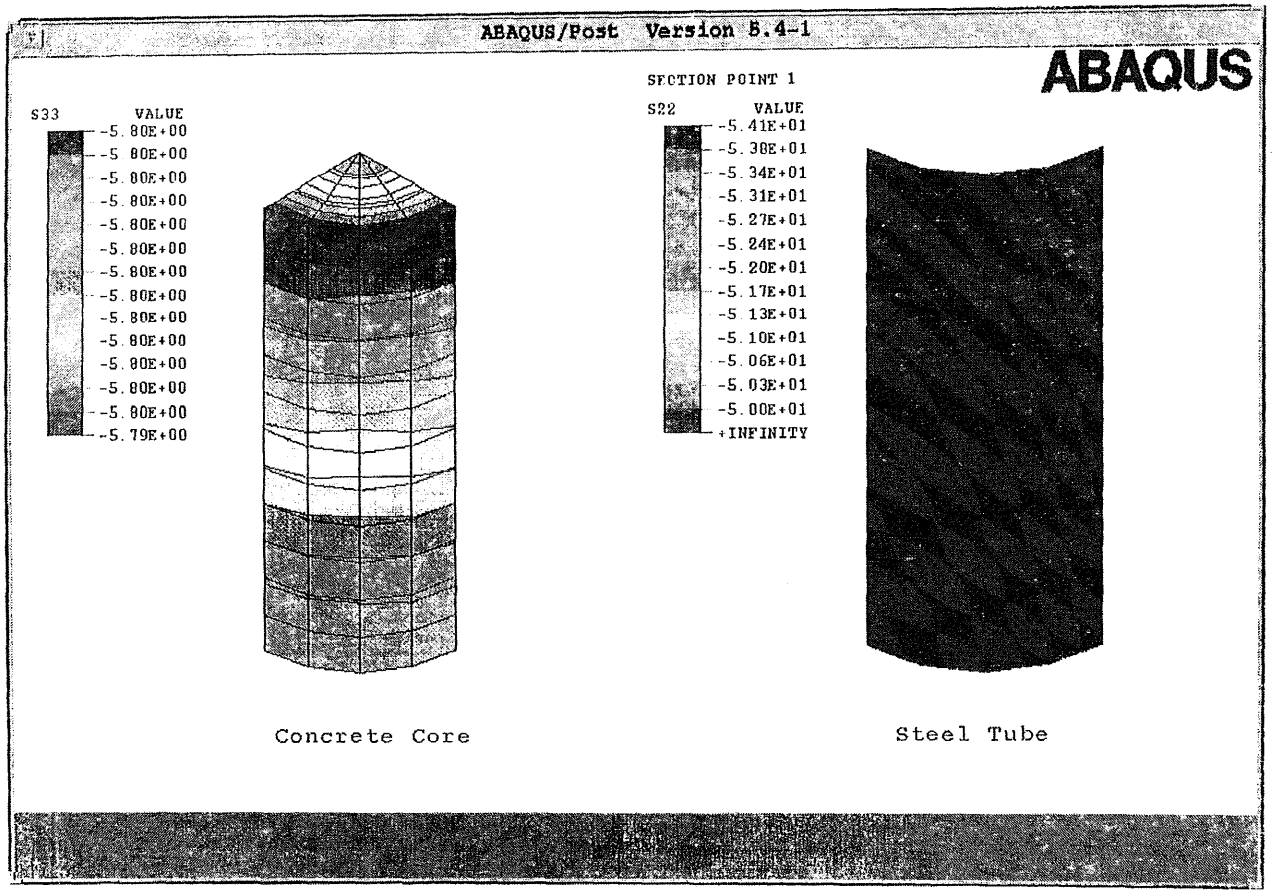

Figure 4.6b Axial stress contours for the steel tube and the concrete core in circular CFT column.

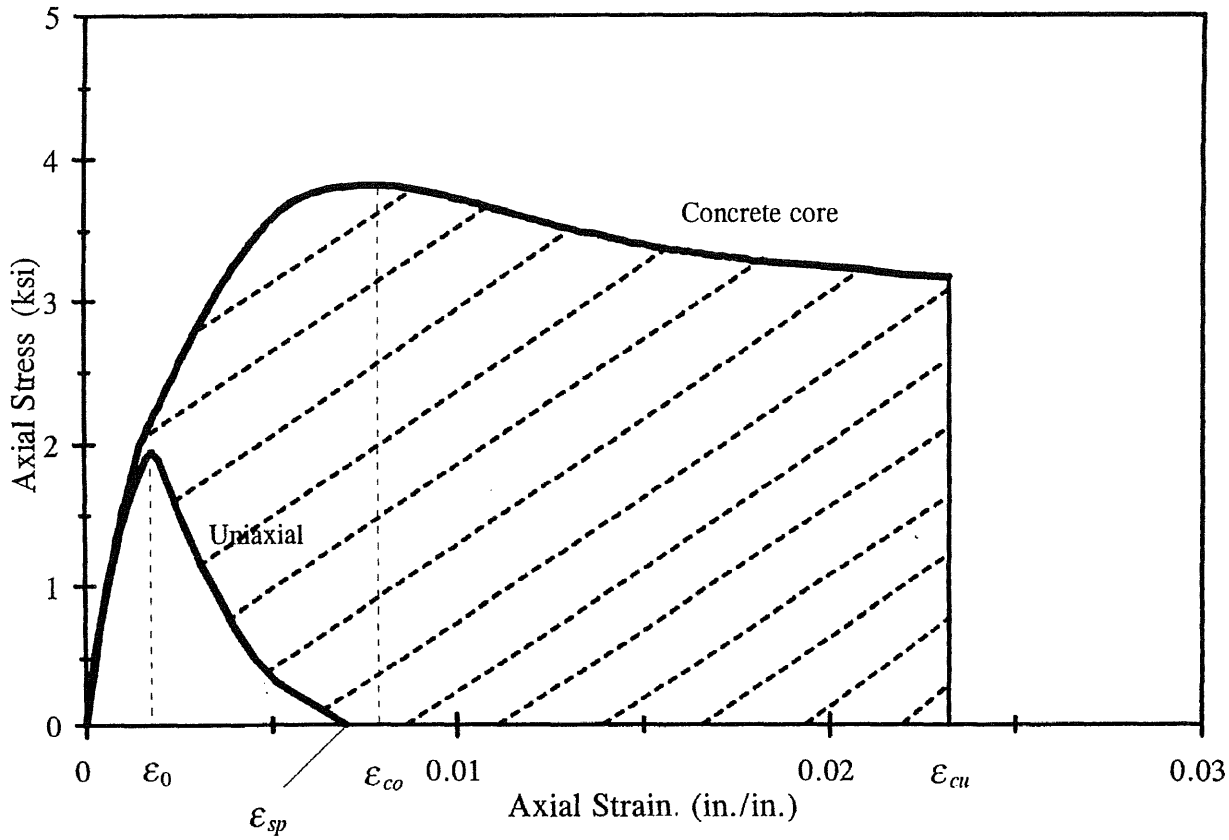

Figure 4.7 Stress-strain relationship for concrete core in CFT columns.

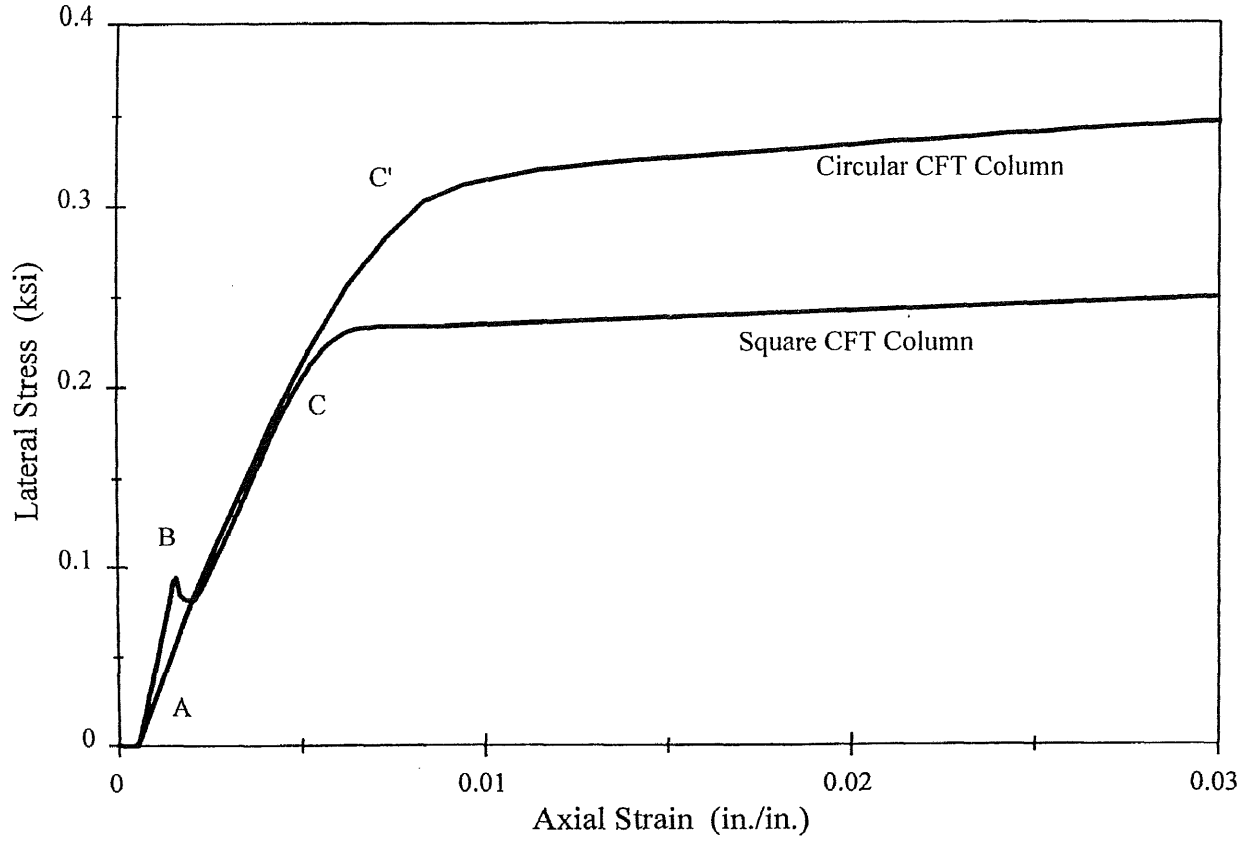

Figure 4.8 Confining stress on the concrete core.

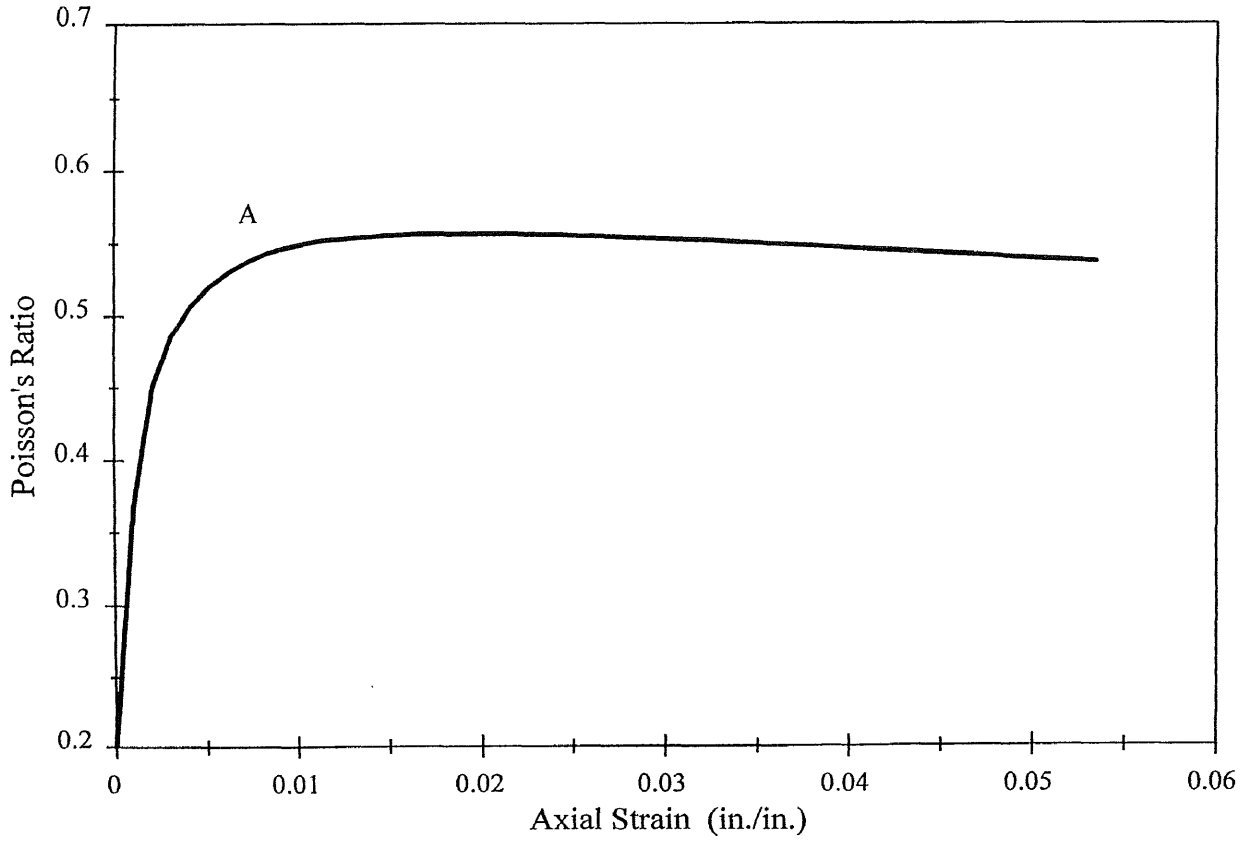

Figure 4.9 Poisson's ratio-axial strain relationship for the concrete core.

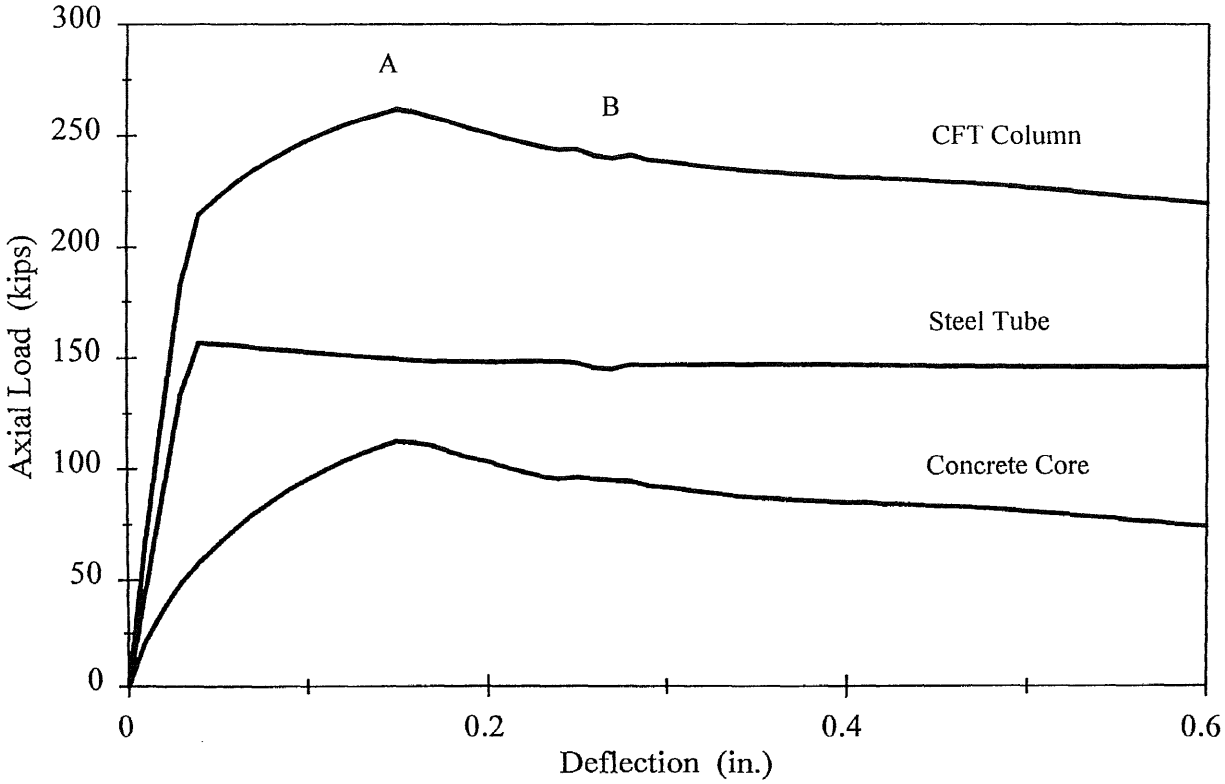

Figure 4.10 Typical axial load-deformation curve for square CFT columns.

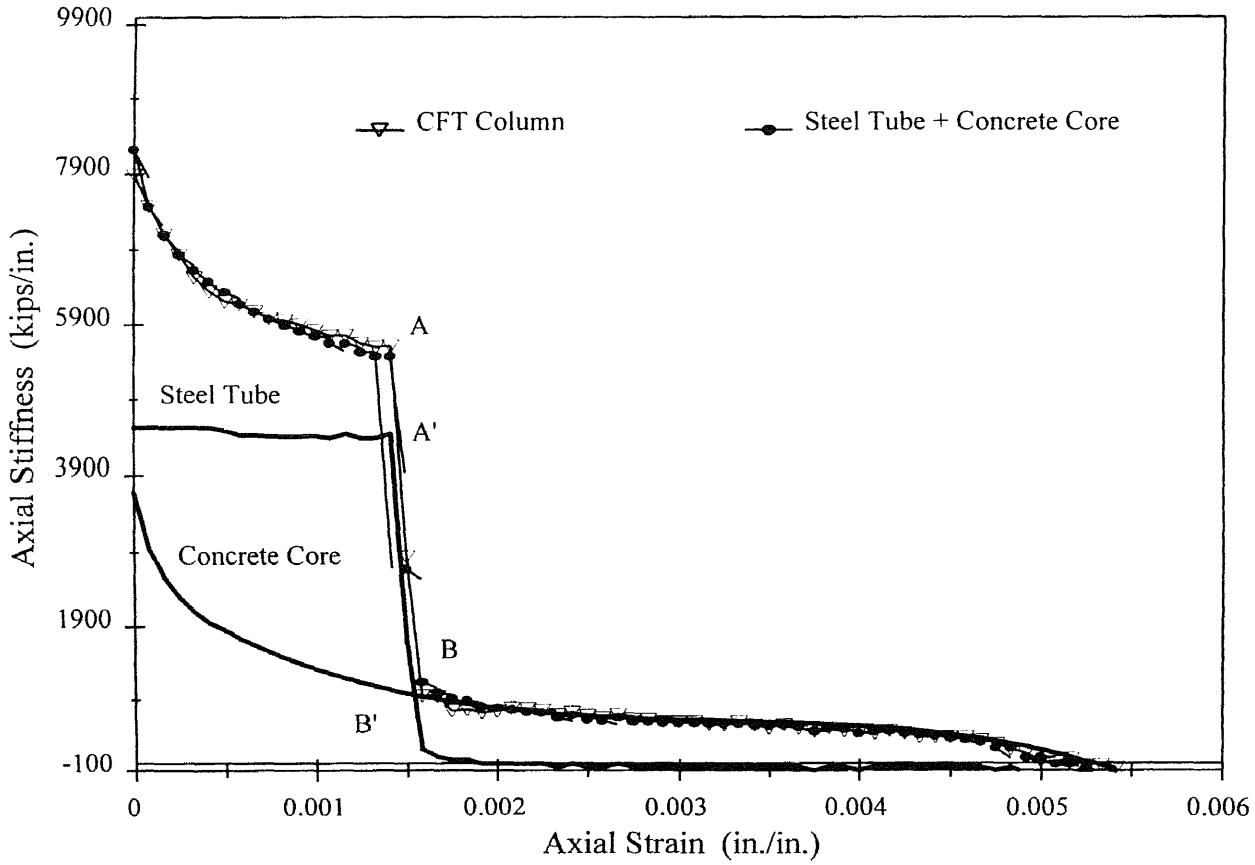

Figure 4.11 Axial stiffness for components of the CFT column.

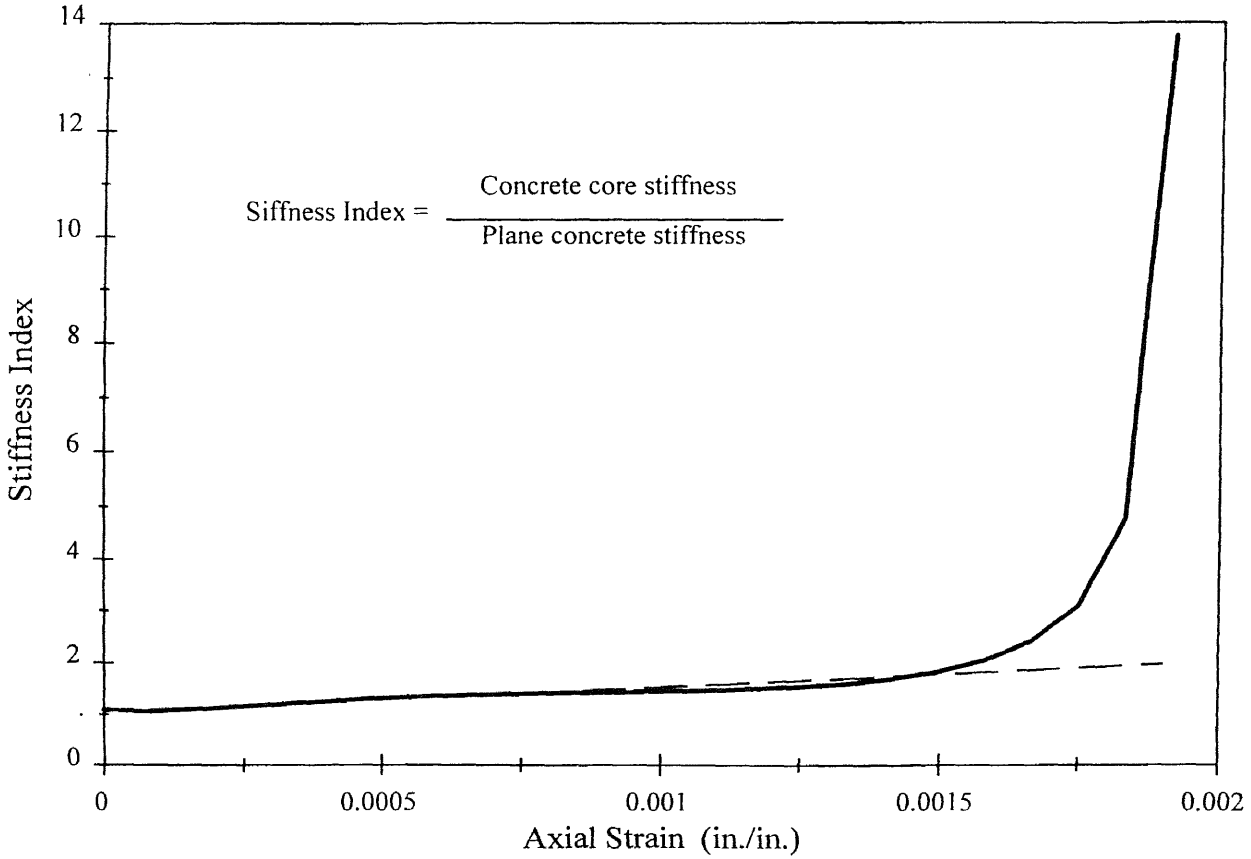

Figure 4.12 Increase in the axial stiffness of concrete core compared with plain concrete.

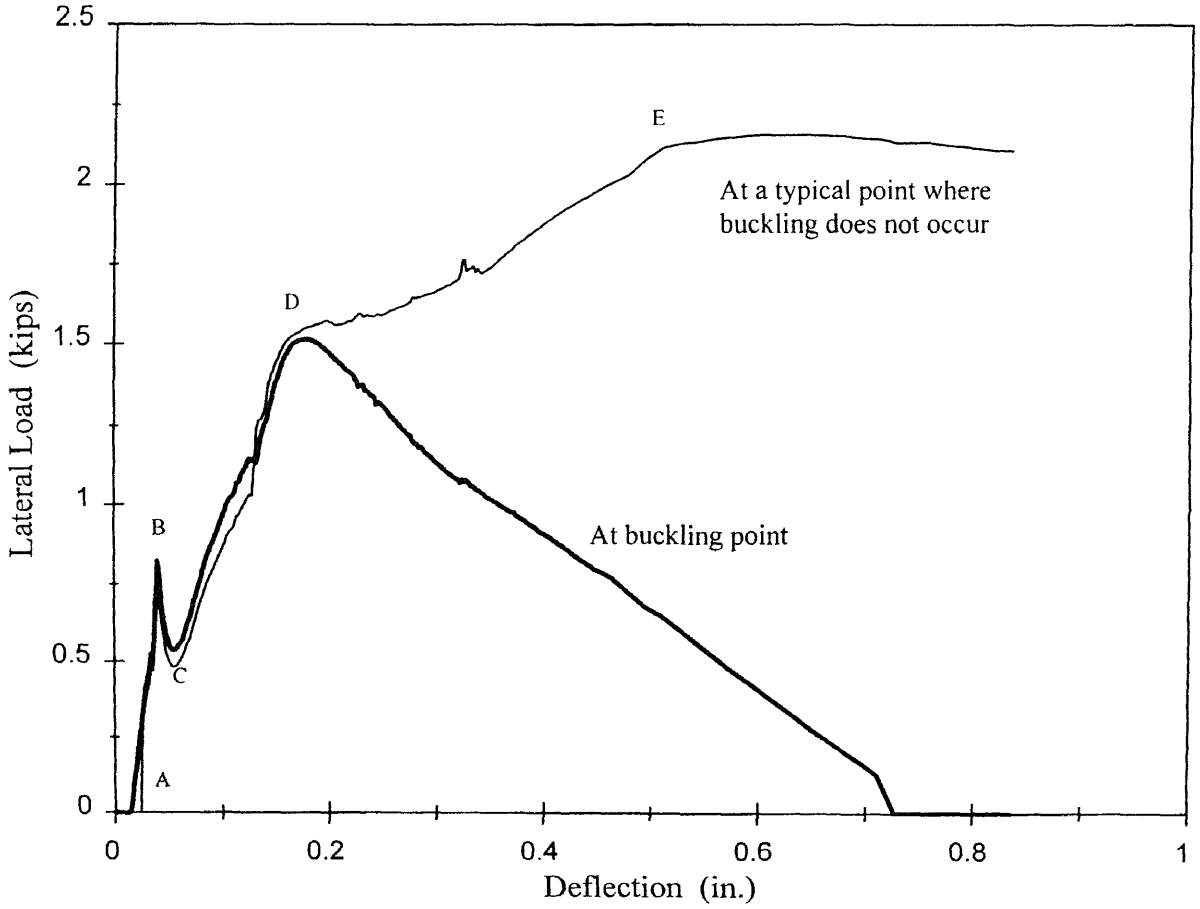

Figure 4.13 Contact force between steel tube and concrete core.

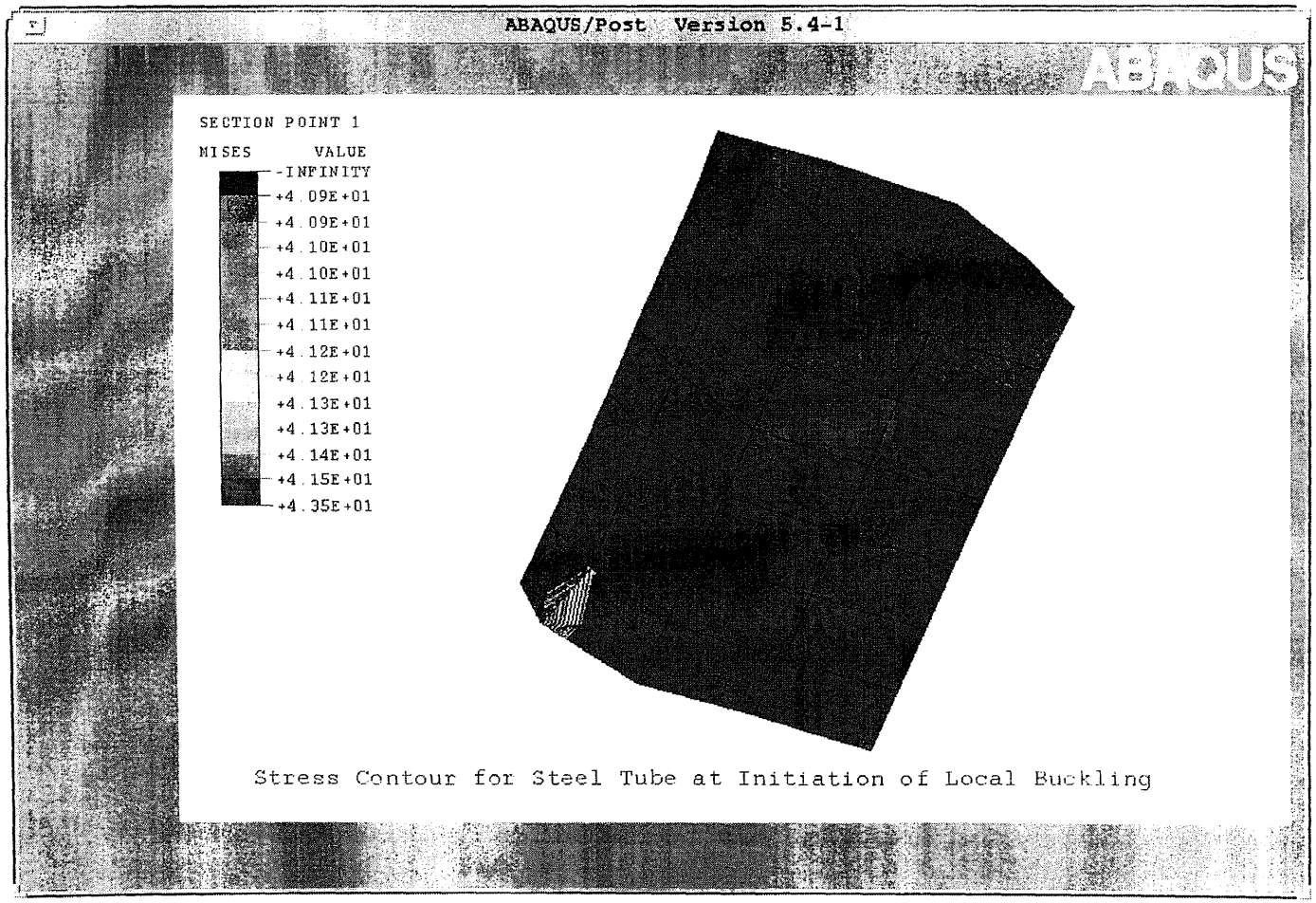

Figure 4.14 Local buckling of steel tube and stress contours.

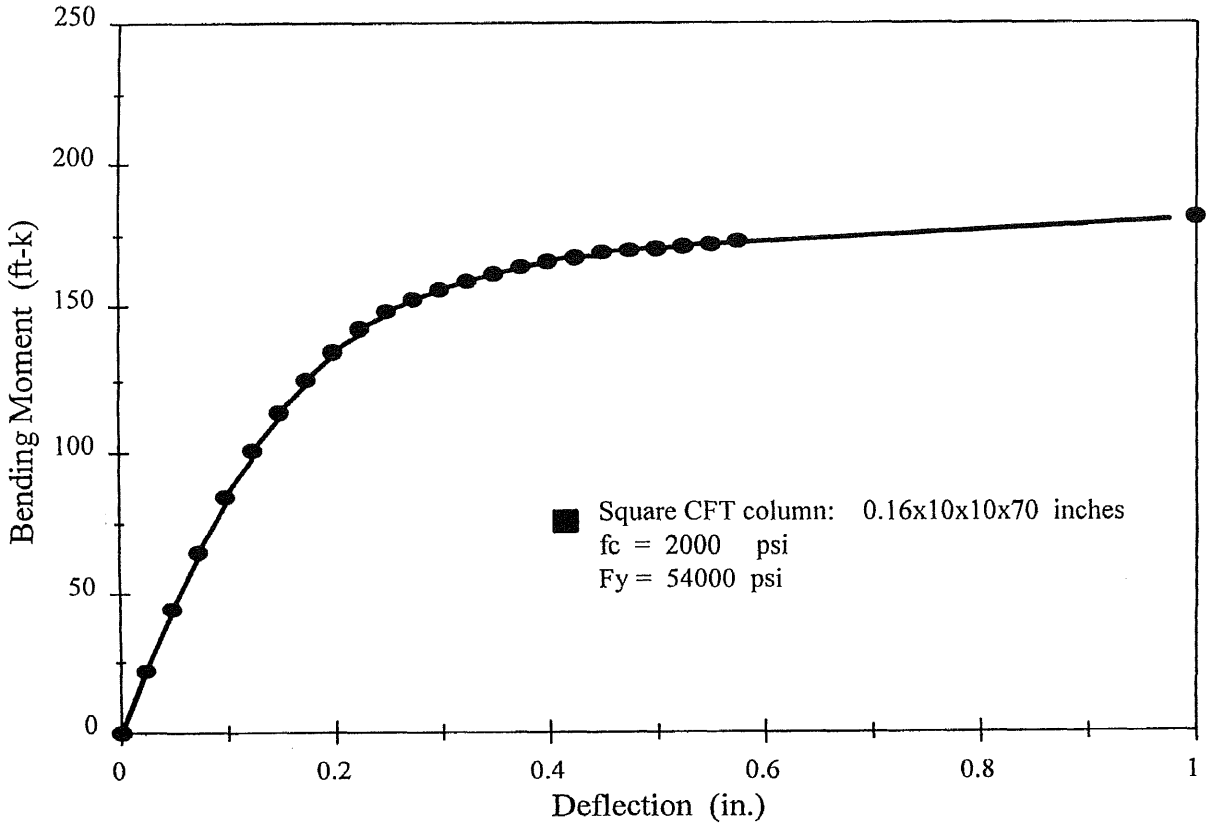

Figure 5.1 Bending moment-defection relationship for Square CFT columns.

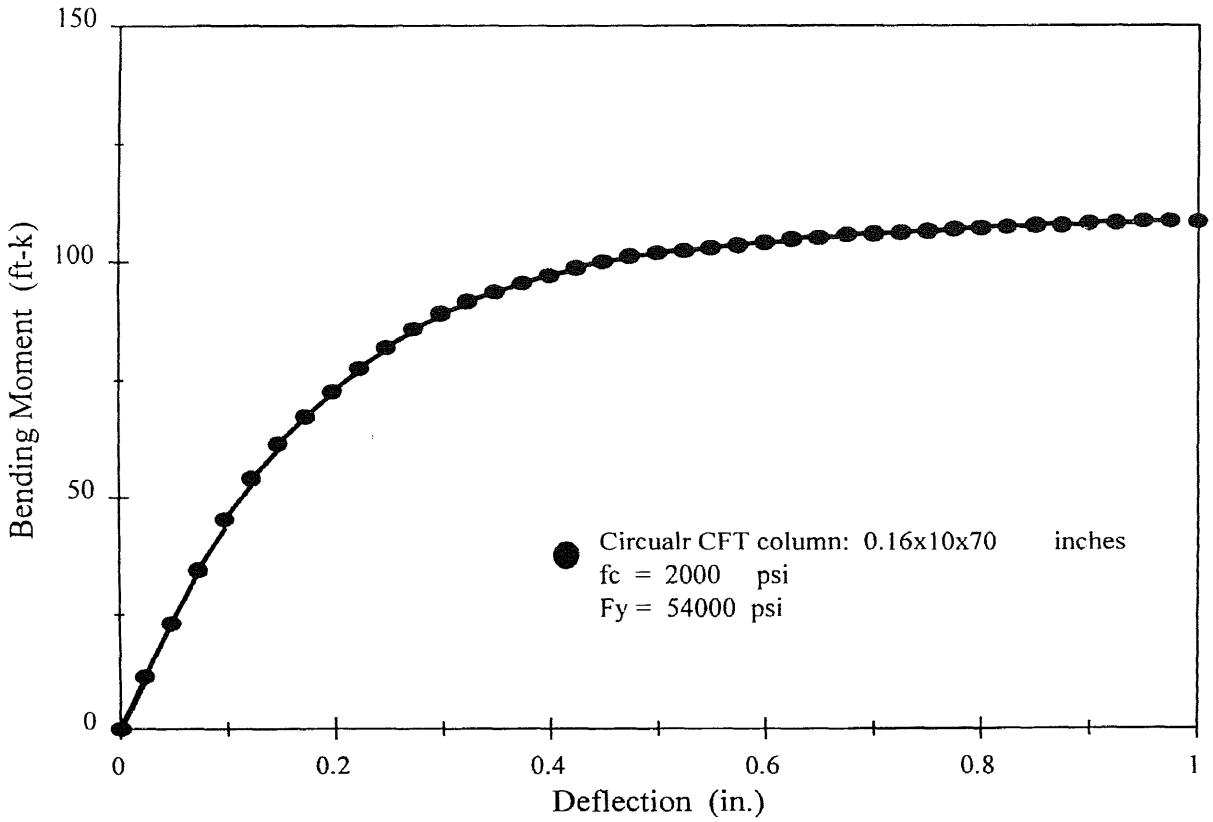

Figure 5.2 Bending moment-defection relationship for circular CFT columns.

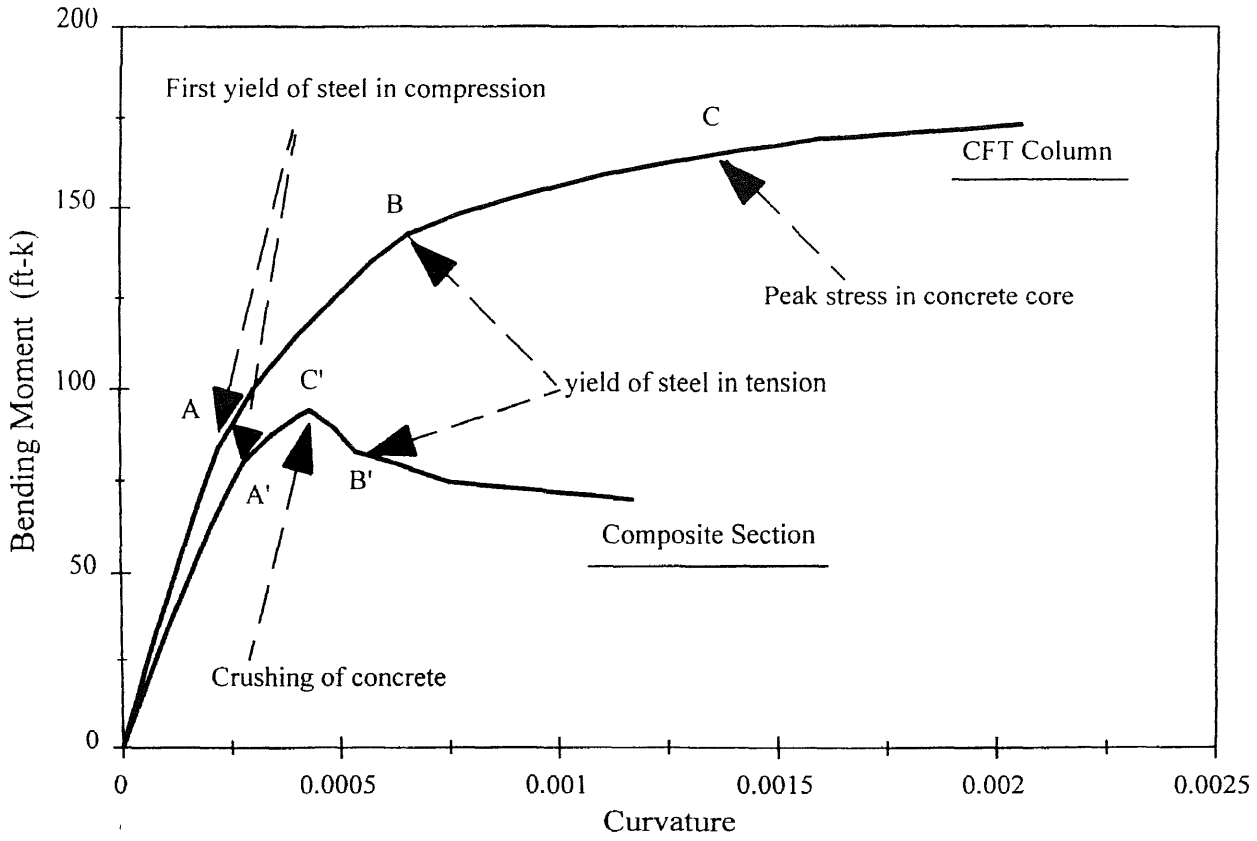

Figure 5.3 Moment-curvature relationships for CFT columns and composite sections.

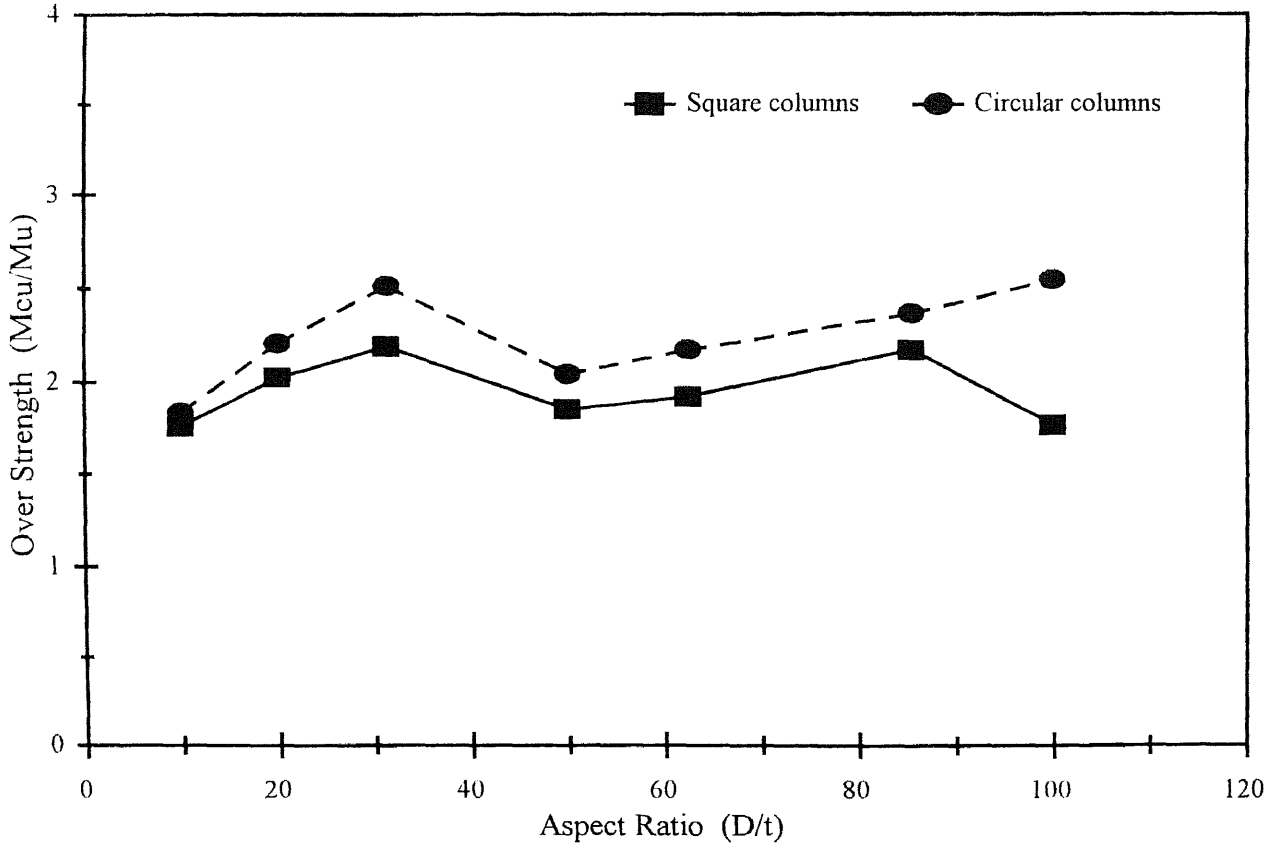

Figure 5.4 Over strength in moment capacity of CFT columns compared to combined sections.

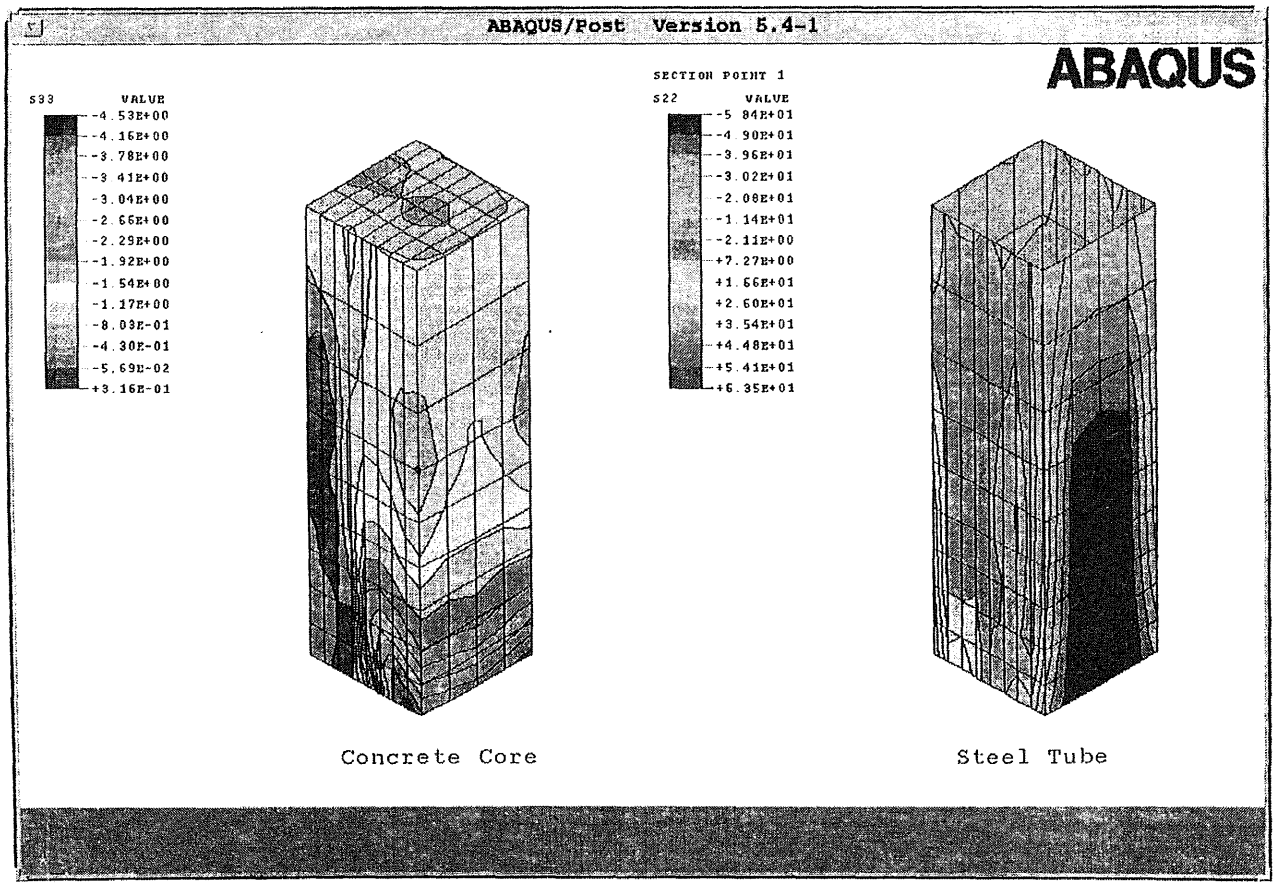

Figure 5.5 Longitudinal stress distributions for steel tube and concrete core in square CFT columns.

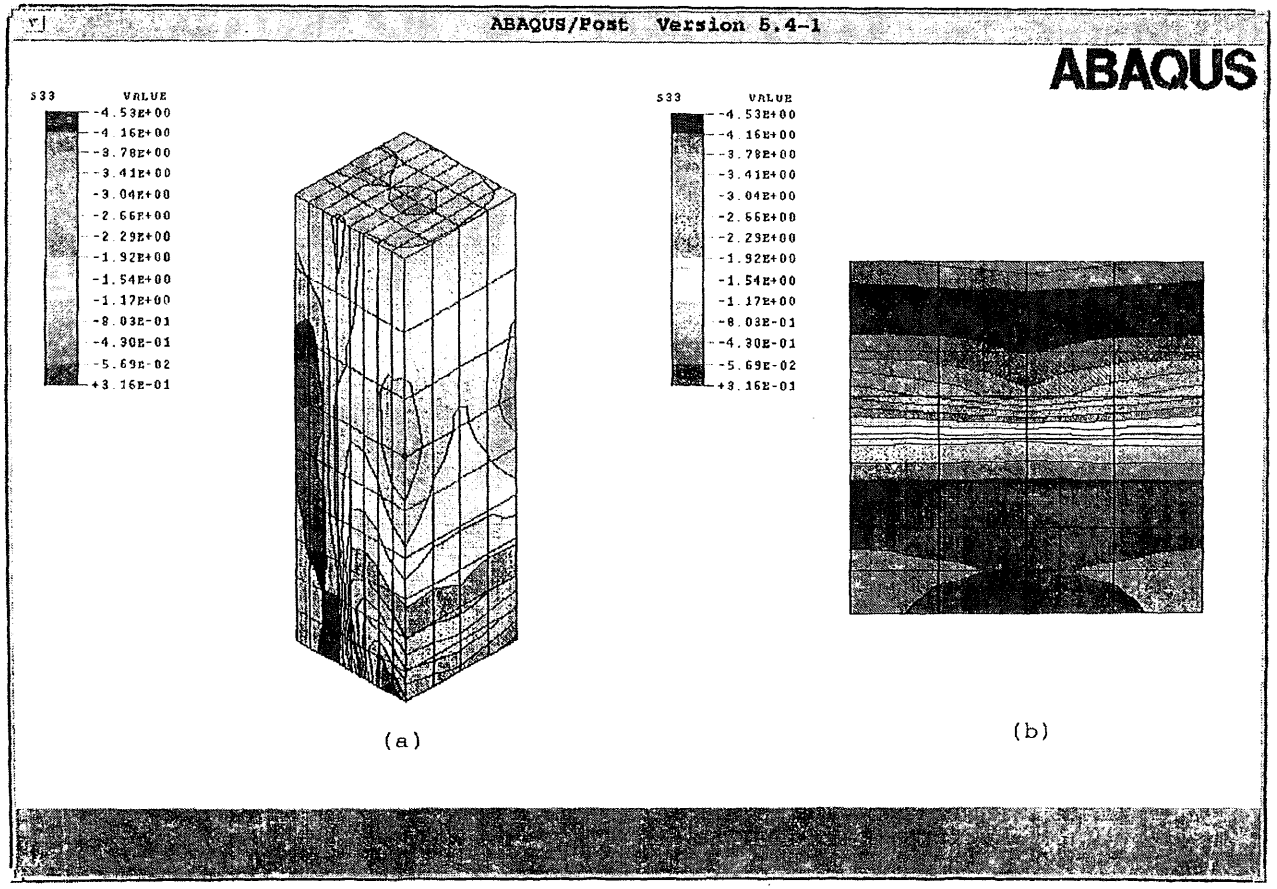

Figure 5.6a Axial stress distribution of concrete core in longitudinal and cross-sectional directions.

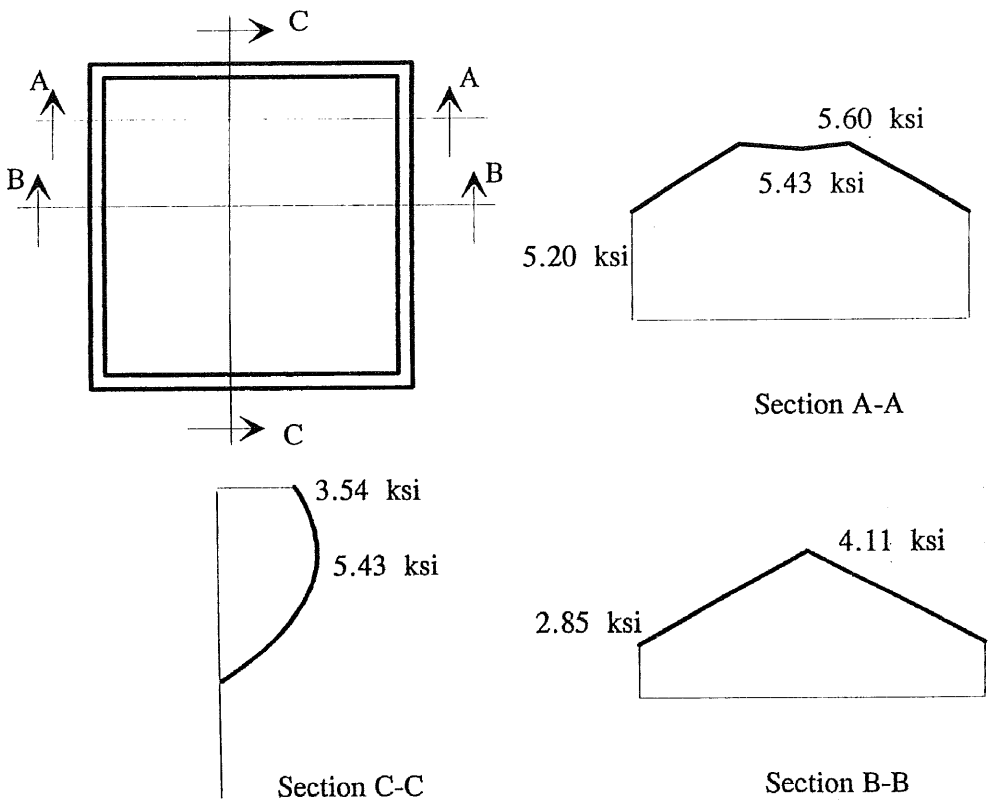

Figure 5.6b Axial stress distribution of concrete core at cross section.

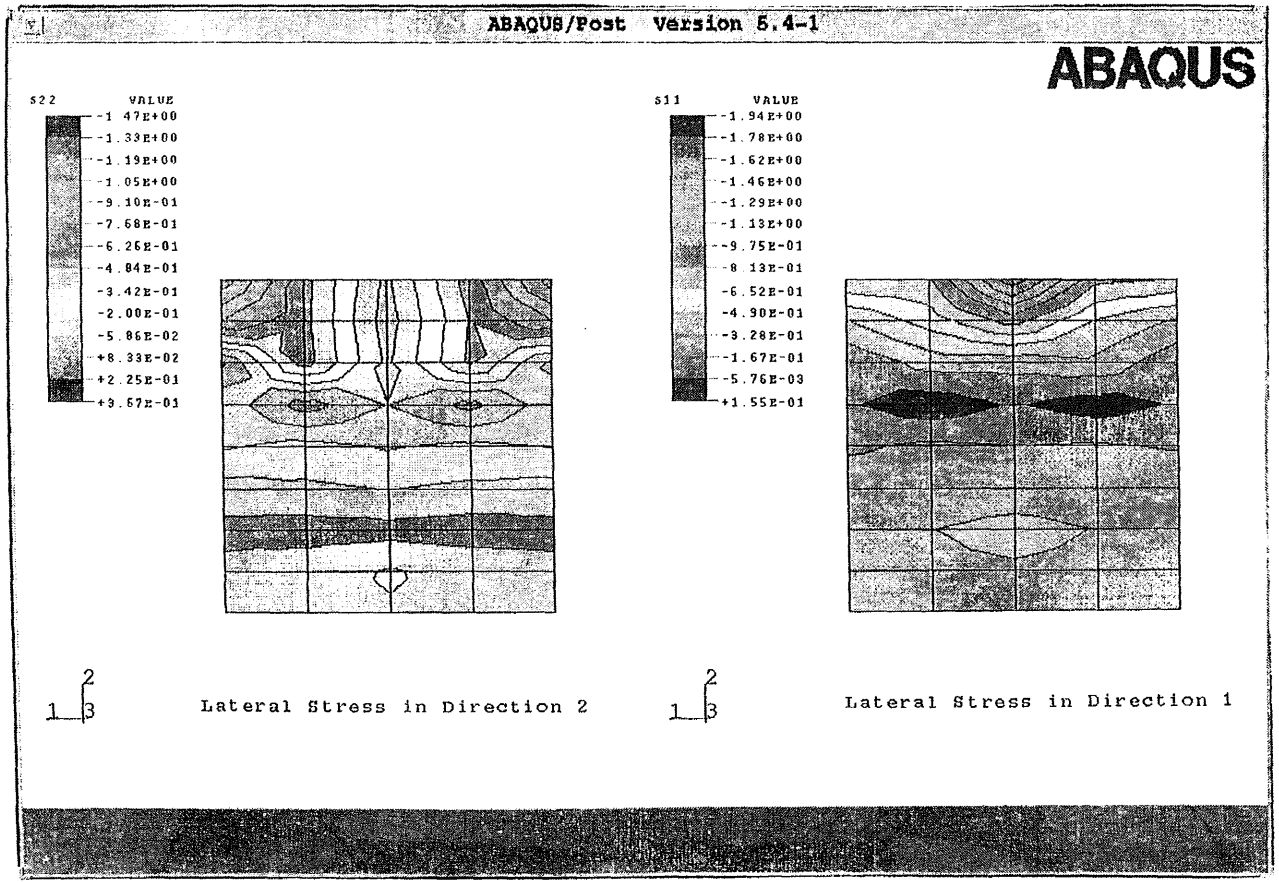

Figure 5.7 Lateral distribution of concrete core at cross section.

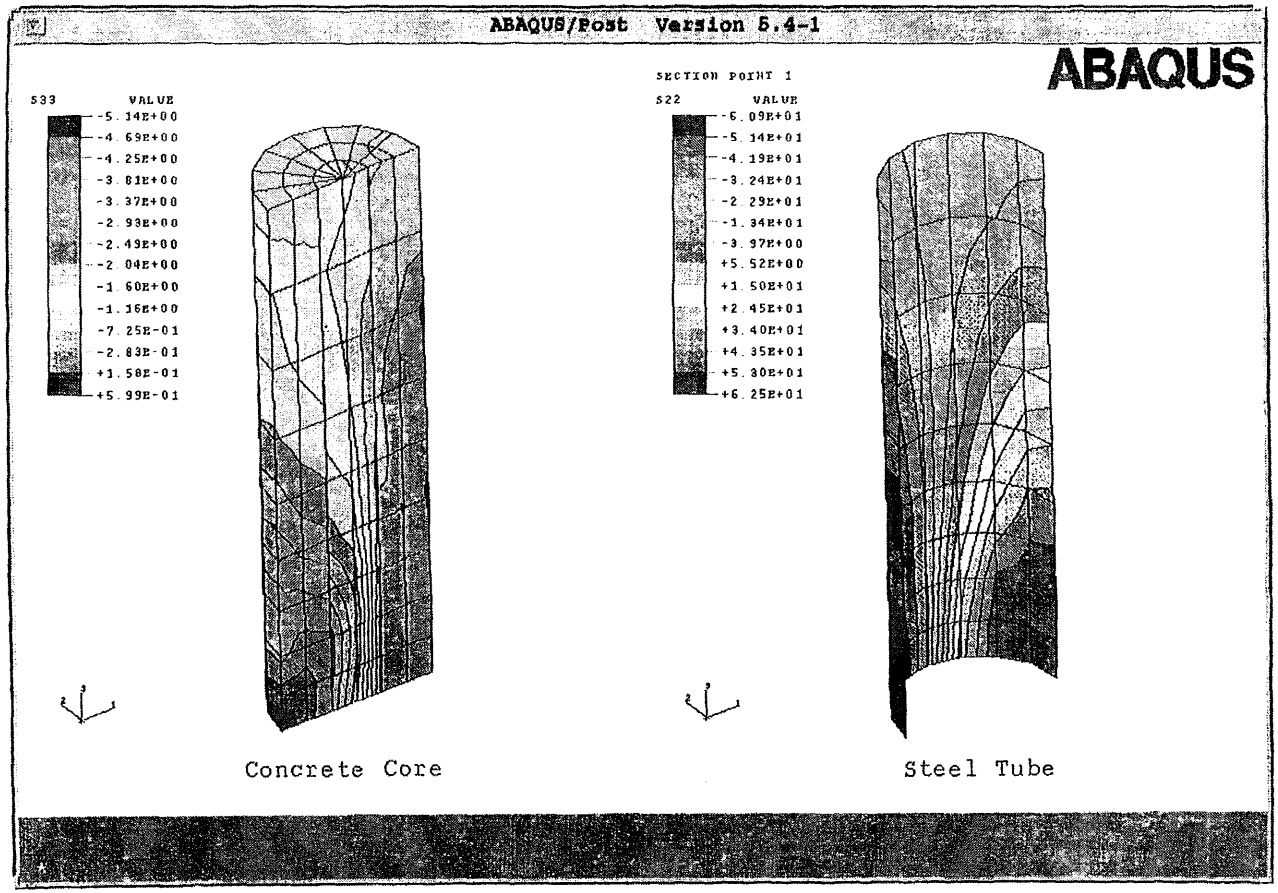

Figure 5.8 Longitudinal stress distributions for steel tube and concrete core in circular CFT columns.

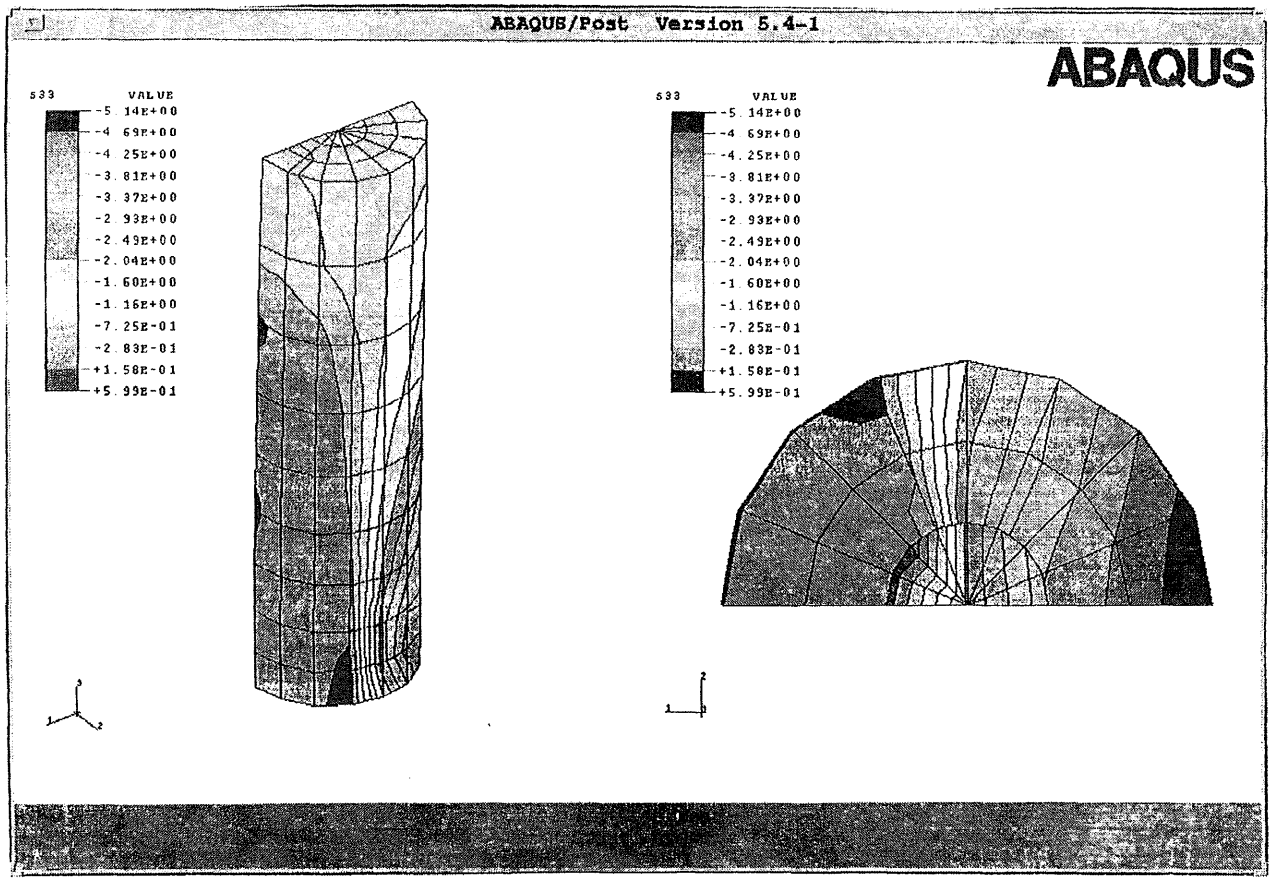

Figure 5.9 Longitudinal and cross-sectional stress distributions for concrete core in circular CFT columns.

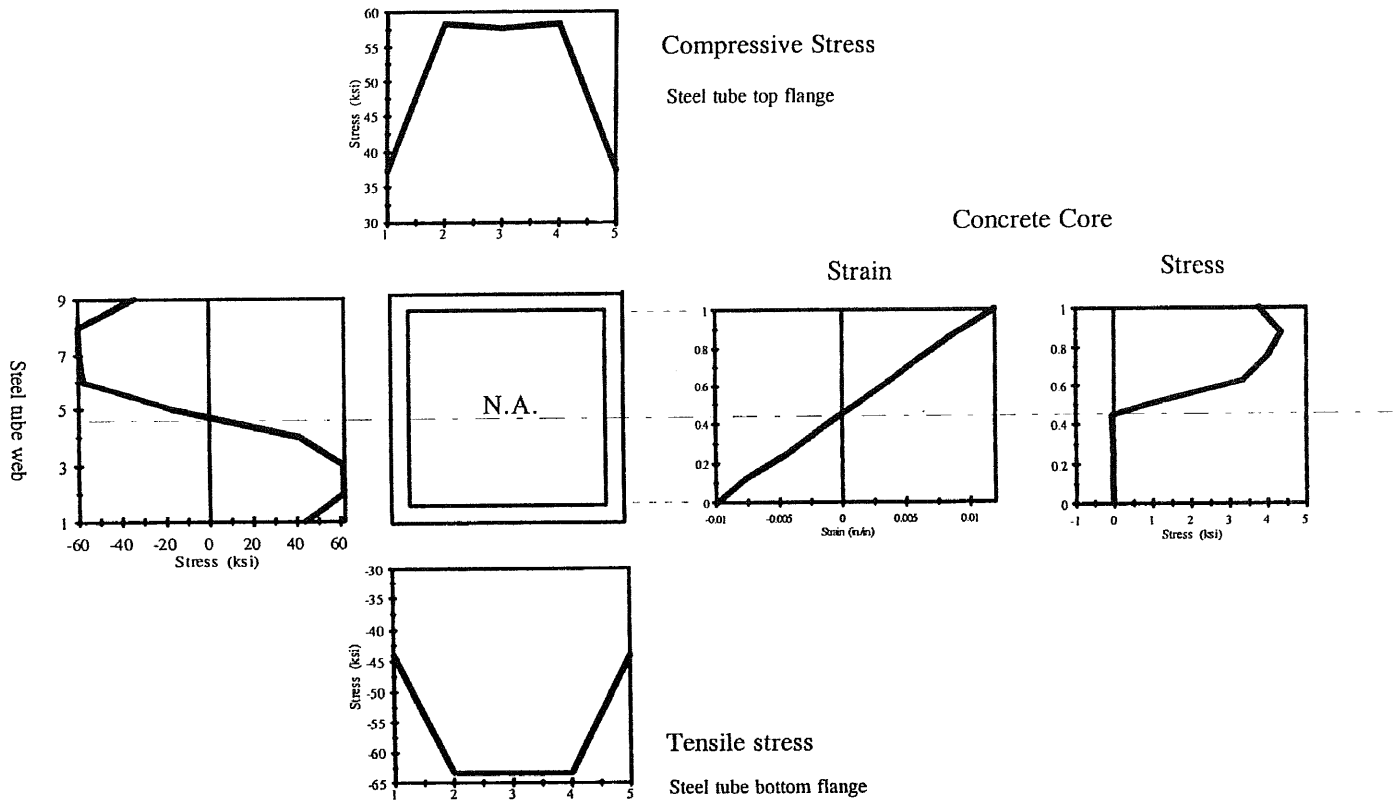

Figure 5.10 Cross-sectional stress distribution for a square CFT column under combined Loading.

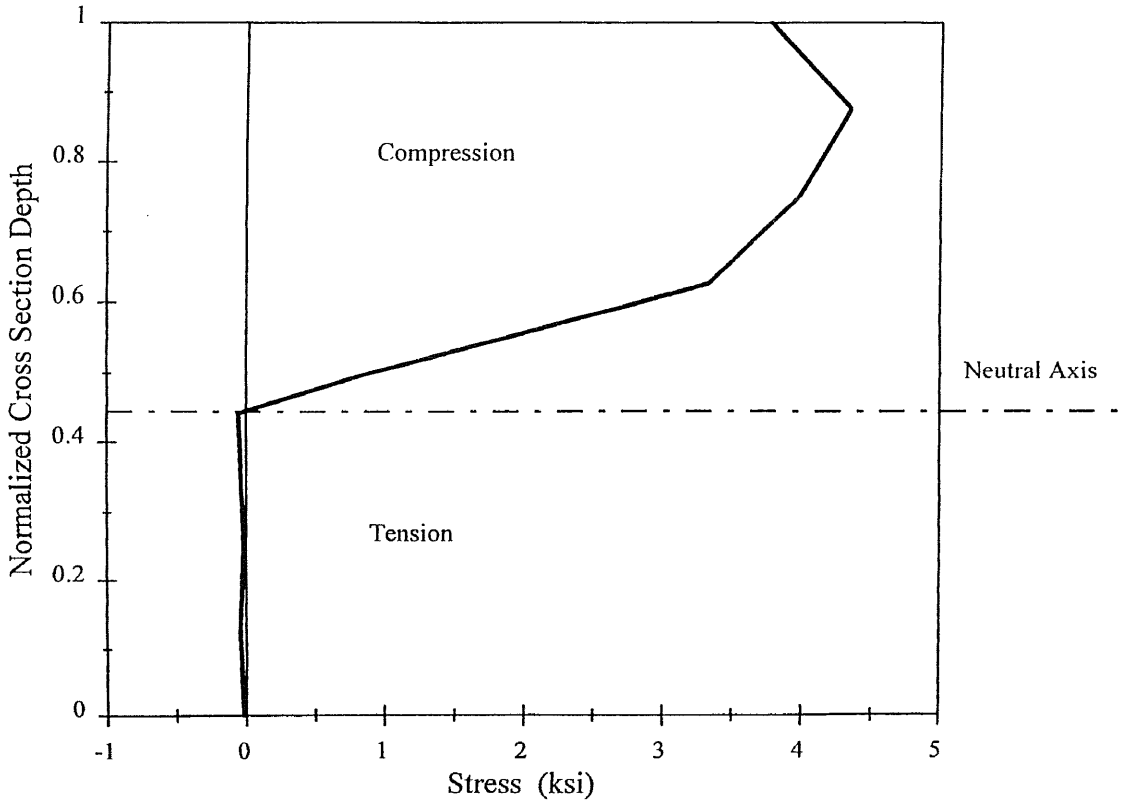

Figure 5.11 Stress distribution of concrete core along the cross section (square column).

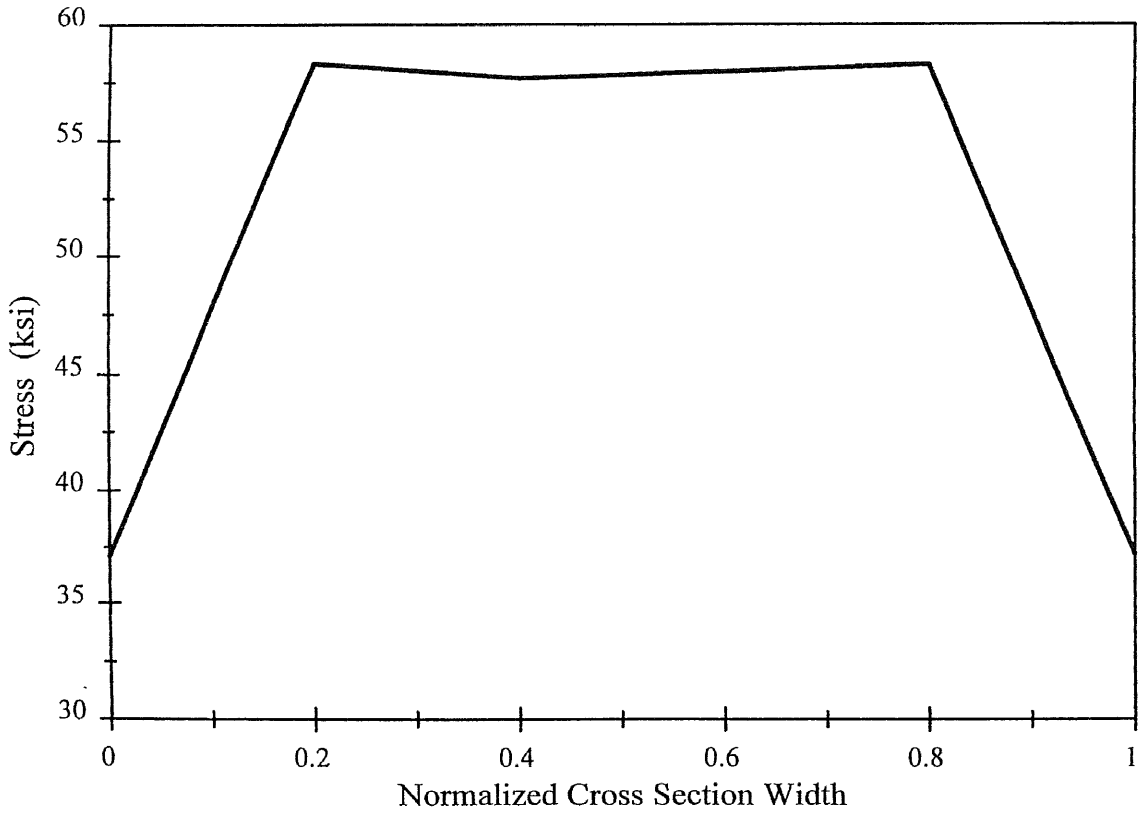

Figure 5.12 Steel tube stress distribution along the cross-section width (square column).

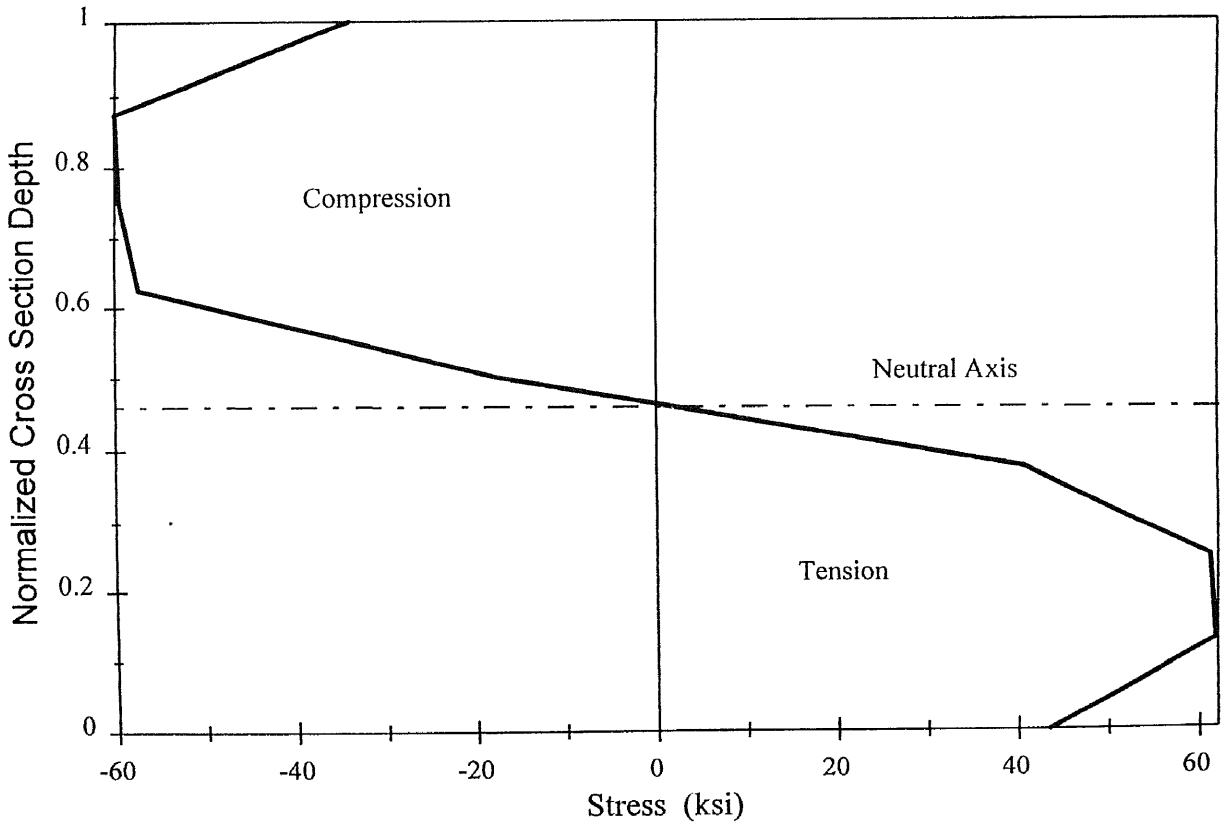

Figure 5.13 Steel tube stress distribution along the cross-section depth (square column).

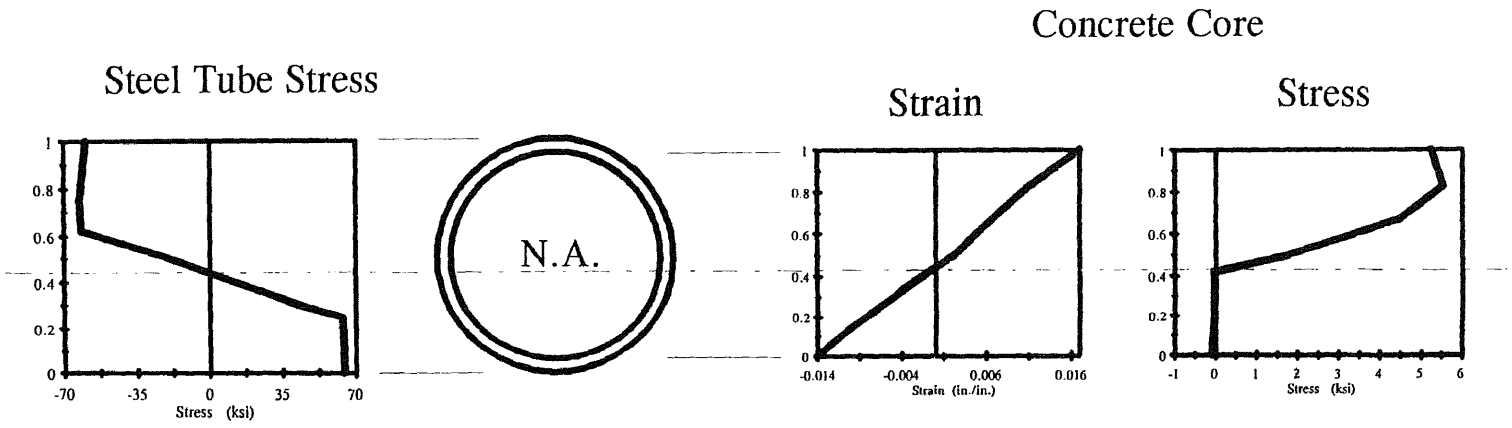

Figure 5.14 Cross-sectional stress distribution for a circular CFT column under combined loading.

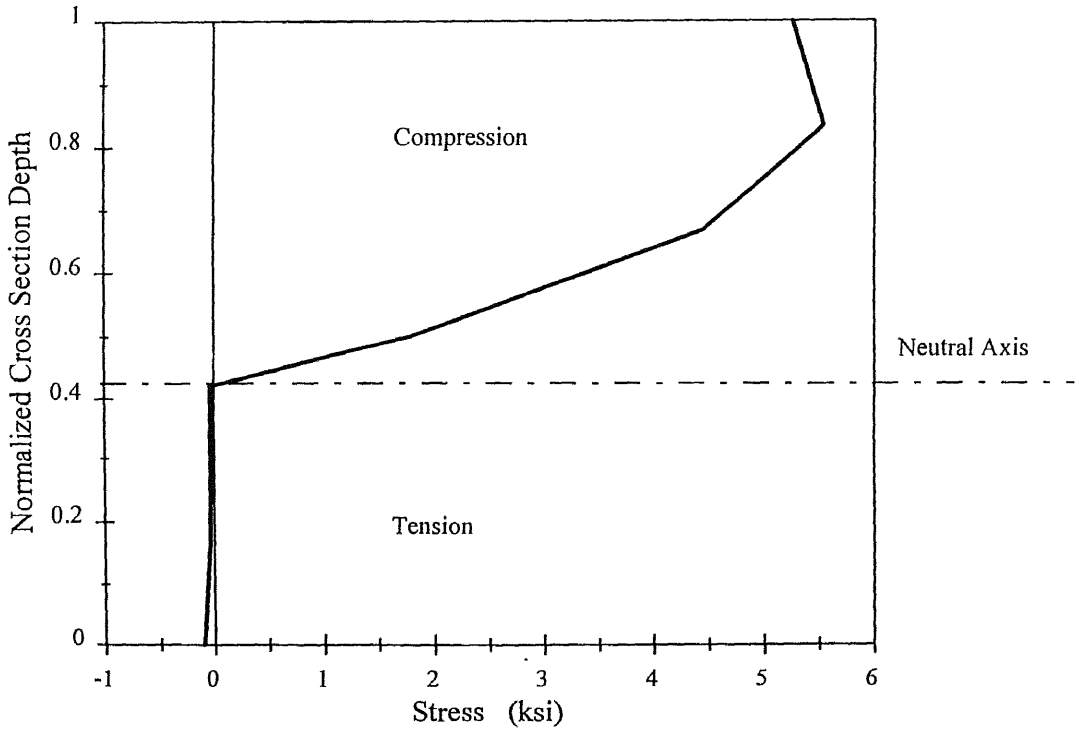

Figure 5.15 Stress distribution of concrete core along the cross section (circular column).

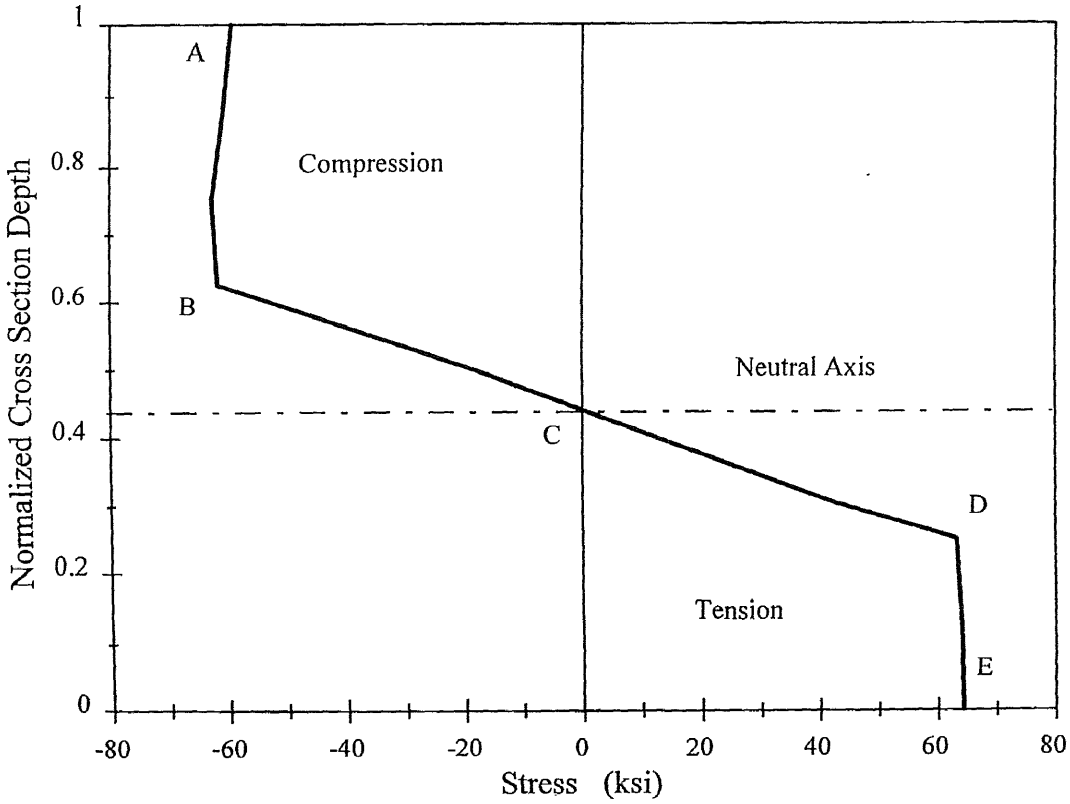

Figure 5.16 Steel tube stress distribution along the cross-section depth (circular column).

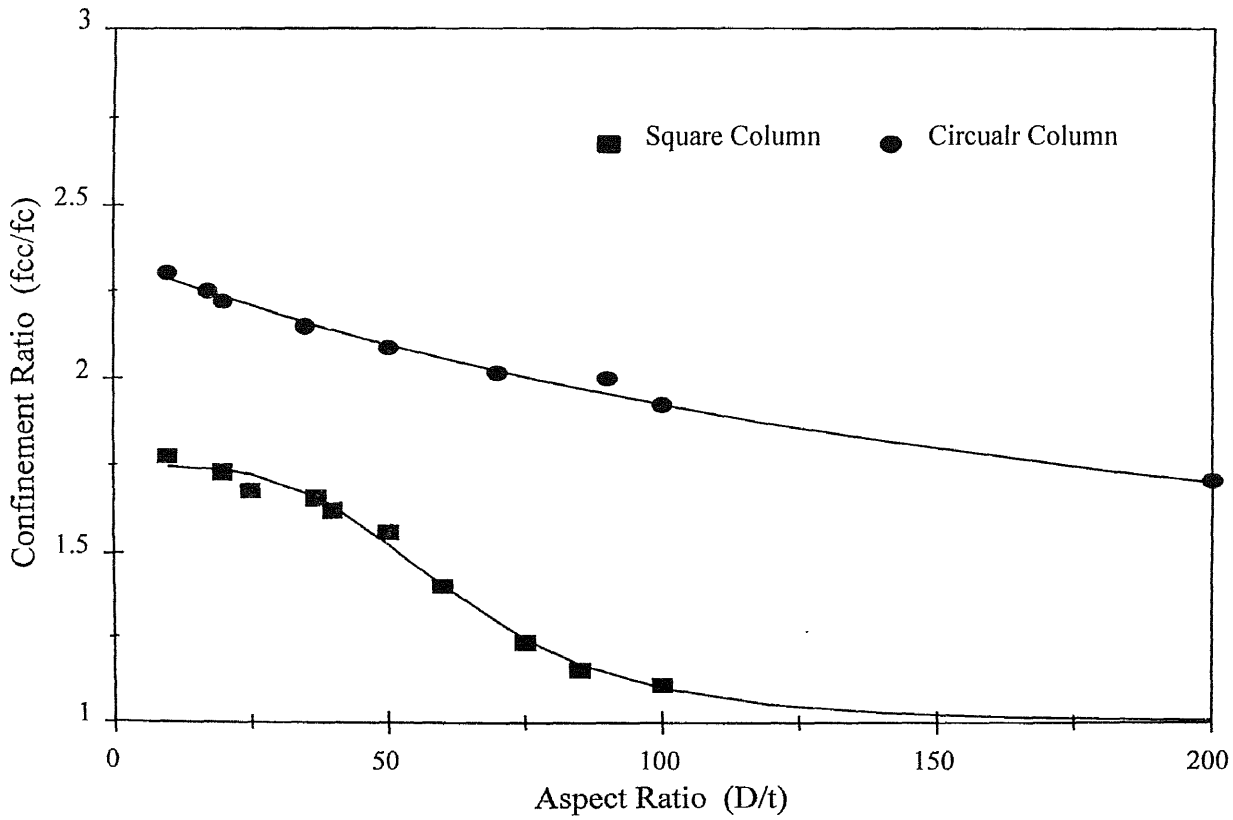

Figure 6.1 Confinement-aspect ratios relationship for circular and square columns.

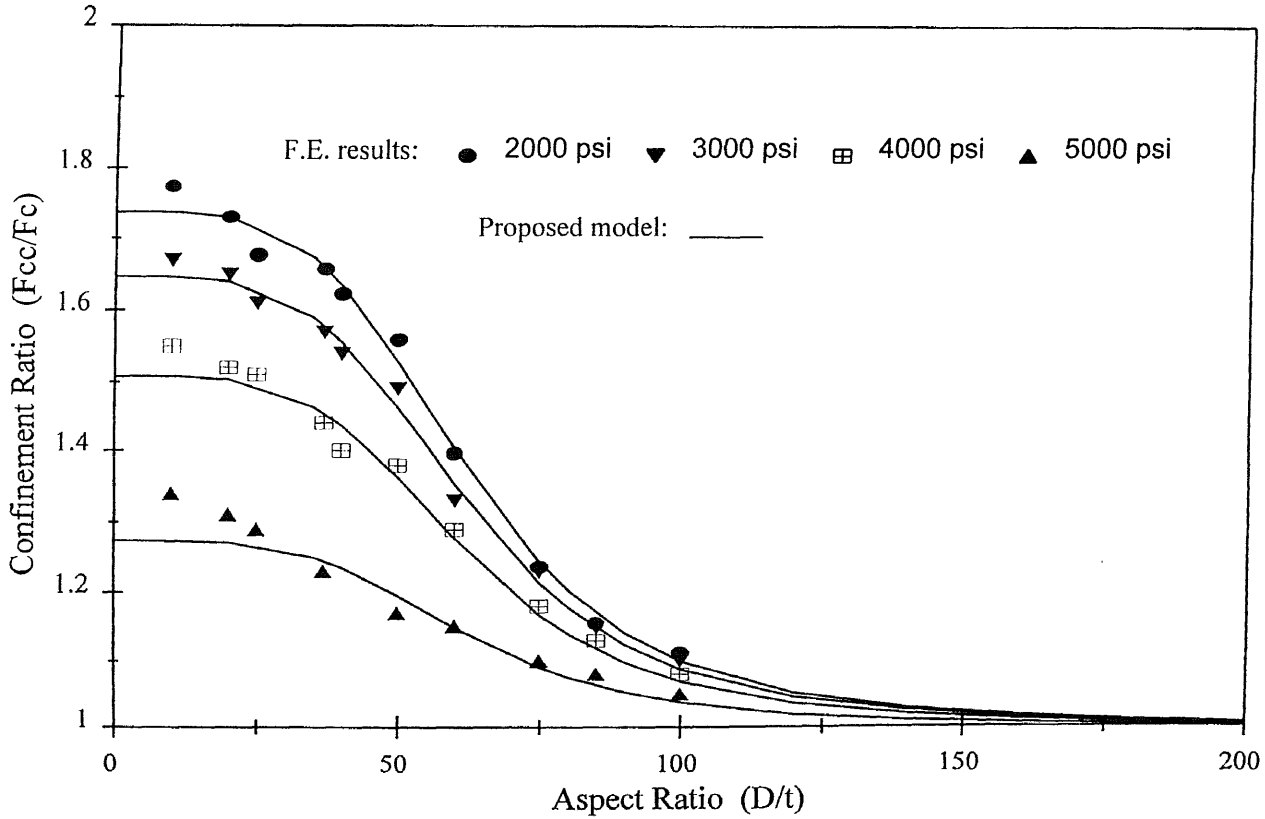

Figure 6.2 Confinement-aspect ratios relationship for square CFTs; comparison between the F.E. results and proposed model.

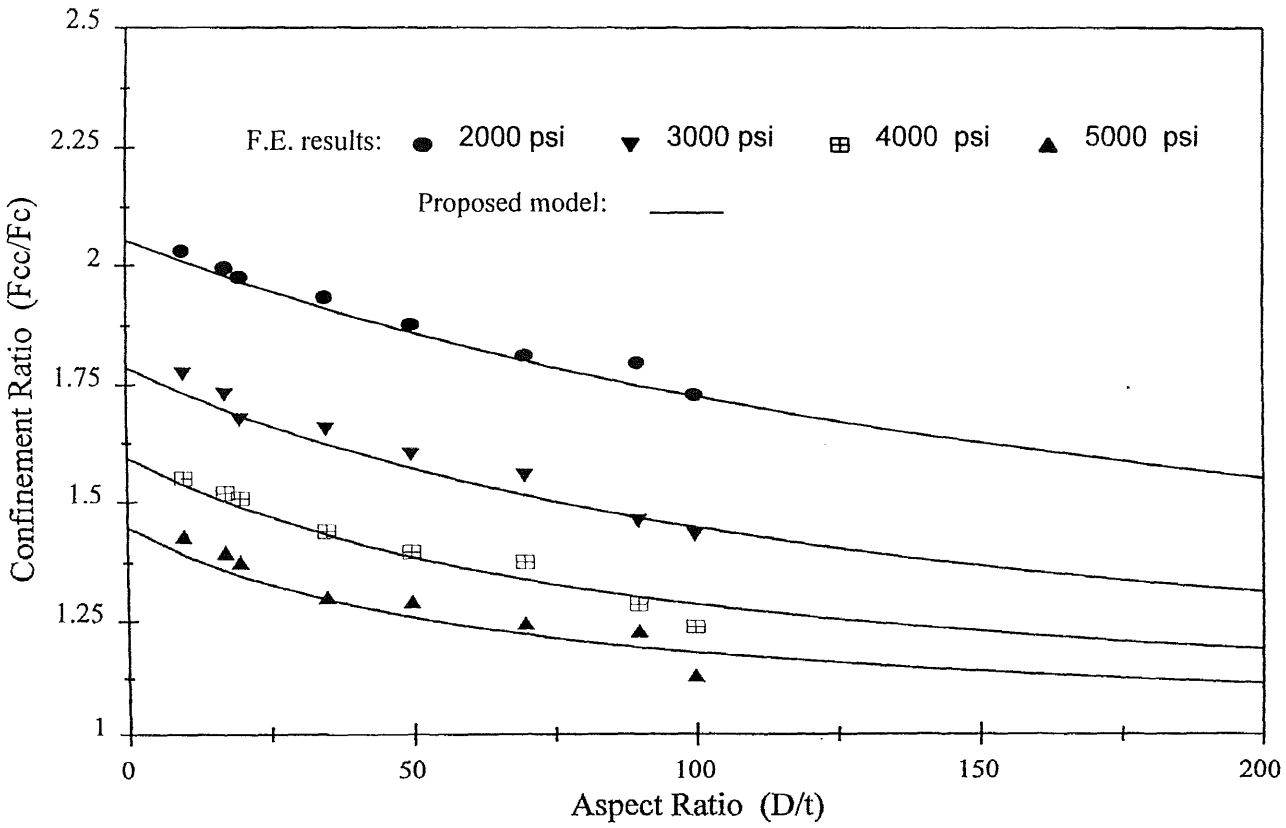

Figure 6.3 Confinement-aspect ratios relationship for circular CFTs; comparison between the F.E. results and proposed model.

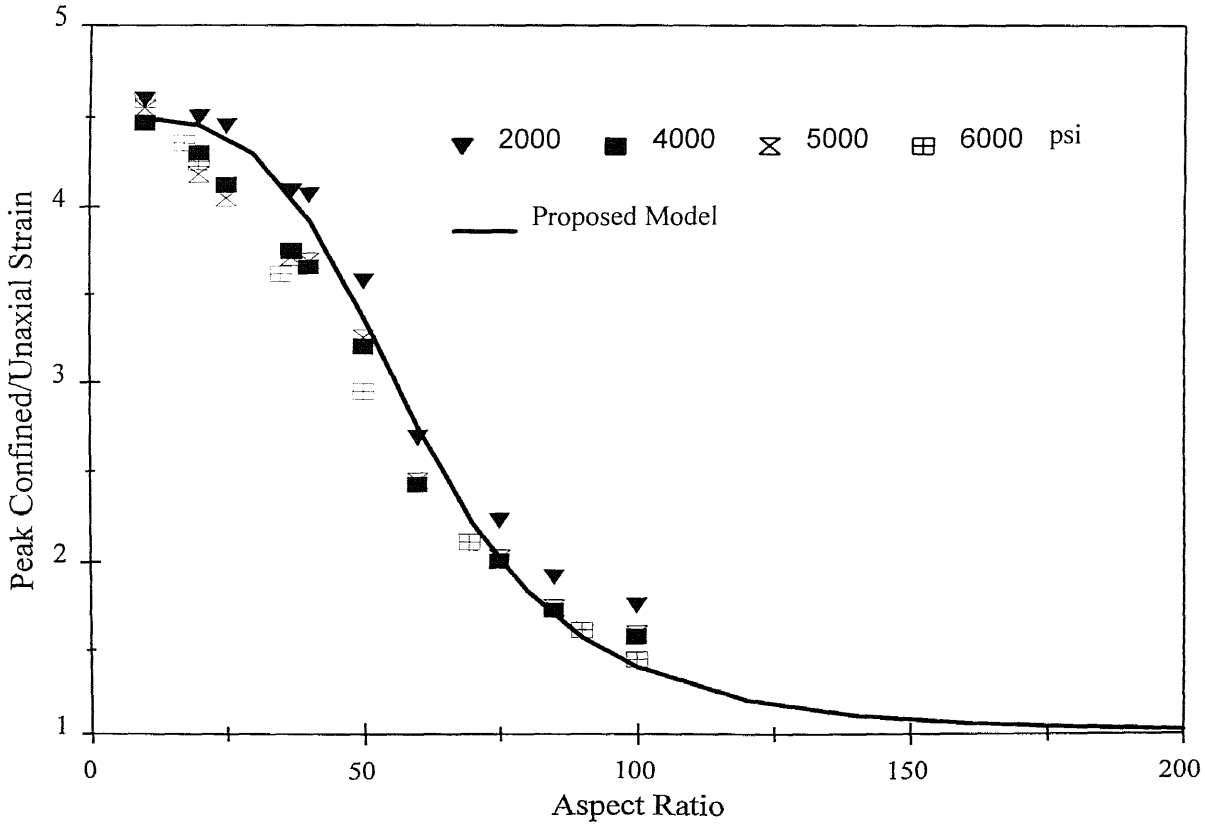

Figure 6.4 Confined peak strain-aspect ratio relationship for square CFT columns.

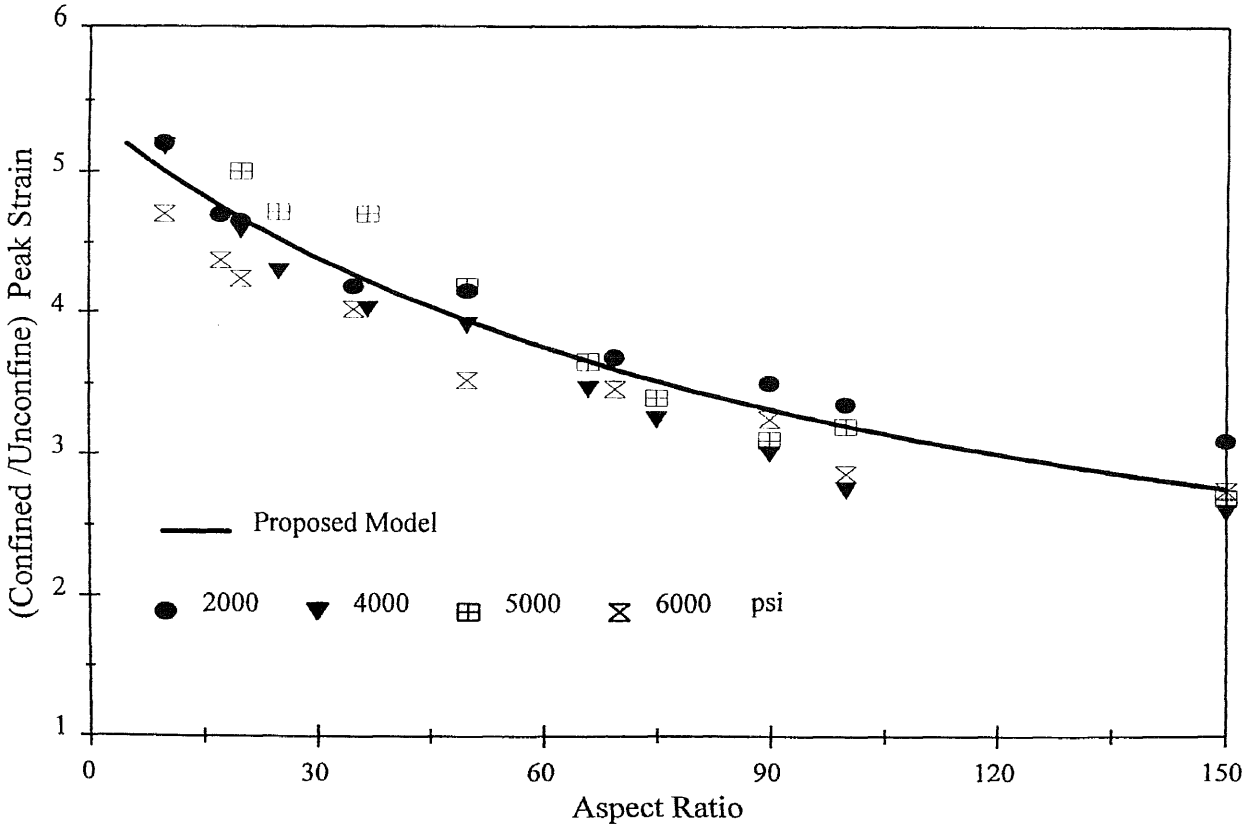

Figure 6.5 Confined peak strain-aspect ratio relationship for circular CFT columns.

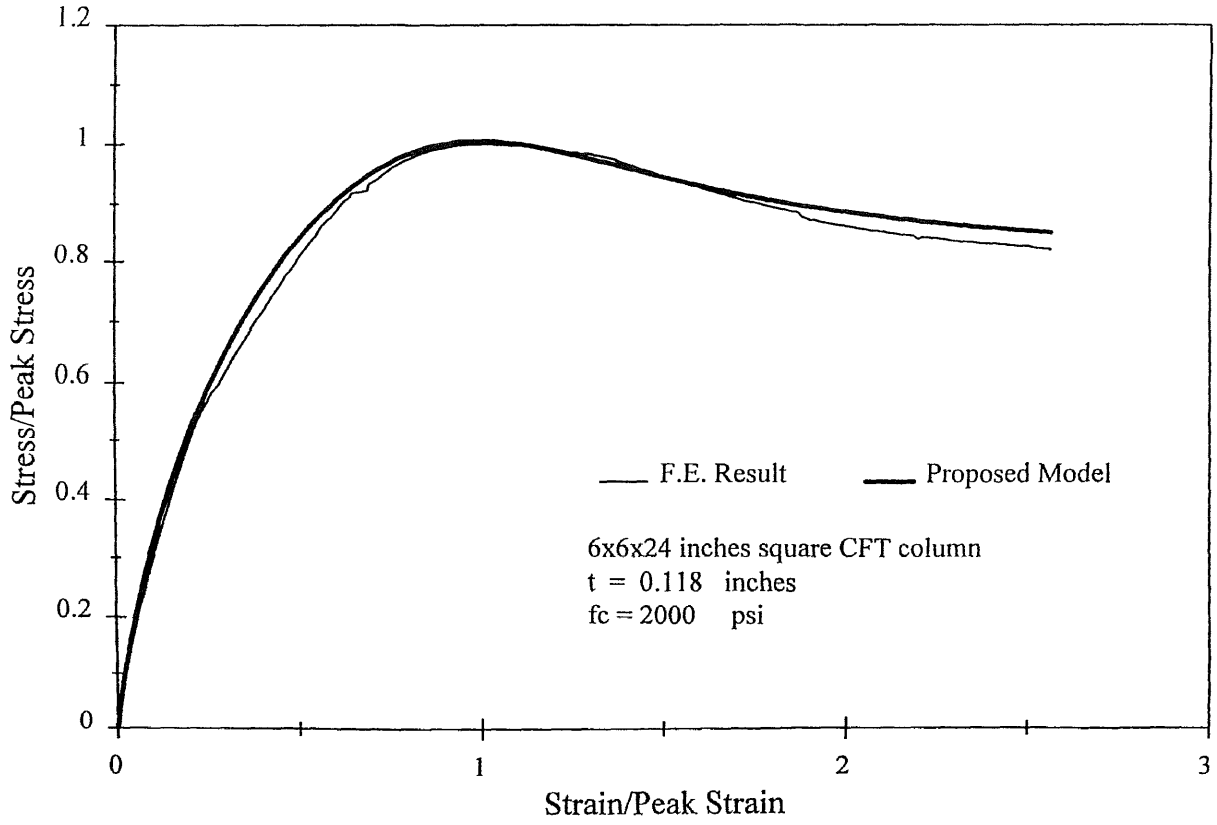

Figure 6.6 Concrete core stress-strain relation for square CFT column.

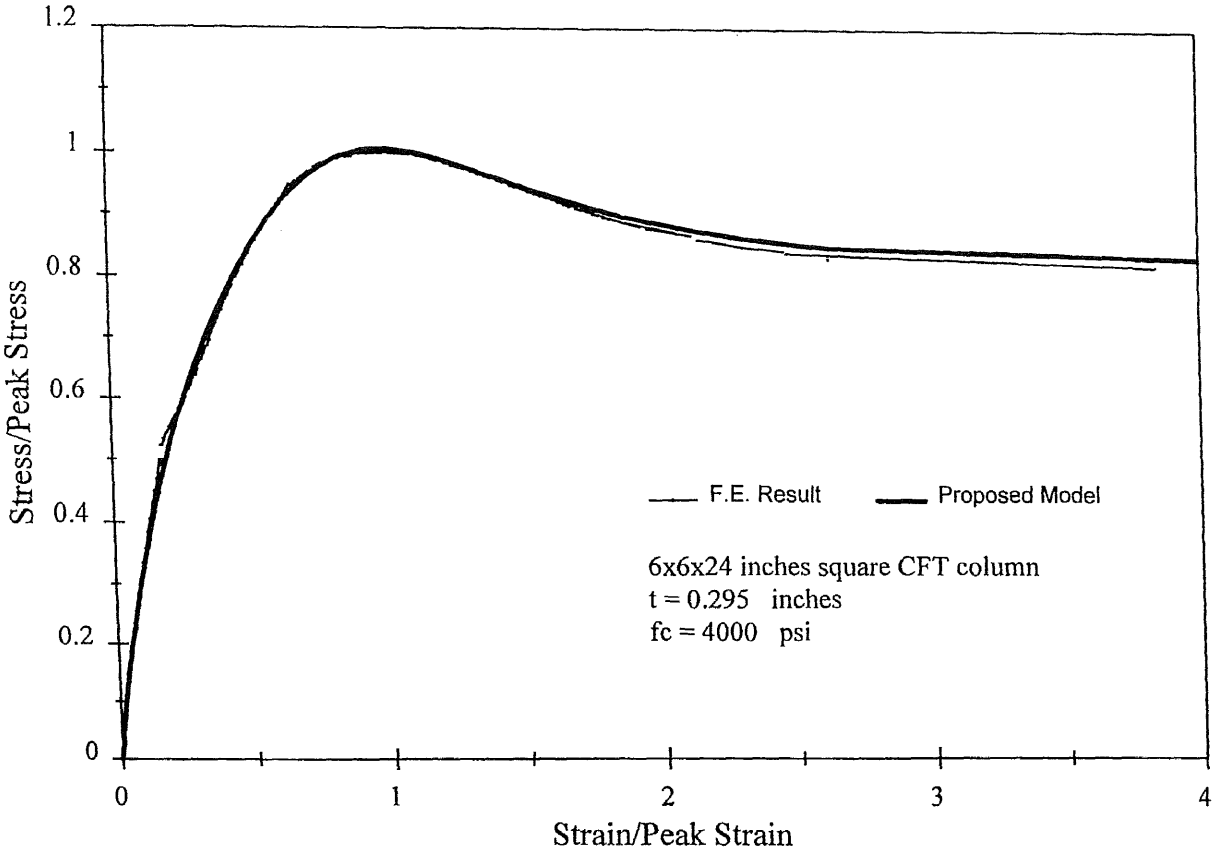

Figure 6.7 Concrete core stress-strain relation for square CFT column.

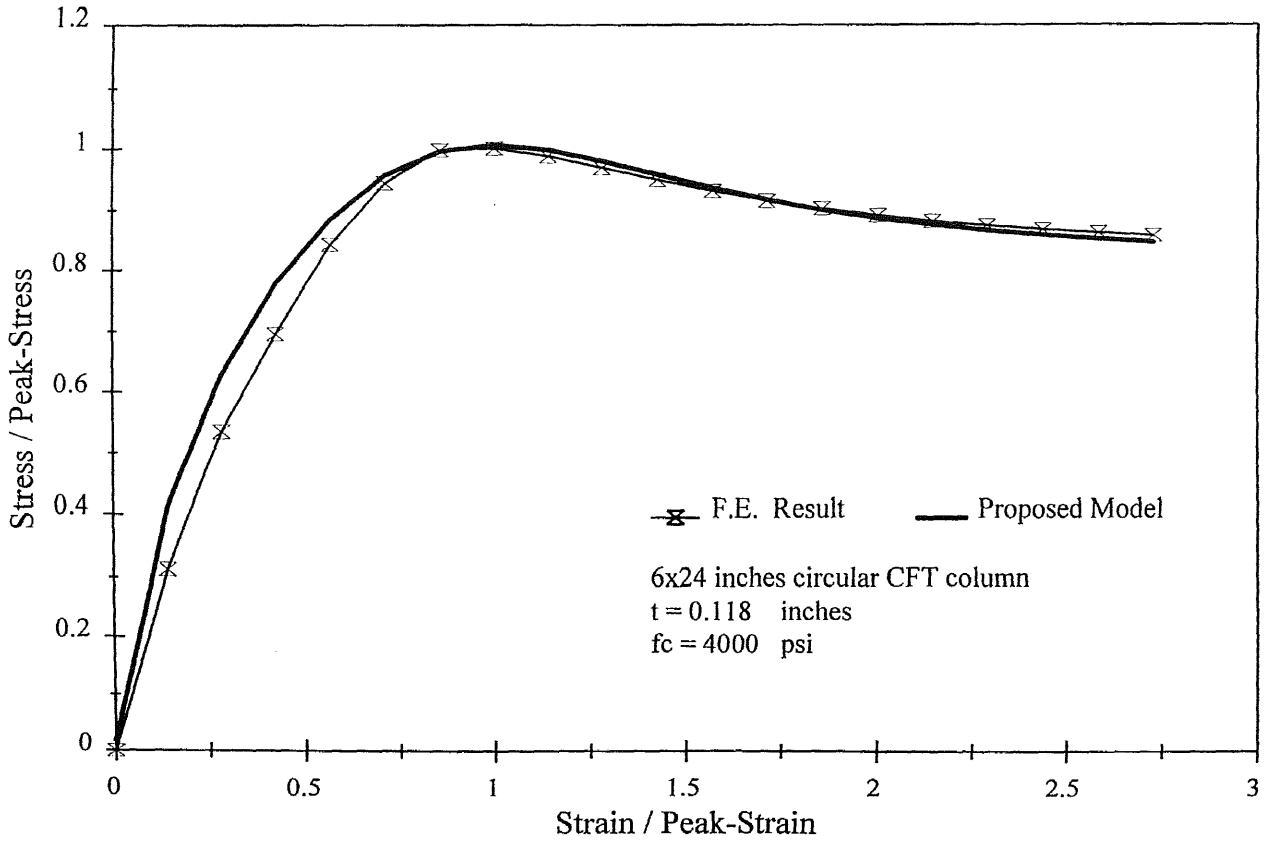

Figure 6.8 Concrete core stress-strain relation for circular CFT column.

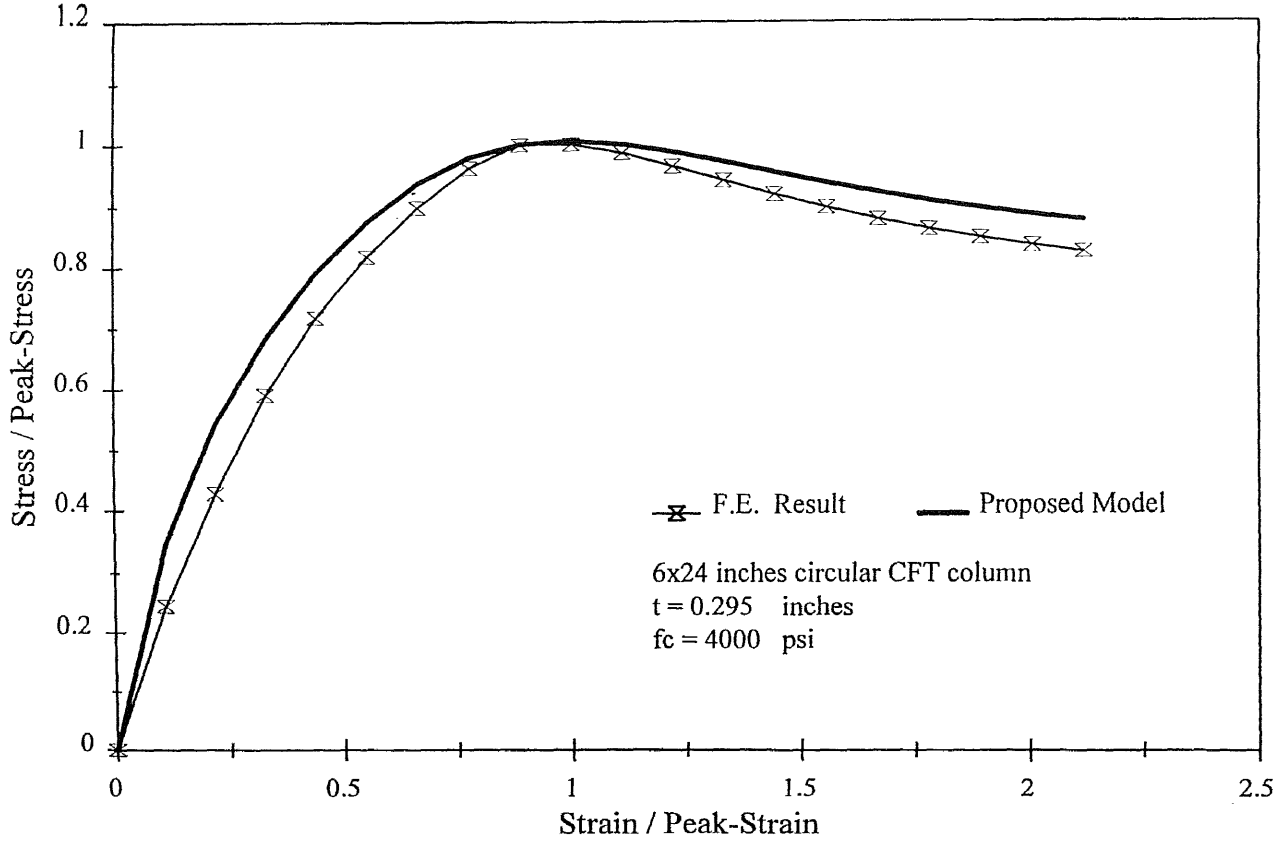

Figure 6.9 Concrete core stress-strain relation for circular CFT column.

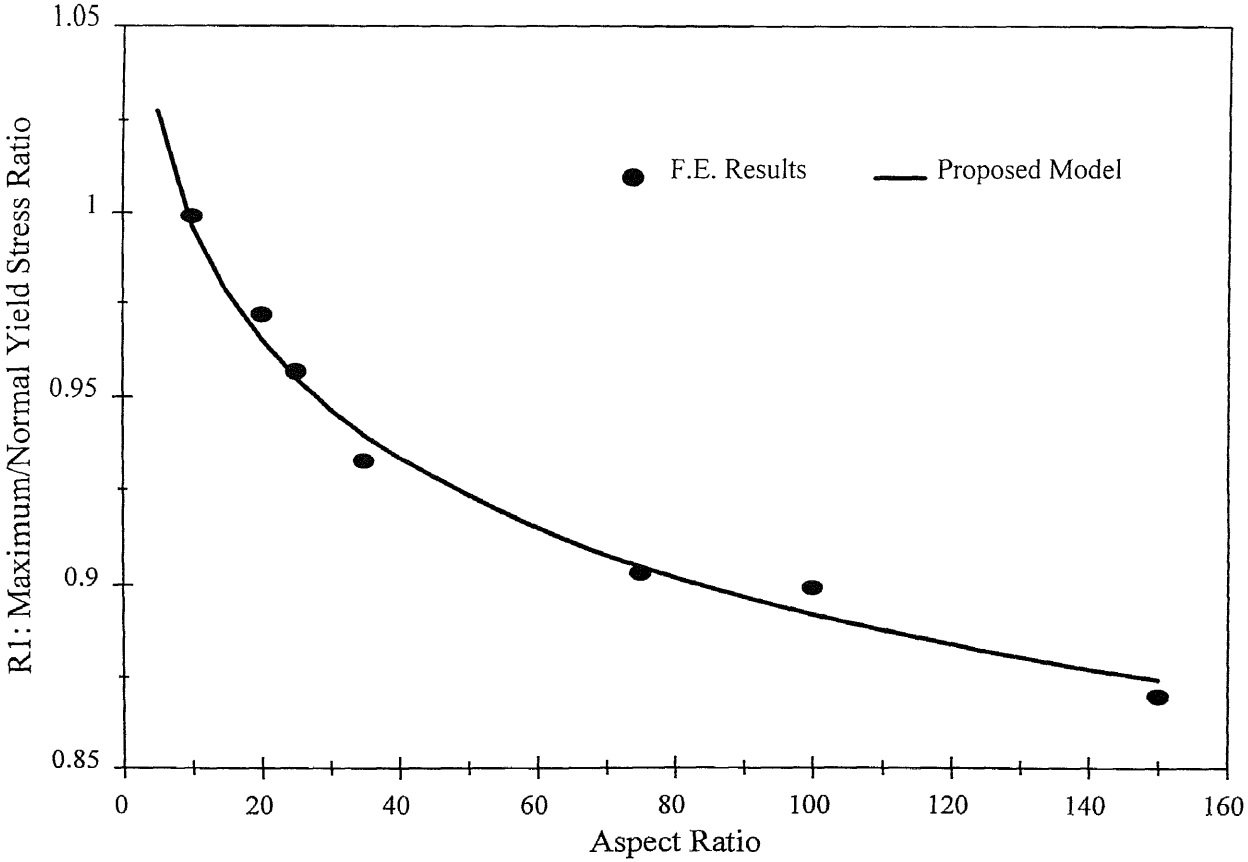

Figure 6.10 Effect of aspect ratio on the yield stress of steel tube in CFT columns.

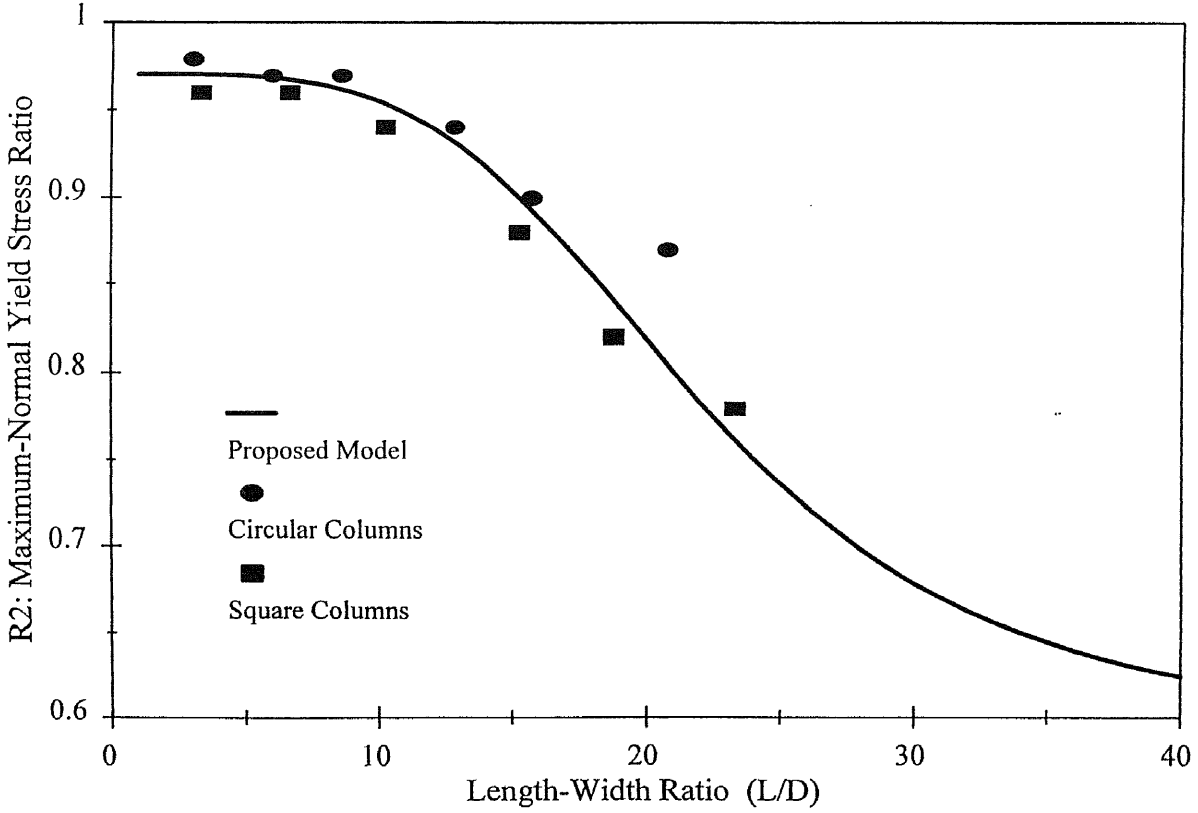

Figure 6.11 Effect of length-width ratio on the yield stress of steel tube in CFT columns.

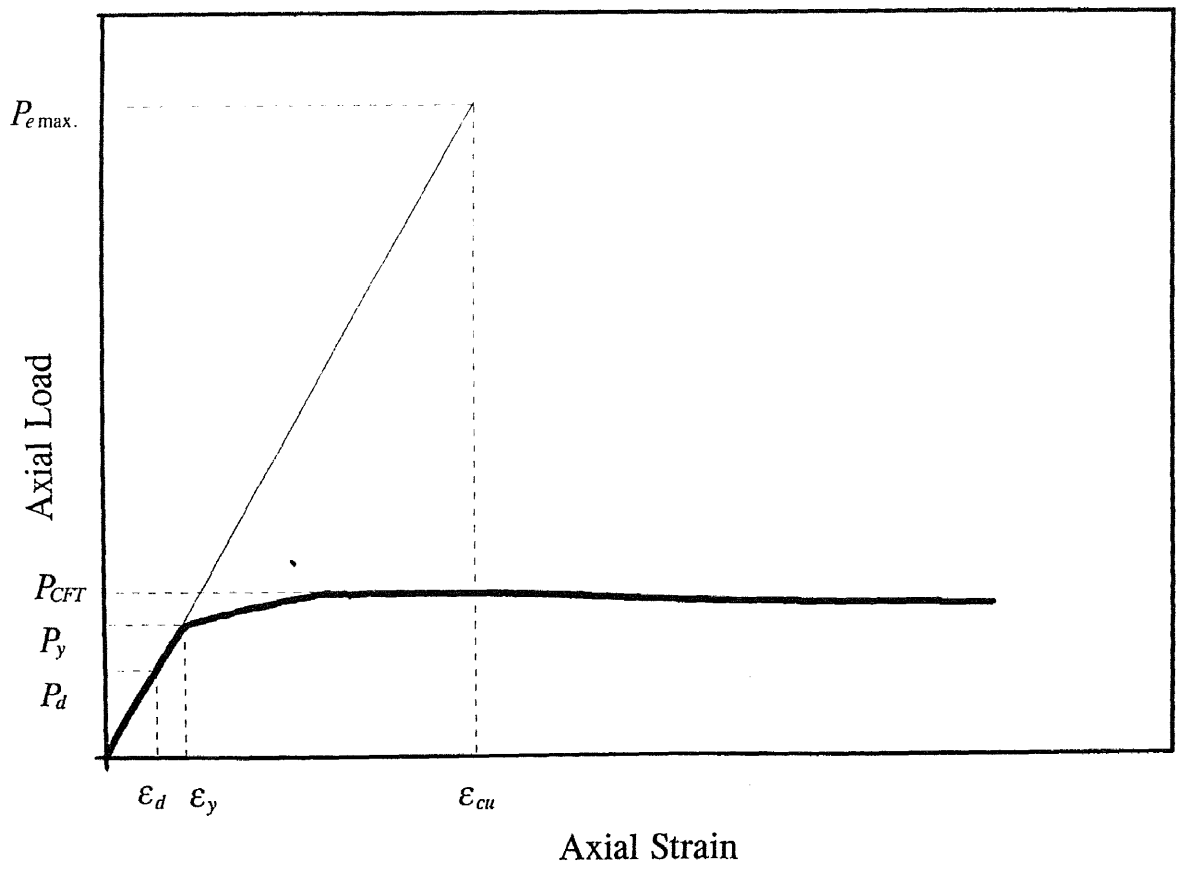

Figure 6.12 Typical axial load-strain curve for CFT columns.

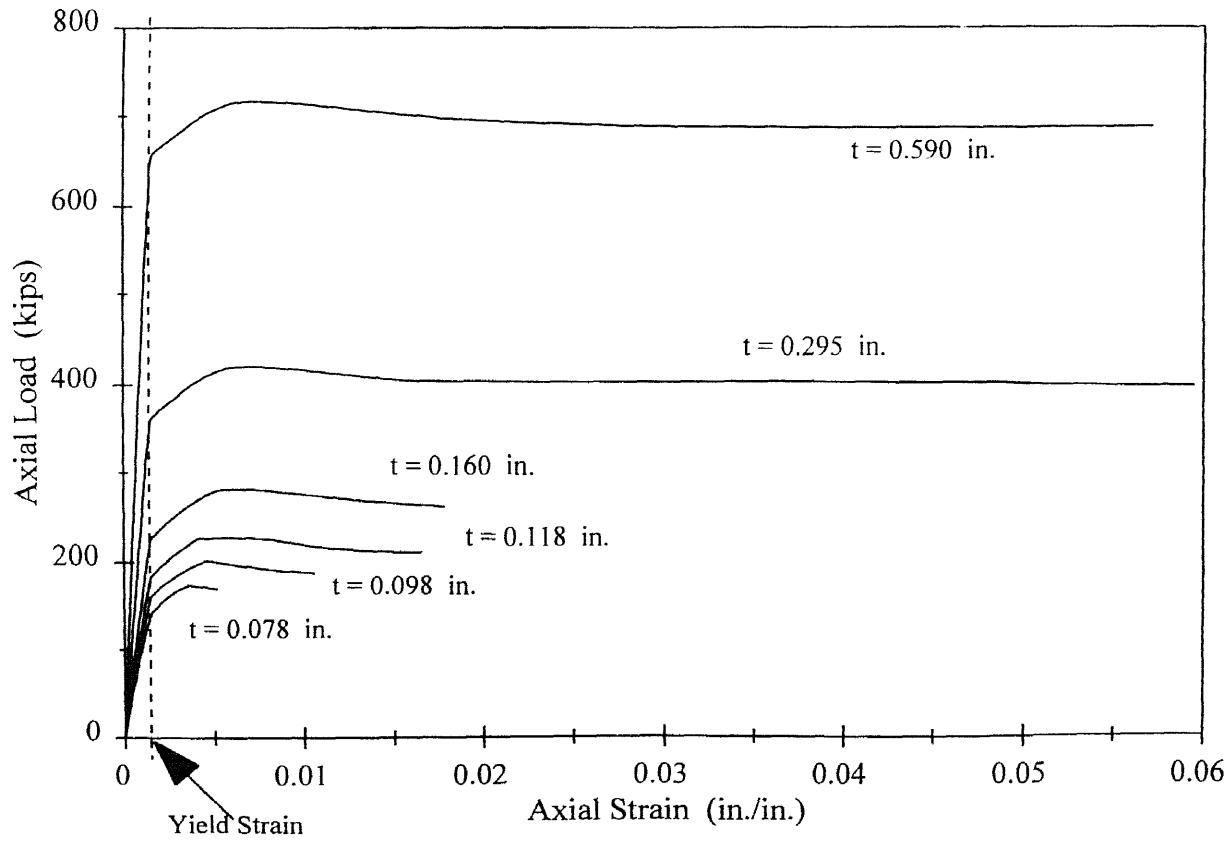

Figure 6.13 Axial load-strain relationships for square CFT columns.

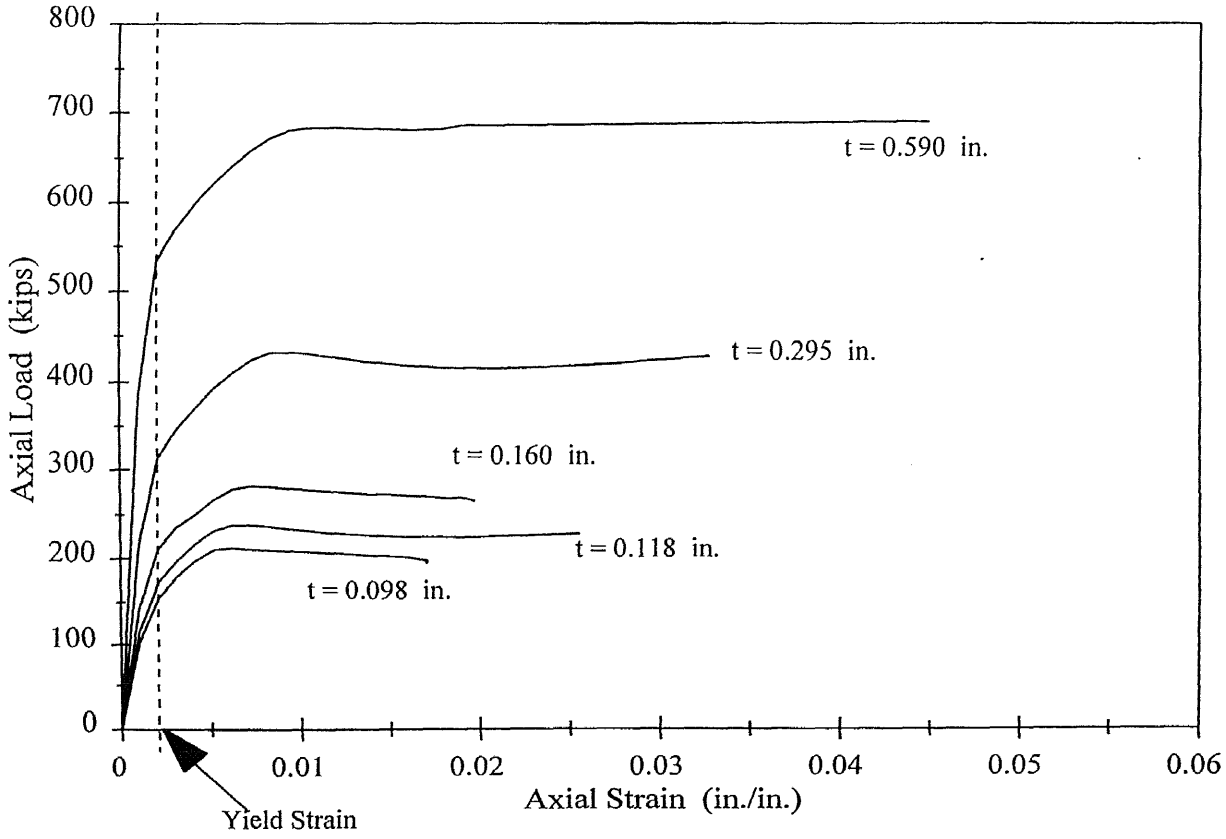

Figure 6.14 Axial load-strain relationships for circular CFT columns.

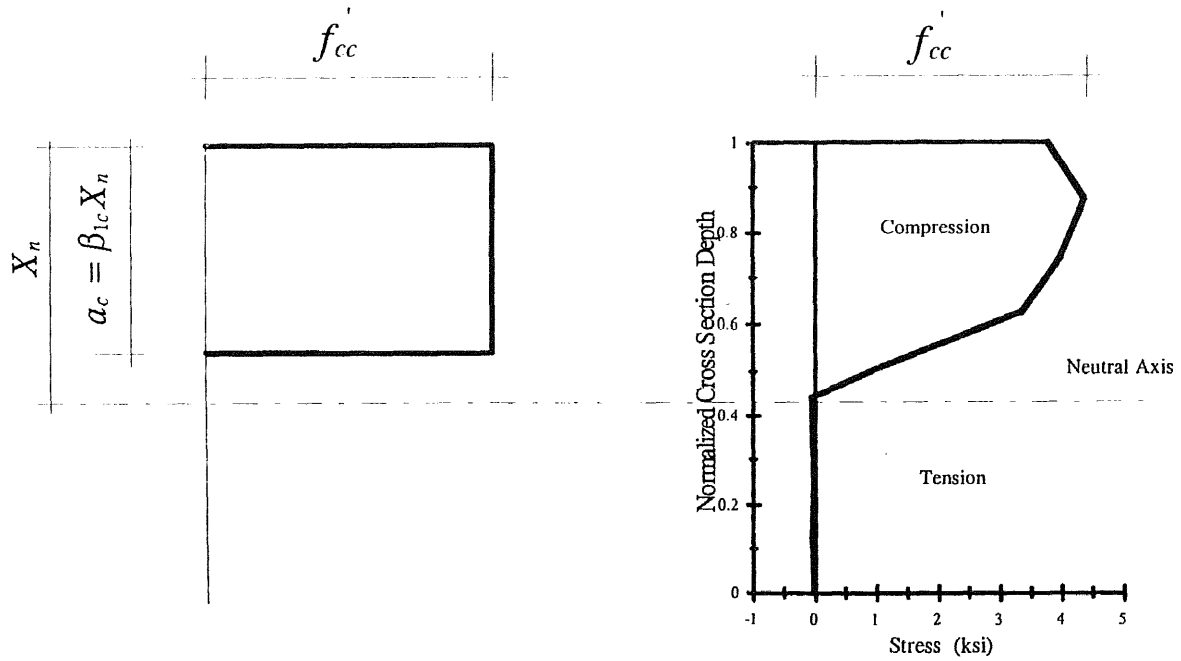

Figure 6.15 Concrete core stress distribution and equivalent stress block at cross section.

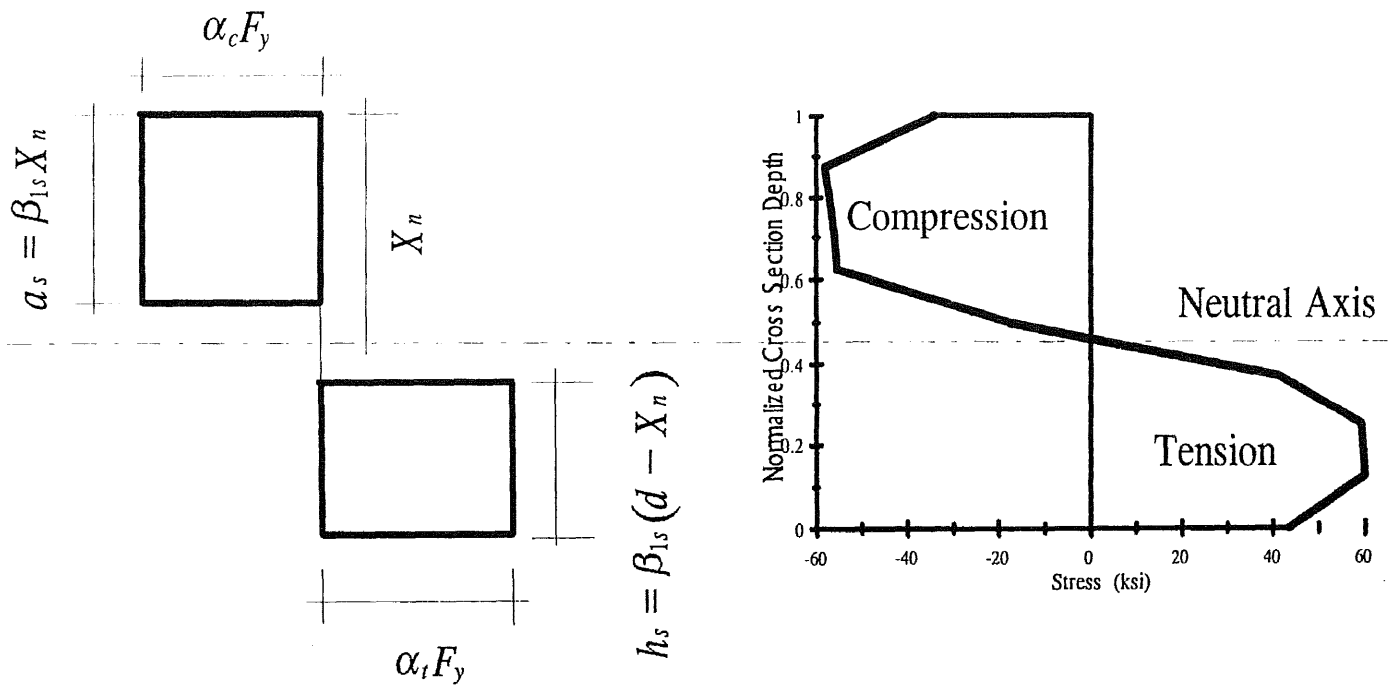

Figure 6.16 Steel tube stress distribution and equivalent stress block at cross section.

REFERENCES

ABAQUS, (1994). "Constitutive Theories; Metal Plasticity Models." Theory Manual, Hibbitt, Karlsson & Sorensen, Inc., Pawtucket, Rhode Island, 4.3.1-1, 4.3.2-6.

AISC, (1994). "Manual of Steel Construction, Load and Resistance Factor Design (LRFD)." Structural Members, Specifications and Codes, Vol. 1.

American Concrete Institute Committee 318, (1995). "Building Code Requirements of Reinforced Concrete," ACI, 318-95, Detroit, Michigan, pp. 130-131.

Baker, A. L., and Amarakone, A. M. N., (1964). "Inelastic Hyperstatic Analysis." Proceedings, International Symposium on the Flexural Mechanics of Reinforced Concrete, ASCE-ACI, Miami, Florida, pp. 85-142.

Barlow, J., (1976). "Optimal Stress Location in Finite Element Models." International Journal for Numerical Methods in Engineering, 10, pp. 243-251.

Bazant, Z. P., and Kim, S. 1979. "Plastic-Fracturing Theory for Concrete." Journal of Engineering Mechanics Division, ASCE, 105, (EM3), pp. 407-428.

Bevington, P. R., (1969). *Data Reduction and Error Analysis for the Physical Sciences*, McGraw Hill, New York.

Bode, H., (1976). "Columns of Steel Tubular Sections Filled with Concrete Design and Application." Journal of Acier, Stahl, Steel, 11-12, pp. 388-393.

Boyd, P. F., Cofer, W. F., and McLean, D. I., (1995). "Seismic Performance of Steel-Encased Concrete Columns under Flexural Loading." Structural Journal, ACI, 92, (3), pp. 355-364.

Brazier, L. G., (1927). "On the Flexure of Thin Cylindrical Shells and other Thin Sections." Proceedings, Royal Society, A, 166, London, England, pp. 104-114.

Bridge, R., and Webb, J., (1992). "Thin Walled Circular Concrete Filled Steel Tubular Columns." Composite Construction in Steel and Concrete II, ASCE, June 14-19, pp. 634-649.

Carreina, D. J., and Chu, K. H., (1985). "Stress-Strain Relationship for Plain Concrete in Compression." ACI Journal, 82, (6), pp. 797-804.

Chapman, J. C., and Neogi, P. K., (1966). "Research on Concrete Filled Tubular Columns." Reports, Progress to October 31, 1964 and April 30, 1966, Engineering Structures Laboratories, Civil Engineering Department, Imperial College, London, England.

Chai, Y. H., (1992). "Seismic Behavior of Steel Jacketed Circular Bridge Columns." Proceedings, Tenth Structural Congress'92, ASCE, Apr. 13-15, pp. 641-644.

Chen, A. T. C., and Chen, W. F., (1975). "Constitutive Relations for Concrete." Journal of Engineering Mechanics, ASCE, 101, (4), pp. 465-481.

Chen, W. F., (1982). *Plasticity in Reinforced Concrete*. McGraw Hill, New York, New York, pp. 744-750.

Chen, W. F., and Han, D. J., (1988). *Plasticity for Structural Engineers*. Springer-Verlag, New York, New York, pp. 606-607.

Chen, W. F., and Yamaguchi, E., (1985). "On Constitutive Modeling of Concrete Materials." Finite Elemental Analysis of Reinforced Concrete Structures, ASCE, pp. 48-71.

Chinn, J., and Zimmerman, R.M., (1965). "Behavior of Plain Concrete under Various High Triaxial Compression Loading Conditions." Report WL TR 64-163, Air Force Weapons Laboratory Technical, Kirtland Air Force Base, Albuquerque, New Mexico.

Enavs, R. J., and Pister, K. S., (1966). "Constitutive Equations for a Class of Nonlinear Elastic Solids." Solids and Structures, 2, (3), pp. 427-445.

Farshad, M., (1994). *Stability of Structures*. Development in Civil Engineering, 43, Elsevier Science, Amsterdam, Netherlands, pp. 225-318.

Filanagan, D. P., and Belytschko, T., (1981). "A Uniform Strain Hexahedron and Quadrilateral with Orthogonal Hourglass Control." International Journal for Numerical Methods in Engineering, 17, pp. 679-706.

Furlong, R. W., (1983). "Columns Rules of ACI, SSLC, and LRFD Compared." Journal of Structural Engineering, ASCE, 109, (10), pp. 2375-2386.

Furlong, R. W., (1968). "Design of Steel-Encased Concrete Beam-Columns." Journal of Structural Division, ASCE, 94, (ST1), pp. 267-281.

Furlong, R. W., (1967). "Strength of Steel-Encased Concrete Beam Columns." Journal of Structural Division, ASCE, 93, (ST5), pp. 113-124.

Gardner, J., and Jacobson, R., (1967). "Structural Behavior of Concrete Filled Steel Tubes." ACI Journal, 64, pp. 404-413.

Ge, H., and Usami, T., (1992). "Strength of Concrete-filled Thin-walled Steel Box Columns: Experiment." Journal of Structural Engineering, ASCE, 118, (11), pp. 3036-3054.

Ghosh, R. S., (1977). "Strengthening Of Slender Hollow Steel Columns by Filling with Concrete." Canadian Journal of Civil Engineering, 4, (2), pp. 127-133.

Granholm, H., (1965). *A General Flexural Theory of Reinforced Concrete*. John Wiley, New York, New York.

Griffis, L. G., (1992). "State of the Art Report Composite Frame Construction in the United States," Proceedings, US-Japan Workshop on Composite and Hybrid Structures, Berkeley, California, Sept. 10-12, pp. 33-49.

Han, D. J., and Chen, W. F., (1985). "A Nonuniform Hardening Plasticity Model for Concrete Materials." Mechanics of Materials, 4, pp. 283-302.

Hognestad, E., Hadson, N. W., and McHenry, D., (1955). "Concrete Stress Distribution in Ultimate Strength Design." ACI Journal, 52, pp. 455-479.

Hurlbut, B. J., (1985). "Experimental and Computational Investigation of Strain-Softening in Concrete." Structural Research Series, No. 8505, Department of civil, environmental and architectural engineering, University of Colorado, Boulder, Colorado.

Kenny, J. R., Broce, D. A., and Bjoohovde, R., (1994). "Removal of Yield Stress Limitation for Concrete Tubular Columns." Engineering Journal, AISC, First Quarter, pp. 1-4.

Kloppel, V. K., and Goder, W., (1957a). "An Investigation of the Load Carrying Capacity of Concrete-filled Steel Tubes and Development of Design Formula." Der Stahlbau, 26, (1), pp. 1-10.

Kloppel, V. K., and Goder, W., (1957b). "An Investigation of the Load Carrying Capacity of Concrete-filled Steel Tubes and Development of Design Formula." Der Stahlbau, 26, (2), pp. 44-50.

Kloppel, K., and Goder, W., (1957). "Collapse Load Test on Concrete Filled Steel Tubes and Derivation of a Design Formula." Der Stahlbau, 26, (2), pp. 76-93.

Knowels, R., and Park, R., (1969). "Strength of Concrete Filled Steel Tubular Columns." Journal of Structural Division, ASCE, 95, (ST12), pp. 2565-2587.

Knowels, R., and Park, R., (1970). "Axial Load Design for Concrete-Filled Steel Tubes." Journal of Structural Division, ASCE, 96, (ST10), pp. 2125-2153.

Launary, P. and Gachon, H., (1971). "Strain and Ultimate Strength of Concrete under Triaxial Stress." Proceedings, 1st International Conference Structural Mechanics and Reactor Technology, Berlin, West Germany, Paper H1/3, pp. 23-34.

Maekawa, K., and Okamura, H., (1983). "The deformational behavior and Constitutive Equation of Concrete Using the Elasto-Plastic and Fracture Model." Journal of Faculty of Engineering, University of Tokyo (B), XXXVII, (2), Tokyo, Japan, pp. 253-328.

Mander, J. B., Priestley, M. J. N., and Park, R., (1988). "Observed Stress-Strain Behavior of Confined Concrete." Journal of Structural Engineering, ASCE, 114, (8), pp. 1827-1849.

Mattock, A. H., (1967). "Discussion of Rotation Capacity of Reinforced Concrete Beams by W. G. Corley." Journal of Structural Division, ASCE, 93, (ST2), pp. 519-522.

Mills, L. L., and Zimmerman, R. M., (1970). "Compressive Strength of Plain Concrete under Multiaxial Loading Conditions." ACI Journal, 26, October, pp. 437-461.

Morino, S., Kaawaguchi, J., Yasuzaki, C., and Kanazawa, S., (1992). "Behavior of Concrete-Filled Steel Tubular Three-Dimensional Subassembleages." Proceedings, Composite Construction in Steel and Concrete II, ASCE, June 14-19, pp. 726-741.

Nagashima, T., Sugano, S., Sawada, H., and Kei, T., (1989). "An Experimental Study on Behavior of Concrete-Filled Steel Tubular Columns under Cyclic Loading Axial Load." Abstracts, Annual Meeting of A.I.J., pp. 1601-1602.

Neogi P. K., and San H. K., (1969). "Concrete Filled Tubular Steel Columns Under eccentric Loading." Journal of Structural Engineering, 47, (5), p. 1123-1342.

Okamato, T., and Maeno, T. 1988. "Experimental Study on Rectangular Steel Tube Columns Infilled with Ultra High Strength Concrete Hardened by Centrifugal Force," Proceedings, Annual Meeting of AIJ, Chiba, Japan, pp. 1359-1375.

Park, R. J. T., Priestley, M. J. N., and Walpole W. R., (1983). "Reinforced Concrete Bridge Piles." Bulletin of New Zealand National Society for Earthquake Engineering, 16, (2), pp. 275-293.

Pramono, E., and William, K., (1989). "Fracture Energy-Based Plasticity Formulation of Plain Concrete." Journal of Mechanical Engineering, ASCE, 115, (6), pp. 1183-1202.

Press, W. H., (1992). *Numerical Recipes in C; The Art of Scientific Computing.* Cambridge University Press, Cambridge, England.

Priestley, M. J. N.,. Seible, F., Xiao, Y., and Verrna, R., (1994). "Steel Jacket Retrofitting of Reinforced Concrete Bridge Columns for Enhanced Shear Strength Part-1: Theoretical Considerations and Test Design." Structural Journal, ACI, 91, (4), pp. 394-404.

Rangan, B. V., (1991). "Design of Slender Hollow Steel Columns Filled with Concrete." Proceedings, International Conference on Steel and Aluminum Structures, ICSAS 91, Singapore, May 22-24, pp. 104-112.

Rangan, B. V., and Joyce, M., (1992). "Strength of Eccentrically Loaded Slender Steel Tubular Columns Filled with High-Strength Concrete." Structural Journal, ACI: 676-681.

Read, H. E., and Hegemier, G. A., (1984). "Strain Softening of Rock, Soil, and Concrete - A Review Article." Mechanics of Materials, 3, pp. 271-294.

Recommendations for US-Japan Cooperative Research Program, (1992), "Phase 5; Composite and Hybrid Structures," Report No. UMCEE92-29, .Ann Arbor, Michigan, pp. 34-37.

Richart, F. E., Brandtzaeg, A. and Brown, R. L., (1928). "A Study of the Failure of Concrete under Combined Compressive Stress." Bulletin 185, University of Illinois, Engineering Station, Urbana, Illinois, pp. 104-121.

Roeder, W. C., (1992). "Composite Members in Seismic Design." Proceedings, US-Japan Workshop on Composite and Hybrid Structures, Berkeley, California, Sept. 10-12, pp. 144-153.

Russell, W. A., (1953). "Structural Properties of Light-Gage Tubular Columns." Housing Research Paper, No. 21, Housing and Home Finance Agency, New York, New York.

Saadeghvaziri, M. A., (1988). "Inelastic Response of R/C Bridges under Horizontal and Vertical Earthquake Motions." Thesis for the Degree of Doctor of Philosophy, Department of Civil Engineering, University of Illinois, Champaign, Illinois.

Saatcioglu, M., (1991). "Modeling Hysteretic Force-Deformation Relationships for Reinforced Concrete Elements." Earthquake Resistant Concrete Structures Inelastic Response and Design, ACI, SP127-5, pp. 153-198.

Saenz, L. P., (1964). "Discussion of Equation for the stress-strain curve of concrete by P. Desai and S. Krishman." ACI Journal, 61, (9), pp. 1229-1235.

Smith, S. H., (1987). "On Fundamental Aspects of Concrete Behavior." Thesis for Degree of Master of Science, Department of Civil, Environmental and Architectural Engineering, University of Colorado, Boulder, Colorado.

Subcommittee on the State of Art Survey of the Task Committee on Composite Construction of the Committee on Metals of the Structural Division, (1974). "Composite Steel Concrete Constructions: Report." Journal of Structural Division, ASCE, 100, (ST5), pp. 1085-1115.

Sugano, S., and Nagashima, T., (1992). "Seismic Behavior of Concrete Filled Tubular Steel Columns." Proceedings, Tenth Structural Congress 92, ASCE, Apr. 13-15, pp. 914-917.

Task Group 20, Structural Stability Research Council, (1979). "A Specification for the Design of Steel-Concrete Composite Columns." Engineering Journal, AISC, 16, (4), pp. 101-115.

Timoshenko, P. S., and Gere J. M., (1963). *Theory of Elastic Stability*. McGraw-Hill International Book Company, New York, New York, pp. 384-439.

Tomii, M., and Yoshimaro K., (1977). "Experimental Studies one Concrete Filled Steel Tubular Columns Under Concentric Loading." International Colloquium on Stability of Structures Under Static and Dynamic Loads, Washington, D. C., May 17-19, pp. 718-741.

Tsai, W. T., (1988). "Uniaxial Compressional Stress-Strain Relation of Concrete." Journal of Structural Division, ASCE, 114, (9), pp. 2133-2136.

Wang, C.-K., and Salmon, C. G., (1985). *Reinforced Concrete Design.* Harper & Row, Publishers, New York, New York, pp. 39-89.

Xie, J., Elwi, A. S., and MacGregor J. G., (1994). "Numerical Investigation of Eccentrically Loaded Tied High Strength Concrete Columns." Structural Engineering Report, Department of Civil Engineering, University of Alberta, Alberta, Canada, No. 204, pp. 35-51.

Yoshioka, Y., (1992). "State of Art of Composite Steel Tube and Concrete Structures In Japan." Proceedings, US-Japan Workshop on Composite and Hybrid Structures, Berkeley, California, Sept. 10-12, pp.119-130.